Long-term expansion, genomic stability, *in vivo* safety and immunogenicity of adult human pancreas organoids

Nikitas Georgakopoulos

Supervisors: Dr. Kourosh Saeb-Parsy, Dr. Meritxell Huch

Department of Surgery
University of Cambridge

This dissertation is submitted for the degree of
Doctor of Philosophy

Queens' College October 2020

Declaration

This dissertation is the result of my own work and includes nothing which is the outcome of work done in collaboration except as declared in the Preface and specified in the text. It is not substantially the same as any that I have submitted, or, is being currently submitted for a degree or diploma or other qualification at the University of Cambridge or any other University or similar institution except as declared in the Preface or specified in the text. I further state that no substantial part of my dissertation has already been submitted, or, is being concurrently submitted for any such degree, diploma or other qualification at the University of Cambridge or any other University or similar institution except as declared in the Preface or specified in the text. This dissertation contains fewer than 60,000 words excluding figures, photographs, tables, supplemental data, appendices and bibliography.

Nikitas Georgakopoulos

October 2020

Abstract

Long-term expansion, genomic stability, *in vivo* safety and immunogenicity of adult human pancreas organoids

Nikitas Georgakopoulos

Pancreatic organoid systems have recently been described for the *in vitro* culture of pancreatic ductal cells from mouse and human. Mouse pancreatic organoids exhibit unlimited expansion potential, while previously reported human pancreas organoid (hPO) cultures do not expand efficiently long-term in a chemically defined, serum-free medium. The aim of this project was to generate a 3D culture system for long-term expansion of human pancreas ductal cells as hPOs to serve as the basis for studies of human pancreas ductal epithelium, exocrine pancreatic diseases and the future development of a genomically stable replacement cell therapy for diabetes mellitus.

hPOs can be generated and expanded in a chemically defined, serum-free, human pancreas organoid culture medium with high efficiency from both fresh and cryopreserved primary tissue. Crucially, the hPO culture system also supports the establishment and expansion of these organoids in a chemically defined, modifiable and scalable, biomimetic hydrogel thus facilitating their translation into the clinic. Moreover, hPOs expanded over months in culture maintain their ductal morphology and biomarker expression of the primary tissue while they can also be expanded from tissue with underlying disease such as type 2 diabetes (T2D).

This project further demonstrates that hPOs maintain stable chromosomal numbers following long-term *in vitro* culture, especially when compared to an established positive tumour organoid control. When clonal hPOs were subjected to whole genome sequencing (WGS), they maintain genomic integrity following culture and acquire less mutations in culture than iPSC-derived cultures, resembling other reported organoid systems. Xenografts of hPOs survive long-term *in vivo* when transplanted into the pancreas of immunodeficient mice. Notably, mouse orthotopic transplants show no signs of tumorigenicity.

To further assess their clinical applicability, hPOs were assessed for the expression of antigenic molecules, demonstrating that under *in vitro* conditions that mimic the inflammatory milieu, hPOs can upregulate HLA Class II. Moreover, this project utilises recently established human immune system (HIS) mice to interrogate *in vivo* hPO immune rejection under autologous and allogeneic conditions. Lastly, preliminary experiments show that hPOs can be genetically manipulated to express GFP and Luciferase which can be used for *in vivo* survival and immune rejection tracking.

Acknowledgements

I would like to thank my supervisor, Dr. Kourosh Saeb-Parsy for giving me the opportunity to undertake this project in his laboratory. Thank you primarily for taking me into your lab as a research assistant and taking that leap of faith in a young researcher without much experience under his belt. That moment has been life defining for me and will shape the rest of my life. Thank you also for entrusting me and giving me the opportunity to undertake this PhD project in your lab. Your continued guidance and support, both in the lab and on a personal level have been an example for me and have set a standard, the level of which I will always try and achieve in my personal career. Thank you also for creating an environment allowing for group and individual success while also breaking the dogmas set by academia. I will always consider myself a member of the KSP lab (a.k.a. Lab Inc.)

I would also like to thank my secondary supervisor, Dr. Meritxell Huch for giving me the opportunity to undertake this project and for welcoming into her lab. Thank you for your guidance and advice throughout my project; I knew that although tough, your advice always came from your heart and drove me to become a better scientist. Your academic excellence is nothing short of admirable and I will always be proud to have been your student.

I would like to especially thank all of my colleagues in both KSP and Huch labs who I'm honoured to have worked with and who I consider lifelong friends. To the OncoID group: Gianmarco Mastrogiovanni, thank you for being a constant source of joy (and gossip) in the lab. Thank you for always being there for me with my endless questions about experiments or to give me some citrate buffer. Mikel McKie, thanks for your pranks. Your science advice was always spot on, but you can use better pranks. Sorry for writing "loser" on your screen. GM made me do it. Lucia Cordero, it took us 3 years, but I finally broke through! Thank you for always being a genius and way too good at science and making me constantly push myself so I didn't look too bad next to you. I finally finished the PhD guys! And…the love car will return! To Luigi Aloia, thank you for being an amazing friend, but also a great mentor both for science and for life. To Flaminia Kalutantridge; we are almost there! Thank you for being such a positive person and for the long life talks in the TC room. It's been amazing to see you grow in the lab and to see what an amazing scientist you have become. To Nicole Prior, thank you for showing me how to be a good scientist and for always challenging me. It was great to have a mentor like you and to work with someone so talented. To the rest of the Huch group: Patricia Inacio, German Belenguer, Anna Dowbaj, Robert Arnes, Daisy Harrison, and Laura Broutier thank you for making the lab an amazing place to work in, for all the stimulating discussions and help, and for all the unforgettable memories I will have from it. Each of you has added important value to the success of this project.

To the KSP group, thank you for always being there to lend a helping hand and for creating such an amazing working environment. Our lab retreats will be lifelong memories for me. To Nikola Doležalová, thank you for being such an amazing friend and for always helping me no matter the

problem or the time. I would have failed all my flow cytometry experiments were it not for you! I will also always strive to be as efficient as you, although I know I can never reach your level. To the rest of the KSP group: Olivia Tysoe, Bethany Bareham, Alba Matas, Abbie Curd, Natasha Ivory, Krishnaa Mahbubani, John Gamble, Anja Gruszczyk, Michelle Curran, Evans Asowata, Maggie Huang, Timothy Elliott Beach, Mazin Hamed, and Jack Martin, thank you for your stimulating discussions and all your help throughout this project.

I would like to especially thank all the collaborators who contributed in this project:

- To Gianmarco Mastrogiovanni from the Gurdon Institute, University of Cambridge for the help in the derivation of hPO lines and characterisation of CFE and doubling time;
- To Daisy Harrison from the Gurdon Institute, University of Cambridge for her work on media optimisation;
- To Nicole Prior from the Gurdon Institute, University of Cambridge for her help in the chemically defined hydrogel experiments, differentiation experiments and general mentorship;
- To Robert Arnes from the Gurdon Institute, University of Cambridge for his help in sectioning, H&E staining and taking care of cultures.
- To Brigitte Angres and Helmut Wurst from Cellendes for the generation of the synthetic hydrogels;
- To Alex Cagan, Federico Abasca and Inigo Martincorena from the Wellcome Sanger institute for the analysis of the whole genome sequencing data, generation of graphs and stimulating discussions;
- To Dawei Sun and Emma Rawlins from the Gurdon Institute, University of Cambridge for provision of the Ef1α-GFP virus;
- To Nikola Doležalová from the Department of Surgery, University of Cambridge for her help with flow cytometry experiments;
- To Olivia Tysoe and Alba Matas from the Department of Surgery, University of Cambridge for their help in planning and carrying out the humanised mouse experiments;
- To the Gurdon Imaging Facility for providing training and support for confocal microscopy;
- To Jackie Higgins from the Department of Surgery for providing excellent care for my experimental animals and helping with animal procedures;

I am grateful to the Horizon 2020 fund for funding the consumables for this project. Thank you to the LSFM4LIFE consortium for the support and stimulating collaborations.

I am grateful to the University Biomedical Services for all their support towards my animal experiments.

I would like to thank the Cambridge Biorepository for Translational Medicine (CBTM) for obtaining and processing human tissue, especially to Dr. Krishnaa Mahbubani, Bethany Bareham, Abbie Curd, Natasha Ivory, and John Gamble. I am also very grateful to Dr. Siong-Seng Liau for provision of the pancreas cancer samples. I am also very grateful to Mr. John Casey and the SNBTS's Islet Isolation Laboratory in Edinburgh for the isolation and provision of human pancreatic islets for research. I am very grateful to all human donors and their families for providing the gift of human tissue for research. Without them this project would not be possible.

I would like to also thank the Department of Surgery technicians and administrative staff for their technical support.

I would like to also thank those who helped with writing and correction of the thesis, especially Dr. Kourosh Saeb-Parsy and Dr. Meritxell Huch.

I would like to thank my family and friends who have been with me and supported me through this difficult but fulfilling journey.

To my love and soulmate, Teddy, thank you for always being there, supporting me through the highs and lows, believing in me and walking this journey with me. You've taught me so much and I'm so lucky to have you by my side.

Lastly, I am grateful to my loving mother and brother who have always unconditionally supported me and loved me. You have been there through all my academic endeavours and have always believed in me.

Table of Contents

List of Figures

List of Tables

Abbreviations

AdSC	Adult stem cell
ALDH	Aldehyde dehydrogenase
ALK3	Activin-like kinase 3
APC	Antigen presenting cells
ASCAT	Allele-specific copy number analysis of tumours
ATMPs	Advanced therapy medicinal products
BLI	Bioluminescence live imaging
BM	Bone marrow
BME 2	Basement membrane extract type 2
BMP	Bone morphogenetic protein
ca19-9	Cancer antigen 19-9
CAG	CMV early enhancer/chicken β actin
CF	Cystic fibrosis
CFTR	Cystic fibrosis transmembrane conductance regulator
CMV	Cytomegalovirus
CNV	Copy number variation
CTP	Cellular therapy product
DAMP	Damage associated molecular patterns
DBD	Donation after brainstem death
DCD	Donation after circulatory death
DEX	Dextranase
DKK-1	Dickkopf-related protein 1
DMEM	Dulbecco's modified eagle medium
DMSO	Dimethyl-sulfoxide
ECM	Extracellular matrix
Ef1α	Elongation factor-1 alpha
EM	Expansion media
EMT	Epithelial-to-mesenchymal transition
EpCAM	Epithelial cell adhesion molecule
ESC	Embryonic stem cell
ESC	Embryonic stem cell
FACS	Fluorescence-activated cell sorting
FGF	Fibroblast growth factor

FSK	Forskolin
G-HA	Glycosil hyaluronic acid
GAD	Glutamic acid decarboxylase
GC	Germinal center
GFOGER	Gly-phe-hyp-gly-glu-arg
GMP	Good manufacturing practice
GvHD	Graft vs host disease
H&E	*Haematoxylin & eosin*
HA	Hyauluronic acid
HbA1c	Glycated haemoglobin
HIS	Human immune system
HLA	Human leukocyte antigen
HNF1β	Hepatocyte nuclear factor β
hPC-org	Human Pancreas Cancer-organoid
hPO	Human Pancreas Organoid
hPO-Opt.EM	Human Pancreas Organoid-Optimised Expansion Medium
HPRT	Hypoxanthine-guanine phosphoribosyltransferase
HSC	Haematopoietic stem cells
Hu-PBL-SCID	Human peripheral blood lymphocytes-SCID
Hu-SRC-SCID	Human SCID-repopulating cell SCID
IA-2	Islet antigen 2
IFNγ	Interferon gamma
IPMN	Intraductal papillary mucinous neoplasm
iPSC	Induced Pluripotent Stem Cell
ITPN	Intraductal Tubulo-papillary Neoplasm
IVIS	*In vivo* imaging system
KRT19	Keratin 19
LGR5	Leucine rich repeat containing g protein-coupled receptor 5
MHC	Major histocompatibility
miH	Minor histocompatibility antigens
mPO	Mouse pancreas organoid
MSC	Mesenchymal stromal cell
MStC	Mesenchymal stem cell
Muc	Mucin
NGN3	Neurogenin 3
NOD	Non-obese diabetic

NSG	Nod scid gamma
NSG-dKO	NSG-double knockout
PAMP	Pathogen associated molecular pattern
PanIN	Pancreatic intraepithelial neoplasm
PCA	Principle component analysis
PDAC	Pancreatic ductal adenocarcinoma
PDL	Partial duct ligation
PDTOs	Patient derived tumour organoids
PDX1	Pancreatic and duodenal homeobox 1
PGE2	Prostaglandin E2
PSC	Pluripotent stem cell
Puro	Puromycin
RGD	Arg-gly-asp
Rhoki	Rho kinase inhibitor
ROCK	Rho kinase
RPE	Retinal pigment epithelial cells
Rspo1	Rspondin 1
RSV	Rous sarcoma virus long terminal repea
SCID	Severe combined immunodeficiency
SLO	Secondary lymphoid organ
SNP	Single nucleotide polymorphism
SNV	Single nucleotide variant
SOX9	Sex-determining region Y-box 9
SpMC	Splenocyte mononuclear cells
T-FH	T follicular helper cell
T1D	Type 1 diabetes
T2D	Type 2 diabetes
TCR	T cell receptor
TGFb	Transforming Growth Factor beta
Tregs	T regulatory cells
VAF	Variant allele frequency
VEGF	Vascular endothelial growth factor
WGS	Whole genome sequencing

CHAPTER 1. INTRODUCTION

1.1 The human pancreas

1.1.1 Development of the human pancreas

The human pancreas is composed of exocrine and endocrine compartments. The former consists of acinar cells, which secrete enzymes into the ductal compartment while the latter is organised into the islets of Langerhans, which are composed of hormone producing cells: α, β, δ, ε, pp cells[1]. The pancreas is composed of approximately 80% acinar cells and 10% ductal cells[2–4] with the endocrine compartment retaining approximately 4.5% of the cell population[5].

Specification of the human embryonic pancreas occurs as early as Carnegie stage 10 (25-27 days post-conception) when the endoderm folds to generate the anterior intestinal portal (AIP) and the endoderm is distinguished into the foregut, midgut and hindgut. Pancreatic and duodenal homeobox factor 1 (*PDX1*) expression is one of the earlier signs of foregut endoderm specification which occurs by the exclusion of sonic hedgehog (*SHH*)[6,7]. The foregut endoderm is subsequently divided into the ventral and dorsal buds marked by co-expression of *PDX1*, SRY (sex-determining region Y)-box 9 (*SOX9*) and GATA binding protein 4 (*GATA4*)[8]. With the early ductal network beginning to form, pancreatic multipotent progenitors become divided with the emergence of Nirenberg and Kim homeobox factor *(NKX 6.1)* into 'tip' progenitors that express *SOX9*, *GATA4* and *NKX6.1* and 'trunk' progenitors with reduced expression of *GATA4*. 'Tip' progenitors further differentiate into acinar cells, an event largely marked by the loss of *SOX9* and *NKX6.1* [8], while 'trunk' bi-potent progenitors give rise to mature ductal and endocrine cells. Although the mechanisms are not fully elucidated, there is evidence that secreted factors such as WNT, fibroblast growth factor 10 (*FGF10*) and epidermal growth factor (*EGF*) drive the proliferation of these early epithelial progenitors [9,10]. Further specification of the 'trunk' progenitors is marked by a transient expression of Neurogenin3 (*NGN3*) and a loss of *SOX9* in cells that further differentiate into endocrine progenitors while ductal progenitors retain expression of *SOX9*[8,11]. Endocrine progenitors further differentiate into the islet cell subtypes with β-cells being characterised by expression of chromogranin A *(CHGA), MAFA, NKX6.1* and Insulin[1] .

1.1.2 Physiology of pancreatic cell subtypes

Ductal cells

Pancreatic ductal cells form a large network of ducts which serve to transport digestive enzymes generated by acinar cells from the small ducts to the main pancreatic duct (of Wirsung) of the pancreas which drains in the duodenum at the ampulla of Vater. The size and histological location of the ducts are important in that larger ducts form a columnar or stratified cuboidal epithelium while smaller

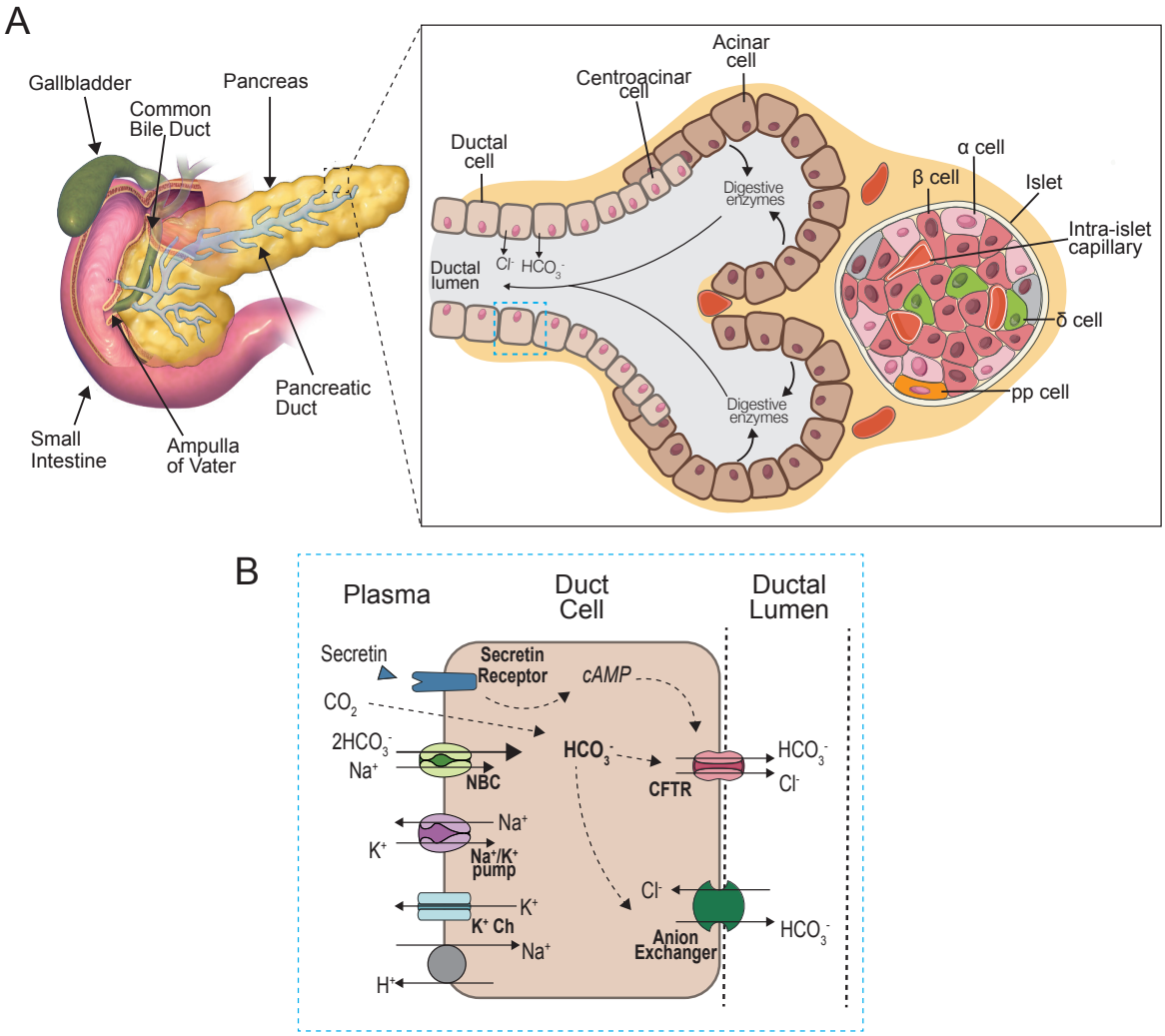

Figure 1.1 Organisation of pancreatic cells and ductal cell function **A**) Schematic showing the anatomy of the human pancreas. The human pancreas contains the main pancreatic duct that runs along the whole organ and further branches out to generate a complex ductal network. The main pancreatic duct connects to the common bile duct, which transverses through the pancreas, and together empty out into the duodenum through the Ampulla of Vater. The pancreas is composed of three main cell types: ductal cells, acinar cells and endocrine cells. The small ductules (lined by ductal cells) which terminate in acinar clusters, transport the digestive enzymes produced by the acinar cells to the duodenum. This is facilitated through the production of chloride ions and bicarbonate ($HCO3^-$) from the ductal cells. Endocrine cells (α, β, γ, δ, pp cells) are organised in cell clusters called Islets of Langerhans and play key role in blood glucose regulation. **B**) Schematic demonstrating the bicarbonate and chloride secretion of ductal cells. $HCO3^-$ ions are generated from CO_2 that enters the cells through passive fusion or $HCO3^-$ can enter through a Na^+ dependent uptake mechanism through the sodium-2-bicarbonate cotransporter (NBC). $HCO3^-$ generation from CO_2 produces protons which are extruded through the Na^+/H^+ exchanger. The driving force for the Na^+/H^+ exchanger is provided by the Na^+/K^+ pump which pumps K^+ in to maintain a hyperpolarised basolateral membrane. $HCO3^-$ ions accumulated through these mechanisms are extruded by an anion exchanger in exchange for Cl- ions. The accumulated Cl^- is transported by Cystic fibrosis transmembrane conductance regulator (CFTR) channel which also conducts $HCO3^-$ into the ductal lumen. The CFTR channel can be activated from secretin binding the secreting receptor causing an increase in cyclic AMP (cAMP) which further activates Protein kinase A which goes on to activate CFTR. (Pancreas image obtained from Blausen Medical Gallery[12]. Figure adapted from Grapin-Botton *et al*. 2005[2])

intralobular ducts form a simple cuboidal epithelium with less connective tissue[2] . Although all pancreatic cell subtypes arise from PDX1+ progenitors, mouse data suggests that the ductal lineage separates from the acinar/endocrine lineage at 12.5 days post conception (dpc)[13]. Due to ethical restrictions, elucidation of the mechanisms driving maturation and ductal network formation in humans has been difficult. However, it has been shown that secreted factors like FGF10, EGF, and Wnt pathway and Notch pathway activation are key in maintaining and expanding the epithelial ductal cell progenitor population[2,9,10,14]. The interplay between these factors and the downregulation of ones such as *FGF10* and *EGF* have been linked to reduced branching and proliferation inferring their importance in the maturation of ductal cells[9,15]. Mature ductal cells serve to produce bicarbonate that neutralises stomach acidity, a process stimulated by secretin produced by the duodenum in response to high acidity. Bicarbonate is secreted along with chloride ions via the Cystic fibrosis transmembrane conductance regulator (CFTR) which is stimulated by cAMP[2,16–18] (Fig. 1.1). Furthermore, ductal cells are responsible for mucin production which lines and protects the epithelium from destructive enzymes[2].

Endocrine cells

Islet cells and perhaps more specifically β-cells are the most studied cells of the pancreas, largely due to the connection to diabetes (discussed in section 1.2.1). Islets are interspersed throughout the pancreas and are round cell clusters composed of distinct cell types including α, β, δ, ε, pp cells and together play a pivotal role in blood glucose regulation[1] (Fig. 1.1). *NGN3* is a key factor driving maturation and proliferation of the endocrine progenitors,[13] however advances of differentiation protocols of pluripotent stem cell (PSCs) have provided evidence of other key factors that are involved (section 1.4.1). β-cells express GLUT-2 receptors which uptake glucose that stimulates insulin secretion by generating ATP, which further increases intracellular Ca^{+} concentration. Insulin release can be also stimulated from incretin hormones produced by the digestive system in response to food digestion[19,20]. Insulin secreted in the bloodstream can be sensed by insulin receptors found in locations such as adipose tissue and muscle cells which, upon insulin binding, will uptake glucose and store it in the form of triglycerols or glycogen. α-cells produce glucagon, a hormone that works in an opposite manner to insulin. During fasting, glucagon is secreted which stimulates glycogenolysis and gluconeogenesis in the liver, thereby increasing glucose levels in the blood. Glucagon production is initiated by hypoglycaemia but the exact mechanism of α-cell stimulated glucagon secretion remains contested[21]. Reports also attribute glucagon release control to paracrine signals. For example, GABA secretion from β-cells has the ability to inhibit glucagon secretion[22], and glucose itself can act as an inhibitory signal. Somatostatin produced by δ cells may also inhibit production of both insulin and glucagon[21]. However, studies have also attributed glucagon release to more intrinsic factors such as membrane potential changes, whereby circulating glucose causes a decrease in the amplitude of action potentials further inhibiting ion channels and further blocking production of glucagon[21]. Although the exact mechanisms are still being studied, it is becoming increasingly clear that precise blood glucose control is dependent

on multiple cell types and a complex network of biochemical reactions functioning in a seamless manner.

Acinar cells

Acinar cells are the most abundant cell of the pancreas and are a secretory epithelial cell. They are organised into acinar clusters which form intercellular canaliculi into which they secrete three main enzymes: α-amylase, lipase and protease responsible for the breakdown of carbohydrates, fats and proteins respectively. The intercellular canaliculi converge into the larger intralobular ducts which further converge into the main pancreatic duct[23]. As mentioned, acinar cells share a common progenitor with endocrine and ductal cells but are the first of the three cell types to diverge at 45-47dpc, in humans, triggered by high levels of *GATA4* [1]. By 10wpc acinar 'tip' cells lose expression of *NKX6.1* and by 14wpc, they lose expression of *SOX9*. In a contrast to *NKX6.1* and *SOX9*, Pancreas transcription factor 1a (*PTF1A*) and Nuclear receptor subfamily 5, group A, member 2 (*NR5A2*) although initially present in pancreatic multipotent progenitors, their expression becomes restricted to mature acinar cells. Together with muscle, intestine, stomach transcription factor 1 (*MIST1*), these factors are essential for the maturation and identify maintenance of acinar cells[24–26]. Mature acinar cells are stimulated by neurohormonal regulators triggered by ingestion of food. These include cholecystokinin, acetylcholine and others which bind to their receptors and trigger downstream signalling pathways. These events stimulate the exocytosis of secretory granules containing of the three aforementioned enzymes[3,23].

1.2 Pathologies of the pancreas

The pancreas is associated with various pathologies that can affect either the endocrine compartment, such as diabetes, or the exocrine compartment such as Cystic Fibrosis or pancreatitis. Furthermore, pancreatic cancer can affect both endocrine and exocrine compartments. Understanding of the pathologies that are associated with the pancreas can help guide strategies for the generation of cellular therapies aimed at treating them. Furthermore, such diseases require complex modelling *in vitro* that can allow better understanding of the native tissue, the disease biology, as well as improved *in vitro* drug testing. Sections 1.2.1-1.2.4 review the most common pancreatic pathologies in terms of disease pathology, prevalence and available treatments.

1.2.1 Diabetes

Diabetes Mellitus describes a series of metabolic conditions associated with hyperglycaemia caused by defects in insulin secretion and/or action. Insulin, produced by the islet β-cells has a series of functions, the most important of which is the stimulation of uptake of glucose by cells in the body. Diabetes is divided into two categories: Type 1 Diabetes (T1D), in which the pancreas is unable to produce

sufficient insulin and Type 2 Diabetes (T2D), which is characterised by impaired glucose tolerance and insulin resistance[27]. In 2019, 463 million people were diagnosed with diabetes worldwide, a figure that is expected to rise to 700 million by 2045. It is estimated that 4.5 million people have diabetes in the UK, of which only 3.8 million are diagnosed[28–30].

Type 1

T1D accounts for 10-15% of all cases of diabetes. It is a multifactorial disease resulting from autoimmune destruction of insulin producing pancreatic β-cells, driven by both genetic predispositions and environmental triggers[31]. B-cell destruction can begin in the first few months or years of life with symptoms, primarily overt hyperglycaemia, evident after 90-95% loss of β-cells[32].

Type 2

T2D is a multifactorial disease which involves genetic, environmental, and lifestyle factors. Over time, cells within the muscle, liver and fat develop resistance to insulin, causing hyperglycaemia, an increased demand and production of insulin. Insulin resistance is thought to arise through various pathways including imbalance in the concentrations of hormones (e.g., increased leptin, reduced adiponectin, and increased glucagon) and increased concentrations of cytokines (e.g., TNF-α, IL-6)[27]. This leads to a gradual decline in β-cell function as well a decrease in β -cell mass. Apoptosis may also be an important contributor. This decline in the function of β-cells leads to hyperglycaemia, lipotoxicity, and oxidative stress with α-cell dysfunction[27].

1.2.2 Treatment options for T1D and T2D

The treatment options for diabetes are primarily determined by disease type - T1D or T2D. Current treatments for T1D, as well as in advanced T2D, include exogenous insulin delivered intermittently (insulin analogues) or continuously (insulin pumps) as well as endogenous insulin production through pancreas or islet transplantation.

Exogenous Insulin

A range of insulin analogues and formulations are available: rapid-acting analogues (aspart, lispro), slow-acting analogues (glargine, determir) and various pre-mixed formulations with both types to replicate normal insulin levels[33]. However, the need for strict patient adherence to insulin regiments as well as the risk of hypoglycaemia are some of the disadvantages of exogenous insulin[34]. Patient adherence can be improved with the use of insulin pumps and the introduction of a closed loop system with integrated sensing technology (i.e., artificial pancreas). Such systems can indeed help achieve better targets of blood glucose levels as compared to daily insulin injections[32], but require carbohydrate

counting or announcing meals to a machine algorithm[35] which in turn reduces flexibility of meals. Significant research has gone into developing artificial pancreases that are based on artificial intelligence (AI) and continuous glucose monitoring, thus removing the need for carbohydrate counting. Promising clinical trials show that such devices are comparable and even perform better than standard care treatment with minimal information required for initialisation and operation[36]. Despite such important advancements, further research is required to assess the long-term usage and physiological effects of such devices.

Whole Organ Transplantation

Whole pancreas transplantation is another treatment option for some patients with T1D, usually if there is concomitant end-stage renal disease. It is generally regarded as the most effective way to achieve euglycaemia. However, pancreas transplants are limited due to shortage of pancreases suitable for transplantation. In 2018/9 in the UK, 176 pancreas transplantations took place while only 32% of patients on the transplant waiting list received a pancreas within one year[37]. Transplantation also requires life-long immunosuppression to prevent immune rejection of the graft. Despite significant advances in pancreas transplantation, in 2018 patient and graft survival at 5 years was reported at 81% and 49% respectively[37]. Furthermore, pancreas transplantation is generally reserved until late in the course of diabetes, therefore reversal of existing complications is unlikely[38].

Islet Transplantation

Islet transplantation is appealing because a much less invasive surgical procedure is necessary and only the insulin-producing islets are transplanted. Shapiro *et al*., with the introduction of the Edmonton protocol performed islet transplants in 7 consecutive patients with a glucocorticoid-free (glucocorticoids induce peripheral insulin resistance and directly damage pancreatic islet β-cells[38,39]), tacrolimus based immunosuppressive regiments. All patients became insulin-independent with no instances of rejection up to 1 year[39]. Despite various successes of islet transplantation over the years, the treatment faces several obstacles. In the first instance, immunosuppression is still required and only a few select patients are chosen for the procedure. In addition, multiple donor pancreases are required for isolation of enough islets, so that organ availability is still the greatest limiting factor with only 28 islet transplants performed in the UK in 2019[37].

1.2.3 Long term complications of diabetes

Individuals with diabetes have a 10-fold higher risk of cardiovascular complications such as myocardial infarction and stroke as well as risk for microvascular complications such as retinopathy, nephropathy, and neuropathy[32]. In addition, diabetes is the most common cause of adult loss of vision, end-stage renal

disease and amputations. Increased risk of cancers (eg, pancreas, liver, and colorectal) have also been attributed to the vascular complications of diabetes[40].

1.2.4 Exocrine pancreas disorders

Cystic fibrosis

Cystic fibrosis (CF) is an autosomal recessive, monogenetic disorder caused by mutations in the cystic fibrosis transmembrane conductance regulator (*CFTR*) gene responsible for generating the CFTR channel. As mentioned, this channel mainly functions as an apical anion channel of chloride and bicarbonate. Severity of the disease is determined by the mutations occurring in the genes of an individual, with some leading to loss of expression of CFTR in the membrane while others lead to loss of function. The main organs affected by CF are the lungs, pancreas and the gastrointestinal tract with airway disease being the main driver of morbidity and mortality. In the lungs, CF leads to mucus accumulation which leads to obstruction of the airways[41]. In the pancreas, the lack of a functional CFTR channel leads to decreased bicarbonate secretion in the ductal lumen which increases the concentration of acinar enzymes and causes damage and obstruction of the ductal network[42]. This process leads to inflammation, destruction of the acini and fibrosis with 85% of CF patients having exocrine pancreatic insufficiency[42]. CF affects 1 in 3,000 individuals born with European descent while the incidence can be as low as 1 in 15,000 in individuals such as African Americans. The projected median survival of children born with CF today is 56 years with the survival rate improving constantly. Treatment of the disease can start with prescription of mucolytics, antibiotics, anti-inflammatory medication and enzyme replacement therapy with more severe cases requiring lung transplants and occasionally pancreas and liver transplants[41,42]. Experimental approaches for treatment are focused on gene therapy to provide the normal copy of the *CFTR* gene in the patient's cells or therapeutic agents that can improve the translation and folding of the CFTR protein and expression on the cell surface[41].

Pancreatitis

This disease is characterised into two different types: acute pancreatitis and chronic pancreatitis. Acute pancreatitis is the most common disease of the pancreas and is characterised by tissue oedema, acinar cell necrosis, haemorrhage and inflammation[3]. The major etiological factors for acute pancreatitis are gallstones and alcoholism. Acute pancreatitis is thought to be initiated by inappropriate activation of the proteolytic enzyme trypsin, which triggers a cascade of events leading to pancreatic autodigestion[43]. Although most patients recover, 10-15% of them will develop severe acute pancreatitis which can lead to complications and potentially death. Treatment includes the use of antibiotics or enteral feeding or cholecystectomy when gallstones are involved[43]. Chronic pancreatitis has a lower incidence rate of 7-10 per 100,000 per year and has various risk factors associated such as environmental (alcohol consumption etc.), hereditary mutations, ductal obstruction and autoimmune factors. It is characterised

by fibrotic destruction of the tissue leading to acinar cell death, matrix deposition, permanent structural changes leading to impairment of both endocrine and exocrine compartments[44]. Treatment of chronic pancreatitis includes pain management, insulin and enzyme therapy to treat pancreatic insufficiency as well as surgical procedures to remove parts or all of the pancreas[43].

Issues relating to the pancreatic ductal compartment have been implicated as causes for both acute and chronic pancreatitis. Patients with mutations in the *CFTR* gene but not necessarily with presence of CF have a higher chance of developing chronic pancreatitis[43,45]. Furthermore, agents such as bile acids or ethanol can significantly impact the ability of ductal cells to secrete bicarbonate or other ions into the ductal lumen thereby causing changes to luminal pH. Decreased extracellular pH can enhance both trypsinogen autoactivation and injury to acinar cells which can further lead to pancreatitis[45].

Pancreatic cancer

Pancreatic cancer can involve either the endocrine (e.g. insulinomas) or exocrine (e.g., adenocarcinomas) component. The most prominent pancreatic cancer type is pancreatic adenocarcinoma of which almost >90% of cases are pancreas ductal adenocarcinoma (PDAC). Pancreatic cancer is the 14th most common cancer worldwide with a very poor 5 year survival of 4-6% in Europe depending on gender and precise region[46,47]. PDAC can develop from benign or pre-malignant lesions, three of which are known and well characterised; pancreatic intraepithelial neoplasia (PanIN), intraductal papillary mucinous neoplasm (IPMN) and mucinous cystic neoplasms (MCN)[48]. PanINs arise in the small ducts of the pancreas, typically less than 0.5cm in size and are classified into three grades (1-3) based on levels of nuclear changes such as pleomorphism, pseudostratification and loss of polarity, as well as general loss of architecture with formation of papillae[49]. IPMNs arise in the main duct or duct branches while different subtypes exist such as intestinal and pancreaticobiliary depending on the level of differentiation[50]. MCNs are predominantly found in women and arise in the pancreatic body or tail without communication to the main pancreatic duct. MCN histology is described as tubular adenocarcinoma, similar to PDACs[51]. Although each of these premalignant lesions can progress to a PDAC with the appropriate mutations, PanINs are the most common precursor. Mutations in the *KRAS* oncogene are associated with nearly all PDACs and are an early event in the progression from premalignancy to carcinoma. Further progression occurs with mutations taking place in tumour suppressor genes identified such as *p16/CDKN2A, SMAD4, TP53* and *BRCA2*[48,52]. Histology of PDACs is primarily characterised by invasive malignant epithelial neoplasm with duct-like glands with varying levels of differentiation and mucin production[53]. Treatment of PDAC includes surgery to remove the affected region. However only 15-20% of patients are eligible for such a procedure due to distant spread of the disease at the time of diagnosis. For some, but not all, of those not eligible for surgery,

chemotherapy or radiation may be a remaining treatment option[48]. This highlights the need for improved or targeted therapies that can increase the pool of eligible patients as well as increase the rate of survival.

1.3 Regeneration and plasticity in the pancreas

1.3.1 Plasticity and β-cell regeneration *in vivo*

Whether the adult human pancreas is capable of regeneration is a subject of intense debate. It is known that organs such the adult liver display a tremendous regeneration capacity, capable of full regeneration after as much as 70% of the liver is removed following a hepatectomy[54,55]. Although the pancreas clearly does not display such regeneration capabilities, scientists have investigated the ability of the pancreas to maintain its cell populations under normal or damaged states, with particular focus on β-cells, the loss of which is implicated in diabetes. Although the exocrine pancreas possesses some capacity for regeneration, such as after acute pancreatitis, it remains unclear whether the human endocrine compartment can regenerate itself to a clinically relevant extent. Understanding of such potential intrinsic pathways of regeneration can help guide strategies towards *in vivo* regeneration or *ex-vivo* generation of β-cells for the treatment of diabetes.

In T1D, ~90% of β-cell loss must occur before patients become fully dependent on exogenous insulin. However, cases where only 50-60% of the pancreas is removed during surgery have also triggered insulin-dependent diabetes[56]. Despite the inability of the endocrine compartment to regenerate in such extreme loss, evidence in rodents demonstrates an increase in β-cell mass in cases such as pregnancy, obesity or experimentally-induced insulin resistance[57–60]. In humans, the β-cell mass has been observed to increase by as much as 50% in non-diabetic obese individuals[61]. Although modest in comparison to rodents, a small increase in β-cell mass is also observed during human pregnancy[62]. Nevertheless, the question remains as to the source of *de novo* β-cells *in vivo* in both diseased states and during homeostasis, i.e., the healthy, undamaged adult state after embryonic and postnatal growth. A landmark study by Dor *et al.*, with the use of genetic lineage tracing in mice using insulin promoter driven inducible expression of Z/AP reporter, showed that existing β-cells rather than stem cells are involved in β-cell replenishment[63]. Indeed, in humans, there is evidence to show that replication underlies the post-natal expansion of β-cells, while it has also been shown that subsets of β-cells in the adults express proliferation markers such as Ki67[64,65]. Nevertheless, it is unclear as to what happens in the adult pancreas while contrasting views have highlighted evidence for the existence of a β-cell progenitor.

Significant functional heterogeneity exists within β-cells; hypoxic subset populations[66] or hub cells (<10% of islet β-cells) have been described that, when silenced, can disrupt islet connectivity, calcium signalling and insulin secretion[67]. Importantly, distinct subpopulations of β-cells have been identified through differential gene expression of CD9 and ST8 alpha-N-acetyl-neuraminide alpha-2,8-sialyltransferase 1 (ST8SIA1)[68]. Interestingly these populations showed a difference in glucose-

stimulated insulin secretion and a shift in populations was evident in T2D patients, suggesting the possibility that diabetes can alter levels of β-cell subpopulations[68]. Interestingly, in mice, an inverse relationship has been demonstrated between proliferative state and maturity of β-cells[69,70]. Consistent with this finding, induced hyperglycaemia in mice has been shown to lead to β-cell de-differentiation towards a progenitor-like state[71]. Furthermore, insulin expressing multipotent progenitors (MPs) have been proposed to exist in pancreases of both mice and humans that could generate β-like cells *in vitro*[72]. Whether these reports of heterogeneity among β-cells and insulin positive MPs underlie the existence of a true and functionally relevant population of adult β-cell progenitor pool remains under investigation.

Other studies have focused on the possibility of trans-differentiation as a mechanism of β-cell regeneration. Thorel *et al.* showed that chemical ablation 90% of β-cells led to significant regeneration of β-cell mass which came from conversion of α-cells[73]. In another study, somatostatin producing δ-cells were shown to be converted to β-cells in a similar injury model in pre-puberty mice[74]. While it is an interesting notion, there is lack of evidence that such islet-cell subtype interconversion exists in a human setting.

1.3.2 Stem cells in the adult human pancreas

One of the most contentious subjects within the topic of pancreas regeneration is the existence of an adult progenitor/stem cell pool which can regenerate multiple types of cells. As mentioned in section 1.1.1, during development, specification of the three pancreatic cell subtypes stems from a ductal progenitor population[1]. Following this notion, many believe that the adult ductal compartment could retain a subset of progenitor cells. Indeed, early studies showed that ductal cells could contribute to islet regeneration following pancreatectomy in the mouse[75]. However, pivotal studies such as from Dor *et al.*[63,64] have challenged the existence of pancreas progenitors. Interestingly, as pointed out in a recent review[76], such studies that have refuted or supported the 'progenitor cell hypothesis' have largely depended on lineage tracing experiments. The investigators however acknowledged the limitations of such techniques, including promoter leakage or low labelling efficiency[76]. Moreover, studies based on lineage tracing variably demonstrated that ductal cells were[77] or were not[78], contributing to β-cell regeneration postnatally. Such contrasting reports could be attributed to a dynamic state within the ductal compartment, whereby cells express or lose expression of specific markers to acquire a more stem-cell identity thereby introducing inconsistency in labelling[76]. Nevertheless, several reports have shown that upon damage, ductal cells can proliferate and differentiate towards a ductal lineage[79] and upregulate the adult stem cell receptor Lgr5[80]. Furthermore, ductal cells were also shown to contribute to acinar and endocrine lineages following damage [79,81–83]. More recently, single cell RNA-sequencing (scRNA-seq) of activin-receptor like kinase 3 (ALK3) positive ductal cells from the adult human pancreas demonstrated multiple subpopulations in the ductal compartment, with a ducto-acinar and

ducto-endocrine axis as assessed by principal component analysis (PCA)[84]. Although the 'replication' vs 'progenitor' debate ensues, both proponents agree that pancreas regeneration *in vivo* during homeostasis is rare and has only been observed after a non-physiological event has taken place. However, such progenitors, even if existent in a rare form, could potentially be expanded *in vitro* and allow investigation of mature stem cell biology or generation of novel cellular therapies.

1.4 Regenerative cellular therapies of the pancreas

Islet transplantation is a potentially curative treatment for T1D and can restore the insulin producing pool of cells, but the treatment is hampered partly by the lack of available donors. Expansion of islets *in vitro* would be an ideal treatment strategy in addressing a shortage of islets; however, this remains a challenge due to the low proliferative capacity of mature endocrine cells and the tendency of islets to undergo epithelial to mesenchymal transition in culture[85]. Stem cell derived therapy aims to replace or repair damaged or diseased tissue. This concept can be applied to diabetes whereby the disease could be treated by stem cell-derived healthy functioning β-cells which can be delivered to a patient in a manner similar to islets. The appeal of stem cells is that they can be derived from the patient, differentiated into the appropriate cell type, grown to sufficient amounts, and re-transplanted into the same individual to treat their disease. Such an 'autologous' treatment might be expected to induce little or no immune response. The stem cells could also be frozen and be readily available for future use while providing a continuous supply. Thus, much research has focused on the *in vitro* reprogramming of stem cells derived from pluripotent stem cells (PSCs) such as embryonic stem cells (ESCs) and induced pluripotent stem cells (iPSCs) or trans-differentiation of terminally differentiated cells.

1.4.1 Reprogramming of pluripotent stem cells (PSCs)

ESCs and iPSCs

ES cells are derived from the preimplantation embryo, from the inner cell mass of the blastocyst. They are defined by their prolonged undifferentiated proliferation and ability to form all three embryonic germ layers (i.e., pluripotency). iPSCs are derived from fully differentiated adult somatic cells and converted to the pluripotent state while presenting identical features to ESCs[86–88]. Phenomenal progress has been made into differentiating ESCs and iPSCs towards a desired cell type as well as translating the technology into a clinical therapy. Despite various successes, concerns regarding tumorigenicity and immunogenicity of these cells remain an issue (this is reviewed in detail in sections 1.6.2 and 1.7.4 respectively). Studies in mouse models have shown that ESCs have the capacity to form undifferentiated tumours[89] which can also be lethal[90]. Similarly, iPSCs have been shown to be genomically unstable due to the use of reprogramming factors as well as the culture process[91,92]. Surprisingly, it was shown that even autologous derived iPSCs were rejected by the immune system (further detailed in section 1.7.3[93]).

PSCs for the generation of β-like cells

Developmental studies utilising mouse models or human embryonic samples within the allowed ethical timeframes have been very informative in the understanding of the development of the pancreas. Nevertheless, practical and ethical barriers have made it difficult to discover the precise steps and soluble factors involved which drive maturation of the pancreas. However, insights have been granted by mapping PSC differentiation protocols for the generation of β-like cells onto human pancreas development. There is significant expectation that PSC derived β-like cells will eventually provide a cellular therapy for the treatment of diabetes.

As outlined in section 1.1.1, pancreatic β-cells arise from the definitive endoderm developing to the primitive gut tube, posterior foregut, pancreatic endoderm, pancreatic endocrine progenitors and finally β-cells (Fig. 1.2). Treatment of pluripotent stem cells with Activin A and Wnt3A (or CHIR99021, a WNT activator) induces definitive endoderm specification in PSCs by stimulating transforming growth factor β (*TGFβ),* Wnt and Nodal signalling[94,95]. Posterior foregut specification can be achieved by activation of *FGF* and retinoic acid signalling and inhibition of sonic hedgehog pathways; SHH inhibition is usually achieved with the use of SANT-1, an SHH antagonist. This stage is marked by expression of forkhead box A2 *(FOXA2)*, and hepatocyte nuclear factor 1-β (*HNF1β)* expression. Further specification to pancreatic endoderm occurs by inhibition of BMP signalling, which favours liver development, though use of BMP signalling antagonist LDN193189 while SHH inhibition assists pancreatic endoderm specification. This stage is marked by expression of PDX1 and NKX6.1[95] . Generation of endocrine progenitors is largely dependent on inhibition of the Notch signalling pathway which is achieved by γ-secretase inhibitors such as DAPT. This allows expression of NGN3, a key marker of endocrine progenitors while further maturation is largely governed by *TGFβ* signalling inhibition achieved by addition of Activin receptor-like kinase 5 inhibitor II (ALK5i)[1,94,95]. The ultimate goal is to generate mono-hormonal insulin producing cells which have arisen from pancreas progenitor cells, defined by co-expression of transcription factors *PDX1, NKX6.1, NKX2.2, PTF1A*, and *SOX9*. In the earlier studies of directed differentiation, expression of these markers had not been achieved. It was then understood that expression of transcription factors required tight control. Landmark papers from Pagliuca *et al.*[96] and Rezania *et al.*[97], using a suspension-based culture system utilised a TGF-β inhibitor, BMP4 inhibitor, thyroid hormone and Notch inhibitor to create PSC-derived mono-hormonal, PDX1 and NKX6.1 double-positive β-like cells. These were also capable of glucose stimulated insulin secretion (GSIS) and were able to ameliorate hyperglycaemia after transplantation into mice[96,97]. This was also recapitulated from human fibroblasts derived from T1D patients[98]. Despite the promise of PSC derived β-cells and the continued improvement of protocols, concerns remain as to the safety of their use in a clinical environment (this is explored in section 1.6.2). Regardless of safety and ethical

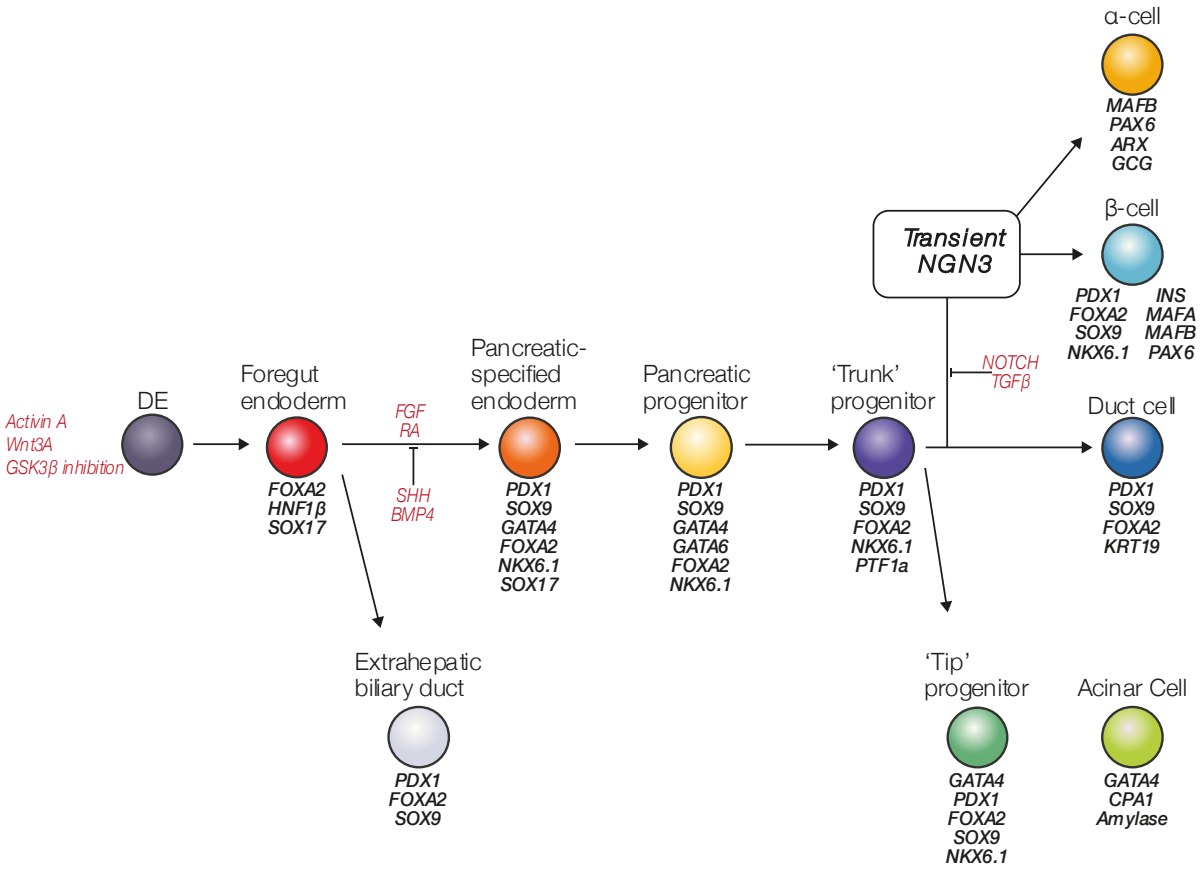

Figure 1.2 Regulatory factors affecting human pancreas developmental stages. Cell stages (coloured circles) of pancreatic cell development from definitive endoderm (DE) to the pancreatic lineages. Differentiation protocols use exogenous factors, some of which are illustrated in red, to direct differentiation towards a specific path. Glycogen synthase kinase 3β (GSK3b); sonic hedgehog (SHH); bone morphogenetic protein 4 (BMP4); Fibroblast growth factor (FGF); Retinoic Acid (RA); Transforming growth factor β (TGFβ); Neurogenin 3 (NGN3); Glucagon (GCG); Insulin (INS).(Figure adapted from Jennings *et al*. 2015[1])

concerns, approaches utilising ESCs or iPSCs are advancing with companies introducing these technologies in clinical trials[99].

1.4.2 Reprogramming of terminally differentiated cells

It has been shown that terminally differentiated cells within the pancreas can be reprogrammed into β-cells. Studies have demonstrated that ectopic expression of *NGN3* through adenoviral infection in adult human pancreatic cells resulted in ductal-endocrine differentiation, which could be improved by inhibition of Delta-Notch signalling. Nevertheless, these studies did not demonstrate functionality of the insulin+ (INS) cells[100,101]. Collombat and colleagues successfully converted adult mouse α-cells into β-cells through ectopic expression of paired box 4 (*PAX4*)[102]. Similar investigations of non-endocrine cells by Zhou *et al.* showed that adenoviral transfection of three key factors, *PDX1, MAFA,* and *NGN3* (3TF) into adult mouse exocrine cells *in vivo* can convert them to β-like cells. These cells resembled

adult β-cells morphologically and functionally and were able to ameliorate hyperglycaemia[103]. In human exocrine tissue, it was shown that adenoviral transduction of four factors (*PDX1, MAFA, NGN3, PAX4*) and silencing of aristaless related homeobox (*ARX*) transcription factor - which favours α cell identity - resulted in functional β-like cells that reversed diabetes in streptozotocin-induced diabetic mice[104]. However, the precise cellular origin of the differentiated cells was not stated. Furthermore, it was shown that persistent overexpression of 3TF caused acinar to ductal metaplasia and inflammation. It was only when inflammation was attenuated by reducing expression levels of 3TF that acinar cells were allowed to be converted to β-like cells[105]. Despite these promising results, the effects of reprograming on the cells, genomically and functionally, as well as their safety in use for clinical therapies has yet to be definitely determined.

1.5 Organoid technology

The development of PSC technologies has both increased the knowledge surrounding the development of organs and has provided realistic hope for a cellular therapy to treat diseases such as T1D. However, such culture systems originally utilised 2D cell culture conditions wherein the investigation of tissue patterning, and organ morphogenesis remains challenging. Recently developed 3D culture systems, in which cells are cultured using an extracellular matrix and subsequently develop into 3D cell clusters (termed 'organoids') have become a novel *in vitro* model for the study of tissue development, organogenesis, cell-to-cell interactions, as well as disease modelling. An 'organoid' is defined as a 3D structure derived from ESCs, iPSCs or adult-tissue-resident cells (stem or differentiated cells) that spontaneously self-organise into functional cell types, in part resembling their tissue of origin[106,107]. The following sections review the use of organoid technology to model development as well as healthy and diseased states of the pancreas.

1.5.1 Embryonic/PSC derived organoids

ESC and iPSC technologies are progressively being used in conjunction with 3D culture systems. Thyroid, liver, intestine, cerebral, and inner ear are some of the tissues from which organoids have been derived using PSCs[108]. Of note, the 3D organoid systems have been reported utilising embryonic tissue in the mouse. Greggio *et al.*[109] reported organoid-like structures after seeding E10.5 pancreas epithelial cells which expressed PDX1, SOX9, and HNF1B. After co-culture of the progenitor organoids with embryonic pancreas, they achieved endocrine differentiation of organoids[109]. Importantly, it was shown that FGF10 was important for growth of the culture and limited acinar differentiation, while FGF1 reduced endocrine differentiation. This is consistent with findings from Bhushnan *et al.* which show that FGF10 promotes epithelial progenitor maintenance and expansion[9]. However, blocking of FGF signalling after 4 days culture had no effect on organoid formation capacity while it induced differentiation into endocrine lineages[109]. Similarly, another group has more recently achieved 'islet-

like organoid' structures from human iPSCs, utilising the iPSC stepwise differentiation protocol. The organoids were grown on non-coated plates, forming 3D clusters that expressed insulin, somatostatin and pancreatic polypeptide in a polyhormonal fashion[110].

Studies based on embryo derived progenitors or PSCs to generate 3D cultures have maintained the use of small-molecule driven protocols to achieve differentiation, although there have been efforts to reduce the use of small molecules to drive differentiation in an *in vivo*-like manner. Bonfanti *et al.* generated 3D organoids from foetal human pancreatic tissue demonstrating the importance of WNT, FGF10 and epidermal growth factor (EGF) for the expansion of pancreatic progenitors long-term in culture. Importantly, removal of EGF from the culture media led to endocrine differentiation[10]. More recently, Koike and colleagues drove differentiation of human iPSCs into definitive endoderm and then into either anterior gut or posterior gut which formed spheroids when placed in air-liquid interphase culture. The researchers fused the two spheroids to recreate the foregut-midgut boundary of a developing embryo. It was shown that hepatic, pancreatic and biliary progenitors could be detected in the boundary of the fused spheroids in the absence of extrinsic factors after 90 days in culture[111]. This was an important step towards driving organogenesis *in vitro* utilising a model that is more faithful to what occurs *in vivo*. Whilst the use of embryonic tissue and or ESCs/iPSCs for 3D culture has clear potential for the study of developmental processes and organogenesis, important biological questions remain once organ growth has terminated. Thereby, a need exists to model maintenance and repair of adult tissue.

1.5.2 Adult-tissue-resident-cell organoids

Adult stem cell derived organoids

The existence of adult stem cell (AdSC) populations has been known since the 1980s when Barrandon and Green[112] expanded epidermal stem cells. Despite the initial difficulty of expanding stem/progenitor cells from primary adult tissue, this has been achieved from tissues and organs such as the mammary gland, bone, small intestine, stomach, colon, liver, pancreas, lung, prostate, salivary gland and tongue[106]. Wnt signalling[113,114] has been shown to have a vital role in regulating AdSCs in various organs[115]. The Lgr5 receptor, through the actions of Rspondin (Rspo1), enhances Wnt signalling (Fig. 1.3) and was shown to mark the actively dividing adult stem cell population in high turnover tissues including the intestine, colon, and stomach[116,117]. In a seminal paper by Barker *et al.,*[116] the authors generated a mouse line with a EGFP-IRES-creERT2 knock in allele in the first codon of the Lgr5 gene crossed with a Cre-activatable Rosa26-lacZ reporter (namely, Lgr5-IRES-creERT). In this study, GFP marked the crypt-base-columnar cells of the intestinal crypt and the lacZ acting as a permanent progeny marker showed repopulation of all the cells in the intestinal crypt[116]. It was later shown that these Lgr5+ sorted single cells could grow small intestinal organoids *in vitro* using a modified 3D culture protocol established by Sato *et al*.[118] while this was later recapitulated in the stomach[117]. Despite Lgr5 not being observed in

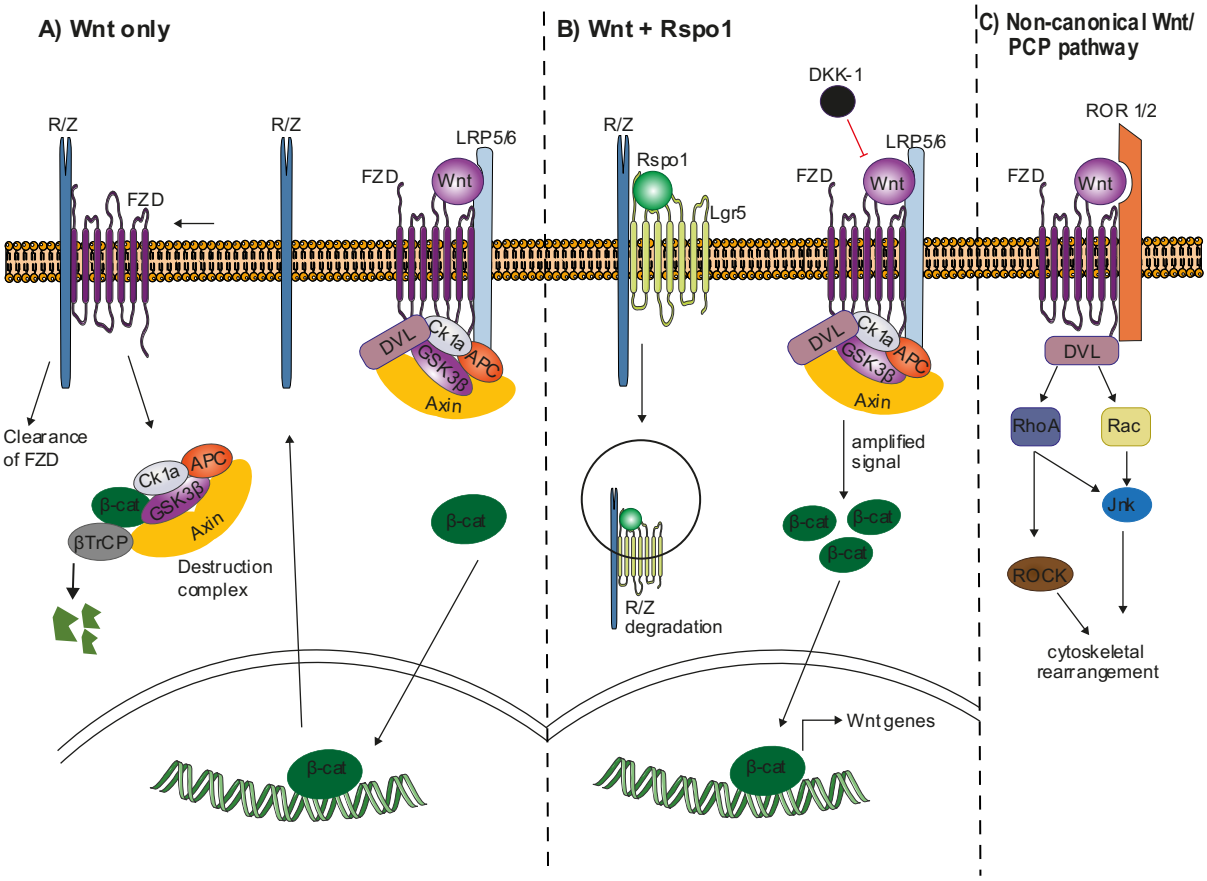

Figure 1.3 Wnt Signalling pathways. **A**) During Wnt signalling (left), Wnt binds to Frizzled receptor (FZD) and LRP5/6 receptor which then bind the destruction complex, made up of Dishiveled (DVL), Axin, GSK3β, CK1a, and APC, sequestrating it. Stabilised β-catenin (β-cat), translocates to the nucleus and induces expression of Wnt signaling genes as well as RNF43/ZNRF3 (R/Z), an E3 ubiquitin ligase. R/Z translocates to the plasma membrane, binding to FZD and subsequently clearing it. The destruction complex can then bind βcat and destroy it, switching off Wnt signaling. **B**) In the presence of Rspondin1 (Rspo1)(Right), Rspo1 enhances Wnt signaling by binding to LGR5 receptor which then binds to R/Z, triggering its internalisation and degradation. This allows more FZD molecules to remain on the cell surface leading to increased stabilisation of β-cat and increased expression of WNT genes. C) During non-canonical Wnt/Planar cell polarity (PCP) signaling, Wnt binds to the ROR-FZD receptor complex to recruit and activate DVL. DVL activates GTPases Rho and Rac which together trigger Jnk and Rho kinase (ROCK) which leads to cytoskeletal rearrangements. Dickkopf-related protein 1 (DKK-1) acts to inhibits canonical Wnt signalling. (Figure adapted from Feng *et al.* 2015[114], Hao *et al.* 2016[113], and Zhan *et al.* 2016[119])

endodermal organs under physiological conditions, it was shown that upon injury, the mouse liver harbours Lgr5+ cells capable of regeneration[80]. EpCAM+ cells could also be isolated from ducts of primary human liver tissue which formed organoid structures and could be expanded long-term *in vitro* without the need of cell transformation, while these cells expressed Lgr5 mRNA. These cells carried a ductal phenotype, were termed 'bi-potent progenitors' and could be differentiated into hepatocytes that were functional *in vivo*[120].

Mouse Pancreas derived organoids

The pancreas is a tissue of low regenerative capacity and Wnt signalling in the adult is thought to be inactive. Therefore, the existence of an Lgr5+ stem cell pool under physiological conditions is unlikely. Nonetheless, it was shown by Huch *et al.* that ductal injury in the mouse pancreas via partial duct ligation (PDL) resulted in significant *Lgr5* activation around the ductal tree of the pancreas. Importantly, the ductal cells could be isolated from primary tissue and grown in Matrigel under conditions containing EGF, Rspo1, Noggin, FGF10, and Nicotineamide[121]. The ductal cells formed hollow cysts with a single layer of epithelial cells which generated buds that expressed Lgr5, while acinar and endocrine cells were incapable of organoid formation[121]. These could be grown *in vitro* for over 10 months without the need for cell transformation and expressed ductal and pancreatic progenitor markers SOX9, PDX1, KRT19. Promisingly, when the adult-derived pancreas organoids were re-aggregated with mouse embryonic pancreas and transplanted under the mouse kidney capsule, they differentiated into mono-hormonal INS+ cells at a low frequency (~5%)[121]. This study not only provided evidence for the existence of a progenitor pool in the ductal compartment of the mouse pancreas but also showed that with the correct signalling cues, adult ductal cells can differentiate into insulin producing cells. Recently, two groups described the expansion of mouse islet cells in 3D culture. Wang and colleagues were able to expand protein C receptor (Procr+) positive cells, a population of progenitor cells in mouse islets. When co-cultured with endothelial cells, these cells maintained endocrine markers and could passaged as organoid structures for at least 6 months[122]. The second group expanded islet clusters from pregnant mice or WT rats in 3D culture with use of a culture medium based on previous organoid studies[121,123] and addition of CHIR99021(GSK3β inhibitor; Fig. 1.3), Exendin-4 (insulinotropic agent) and Forskolin (FSK). These clusters maintained islet identity and could be expanded *in vitro*, but only up to 9 days[124].

Culture of human primary ductal cells

The human pancreas ductal compartment remains a focus point for research due to its potential to retain a progenitor pool and potential contribution to β-cell neogenesis *in vivo*. Early studies aimed to expand ductal tissue *in vitro* as a means to uncover ductal progenitors capable of endocrine differentiation. Boner-weir *et al.* utilised islet-depleted exocrine tissue which was cultured in non-treated flasks. Upon near confluency after 1 to 2 weeks in culture, the cells were overlaid with Matrigel, after which they reported formation of cysts. The study showed that the cultured cells could differentiate towards an endocrine lineage but it remained unclear whether those endocrine cells were islet cell contaminants from the initial cell preparation[125]. A later study was able to derive ductal cells from deceased donor pancreases after ficol gradient separation which were cultured on human fibronectin-coated dishes. Importantly this study demonstrated the need for EGF signalling for the culture of ductal cells which worked to activate the MEK/ERK pathway[126]. Furthermore, the same group from the Bonner-weir *et al*. 2000 study demonstrated the ability to culture purified ductal cells, based on cancer antigen 19-9

(CA19-9) expression, while these cells showed very low (<1%) endocrine differentiation after transplantation in immunodeficient mice. Of note, graft survival of purified ductal cells after 4 weeks of engraftment was 40%[127]. Recently, a group reported improved endocrine differentiation of human non-endocrine epithelial tissue after expansion in culture with BMP-7and subsequent withdrawal. They reported an insulin response when stimulated with glucose, although the cells failed to improve hyperglycaemia after transplantation in mice. Lineage tracing experiments demonstrated that non-endocrine PDX1+ cells are the cell source for the BMP-7-induced insulin expressing cells[128]. Further work from the same group showed that PDX1+/ALK3+ cells, found in the ductal compartment can be expanded *in vitro* in a BMP-7 based culture medium and can differentiate into C-peptide+ cells upon withdrawal of BMP-7. Furthermore, BMP-7 induced a progenitor profile which was lost when BMP-7 was removed[129]. Nevertheless, while the differentiation ability of ductal cells remains contested, these studies were not able to expand ductal cells beyond a few weeks in culture.

Human pancreas derived organoids

Differences between mice and humans are well documented and while significant evidence exists for the presence of a ductal progenitor pool (namely Lgr5+ cells) in the adult mouse pancreas, such a progenitor pool has remained elusive in humans. This is partly hampered by the inability to perform *in vivo* reporter or lineage tracing experiments in human tissue. Nevertheless, several studies have modified the mouse pancreas organoid culture system by Huch *et al.*[121] to generate adult human primary ductal pancreas tissue derived organoids[123,130–132]. Lee *et al*. was able to generate organoids from CD133+ ductal cells and expand them *in vitro* demonstrating that these cells maintain ductal markers[130]. More recently two studies [123,131] demonstrated the ability to generate human pancreas organoids (hPOs) from ductal fragments of pancreases procured from deceased organ donors. Both studies utilised similar media components which closely mirrored the media used by Huch *et al*. 2013b[121]. However, it was shown that TGFβ inhibition, via ALK5 inhibitor A83-01, was important for propagation of human pancreatic organoids. More recently, a study by Loomans *et al*. demonstrated the propagation of hPOs from islet depleted exocrine tissue highlighting that cells with high expression of aldehyde dehydrogenase ($ALDH^{hi}$) were the organoid initiating cells[132]. These $ALDH^{hi}$ cells clustered with foetal pancreatic organoids on PCA analysis following RNA sequencing, hence demonstrating progenitor features[132]. It is important to note that all studies failed to show robust long-term *in vitro* expansion of hPOs while the culture medium utilised was not chemically defined, an essential component for GMP translation (Further detailed in section 1.6.1).

Furthermore, in order to address whether hPOs retain the capacity for endocrine differentiation Lee *et al*., demonstrated that adenoviral transduction of these cells with *NGN3, PDX1, MAFA* resulted in insulin production *in vitro*[130]. However, as mentioned in section 1.4, induced expression of the *NGN3, PDX1, MAFA* factors is enough to induce endocrine differentiation not only in closely related exocrine

cells[103,104], but also in more distant cell types such as intestinal[133]and stomach cells[134]. Furthermore, Loomans *et al.* reported differentiation of hPOs towards insulin producing cells following a 7-day differentiation protocol and subsequent transplantation of the organoids in the kidney capsule of immunodeficient mice[132]. However, as the differentiation process took place in the first 7 days following organoid isolation from the primary islet-depleted exocrine tissue, it is difficult to conclude whether the endocrine cells originated from differentiated hPOs or contaminating islet cells. Thus, further studies are needed to provide robust evidence for the existence of bi-potent progenitors in the adult human pancreatic ductal compartment.

1.5.3 Organoid models of pancreatic cancer

Traditional cancer models have utilised 2D cell lines or patient derived xenografts. Whilst these have been incredibly useful in understanding cancer biology and generation of cancer therapies, they present certain limitations. 2D cell lines are associated with failure to recapitulate the histoarchitecture of the parental tissue and maintain the intratumor heterogeneity. Furthermore, establishment of cell lines frequently results in clonal selection with significant genetic differences reported across individual cancer cell lines[135]. Contrastingly, patient derived xenograft (PDX) models are able to maintain the heterogeneity of tumours while also allowing stromal interaction[136]. However, establishment of PDX models requires a large amount of starting patient material, the use and maintenance of multiple mice to generate and expand the tumour cells, and often requires many months to generate enough material for assays or drug testing. 3D patient derived tumour organoids (PDTOs) have the potential to remove the shortcomings of faithful recapitulation observed in 2D cell lines while significantly reducing the costs and expansion timescales associated with PDX models. Therefore, this section will review the use of PDTOs to model pancreatic cancer.

Boj *et al.* described the first organoid culture from human pancreatic ductal adenocarcinoma (PDAC) utilising an adapted culture system from Huch *et al.* 2013b. The PDAC derived organoids could be propagated in culture indefinitely and were less dependent on culture factors than their healthy counterparts. However, removal of Rspo1 and Wnt was detrimental for their growth. Wnt signalling is known to be important in cancer and many Wnt target genes are mutated in cancer,[115,131] which may explain the need for Wnt factor for PDAC organoid cultures. Importantly, the PDAC organoids could recapitulate histological features of the original tumour *in vitro* while targeted sequencing showed that the organoids carried mutations in genes implicated in pancreatic cancer (e.g. KRAS). Following orthotopic mouse transplants of the PDAC organoids, it was shown that the organoids generated early and late PanIN lesions with expression of cancer markers such as Mucin 5AC (MUC5AC) while also retained the metastatic potential of the primary tumour[131]. More recent studies have demonstrated the translational applications of tumour derived organoids. Tiriac *et al.* demonstrated that biobanks of pancreas PDTOs can be generated that recapitulate all stages of pancreatic cancer. Furthermore, these

PDTOs could be used to generate a transcriptomic signature based on drug-sensitivity assays and these signatures correlated with responses seen in a separate cohort of patients[137]. In addition, other groups have shown that pancreas PDTOs can be subjected to high-throughput drug screening, demonstrating that the sensitivity or resistance to drugs *in vitro* correlated with patient outcomes in the clinic[138]. Indeed, studies have shown strong correlation between *in vitro* drug screening assays and patient clinical outcomes among different types of tumour derived organoids models[139–141]. Nevertheless, while PDTO models can recapitulate features of the tumour, the microenvironment including stromal and immune components has a significant impact on the progression of a tumour and PDTO models are limited in their ability to be expanded in a multi-cell type co-culture manner. While progress is being made in generating PDTO co-culture systems to include cell types such as T-cells or fibroblasts[142] it will be interesting to see the evolution of PDTO models as the complexity of the culture systems increases.

1.6 Translation of cellular therapies to the clinic

1.6.1 GMP criteria

Any medicinal product which is used in the clinic must meet the specific production guidelines in order to ensure the quality and safety of the product. These guidelines are set out by various regulatory bodies such as the European Medicines Agency (EMA) or the U.S.-based Food and Drug Administration (FDA). These guidelines are generally referred to as Good Manufacturing Practice (GMP) and establish a quality control system which ensures that each product generated meets a certain standard. While all medicinal products (i.e. vaccines, medications) must meet these guidelines, specific regulation has been published for cell therapy products which are typically referred to as Advanced Therapy Medicinal Products (ATMPs)[143,144]. ATMP's GMP criteria aim to control the collection, processing, storage and release of cell therapy products and also address the following elements a) facilities (design, access and maintenance); b) equipment (purchase, use and maintenance); c) materials (specifications, purchase, storage and use); d) quality assurance (quality control, validation, qualification and document control)[144]. The regulation also aims to tackle the following points with regards to cell therapy products: 1) demonstration of preclinical safety and efficacy; 2) no risk for donors of transmission of infectious or genetic diseases; 3) no risk for recipients of contamination or other adverse effects of cells or sample processing; 4) specific and detailed determination of the type of cells forming the product and what are their exact purity and potency; 5) "*in vivo*" safety and efficacy of the product[144]. Specific safety issues for stem cell-based products typically involve the potential malignant transformation after *in vitro* culture, propensity of cells to migrate from the transplantation site, initiation of an immune rejection event and the biological impact of impurities in the final product[145].

With this in mind, it can be argued that three areas of stem-cell based therapy production have hindered their introduction to the clinic: 1) risk of tumour formation resulting from contamination of

undifferentiated cells or malignant transformation, 2) production of the cells in a chemically-defined culture system and 3) risk of immunogenicity of the transplanted cells.

1.6.2 Risk of tumorigenicity of ESC/iPSC technology

The potential benefits of ESC and iPSC technologies as regenerative cellular therapies in the clinic are well understood. It is generally accepted that treatment of disease in the future will at least in part depend on cutting edge stem cell therapy rather than organ transplantation or therapeutic drugs. However, significant concerns remain regarding use of ESCs and iPSCs as a cell therapy product in the clinic. While ESCs have the added complexity of the ethical and regulatory barriers surrounding their use, since they require the destruction of an embryo for their derivation, both ESC and iPSC technologies are burdened by the risk of tumour formation. These tumours can arise for various reasons including remaining residual undifferentiated cells in the final product, accumulation of genomic aberrations, mutations in oncogenes or tumour-suppressor genes or genomic instability following long-term culture[146]. While regulatory frameworks exist to consider quality, safety and efficacy of products destined for clinical trials, there is no guidance for the specific assays that need to be conducted to determine safety of a product[147]. Therefore, rigorous, robust and universal safety assessment strategies are needed for translation of cell therapies into the clinic.

ESCs

Human ESCs (hESCs) express pluripotent stem cell markers octamer-binding transcription factor 3/4 (OCT3/4), stage specific embryonic antigens 3 and 4 (SSEA-3 and SSEA-4), TRA-1-60, TRA-1-81 and alkaline phosphatase, possess high levels of telomerase activity and show normal karyotype[148]. However, while this pluripotency underlies their benefit, it also means that hESCs share many similarities with cancer lines including a rapid proliferation rate, propensity for genomic instability and high expression of oncogenes (e.g. MYC, KLF4)[91]. When undifferentiated hESCs are transplanted in mice they will form a benign tumour (teratoma) with all three germ layers present[90,148,149] while some studies have also demonstrated that hESCs can undergo *in vitro* transformation and form more aggressive teratocarcinomas[150]. To avoid this, differentiation of hESCs *in vitro* is necessary. However, despite following stringent protocols to remove undifferentiated hESCs, Roy *et al.* reported persistent proliferation of undifferentiated cells 10 weeks after transplantation of hESC derived dopamine neurons[151]. Nevertheless, in more recent studies including a phase 1/2 clinical trial, hESC-derived retinal pigment epithelial cells (hESC-RPE) were used to treat macular degeneration in patients with no reports of tumorigenicity after a 1-year follow-up[152,153].

iPSCs

Human iPSCs (hiPSCs) are pluripotent cells derived from fully differentiated adult somatic cells. In 2006, Takahashi and Yamanaka converted mouse fibroblasts into iPSCs through retroviral expression of four key factors: *OCT3/4, SOX2, c-Myc* and *KLF4*[154]. This was repeated in human fibroblasts using the same four factors by the same group[87] while another group[155] generated iPSCs using the factors Oct3/4, Sox2, Nanog, and LIN28 using a lentiviral system. Indeed, Oct4 and Nanog have been shown to be key markers for pluripotency. However, the core reprogramming process represents a risk for tumorigenicity as factors such as c-Myc are well known oncogenes while others are overexpressed in various cancers[91]. Additionally, the use of integrating vectors poses an obvious risk for genomic alterations, by inserted mutagenesis, thereby preventing their clinical use[91]. To remove this risk, studies have looked towards protocols for iPSC generation with non-integrating adenoviruses thus removing the need for insertional mutagenesis[156]. However, it was shown that the reprogramming process, regardless of the use of integrating or non-integrating vectors, generates mutations in protein-coding regions as well as copy number variations (CNVs) which were not in the parental fibroblast cells[157,158]. Furthermore it was shown that hiPSCs acquire chromosomal aberrations as a result of the long-term culture process, otherwise referred to as culture adaptation and high levels of aneuploidy in early passages suggesting a selective pressure effect of the reprogramming process[92,159]. However, studies have questioned the true source of these genetic variations particularly single nucleotide polymorphisms (SNPs) and CNVs and whether they have arisen due to the iPSC culture process or whether they existed in rare populations of the parental pool of cells. Kwon *et al.* generated clonal fibroblast lines and clonal hiPSC lines from two different donor fibroblast pool of cells. This allowed identification of new variants in the daughter lines that were not found in the parental pool of cells. Once these new variants were identified, the researchers performed deep targeted sequencing on the on the parental pool of cells and demonstrated that 90% of the new variants found in the daughter lines existed in small frequencies in the parental population. They also demonstrated that hiPSC and fibroblast clonal lines have similar number of de novo variants. This study demonstrated that the hiPSC do not acquire increased numbers of de novo mutations. However, the researchers acknowledged that the hiPSC lines carried a higher mutational load than their fibroblast counterparts which needs further investigation[160].

In summary, uncertainties remain regarding whether ESC or iPSC technologies pose a real threat as a clinical therapy and clarification of this important safety concern is an essential prerequisite for the successful translation of cell therapies to the clinic.

1.6.3 Somatic mutations and mutational burden

The link between somatic mutations (i.e., mutations in developing somatic tissues) and cancer is well known, and it is well understood that a gain of function mutation in oncogenes or loss of function mutation in tumour suppression genes can lead to cancer. However, greater understanding of mutational processes has led to the theory that cancer does not always arise from a single mutation affecting one

gene and can be a result of the accumulation of mutations. Somatic cells acquire mutations throughout life due to errors in DNA replication, mutagen exposure, enzymatic modification of DNA or defective DNA repair. These mutations can be classified into three categories: "driver" mutations- those that confer a selective advantage, increasing survival or proliferation (i.e. positively selected), selectively neutral mutations, and negatively selected mutations that lead to cell death or senescence[161]. The amount of somatic mutations in cells is shown to increase with age, a concept referred to as mutational burden, while age has a strong correlation with incidence of cancer[162]. However, mutational burden alone does not explain the switch of a normal cell to a cancerous one. Normal cells are shown to acquire mutations at a rate similar to some cancers; a study showed that normal skin cells presented 2-6 somatic mutations/Mb/cell which was higher than the number of mutations found in breast and ovarian cancers[163]. Indeed, the number of driver mutations in a cell may be a critical determinant of the risk for oncogenesis. Interestingly, driver mutations largely affect protein coding regions while a cell can contain many neutral or mildly deleterious mutations (in coding or non-coding regions) which act as "passenger" mutations that have "hitchhiked" onto cells positively selected due to their driver mutation(s)[162]. Such driver mutations can lead to clonal expansions while this occurs only if the mutations transpire in stem cells or proliferating cells. Therefore, cancer can arise as a result of a clonal lineage acquiring a complement of driver mutations that allows the cells to evade normal restraints of cell proliferation[161]. Interestingly, studies on precancerous lesions such as Barrett's oesophagus show that the majority of driver genes are mutated prior to progression towards oesophageal carcinoma[164]. This suggests a stepwise model of progression from normal to cancer whereby successive clonal expansions lead to a more disordered phenotype. The occurrence of mutations, whether gradual or sudden, that take place due to various mutational processes leave patterns which are termed "mutational signatures". These signatures contain features such as classes of mutations (e.g. substitutions, indels etc.), sequence context, distribution across the genome, evidence of repair and timing during cancer evolution[162,165]. Analysing catalogues of 7,000+ cancers, Alexadrov *et al.* revealed 21 distinct mutational signatures based on the six classes of base substitution (C>A, C>G, C>T, T>A, T>C, T>G) and information on the bases immediately 5' and 3' to each mutated base. Notably, signatures were correlated to processes such as over activity of members of the APOBEC family of cytidine deaminases (signature 2), and UV induced mutations (signature 7). A later study by the same group was able to correlate signature 4 to a known chemical in cigarettes, benzo[a]pyrene[165,166]. This understanding of mutational processes will greatly increase the ability to pinpoint the aetiology of each cancer.

1.6.4 Regulatory guidelines for safety assessment

To understand the risk of tumorigenicity for cellular therapies, studies have relied on karyotyping or assessment of tumour formation after *in vivo* transplant. However, rigorous assessment of cell cultures is needed to understand the risk of tumour formation after transplantation into a patient. Doses in the

range of 10^8-10^9 cells have been reported to be administered to patients in trials assessing stem cell therapies[167]. Such numbers mean that even protocols that ensure 99.99% efficacy, result in 100,000 cells (0.01%) that could be either undifferentiated or carry driver mutations which could cause cell transformation. Therefore, conventional tumorigenicity assays whereby cells are transplanted in immunodeficient mice and monitored for tumour masses may not be sensitive enough to detect small numbers of contaminating transformed cells[147]. Notably, guidance from regulatory bodies such as the Food and Drug Administration (FDA) or European Medicines Agency (EMA) for cellular therapy products remains vague. While the risk of tumour formation from hiPSC or hESC cells is understood, the EMA suggests that prolonged cell culture might help to evaluate tumorigenicity and makes a distinction between hiPSCs/ESCs and somatic stem cells such as haematopoietic stem cells (HSCs)[147,168]. The FDA further states that animal studies designed to show tumorigenicity must do so for a sufficient length of time[147,169]. However, this leaves open questions such as what steps are to be taken in the case of positive results? Are there allowed limits of transformed cells in the final product? Should the safety assessment tests be different for each type of cell (iPSC/adult stem cells etc.)? Will safety tests need to be conducted for each batch released?

In summary, a combination of *in vivo* and *in vitro* technologies will be needed to assess safety of cellular therapy products. While *in vivo* assays do not recapitulate the human environment, they remain the closest thing to assessing cell therapies in a human setting. Equally, *in vitro* assays such as karyotyping, or next generation sequencing will be needed to assess mutational burden and genomic stability of the final product.

1.6.5 Safety of adult somatic cell derived technologies

While adult stem/progenitor cell derived culture systems pose a lower risk of tumorigenicity from contaminating undifferentiated cells than hiPSCs or hESCs, the risk of obtaining driver mutations throughout the culture process and or differentiation protocols resulting in cell transformation remains a possibility worthy of investigation. Huch *et al.* demonstrated that human liver organoids maintained normal ploidy after long-term in culture. Importantly, the culture protocol allowed derivation of clonal organoid lines and subsequent whole genome sequencing (WGS). This manner of sequencing allowed differentiation of somatic mutations acquired *in vivo* throughout the lifetime of the patient and those acquired *in vitro*. It was shown that 3 months of *in vitro* culture of liver organoids introduced 10-fold less substitutions than iPSC reprogramming while most of these substitutions were not in protein coding regions. Furthermore, CNV analysis showed only 2 heterozygous gains which were present in early passage clones and were not likely caused by the culture process[120]. Interestingly it was shown that adult stem cells from liver, colon and small intestine acquired approximately 40 novel mutations per year *in vivo* despite differences in proliferation rates among the organs. However, the mutation

signatures were tissue specific with the organs containing more rapidly cycling AdSCs, namely colon and intestine, demonstrating signatures attributed to deamination of methylated cytosine residues[170].

A more recent study from the same group utilised clonal and sub-clonal organoid lines from liver and small intestine AdSCs as well as an iPSC derived clonal line. WGS of the clones allowed deduction of mutations caused by the cell culture process. Although iPSCs had higher amounts of total single-base-pair substitutions, surprisingly, the AdSC lines showed nearly double the amount of substitutions per population doubling which amounted to 40-fold higher mutations per year when compared to their *in vivo* counterparts. Using mathematical modelling, the researchers aimed to model the risk of an oncogenic mutation occurring *in vitro* which showed that in small intestine AdSCs there is 1 oncogenic mutation per $1.3x10^7$ cells and in iPSCs 1 per $2.4x10^7$ while the risk was significantly lower for cancer relevant genes. Obtaining 1 oncogenic mutation *in vitro* in small intestine AdSCs was equivalent to 100 days in their *in vivo* counterpart[171]. This type of study demonstrates the tools that may be used to quantify the relative risk of tumorigenicity of a cellular therapy product.

1.6.6 Synthetic matrices for organoid *in vitro* culture

One of the main areas of concern with regards to translating 3D-based culture systems to the clinic is the use of Matrigel (or similar products such as BME 2). Matrigel is universally used as the extracellular matrix (ECM) for the generation and expansion of organoids or spheroids. It is an assortment of ECM proteins, mainly laminin, collagen IV, and enactin, that are derived from the Englebreth-Holm-Swarm tumours in mice, however the exact composition of Matrigel is not known[172]. This lack of a chemically defined composition and xenogeneic derivation makes it very difficult to meet GMP-level criteria and subsequently translate into the clinic. This is compounded by the batch to batch variability associated with Matrigel[172]. In order to facilitate translation of 3D culture-based models either for pre-clinical (drug testing) or clinical (transplantation) translation, various groups have worked towards generating chemically defined synthetic hydrogels which support the growth of organoids in a comparable manner to Matrigel. Greggio *et al.* generated polyethylene glycol (PEG)- based hydrogels linked with laminin-1 that could support generation of mouse progenitor pancreas derived organoids[109]. Furthermore, synthetic matrices have been used to uncover the required ECM properties to support expansion and maintenance of intestinal stem cells (ISCs), or their differentiation. Use of RGD (Arg-Gly-Asp; as substitute for full length fibronectin) -PEG-laminin hydrogels demonstrated that high-matrix stiffness supported the expansion of ISCs, while a softer matrix supporter their differentiation[173]. An RGD-PEG based hydrogel further allowed expansion and limited passage of PSC-derived human intestinal organoids while another study demonstrated that human derived fibrin with laminin allowed generation and expansion of multiple epithelial organoids including human liver and pancreas organoids[174]. Use of other binding peptides such as GFOGER (collagen-derived) and use of metalloprotease susceptible crosslinkers further showed the support for the generation and serial passaging of human intestinal and

endometrial organoids from the single cell level[175]. However, the synthetic hydrogels did not demonstrate the same efficiency in terms of expansion capacity compared to Matrigel. Furthermore, these studies utilising primary tissue derived organoids, generated organoids first in Matrigel and subsequently transferred them onto the synthetic matrix culture[173–175]. Therefore, a chemically defined, synthetic matrix that supports growth of organoids from the primary tissue level, in a comparable or improved manner to Matrigel has not yet been demonstrated.

1.6.7 Cost of treating Pancreatic diseases

It is difficult to place a value on cellular therapies and at which 'price-tag' they become a more financially viable option than the alternative standard-of-care treatment. This is particularly difficult for diseases where patients live a long time with the disease. Using diabetes as an example, given that it is one of the primary diseases affecting the pancreas, life expectancy of T1D patients under current therapeutic regimes is 10 years less than those without diabetes[28]. Furthermore, the costs for the production of insulin (or insulin analogues) ranges between £35 to £280 per patient per year. Even though governmental bodies such as the National Health Service, UK pay 5-7 times more than the cost of production, it can be argued that the cost of medications for diabetes is cheap[176]. This is particularly striking when comparing to advanced cell therapies that have been reported to cost anywhere between £20k to £170k per batch with each batch producing 1 to 88 doses[177]. However, while drug cost for the treatment of diabetes may be low, the total direct and indirect costs of diabetes in the UK, including non-diabetes drugs, inpatient and outpatient care to treat diabetes complications, social services, cost of absenteeism, early retirement and social benefits surmounted to more than £40b for the year of 2010[178]. Moreover, insulin treatment does not prevent complications of diabetes. A curative treatment that prevents these complications may be most cost-effective even if it costs more than insulin. Therefore, careful economic analyses are required in order to generate an inclusive cost-benefit analyses for future cell therapy products.

Logistical considerations for autologous vs allogeneic cell therapies

Despite careful economic analyses however, it is still true that the cost of production for cell therapies needs to be reduced. One significant cost driver for cell therapies is the choice between allogeneic (donor to patient) or autologous (patient to self) modalities of treatment. While autologous treatments have the advantage of a reduced risk of immune rejection (further discussed in section 1.7), they have certain limitations. Cost of allogeneic treatments can be reduced as the processes are scaled up, but autologous therapies do not benefit equally from economies of scale as one donor equals one patient[179]. Furthermore, as each autologous therapy is for a specific patient, labour costs cannot be divided across multiple patients such as in the case of allogeneic therapies and therefore naturally, cost of autologous therapies per dose is higher than that of allogeneic therapies[179]. Furthermore, there are logistical

challenges to autologous therapies. For allogeneic therapies, donors can be recruited to centralised processing centres whereby cell banks can be generated from which potentially all patients can be treated, and the cell therapy product can be delivered to the clinic at the time of need. However, particularly for cell therapies that require significant manual handling to reach a final product, performing patient recruitment, cell processing, quality control and therapy delivery for each patient specifically at the local level (i.e., treatment clinic) requires significant demands for establishment of multiple facilities as well as availability of highly trained staff in each centre.

With this in mind, a likely scenario for future cell therapies is the use of both allogeneic and autologous treatment modalities which will be based on the specific requirements of the disease treated as well as the cost-benefit analysis of that disease.

1.7 Immunogenicity of regenerative cellular therapies

1.7.1 Alloimmune rejection

The alloimmune response is defined as the recognition of donor antigens by the recipient immune system. In the context of transplantation and without immunosupressive drugs, an alloimmune response leads to rejection of the transplanted tissue. Allograft rejection can be divided into acute and chronic rejection which are largely divided by timing of the response. Both innate and adaptive immunological mechanisms underlie both types of rejections, however the adaptive mechanism plays a more central role. Notably, acute rejection is largely driven by the T cell response (cellular immunity) while chronic rejection is more antibody mediated (humoral response)[180–182]. Nevertheless, it is important to note that there is no clear distinction between the phases of alloimmune rejection as cells from the innate and adaptive systems as well as cellular and humoral responses interact across all phases to mount a response.

Innate immune response

Injury such as the one taking place in clinical transplantation results in the release of damage-associated molecular patterns (DAMPs) and pathogen-associated molecular patterns (PAMPs). These are recognised by pattern-recognition receptors (PRRs) expressed among hematopoietic cells and their activation leads to antigen-presenting cell (APC) maturation, up-regulation of costimulatory molecules, and secretion of proinflammatory cytokines[180,183]. This results in activation of naïve T cells into effector CD4+ T helper cells which further activate macrophages and granulocytes that have migrated to the graft due to the inflammatory stimuli. Furthermore, the inflammatory cascade from PRR activation leads to activation of NK cells and the complement system which work to kill foreign cells[180,184].

Adaptive immune response

Initiation of the adaptive immune response occurs by T cell activation which conventionally occurs via binding of the T cell receptor (TCR) on the peptide binding groove of major histocompatibility (MHC; also referred to as human leukocyte antigen [HLA] in humans) molecules which are found on antigen presenting cells (APCs) and/or target cell. CD8+ T cells recognise peptide-HLA Class I complexes which are presented on all nucleated cells via the endogenous pathway, while CD4+ T helper cells recognise peptide-HLA Class II complexes on APCs which present peptides via internalisation of exogenous antigens (Fig. 1.4)[182]. T cell allorecognition in the context of transplantation happens via three known pathways: the direct, indirect and semi-direct pathways which are implicated in acute and chronic rejection and involve pathways associated to direct T cell killing or antibody mediated killing.

The **direct pathway** (Fig. 1.4) involves recognition of intact donor HLA-peptide complexes by recipient T cells. These are presented by donor derived APCs which are primarily composed of tissue resident dendritic cells (DCs). Upon receiving inflammatory signals such as IL-1β, TNF-α or CD40, DCs can undergo maturation. In their immature state however, they are found abundantly in organs and can express both HLA Class I and class II[185]. CD4+ T helper cells recognise the foreign HLA Class II-peptide complex on donor APCs and propagate the effector function of CD8+ T cells which may also be bound to the same APC[186]. This activates the cytotoxic activity of CD8+ T cells which induce killing of the graft cells by granzyme B, or by the Fas/FasL pathway which induces apoptosis[180,185]. Nevertheless, it has been shown that direct pathway CD4+ T cell allorecognition is more relevant to acute allograft rejection as it is short lived since donor APCs are eliminated quickly[185].

The **indirect pathway** (Fig. 1.4), which represents the typical process of (allo)antigen recognition, involves internal processing of donor peptides by professional recipient APCs and presentation via the HLA Class II pathway. APCs phagocytose allogeneic HLA peptides which are found in the 'debris' of necrotic donor cells. CD4+ T cells in turn recognise the self HLA-allopeptide complex presented by APCs in the secondary lymphoid organs (SLOs) and become activated. Indeed, these activated CD4+ T cells can contribute to CD8+ T cell activation and cytotoxic killing[187], but it is argued that this is less relevant than the direct pathway[185]. Primed indirect pathway CD4+ T helper (Th) cells migrate to the T-cell-B-cell zone of the B cell follicles in secondary lymphoid organs (SLOs; lymph nodes and spleen) whereby Th cells interact with B cells that are alloantigen specific. This generates short-lived plasma cells that secrete less-specific antibodies. A percentage of the CD4+ Th cells acquire a follicular helper (T-FH) phenotype and migrate to germinal centres (GCs) formed by activated B cells in SLOs. B cell interaction with alloantigen as well as cytokines from T-FH cells (IL-21, IL-6) drives B cell maturation which further undergo antibody class switching and affinity maturation which is directed by somatic hypermutation and produce highly specific IgG alloantibodies. A subset of these B cells will travel to the bone marrow as long-lived plasma cells and will likely last throughout the lifetime of the individual[185,188]. While antibody mediated rejection has been implicated in acute rejection, production of highly specific antibodies likely governs chronic allograft rejection[185]. Generation of these *de novo* antibodies results in complement pathway activation and recruitment of

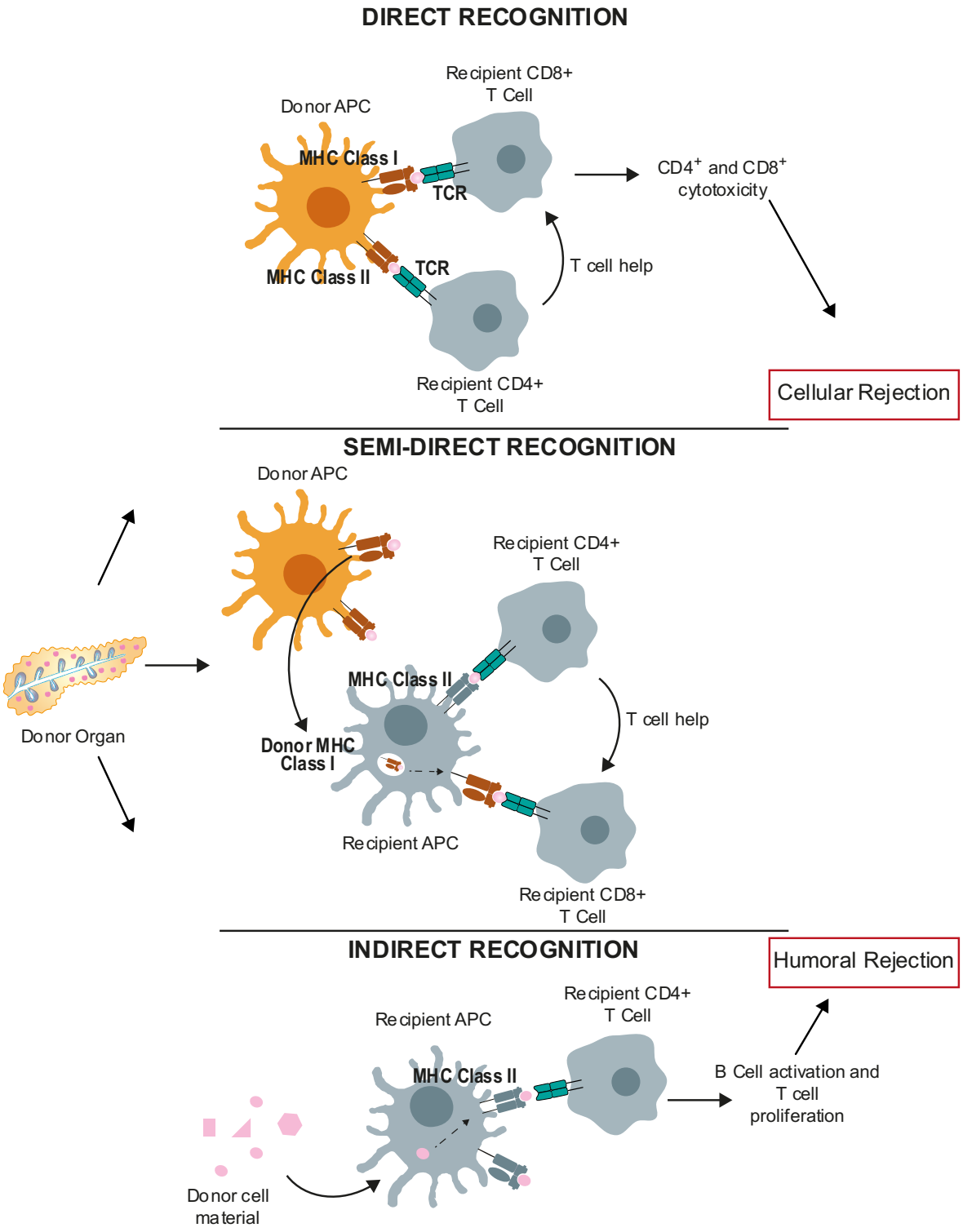

Figure 1.4 Pathways of T cell allorecognition. Direct pathway allorecognition (top) involves intact donor MHC class I or II molecules presented on donor APCs and recognised by the T cell receptor (TCR) on recipient T cells. In the indirect pathway (bottom), recipient APCs present allopeptides that have been loaded onto MHC Class II molecules and are presented to and activate recipient $CD4^+$ T cells. The semi-direct pathway (centre) involves recipient APCs acquiring in-tact donor MHC molecules and presenting them intact on their surface to recipient T cells. (Adapted from Sanchez-Fueyo *et al.*, 2011[189] and Afzali *et al.* 2008[190])

neutrophils and macrophages to the graft whose Fc receptors recognise the heavy chain of antibodies[189,191].

The **semi-direct pathway** (Fig. 1.4) occurs through the acquisition of intact HLA molecules from donor cells by recipient APCs. Recipient APCs can then present both allo-HLA as well as self-HLA-allopeptide complexes which can activate recipient immune cells via both direct and indirect pathways[190,192]. While the involvement of direct and indirect pathways is generally linked to acute and chronic responses respectively, the relative contribution of the semi-direct pathway in either response is unknown[190].

Co-stimulation

To develop effector function and mount a response against a foreign graft, T cells require two activation signals: Signal 1 delivered through TCR binding and signal 2 delivered through binding of co-stimulatory molecules. A lack of co-stimulation can lead to T cell anergy or suppression[182]. T cells express CD28 costimulatory molecule which binds to CD80 and CD86 on APCs. In addition, CD40L is a costimulatory molecule expressed on activated T cells and binds CD40 on APCs. Binding of co-stimulatory molecules leads to CD8+ T cell activation and proliferation into CD8+ cytotoxic T lymphocyte (CTLs) cells, a process which is dependent by cytokine production (IL-2, IFN- γ) from CD4+ cells (also known as signal 3)[182] .

1.7.2 Preventing allograft rejection

Graft tolerance and immunosuppression

Tolerance in the immune system is governed by central and peripheral tolerance. In central tolerance self-reactive T and B cells are removed by negative selection. In peripheral tolerance, self-reactive T cells undergo clonal deletion, anergy or suppression by regulatory T cells (Tregs)[193]. Ideally, clinical transplantation aims to achieve operational tolerance whereby the immune cells become unresponsive to alloantigens in the absence of immunosuppressive therapy and there are no signs of immune rejection[194]. As central tolerance occurs in the thymus during embryonic development, it is not applicable to transplant tolerance. Peripheral tolerance may be induced by depleting alloreactive effector T cells and by increasing numbers of alloreactive Treg cells[195]. Strategies to remove alloreactive T cells include co-stimulation blockade or T cell depletion therapy while Treg numbers can be increased by cellular therapy to introduce *in vitro* expanded Tregs with administration of cytokines such as IL-2 to promote Treg survival or tolerogenic cytokines such as IL-10 and TGFβ[195,196]. However, obtaining operational tolerance remains difficult in a transplant scenario.

HLA matching

It has been known that organs transplanted between HLA identical individuals, i.e., twins, are accepted whereas in HLA mismatched individuals and in the absence of immunosuppression, the organ is rejected. In order to avoid or reduce immune rejection, HLA matching between donor and recipient is required and is an important consideration in the organ allocation process. The HLA system is a group of proteins encoded by the MHC gene region in chromosome 6. These are structurally and functionally divided into two major classes: HLA Class I and Class II. There are three classic loci related to Class I that encode HLA-A,-B,-C molecules and 3 loci related to Class II encoding HLA-DR,-DP,-DQ molecules[197]. HLA genes are highly polymorphic, and to date, more than 20,000 alleles have been identified[198]. The degree of HLA matching is important but can have varying effects depending on the organ type. In kidney transplants, matching takes place at the HLA-A, -B and -DR loci with clear benefits shown between total mismatch and full matched transplants, while the HLA-DR loci has the strongest effect if mismatched[197]. In the case of pancreas or simultaneous pancreas and kidney (SPK) transplants, it is less clear whether HLA matching has a strong correlation with improved graft survival but might bear an advantage for reduced acute rejection[199]. Therefore, due to the low numbers of available donor organs the level of HLA matching varies greatly in each case.

Immunosuppression

Suppression of the immune system via administration of therapeutic agents remains one of the most effective ways in preventing allograft rejection and promoting long-term graft survival. The target level of immunosuppression must balance between the benefit of preventing rejection and the adverse side effects of the drug regime (including risk of toxicity, infection and cancer), hence it is specific to each patient and type of organ transplanted. Immunosuppression is divided into three phases: induction immunosuppression in the early phase, maintenance in the late phase, and treatment of organ rejection[200]. It can be either chemical agents or biological agents such as monoclonal antibodies aimed at blocking release of cytokines from activated T cells, downregulating expression of T-cell surface receptors, inhibiting T cell proliferation and inducing T cell depletion[201]. Corticosteroids can be used in induction immunosuppression alongside monoclonal antibodies (e.g. Basiliximab) to inhibit or deplete recipient T cells[200]. Cyclosporine and the newer agent, tacrolimus are calcineurin inhibitors blocking Signal 2 dependent T cell activation typically used in the early and maintenance phase. Notably, their use in clinical practice led to vastly improved survival rates than previously used regiments[200,202]. For episodes of acute rejection, use of higher doses of corticosteroids is the first line treatment followed by various patient dependent strategies[200]. Despite the continuous improvement of therapies and strategies, immunosuppression is associated with toxic side effects such as nephrotoxicity or increased susceptibility to infections and cancer[203]. Therefore, improved strategies for reducing immunogenicity of transplanted organs and cells are key for the long-term health of patients.

1.7.3 Immunogenicity of stem cells

The assumption that allogeneic and not autologous derived stem cell-derived cellular therapies will have immunogenic potential has existed for many years. However, this idea has been challenged, as summarised below. Several groups have attempted to elucidate how a stem cell can pose an immunogenic threat. ESCs can express low levels of MHC antigens which may not be enough to activate T cells but could elicit a Natural Killer (NK) cell response[204]. In addition, MHC expression has been shown to be upregulated upon cytokine induction such as INFγ, a common product of the allograft immune response[205]. Furthermore, it was also shown that despite MHC matching in mice, acute rejection can be elicited due to the expression of differential peptides capable of generating an immune response; these are alternatively known as minor histocompatibility (miH) antigens[206]. This, along with other studies highlighted the capacity of embryonic derived cells to be immunogenic[204].

A seminal paper by Zhao *et al.* demonstrated that non-viral integration derived iPSCs from fibroblasts, when transplanted into syngeneic mice, elicited an immune response. Gene expression analysis of the rejected teratomas highlighted two proteins involved: zymogen granule protein 16 (Zg16), which can play a role in protein trafficking in the cell, and HORMA domain-containing protein 1 (Hormad1), which plays a role in cell division. Upon ectopic expression of these two proteins and subsequent transplantation of the iPSCs, teratomas failed to form due to rapid immune rejection and T cell infiltration[93]. The findings of this paper were criticised both in that undifferentiated iPSCs are unlikely to be used clinically, and that the two proteins failed to induce an immune response in a human setting[204,207]. It was later shown that human derived smooth muscle cells and retinal epithelial cells, derived from the same iPSC line, had differential immune rejection when transplanted into mice whose immune system was reconstituted from foetal cells of the same individual-referred to as humanised immune system (HIS) mice (further detailed in section 1.8)[208]. This further propagated the debate of whether autologous derived stem cells have immunogenic potential. More importantly, these studies highlight the importance for the strict characterisation of the immune profile of stem cells, especially those destined for clinical applications.

1.7.4 Immunogenicity of pancreatic cell subtypes

Whether non-professional APCs can express immunogenic markers such as HLA Class II has been an ongoing debate. Although some studies have sought to investigate HLA expression in islets, investigations in the rest of the pancreatic cell subtypes are limited. Despite this, earlier work has shown that isolated ductal and exocrine cells show low levels of HLA Class I expression and no HLA Class II expression under normal conditions. However, treatment of pancreatic tissue monolayer cultures with IFN-γ can lead to significant upregulation of both HLA classes[209]. Immunohistochemical analysis of normal human pancreas biopsies demonstrated that exocrine and ductal tissue were negative for HLA Class II expression[210]. As previously stated, CD40 is an important co stimulatory molecule found on

APCs which induces T cell activation. Additionally, blocking of CD40-CD40L interactions in non-obese diabetic (NOD) mice inhibits spontaneous development of diabetes. Reports have shown that CD40 is expressed on human pancreatic ductal cells[211] and in human pancreatic islet cells, while its expression on islets was upregulated by pro-inflammatory cytokines (IL-1β, IFN-γ and TNF-α)[212]. Furthermore, activation of CD40 in pancreatic islets resulted in chemokine production while in pancreatic ductal cells, it resulted in secretion of TNF-α and IL-1β[213]. A more recent study has challenged the assumption that pancreatic β-cells do not express MHC Class II. NOD mice were made to develop diabetes by diabetogenic CD4+ T cells that recognise β-cell antigens. Islets isolated from these mice showed MHC class II mRNA and protein expression. In addition, exposure of both mouse and human isolated islets to IFN-γ resulted in MHC class II expression; specifically, HLA-DR in human cells[214]. Despite this impressive result, the study failed to show whether this HLA Class II expression in human cells could lead to T cell activation and subsequent effector function. In addition, they did not address whether MHC Class II expression was due to *in vitro* manipulation of the human cells and what effect it may have *in vivo*, particularly whether HLA-DR will have any significance in a diabetic setting.

1.7.5 Autoimmune response in T1D

The precise trigger of autoimmunity in T1D remains to be elucidated and is part of ongoing research. Despite incomplete understanding of the mechanisms involved in this disease, in the past decades much has been discovered about the pathways involved in the destruction of β-cells. Histologically, T1D is characterised by loss of β-cells, overexpression of HLA Class I, β-cell necrosis, diminished insulin in remaining β-cells, expression of INFα in β-cells and insulitis[32]. Insulitis is characterised by presence of lymphocytes and increased expression of cytokines in the islets of the pancreas[215,216].

Susceptibility in T1D includes a strong genetic component and over 40 genetic loci have been associated with the disease[217]. The HLA gene region has the strongest attributable risk specifically the IDDM1 locus of chromosome 6[31]. The likely mechanism is that these gene polymorphisms result in insufficient presentation of self-antigen (or presentation of different self-antigen repertoire) from MHC Class II, or low expression of, for example insulin to naïve lymphocytes during development of central tolerance thus leading to inefficient deletion of autoreactive lymphocytes[218].

Another component which drives development of T1D is the presence of autoantibodies against autoantigens. Presence of autoantibodies against four known peptides, insulin, glutamic acid decarboxylase (GAD), islet antigen 2 (IA-2), and zinc transporter 8 (ZnT8) predictably results in a nearly 100 % progression to clinical T1D[218]. It is hypothesised that polymorphisms in the genes encoding these peptides lead to amino acid changes which reduce chances of binding MHC Class II or cannot properly activate T cell receptors during thymic education, thus resulting in the 'escape' of autoreactive T cells much like in the case of altered MHC Class II function[218].

T1D is a T cell-mediated autoimmune disease wherein autoantibodies to islet cell antigens can be detected before clinical symptoms arise[215]. Despite presence of autoantibodies, some individuals never develop diabetes, suggesting that external factor(s) such as enteroviruses, or dietary toxins are sometimes needed to trigger T cell autoimmune destruction of β-cells[219]. This is followed by T cell recruitment to islets by a process not yet well understood. Resident activated APCs release chemokines recruiting macrophages and non-resident APCs which in turn release inflammatory cytokines. This recruits CD4+ T helper cells which release IL-2 and IFN-γ inducing secretion of key cytokines such as IL-1β and TNF-α which recruit CD8+ cytotoxic T cells[31]. T cell destruction of β-cells can occur via several pathways. CD8+ T cells can cause cell death via the perforin/granzyme pathway, through insertion of tubular perforin complexes into the membrane causing cell death. In addition, ligation of Fas ligand on T cells with Fas receptor on β-cells leads to apoptosis through the caspase pathway[216,220]. Proinflammatory cytokines IL-1β, TNF-α and INF-γ result in enhanced Fas expression[216]. Furthermore, destruction of β-cells may occur through Nitric Oxide (NO) production as a result of IL-1β secretion and APC activation, though direct evidence has only been shown in rat β-cells[220,221]. Cytokines are also important for β-cell death in a T cell independent manner. IL-1β, IFN-γ, and TNF-α bind to their respective receptors and can cause β-cell apoptosis through the caspase pathway. IL-1β alone affects β-cell function by inducing early release of insulin and inhibition of glucose-stimulated insulin secretion as shown in rodent β-cells[31]. Furthermore, IFN-γ and TNF-α alone or in combination can induce *in vitro* expression of MHC Class I and II as well as I-CAM-1 in both murine and human β-cells[216,222]. IL-1β has also been shown to induce expression of I-CAM-1 on the cell surface which subsequently leads to improved binding and activation of effector T cells[216].

1.8 Mouse models

1.8.1 Development of immunodeficient mice

Studying complex human biological processes such as the immune system *in vivo* is hampered by ethical and technical constraints. Immunodeficient mice are used for *in vivo* studies of immunology, infectious disease, cancer and stem cell biology without rejection of the transplanted cells. These mice present an important platform for recreating the human immune system *in vivo* and are referred to as human immune system (HIS) mice. An important discovery for HIS mice was the random mutation of the *Prkdc*^{scid} *(scid)* gene in CB17 mice which resulted in severe combined immunodeficiency (SCID) including lack of functional B and T cell generation but presented an environment that could support their development[223]. However, these mice presented leakiness (spontaneous development of B and T cells) and had high levels of Natural Killer (NK) cells[224]. A breakthrough in immunocompromised mice came from crossing the scid mutation into non-obese diabetic (NOD) which had lower NK cell activity, reduced macrophage activity and further abrogation of functional B and T cells[225]. Furthermore, it was discovered that a mutation in the IL-2rγ chain (*IL2Rγ*^{null}) resulted in deficiency of the γ-chain of the IL-

2 receptor which led to blocking of NK cell development and defects in innate immunity. NOD-scid IL2Rγnull (NSG) mice therefore presented a great SCID model, which overcame previous mouse strain limitations such as short life span and development of thymic lymphomas[226].

1.8.2 Human immune system (HIS) mice

Derivation of immunodeficient strains such as the NSG mice allowed for an environment, whereby human hematopoietic stem cells (HSC) could be engrafted and expanded into their lineages, thus replacing the mouse immune system. Two main models are used in order to engraft adult human hematopoietic cells: The Human SCID-repopulating cell SCID (Hu-SRC-SCID; also referred to as Hu-SRC in this project), and the Human PBL-engrafted SCID (HU-PBL-SCID; also referred to as Hu-PBL in this project)[224]. The HU-SRC-SCID model is optimally suited for studies of haematopoiesis and is created by engraftment of HSCs into immunodeficient mice. Efficiency of engraftment in this model vastly improved after the introduction of *IL2Rγ^{null}* strains. *IL2Rγ^{null}* mice require sublethal gamma radiation before engraftment of HSCs. This allows for eradication of any remaining mouse lymphocytes to allow for an appropriate niche for HSC differentiation[227]. The level of HSC engraftment and differentiation depends on factors such as strain background, age of recipient, and engraftment route and source of HSCs (cord blood, bone marrow, of foetal liver)[228]. Routes such as intravenous, intraperitoneal, and intrahepatic have been used[227]. Importantly, HU-SRC-SCID models of *IL2Rγ^{null}* mice have shown production of multiple lineages of HSCs including B and T cells, APCs, and NK cells[225] as well as myeloid cells including platelets and red blood cells[227,229]. The main caveats of the model include the time to establish the model (usually 16 weeks or more) or impaired function of the lymphocytes. B cells do not receive adequate CD4 T cell help, impairing their function, while T cell response to antigens can also be impaired. The absence of human primary lymphoid organs results in limited differentiation of human lymphocytes in the mouse while the lack of human leukocyte antigen (HLA) on thymic epithelium results in a lack of T cell education[228].

The HU-PBL-SCID model is suited for studies of mature immune responses and allograft rejection and is created by injection of human peripheral lymphoid cells derived from blood, spleen, or lymph node[230]. Human lymphocytes can be found circulating in the mouse blood after a few days and can be maintained for 4-6 weeks. This limited time scale is due to the development of graft-versus-host-disease (GvHD) defined by human lymphocyte activation against mouse antigen (i.e., MHC molecules) and subsequent attack of the host[226,230]. Engraftment of cells consists of mostly T cells while B and myeloid cells do not engraft well, likely due to the lack of human cytokines needed for their survival[228]. Furthermore, GvHD development confounds studies of allograft rejection. Therefore, use of this model requires first the transplant of the cells of interest followed by reconstitution with lymphoid cells while it is only suitable for short-term studies[231]. However, new mouse strains which are knock-outs for MHC

Class I and II (referred to in this project as NSG-dKO mice) have been generated to slow down the progression of GvHD and increase the time frame of the HU-PBL HIS mouse model[232].

1.9 Project aims

The overarching objective of this project was to establish a model of human pancreas organoids (hPOs) for the advancement in understanding of pancreas cell biology and towards clinical translation of a cellular therapy for T1D. Achieving this required a cell-culture model that allowed expansion of hPOs long-term and from a single-cell, without need of cell transformation. I aimed to utilise this model in order to assess the risk of hPOs to form tumours when transplanted *in vivo* following *in vitro* expansion, as well as to explore the immunogenicity of the cells through *in vitro* assays and HIS mouse models.

The specific aims of this project were to:

- Establish and characterise a 3D organoid model allowing long-term expansion of hPOs in a chemically defined, serum-free culture system and explore use of the model in disease modelling.
- Assess the genomic stability and mutational burden of hPOs during *in vitro* culture and investigate the risk of tumorigenicity after long-term engraftment in mice.
- Understand the level of antigenic expression of hPOs *in vitro* and their ability to induce an immune response in an autologous and allogeneic *in vivo* setting.

Statement of source

This thesis is largely comprised of work based on my first author publication[233] listed below. As such certain sections and figures related to chapters 2-5 have been taken verbatim or slightly modified from the source.

Georgakopoulos, N., Prior N., Angres B., Mastrogiovanni G., Cagan A., Harrison D., Hindley C.J., Arnes-Benito R., Liau SS., Curd A., Ivory N., Simons B.D., Martincorena I., Wurst H., Saeb-Parsy K., Huch M. Long-term expansion, genomic stability and in vivo safety of adult human pancreas organoids. BMC Dev. Biol. 20, 4 (2020)

CHAPTER 2. MATERIALS AND METHODS

2.1 Human tissue collection

2.1.1 Obtaining pancreatic healthy tissue, tumour tissue and isolated islets

Primary pancreas tissue was obtained by the Cambridge Biorepository of Translational Medicine (CBTM) from deceased organ donors from whom multiple organs were being retrieved for transplantation. Pancreas samples were taken via two routes: from donors during the organ retrieval operation (in which organs other than the pancreas were taken for transplant) or from pancreases which were initially removed for organ transplantation but were subsequently declined and allocated for research. Tissue from both donation after circulatory death (DCD) and donation after brainstem death (DBD) donors were used (Appx. Table 1). Tissue samples were placed in cold 4 °C University of Wisconsin (UW) organ preservation solution prior to transportation to the laboratory.

Donor tissue was taken after obtaining written informed consent from the donor's family for studies approved by the NRES Committee East of England, Cambridge South for the Department of Surgery, University of Cambridge, REC reference; 15/EE/0152 and the NRES Committee East of England - Cambridgeshire and Hertfordshire Research Ethics Committee for the Department of Surgery, University of Cambridge, REC reference; 16/EE/0227. Pancreas cancer tissue was obtained from patients undergoing pancreatic resection surgery who had given full written informed consent for studies approved by the NRES Cambridgeshire 2 Research Ethics Committee for Human Research Tissue Bank, Addenbrooke's Hospital, REC reference; 11/EE/0011 and NRES Committee London - Westminster Research Ethics Committee for the Department of Surgery, University of Cambridge, REC reference; 15/LO/0753. Samples from clinical (non-transplant) cancer resections were taken by clinical histopathologists after gross examination of the resected tissue. Pancreatic islets were obtained from the Scottish National Blood Transfusion Service (SNBTS) Islet Isolation Center (NRES West Midlands- South Birmingham Research Ethics Committee, REC reference; 16/WM/0093). All human tissue used was handled according to Human Tissue Authority (HTA) guidelines.

2.1.2 Isolation of primary pancreatic duct(s)

Isolated primary pancreatic ducts for qRT-PCR analysis were collected via two methods: either by manual handpicking of ductal fragments following pancreas tissue digestion (as detailed in 2.2.1) or via surgical dissection of the main pancreatic duct from the pancreases allocated for research. In order to achieve this, the common bile duct was separated from surrounding tissue and followed towards the ampulla of Vater where it connects to the primary pancreatic duct (Fig 1.1;3.11). The primary pancreatic duct was then separated from surrounding tissue and a segment was isolated. The duct was then placed in RNAlater (ThermoFisher Scientific) and incubated for a minimum of 24 h at 4°C. The tissue was

then dried, placed in an eppendort tube, snap frozen on dry ice and stored at -80°C for subsequent RNA analysis.

2.1.3 Isolation of mononuclear cells from primary spleen tissue

Fresh primary spleen segments (5 cm^3) were retrieved form deceased organ donors in the operating theatre after the organ retrieval process, as described in 1.1.1. The spleen segments were placed in UW solution on ice and transported to the laboratory and stored in 4 °C up to 24 h before being processed. Using a sterile scalpel in a Category II Biological safety cabinet, the tissue was cut into small pieces approximately 5 mm^3 in size and placed in a gentleMACS™ 'C' tube with 10 ml of PBS supplemented with 2% Fetal Bovine Serum (FBS) (Life Technologies), referred to from now on as PBS-2%FBS. The tube was then placed onto a gentleMACS™ Dissociator (Miltenyi Biotec) which was used to dissociate the tissue to a single cell suspension. The tissue was subjugated to 3 cycles of the pre-set 'B-0' programme and the resulting cell suspension was filtered through a 70 µm nylon filter to remove any intact tissue. 50 ml Falcon tubes were prepared by placing 15 ml of room temperature Lymphoprep™ (STEMCELL Technologies) and topping up with 20 ml of the splenocyte mononuclear cell (SpMC) suspension. The tubes were centrifuged at 800g for 25 min at 20°C without brake. Following this, the buffy layer in between the Lymphoprep™ and the cell suspension was collected in order to collect the SpMCs. The collected SpMCs were washed twice with PBS- 2% FBS, after which they were resuspended in 10ml of Red Blood Cell Lysis 1X buffer for 10 min at 4°C to remove contaminating red blood cells. The cell suspension was further washed twice with PBS and SpMCs were placed in cryopreservation solution made up of FBS supplemented with 10% DMSO (Sigma Aldrich). The cells were cryopreserved in cryovials at a concentration of $5x10^7$/ml, placed in pre-cooled Nalgene Mr. Frosty™ freezing container and stored at -80°C for 24 hours prior to transferring into liquid nitrogen (LN_2) for long-term storage.

2.1.4 Isolation of mononuclear cells from primary bone marrow

Bone marrow samples were retrieved from deceased organ donors in the operating theatre after the organ retrieval process as described in 1.1.1. Bone marrow was extracted from the spine using T-handle Jamshidi™ bone marrow aspiration trephine needle (BD) which was inserted into the lumbar or thoracic vertebrae while a heparinised Leur lock 50ml syringe was used to remove the bone marrow. The bone marrow was transported to the laboratory and stored on an orbital shaker at room temperature up to 12 h prior to processing. For processing, the bone marrow was filtered through a 70µm nylon filter and diluted 7:1 into PBS- 2% FBS (7 parts bone marrow to 1 part PBS- 2%FBS). Mononuclear cells were isolated and cryopreserved following the same procedure as described in 1.1.3 after the filtration stage.

2.2 Cell culture of hPOs

2.2.1 Generation and culture of hPO

To generate organoid cultures, approximately 5 mg of pancreas sample was manually minced and further dissociated with the gentleMACS dissociator (Miltenyi Biotec) for a total of 2 min. Minced tissue was washed twice in wash medium [Dulbecco's Modified Eagle Medium (DMEM), high glucose, GlutaMAX, pyruvate supplemented (Life Technologies) with 1% FBS and 1% Penicillin/Streptomycin (10,000 U/mL) (Life Technologies)] and digested in 40 ml of digestion solution [Collagenase Type I (Sigma-Aldrich) and Dispase II (Life Technologies) at a concentration of 0.125 mg/ml in DMEM containing 0.1 mg/ml DNase I (Sigma-Aldrich)] and placed at 37 °C for 1 to 2 h. Isolated ducts were either hand-picked with a pipette or the whole digestion mixture was filtered with a 100 μm pore nylon cell strainer (Falcon). Ductal fragments were washed in Basal medium [Advanced DMEM/F12 (Life Technologies) supplemented with 1% Penicillin/Streptomycin, 1% Glutamax 100x (Life Technologies), and Hepes (Life Technologies) 10 mM] and spun at 200g for 5 min. The cell pellet was mixed with reduced growth factor BME 2 (Basement Membrane Extract Type 2; Cultrex), seeded in a 24 well plate and overlayed with the optimised hPO expansion medium (hPO-Opt.EM), unless specified otherwise. BME 2 was used as ECM for all experiments except for those specified in Fig. 5 and Fig. S5 in which hPOs generated in BME 2 were compared with those cultured in the chemically defined hydrogel. hPO-Opt.EM composition: [Basal medium (described above) supplemented with 1X N2 and 1X B27 (both from GIBCO), 1.25 mM N-Acetylcysteine (Sigma-Aldrich), 10% Rspo1 conditioned serum-free media (homemade as previously described[123]), 10 nM [Leu[15]]-Gastrin I human (Sigma-Aldrich), 50 ng/ml EGF (Peprotech), 25 ng/ml Noggin (Peprotech), 100 ng/ml FGF10 (Peprotech), 10 mM Nicotinamide (Sigma-Aldrich), 5 μM A83.01 (Tocris), 10 μM FSK (Tocris) and 3μM PGE2 (Tocris)]. hPO-Opt.EM was supplemented with 10 μM Rho Kinase inhibitor (Y27632, Sigma-Aldrich) during the first 7 days.

2.2.2 Cryopreservation of pancreas tissue

Samples were manually minced and further dissociated using the gentleMACs dissociator (Miltenyi Biotec) for a total of 2 min. Samples were resuspended in 1 ml Recovery Freezing medium [(Dulbecco's Modified Eagle Medium (High Glucose), 10% FBS, and DMSO (10%);Gibco)] and cryopreserved in a Cell freezing container at -80 °C. To initiate hPO generation after cryopreservation, the sample was thawed at 37 °C and washed twice in Wash medium. The procedure was then conducted as described above, beginning with the addition of Digestion solution.

2.2.3 Passaging and dispersion of hPOs to single cells

Confluent hPO wells were collected and washed with cold Basal medium. Cells were centrifuged at 200g for 5 min and the supernatant was removed leaving 2 ml of medium. The organoids were then mechanically dissociated using a narrowed glass Pasteur and further washed with cold basal medium and centrifuged at 200g for 5 min. the pelleted organoids were then resuspended in the correct volume of BME 2, seeded, and overlaid with the appropriated culture medium. For generation of single cells, cells were collected and washed with cold Basal medium. Cells were centrifuged at 200g for 5 min and resuspended in 1 ml of pre-warmed trypsin (TrypLE™ Express Enzyme (1X)-Thermo Fisher Scientific) or Accutase (StemPro™ Accutase™ Cell Dissociation Reagent-Thermo Fisher Scientific). Organoids were pipetted using a narrowed Pasteur 10 times and incubated for 5 min at 37 °C to make single cells. After incubation, the cells were pipetted 10 times and checked for single cells. The process was repeated until most of the organoid fragments were made into single cells. Digestion was stopped by adding cold Basal medium and the digest was filtered through a 40 µm pore nylon cell strainer (Falcon) to remove doublets.

2.2.4 Cryopreservation and thawing of established hPOs

Upon reaching confluency, organoids were dissociated from the well as described above. Organoid fragments were re-suspended in Recovery Freezing medium in 500µl per well and placed in cryovials. Cryovials were stored in -80°C using a Cell freezing container. For long-term storage, cryovials were transferred to LN_2. Cryovials were quickly thawed in a 37°C water bath until the last ice crystal could be observed. The cells were transferred to a 50ml centrifuge tube and 15 ml of pre-warmed media (90% Basal medium, 10% FBS) was added dropwise while shaking. Cells were then centrifuged at 300g for 5min at 8°C and supernatant was discarded. The cells were washed with Basal medium, centrifuged and re-suspended in BME 2. hPO-Opt. EM medium was used with addition of 10 μM Rho Kinase inhibitor (Y27632, Sigma-Aldrich) for the first 7 days of culture.

2.2.5 Generation of clonal and sub-clonal cultures

hPO cultures were initiated from ductal fragments as described above and cultured for 10-14 days. P0 hPOs were made into single cells as described above. Single cells were centrifuged at 500g for 5 min, re-suspended in BME 2 and then seeded in a 48 well plate at a density of 300-500 cells/well and allowed to expand for 15-20 days. Individual organoids were then picked out and reseeded (1 organoid per BME 2 drop). The single organoid was allowed to expand and then passaged as normal[123]. Clonal organoids were collected as early as possible, once they had reached confluency of 2-4 wells (of a 24-well plate) so as to allow enough cells DNA for sequencing. At two months after the clonal step, clonal cultures were subjected to a further single-cell step as described above. From each clonal culture, individual

sub-clones were picked out and passaged as normal. Sub-clonal cultures were collected for WGS when reaching confluency of minimum 1 well (of a 48-well plate). Clones and sub-clones were snap frozen in PBS and submitted for genome sequencing.

2.2.6 Doubling time calculation

Doubling time was calculated as follows; the hPO cultures were dissociated into single cells as described in section 2.2.4. Cell numbers were counted by trypan blue exclusion at the indicated time points. From the basic formula of the exponential curve y(t) = y0 x e(growth rate x t) (y = cell numbers at final time point; y0 = cell numbers at initial time point; t = time) the growth rate was derived. The doubling time was calculated as doubling time = ln(2)/growth rate for each time window analysed.

2.3 Isolation and culture of human pancreas cancer (hPC) organoids

Human pancreas cancer organoids were cultured with a modified protocol based on the one described in Boj et al.[131]. Briefly, the tumour sample was minced and placed in tumour digestion medium [Collagenase type II (5 mg/mL) made up in tumour organoid culture medium (hPC-EM)]. hPC-EM composition: [Basal medium (described above) supplemented with 1X N2 and 1X B27 (both from GIBCO), 1.25 mM N-Acetylcysteine (Sigma), 10 nM Gastrin (Sigma), 50 ng/ml EGF (Peprotech), 40% Wnt3a conditioned medium (homemade), 10% Rspo1 conditioned media (homemade), 100 ng/ml FGF10 (Peprotech), 100 ng/ml Noggin (Peprotech), 10 mM Nicotinamide (Sigma), 0.5 µM A83.01 (Tocris), and 10 µM Rho Kinase inhibitor (Y27632, Sigma Aldrich)] and was digested overnight at 37°C or until there was no more visible tissue chunks left. The digest was spun at 300g for 5 min, the digestion medium as discarded and the tissue was subsequently washed in Advanced DMEM/F12. The cell pellet was mixed with reduced growth factor BME 2, seeded in a 24 well plate and overlayed with human pancreas cancer expansion medium (hPC-EM) medium. IPMN-derived tumour organoids were cultured in hPC-EM while PDAC-derived organoids were cultured in hPC-EM with 1µM PGE2 (Tocris).

2.4 Chemically-defined hydrogel culture

2.4.1 Hydrogel generation (performed by Cellendes GmbH)

For the chemically defined dextran-based hydrogel (DEX-hydrogel) used in section 3.2.5, SG-Dextran (Cellendes Cat. No. M91-3) and RGD Peptide (Cellendes Cat. No. 09-P-001) were used with a thiol-modified hyaluronic acid cross-linker. Thiol-modified hyaluronic acid was prepared as previously described[234], except that 4-(4,6-dimethoxy-1,3,5-triazin-2-yl)-4-methylmorpholinium chloride

(DMTMM, TCI Chemicals) was used instead of N-(3-dimethylaminopropyl)-N'-ethylcarbodiimide hydrochloride (EDC) and N-hydroxysuccinimide (NHS) for attachment of cystamine to hyaluronic acid (Lifecore) with an average molecular weight of 57 kDa[235]. Additionally, tris(2-carboxyethyl)phosphine (TCEP, Sigma-Aldrich, Cat. No. C4706) was used instead of dithiothreitol (DTT) to reduce the disulfide bond of the attached cystamines. Thiol-modified hyaluronic acid was purified by extensive dialysis against phosphate buffer at pH 3-5. This procedure yielded a modification of 12% of the D-glucuronic acid and N-acetyl-D-glucosamine disaccharides of hyaluronic acid with thiol groups as determined with the assay as previously described[236].

Organoid hydrogel embedding and in vitro culture

Preparation of 50µl DEX-hydrogel: Buffer, water and SG-Dextran of the SG-Dextran Kit (Cellendes Cat. No. M91-3) were used; 3µl buffer (10x CB (pH 7.2)), 12.5µl Water, 3.4µl of SG-Dextran (30 mmol/L thiol-reactive groups) and 2.5µl of RGD Peptide (20 mmol/L thiol groups) were combined and incubated for 20 min at room temperature. Thereafter, 20µl organoid fragments were added and hydrogel formation was initiated by adding 8.6µl of thiol-modified hyaluronic acid (50 nmol of thiol groups). The hydrogel/organoid suspension was seeded into 24 well plate during the 8 min pre-gel period and placed in the 37ºC incubator. 30 min after the initiation of crosslinking, the hydrogels were overlaid with the appropriate culture medium.

Preparation of 50µl of GFOGER-hydrogel: Buffer, water and SG-Dextran of the SG-Dextran Kit were used as above. 3.5µl buffer (10x CB (pH 7.2)), 14.78µl Water, 2.68µl of SG-Dextran (30 mmol/L thiol-reactive groups) and 3.7µl of GFOGER Peptide III (6.34mmol/L thiol groups) instead of RGD peptide were combined and incubated for 20 min at room temperature. Thereafter, 15µl organoid fragments were added and hydrogel formation was initiated by adding 10.34µl of thiol-modified hyaluronic acid (50 nmol of thiol groups). The hydrogel/organoid suspension was seeded in a similar fashion to the DEX-hydrogel but with a 1 min gelation period due to increased concentration of the SH-HA crosslinker (1.2 mmol/L instead of 1 mmol/L).

2.4.2 hPO expansion in chemically defined hydrogel (early protocol)

Passaging of organoids grown in DEX-hydrogel was achieved by first digesting the hydrogels with Dextranase (Cellendes Cat. No. D10-1) diluted 1:20 for 30-40 min at 37 °C according to the manufacturer's recommendations. Once the gel was digested, organoids were fragmented by passing through a syringe with 27ga needle 3-5 times. Organoid fragments were washed 4 times with Basal medium and twice with Basal medium containing 11 mg/ml Dextran 6 (Carl Roth; Cat. No. 7615.1) to remove any Dextranase contamination. After the first passage, hPOs in DEX-hydrogel were cultured with hPO-Opt.EM medium supplemented with 10 mg/ml Dextran 6, acting as a competitive inhibitor

to Dextranase, to inhibit gel degradation from leftover contaminating Dextranase; fresh medium was applied every day for 3 days post-passaging.

2.4.3 Optimised protocol for hPO expansion in chemically defined hydrogel

The optimised protocol for passaging of organoids grown in DEX-hydrogel or GFOGER-Hydrogel was achieved by scraping of the gel from the well with a pipette. The gel was fragmented by pipetting up and down and placed in a 15ml falcon tube. Basal media was added to a total volume of 2ml and the cell suspension was homogenised by passing 10-15 times through a syringe with a 30ga needle. The cell suspension was washed 3 times by centrifuging at 300g for 5 min and adding 10ml of Basal medium. After each wash, the cell suspension was pipetted up and down to detach the organoids from hydrogel fragments. The relevant hydrogels were prepared as stated in sections 1.4.1. 30 minutes after the initiation of crosslinking, the hydrogels were overlaid with hPO-Opt. EM medium and media was changed in a similar fashion to hPOs grown in BME 2.

2.5 Whole genome sequencing

2.5.1 Library preparation, sequencing and sequence read alignment

(Performed by Alex Cagan in the Martincorena lab, Wellcome Sanger Institute)

Cells were lysed using a commercially available kit (Arcturus PicoPure DNA extraction kit; Thermo Fisher Scientific, ca. No. KIT0103). The DNA for each sample was quantified and 14 samples with sufficient DNA yields were selected to proceed with genome sequencing. We sequenced 3 independent clonal organoids derived from donor Donor 14, including 6 subclones and 4 independent clones from Donor 10. Libraries were prepared using enzymatic fragmentation, adapter ligation and whole-genome sequencing using the Nextera XT DNA library preparation kit, designed for low volumes of input DNA. Samples were multiplexed and sequenced using Illumina Novaseq 6000® machines to generate 150 base pair (bp) paired-end reads. Samples were sequenced to ~30x depth (Appx. Table 3). Sequences were aligned to the human reference assembly GRCh37 (hg19) using the BWA-MEM aligner[237] and duplicates were marked. Some samples received additional sequencing due to an administrative error in the sequencing pipeline.

2.5.2 Variant calling and copy number calling

(Performed by Alex Cagan in the Martincorena lab, Wellcome Sanger Institute)

Variant calling was performed using the Cancer Variants through Expectation Maximization (CaVEMan) algorithm[238]. CaVEMan operates using a naive Bayesian classifier to derive the probability of all possible genotypes at each analysed nucleotide. For each sample, CaVEMan was run using DNA sequenced from splenocytes from the same donor as a matched normal to identify germline SNPs.

CaVEMan requires pre-input copy-number options, which were set to major copy number 5 and minor copy number 2 for normal clones, as this maximizes detection sensitivity. After variant calling, post-processing filters were applied. We filtered against a panel of unmatched normal samples to remove single-nucleotide polymorphisms (SNPs) commonly present in the population. We also applied two filters designed to remove mapping artefacts associated with BWA-MEM: the median alignment score of reads supporting a mutation should be greater than or equal to 140, and below half of these reads should be clipped. Copy-number changes were called using the allele-specific copy number analysis of tumours (ASCAT) algorithm[239]. The same matched normal sample was used as for calling single nucleotide variants with CaVEMan.

2.5.3 Variant filtering

(Performed by Alex Cagan in the Martincorena lab, Wellcome Sanger Institute)

A number of post-processing filters were applied to the variant calls to remove false positives.

Quality flag filter: CaVEMan variant calls with a series of quality flags. The 'PASS' flag indicates that no quality issues affect the call[238]. Only variant calls that presented the 'PASS' flag were considered for further analysis.

Alignment quality filter: Variants were excluded if > half of the reads supporting the variant were clipped. As the library preparation methods create short insert size libraries this can result in reads overlapping. In such cases in order to avoid the risk of double-counting mutant reads we used fragment-based statistics. Variants without ≥ four high-quality fragments (alignment score ≥ 40 and base Phred quality score ≥ 30) were excluded.

Hairpin filter: To remove variants introduced by erroneous processing of cruciform DNA during the enzymatic digestion, which can lead to false positive single nucleotide variants, we applied a custom filter to remove variants in inverted repeats.

Contamination: To identify samples where the sequencing was contaminated from with cells from other human individuals, we ran VerifyBAMID[240]. While very low levels of contamination are difficult to avoid in genome sequencing experiments, we identified four samples where contamination levels were >5%, which we deemed high enough to warrant excluding the samples from further analysis (Appx. Table 3). This contamination could have been introduced at any time from culturing of the organoids to preparation and sequencing of the libraries. Notably the four excluded samples were from organoids that had spent longer in culture and undergone a second clonal step, suggesting that this may be connected to higher risk of exposure to contamination from human cells not derived from the donor, though this is purely speculative.

2.6 Genetic manipulation of hPOs

2.6.1 Lentiviral transduction with commercial, pre-packaged lentivirus

hPOs were expanded to passage 3, after which organoids were made into single cells as described in 2.2.4. $1x10^5$ cells were resuspended in virus infection medium containing one of two viruses. The first virus used was a 'CMV-GFP-T2A-Luciferase' pre-packaged virus (Systems Bioscience, Cat. No. BLIV101VA-1). The second virus used was a 'CAG-Luciferase-F2A-RFP-RsvPuro' pre-packaged virus (GenTarget Inc., Cat. No. LVP572). The viruses were used at a multiplicity of infection (MOI) of 5 ($5x10^5$u/µl) for the GFP virus while both MOI 5 and 10 were used for the RFP virus. The viruses were resuspended with 1:200 TransDux (System Bioscience) and 1:5 MAX Enhancer (Systems Bioscience) with hPO-Opt.EM and 10 µM Rho Kinase inhibitor. The cell suspension was added to a 24 well plate, spun at 32 °C at 600g for 10 min and then incubated at 37 °C for 6 h. Cells were then transferred to a 15 ml centrifuge tube, washed twice with Basal Medium and seeded in a 48 well plate with BME 2 and overlayed with hPO-Opt.EM supplemented with Rho Kinase inhibitor.

2.6.2 Assessing luciferase activity *in vitro*

Cells were expanded to 4 wells per condition to allow 3 technical replicates when measuring luciferase activity, as well as 1 well to count the number of cells per condition. Once the wells had reached confluency, 1 well per condition was taken for counting by dispersing hPOs into single cells as described in 2.2.4. Cells were then counted under a brightfield microscope by trypan blue exclusion. In order to generate cell lysates, the Reporter Lysis 5X Buffer (RLB) (Promega, Cat. No. E3971) was diluted to 1X by mixing 4:1 buffer and water. The culture medium was then removed from the wells and each well was rinsed with PBS. Then the 1X RLB was added to each well ensuring the cells were completely covered, the cells were then scraped and transferred to an Eppendorf tube and were pipetted up and down to homogenize the cell mixture. Each Eppendorf was then subjugated to a freeze-thaw cycle by embedding each tube in dry ice for a few minutes. Once thawed, each tube was vortexed for 10-15 seconds, centrifuged for 1 min at 12,000g at 4 ºC, and placed on ice. *In vitro* luciferase levels were quantified using the Promega GloMax® 96 Microplate Luminometer (Promega). First, the Luciferase Assay Reagent (LAR) was prepared by adding the Luciferase Assay Buffer (Promega, Cat. No. E152A) to the lyophilised Luciferase Assay Substrate (Promega, Cat. No. E151A). Then, 100µl of LAR was added to a well of a 96 well plate for each sample tube and the luminometer was set for a 2-second measurement delay followed by a 10 s measurement read for luciferase activity. 20 µl of the cell lysate were then added to the well containing LAR and the plate was inserted for reading. Readouts were collected and luciferase levels were normalised to 50,000 cells.

2.6.3 Fluorescence activated cell sorting of GFP-Luciferase+ hPOs

Following the step in 2.6.1, hPOs were expanded for 2 passages to increase cell numbers in preparation for cell sorting. The cells were again subjected to a single cell dissociation step as described above. Single cell preparations, along with negative controls (non-transduced hPOs) were placed in hPO-Opt. EM media with Rho Kinase inhibitor for transport to the sorting facility, while collection tubes were also generated with the same media composition. The cells were sorted using a MoFlo cell sorter (MRC Stem Cell Institute Facilities). GFP+ cells were seeded into 48 well plates with BME 2 and hPO-Opt.EM medium (with Rho Kinase inhibitor for the first 7 days). Organoids were expanded for 2 passages and imaged with the Evos Fl Imaging system (Thermo Fisher Scientific) for expression of GFP.

2.6.4 Lentiviral transduction under the Ef1a promoter

2.6.4.1.Plasmid cloning (performed by Dawei Sun, in the lab of Emma Rawlins)

The membrane targeted EGFP lentiviral vector was created by using the In-Fusion HD Cloning Plus (Takara Bio, Cat. No. 638909) to replace the *PGK-BFP-2A-GFP* sequence with the *EF1α* promoter and *EGFP-CAAX* sequence in a pKLV2-U6gRNA5(Empty)-PGKBFP2AGFP-W vector (a gift from Kosuke Yusa, Addgene plasmid, Cat. No. 67979). The non-targeting gRNA sequence, which was designed not to bind to human genome: *GCTGATCTATCGCGGTCGTC* was inserted in between two BbsI sites.

2.6.4.2.Lentiviral production (performed by Dawei Sun, in the lab of Emma Rawlins)

We grew HEK293T cells in 10 cm dishes to a confluence of 80% before we transfected the lentiviral vector (10 µg) with packaging vectors including 3µg pMD2.G (Addgene, Cat. No. 12259), 6µg psPAX2 (Addgene, Cat. No. 12260) and 3µh pAdVAntage (Promega, Cat. No. E1711) using Lipofectamine 2000 Transfection Reagent (Thermo Fisher Scientific, Cat. No. 11668019) according to manufacturer's protocol. After 16 h, medium was refreshed. Supernatant containing lentivirus was harvested at 24 hrs and 48 hrs and pooled together. Lentivirus was then concentrated using Lenti-X™ Concentrator (Takara Bio, Cat. No. 631232) according to manufacturer's protocol. Lentivirus pellets were dissolved in 200 µl PBS.

2.6.4.3.Transduction and expansion of hPOs with the Ef1a-GFP lentiviral vector

hPOs were expanded to allow for 100,000 cells per 200µl vial of virus and were transduced in a similar manner as described in 1.6.1. hPOs were allowed to grow and were passaged once to expand further. Growing organoids that were homogeneously expressing GFP were handpicked out, fragmented, and placed into separate wells. Organoids that remained in the well and were too small to pick out were split in a 1:1 manner in order to fragment organoids and stimulate expansion as well as to allow for any

further GFP+ organoids to be expanded. Once they reached confluency, GFP+ positive cultures were passaged normally as described in 2.2.1.

2.7 Mouse xenograft studies

2.7.1 Experimental use of mice

All animal experiments were performed in accordance with UK Home Office regulations (UK Home Office Project License number PPL 70/8702 and PPL P57643EBB). Immunodeficient NOD.Cg-Prkdc^{scid} Il2rg^{tm1Wjl}/SzJ (NSG) mice which lack B, T and NK lymphocytes[224,225] were bred in-house with food and water available *ad libitum* pre- and post-procedures. NSG-(K^bD^b)^{null} (IA)^{null}, (referred to as NSG-dKO) which lack expression of MHC Class I and MHC Class II molecules [232] were bred in-house similarly to NSG mice. For the xenograft studies male and female NSG mice were used, whereas for the haematopoietic stem cell (HSC) human immune system (HIS) mouse studies only female mice were used. For splenocyte mononuclear cell (SpMC) HIS mouse studies male and female NSG-dKO mice were used. All mice for the HIS mouse studies were aged between 6-8 weeks while for the xenograft studies mice used were between the ages of 6-12 weeks. All animals had approximately the same weight (~20g). Animals were allocated at random to experimental groups, tissue sections obtained from animals were processed, stained and analysed without reference to the identity of the animal groups.

2.7.2 Preparation of cells for mouse transplantation

hPO and human pancreas cancer organoid (hPC-org) cultures were expanded as described in sections 1.2.1 and 1.3 in order to inject 5x10^5-1x10^6 cells per mouse. Organoids were mechanically dissociated as described for normal passaging and resuspended in the appropriate injection medium as outlined in (Table 2; Appx Table 2). The cells were transported to the animal facility and kept on ice. The surgery area was prepared, and the animal cages were brought into the pre-op surgical area. The cells were loaded into a 250 µl glass gastight syringe (Hamilton) with removable 26ga blunt needles (ESSLAB) for injection into the kidney capsule or custom made 26ga sharp needles, bevelled at a 60^o angle (ESSLAB) for injection into the pancreas capsule. For portal vein injections described below, 1 ml syringe with a 32ga needle was used. The loaded syringe was kept on ice on top of sterile aluminium foil to maintain sterility. Mice were anesthetised using isoflurane gas (flow rate 2.5%) and the left side of the abdomen or peritoneal abdomen was shaved and cleaned with disinfectant. During the procedure, the mice were maintained under anaesthesia (flow rate ~1.5%) on heat pads at 37°C. Injections were performed as described below into the kidney capsule, pancreas capsule or portal vein. Following the xenograft procedure, all animals were kept alive for either 1 or 3 months after which they were humanely euthanised under terminal anaesthesia. Tissue was then retrieved for further histological analysis.

2.7.3 Kidney capsule injections

An incision of the skin was made near the anatomical position of the kidney, the kidney was localised and a further incision of the abdominal wall was made to expose the kidney. The kidney was gently pushed out of the abdomen and kept wet with sterile saline. A small incision to the kidney capsule was made with a sharp needle, then 20 μl of the organoid suspension was injected under the capsule using the blunt needle syringe. A sterile cotton bud was used to apply pressure to the point of insertion to stop bleeding and prevent cell leakage. The kidney was then gently replaced into the abdomen through the muscle wall incision. The muscle wall was sutured close using continuous 5-0 vicryl sutures. Interrupted sutures were used to close the skin layer after which 9mm autoclip wound clips (Harvard Apparatus) were placed on the skin to keep the sutures intact.

2.7.4 Pancreas capsule injections

An incision of the skin and abdominal wall was made along the midline of the abdomen to expose the visceral organs. The abdomen was kept open by an Alm self-retaining retractor and the pancreas was exposed and kept wet with sterile saline. Using a sterile cotton bud for traction, organoids were injected into the tail of the pancreas, through the parenchyma, and placed between the inter-lobular space. The cotton bud was then used to stop leakage by applying pressure for 10-15 s. The pancreas was gently placed back to the correct anatomical position and the abdomen wall and skin were sutured using two layers of continuous 5-0 vicryl sutures.

2.7.5 Portal vein injections

An incision of the skin and abdominal wall was made as described in section 1.7.4. The small and large intestine were either moved to the side or placed outside of the abdomen of the mouse, on a sterile gauze, in order to visualise the portal vein. The needle was the inserted 3-5mm into the portal vein 5-10mm below the liver. Once the cells were fully injected, the needle was withdrawn, and pressure was immediately applied using a sterile cotton bud. To reduce the amount of bleeding, haemostatic powder (SURGICEL, Johnson & Johnson) was applied to minimise bleeding from the entry site. Once bleeding had completely stopped, the organs were gently moved back into the correct anatomical position and the abdomen wall and skin were sutured using continuous suturing with 5-0 vicryl sutures.

2.7.6 Bioluminescent live imaging of transplanted mice

Luciferin (VivoGlo^{TM} Luciferin, Promega) was reconstituted in sterile deionised water at a concentration of 20mg/ml and aliquoted into 1 ml aliquots and stored at -20°C. Animals were transferred to the In Vivo Imaging System (IVIS) imaging room and the IVIS imager was initialised.

The IVIS chamber and stage as well as the nose cones, separators and anaesthetic chamber were cleaned. 1ml syringes with 30ga needles were prepared with luciferin so as to inject 150μl per mouse, up to 2 mice per needle. Each mouse was injected intraperitoneally with Luciferin and was placed into the anaesthetic box, set at 2% flow rate, for 10 min. Each cage of mice was injected and imaged separately to prevent mixing of mice or inconsistent timings of luciferin exposure. After 10 min post luciferin injection, the animals were placed on the IVIS stage, taking note of the ear notch numbers to ensure the same position for each imaging session. Images were taken using the automatic exposure settings as well as the manually set exposure of 120 seconds. Whilst the automatic setting allowed for higher quality images, the manual setting allowed for an unbiased comparison between imaging sessions. Once imaged, the mice were transferred back into their cages.

2.7.7 Non recovery removal of organs/tissue under general anaesthetic

The surgical area was prepared as described in sections 1.7.3-5. Mice were anaesthetised and placed on the heat pad at 37°C. An incision was made to the abdominal wall and the organs were exposed with the use of an ALM self-retaining retractor. The Inferior Vena Cava (IVC) was exposed using a sterile cotton bud and a 1ml syringe with a 27ga needle was used to exsanguinate the animal by removing blood from the IVC, typically 700-800µl per animal. The blood collected was place into Eppendorf tubes with heparin for blood destined for flow analysis or without heparin for blood plasma collection. Pancreas or kidneys that had been engrafted with hPOs were carefully removed under the microscope using fine surgical scissors and forceps in order to ensure the engrafted site was not damaged. Engrafted organs were washed with PBS solution and immediately placed into 10% buffered formalin. If required, the spleen and/or femur were removed for subsequent flow cytometry analysis and were placed in Hank's balanced salt solution (HBSS; Gibco) for later processing.

2.8 Human immune system (HIS) mouse methods

2.8.1 Thawing cryopreserved spleen and bone marrow mononuclear cells

Thawing media (50% RPMI (Gibco) -50% FBS) was pre-warmed to 37 ºC and the cryovials were removed from liquid nitrogen and placed on dry ice. The cryovials were quickly thawed in a 37 ºC water bath until the last ice crystal could be observed after which they were quickly transferred to the Category II Biological safety cabinet and into a 50ml falcon. 15ml of thawing media was added to the tube in a drop-wise fashion while shaking. If more than one cryovial was thawed, up to 3 cryovials were thawed in a 50ml falcon and 45ml of thawing media was added. The cells were then spun at 300g for 5 min, the cell pellet was resuspended by a flicking action and the cells were washed with RPMI supplemented with 20% FBS. If cell clumps were present, 5mg/ml of DnaseI was added and the cells were incubated at 37 ºC until all cell clumps disappeared. The cells were then further washed twice with RPMI

supplemented with 20% FBS and were counted using an automated cell counter and trypan blue exclusion.

2.8.2 Mouse engraftment with splenocyte mononuclear cells (SpMCs

Cryovials with SpMCs from selected donors were thawed such that $1x10^7$ cells could be injected per mouse. SpMCs were thawed and counted as described in 1.8.1. SpMCs were resuspended in PBS- 2% FBS and transported to the animal facility on ice. The mouse cages were transferred into a Category II biological safety cabinet and each mouse was injected intraperitoneally with 200µl of the cell suspension.

2.8.3 Mouse engraftment with bone marrow HSCs

2.8.3.1. Mouse irradiation

The cages of NSG mice to be irradiated were transferred to the irradiation room early in the morning so as to allow as much recovery as possible between irradiation and injection with lymphocytes. The amount of time to generate 2.5Gy of irradiation was calculated and the mice were placed into the irradiator according to standard procedures. Once finished, the mice were placed back into their allocated cages and were injected with CD3-depleted bone marrow lymphocytes no later than 24 h post irradiation. Any irradiated animals that could not be reconstituted for reasons such as lack of available cells, were culled.

2.8.3.2.CD3 Depletion of bone marrow lymphocytes

Cells were thawed and counted as described in 1.8.1 and the cells were resuspended in 80µl of MACS buffer (Miltenyi Biotec) per 10^7 cells and 20µl of MACS CD3 MicroBeads (Miltenyi Biotec) and were incubated for 15 min at 4ºC. The cells were then washed with 2ml of MACS buffer per 10^7 cells and centrifuged at 300g for 10 min. The cells were then resuspended with 5ml of MACS buffer. The cell suspension was then placed onto the correct position of the AutoMACS cell sorter and the "depleteS" programme was run, collecting the "negative" population in order to collect the CD3 depleted fraction of cells. The cells were then counted, centrifuged at 300g for 5 min and re-suspended in the appropriate amount of PBS-2% FBS in order to inject $1x10^7$ cells per mouse.

2.8.3.3. Tail Vein injection of CD3-depleted bone marrow lymphocytes

The CD3 cell-depleted cells suspension was transported to the animal facility and the Cat. II biological safety cabinet was prepared with the heating unit. The irradiated mice were transferred into the heating unit and were left to warm up for ~10 min. While heating up, individual 1ml syringes with 30G needles were prepared with 200µl of the cell suspension, taking care to remove any air bubbles. Tissues were

prepared along with the tail vein mouse restraint which was thoroughly cleaned. Each mouse was placed into the restraint, the tail vein was visualised and 200µl of the cell suspension was injected intravenously. Bleeding was stopped with a sterile tissue and the mice were transferred back into their allocated cages.

2.8.4 Tail vain bleeds

Animal cages were retrieved from the holding room and were placed into a cleaned and prepared Category II biological safety cabinet. The heating unit was cleaned, placed into the cabinet and set to 37 °C. Labelled bleeding tubes (with a small amount of heparin), 27ga needles (one per mouse) and sterile tissues were also placed into the cabinet. After a 10-minute incubation, each mouse was placed onto a tail vein mouse restraint and one of the two tall veins in the tail was pricked with the sterile needle. 4-6 drops of blood were collected with the heparinised bleeding tube and pressure was applied to the bleeding site using sterile tissue. Once the bleeding had stopped the mice were placed back into their cages.

2.9 Histology and immunostaining of organoids and tissues

2.9.1 Fixation and paraffin embedding of tissues

Fresh human or mouse tissue was washed 1-2 times with PBS and placed into 10% neutral-buffered formalin (Sigma-Aldrich) overnight or a maximum of 24hrs at room temperature on a tube roller. Tissues were then washed 3 times with PBS and placed in 70% EtOH. Tissue was either placed in 4 °C for short-term storage or processed immediately for paraffin embedding. The tissue was placed in increasing ethanol concentrations (70%-100%) for 2 hours at room temperature in each concentration. Tissue was then immersed in xylene (Fisher) for 2 hours at room temperature and subsequently in pre-warmed paraffin (Shandon Histoplast; Thermo Fisher Scientific) and left overnight at 60 °C. The tissue was then placed onto paraffin moulds using a paraffin embedding station (Leica EG1150) and stored at room temperature once they had cooled. When needed, the paraffin blocks were sectioned, and sections were cut at 5 μm thickness and were placed at 60 °C for 2-24 h.

2.9.2 Fixation and paraffin embedding of organoids

Organoids were gently collected from wells using a widened plastic Pasteur. Organoids were then washed with Basal medium and incubated with Corning Matrigel Cell Recovery Solution (Scientific Laboratory Supplies) for 30 min on ice. They were then washed 2 times with PBS and fixed in 10% neutral-buffered formalin for 30-40 min on ice. The organoids were washed 2 times with cold PBS and those destined for wholemount immunostaining were kept in PBS while those destined for paraffin embedding were placed in 70% EtOH. The organoids were then transferred to a 5ml flat bottom glass

tube and were stained with 96% ethanol-Eosin (Sigma Aldrich) for 30 min at room temperature. The organoids were then further dehydrated 3 times for 30 min in each of the following solutions: 100% EtOH, Xylene, and pre-warmed paraffin. The paraffin was removed, and the organoids were moved onto a paraffin mould with fresh paraffin, using pre-warmed plastic Pasteurs. The moulds were allowed to cool before being sectioned as described in section 2.9.1.

2.9.3 Fixation of hPOs grown in hydrogel

2.9.3.1. Original protocol

hPOs in DEX-hydrogel were digested with Dextranase for 30-40min at 37 °C until the point that hPOs detached from the gel and flowed free in the media. The organoids were then gently collected using a widened plastic Pasteur and placed in a 15ml falcon tube. The organoids were then washed twice with PBS and fixed in 10% neutral-buffered formalin for 30-40 min on ice. The organoids were washed twice with cold PBS and were stored in PBS for immunostaining.

2.9.3.2.Optimised protocol

hPOs in DEX-hydrogel or GFOGER-hydrogel were removed from the incubator, the culture media was removed, and each well was washed twice with PBS. Thereafter, 1 ml of 10% neutral-buffered formalin was added to each well, the plate was placed on ice and the organoids were fixed for 30-40min. Once fixed, the wells were gently washed with cold PBS and each fixed hydrogel was gently removed with a widened Pasteur taking care to not disrupt the gel and placed in Eppendorf tubes. The PBS was removed, and Dextranase was added in a 1:20 dilution in a similar fashion to section 1.4.2. The hydrogel was digested for 30-40 min at 37 °C and once the organoids were detached from the hydrogel, they were washed twice with cold PBS. The organoids were then stored in 4°C until they could be immunostained.

2.9.4 H&E of organoids, primary tissue and xenograft tissue

Paraffin slides were rehydrated by being placed in xylene for 20 min and subsequently in decreasing concentrations of ethanol (100% - 50%) for 5 min in each concentration. They were washed twice in water and were then immersed in Haematoxylin (Sigma Aldrich) for 8-20 min depending on the tissue type. Slides were then washed with water and dehydrated in increasing ethanol concentrations (50-100%). A 10-20 s wash step of Eosin (Sigma Aldrich) occurred at the 96% ethanol step. Dehydration was completed with immersion of the slides in xylene for 10 min. The slides were then mounted with DPX mounting solution (Fisher Scientific) and cover slip was placed on each slide.

2.9.5 DAB staining of tissue sections

Paraffin slides were rehydrated by being placed in xylene for 20 minutes and subsequently in decreasing concentrations of ethanol (100% - 50%) for 5 min in each concentration. They were then washed 2 times with water and then washed for 5 min in Tris-Buffered Saline (TBS). the slides were then subjected to antigen retrieval by heating to 80 °C in 10 mM Sodium Citrate (Sigma), pH 6 for 20 min. Once the slides had cooled to room temperature they were washed once with TBS and incubated with blocking/permeabilization solution [Triton X100 (1% for nuclear antibodies and 0.1% for membrane and cytoplasmic antibodies), 1% Bovine Serum Albumin (BSA), 2% donkey serum in TBS] for 2 h at room temperature. Primary antibodies were applied at specified dilutions overnight at 4 °C. Thereafter, slides were washed 3 times with water and were incubated with 3% H_2O_2 (Sigma Aldrich) in methanol (Fisher) for 15 min at room temperature. They were then washed once in water and once in TBS and were incubated with BrightVision+ Poly- HRP-Anti Mouse/Rabbit IgG (Immunologic) for 30 min at room temperature and were subsequently washed twice in TBS. 3,3'-Diaminobenzidine (DAB) reagents (Immunologic) were then prepared by adding 1 drop of DAB to 1 ml of DAB buffer. Each slide was incubated with 200-300μl of the DAB mixture for the amount of time specific to each antibody and no longer than the timepoint of seeing background signal in the negative control slide. The slides were then washed twice with water and counterstained with haematoxylin for up to 10 min. Slides were then washed in water and dehydrated in increasing concentrations of ethanol (50-100%), ending with xylene with the same timepoints as for the rehydration steps. Slides were then mounted with DPX (Fisher Scientific) and a cover slip was placed on each slide.

2.9.6 Immunofluorescence (IF) staining of organoids in solution

Organoids were washed in PBS with 0.05% BSA following formalin fixation as described in section 2.9.2. Organoids were incubated with blocking/permeabilisation solution [Triton X100 (1% for nuclear antibodies and 0.1% for membrane and cytoplasmic antibodies), 1% BSA, 2% donkey serum, 2% DMSO in PBS] for 2 h at room temperature. Primary antibodies were applied at specified dilutions overnight at 4 °C (Appx. Table 5). Organoids and tissues were washed 3 times with PBS with 0.05% BSA and after each wash step, organoids were allowed to settle. Centrifugation of organoids was avoided to as to not disrupt the organoid structure. In the case that organoids had been of small size when they were fixed, they were centrifuged at 50g for 1-2 min to assist with the settling of the organoids. Appropriate secondary antibodies were applied for 2 h at room temperature, washed 3 times with PBS and nuclei were counterstained with Hoechst33342 (Molecular Probes, Life Technologies) or 15min at room temperature. IF stained organoids were kept at 4 °C until imaging.

2.9.7 Immunofluorescence (IF) of paraffin tissue sections

Tissue sections were rehydrated as described above for H&E staining. Following rehydration, slides were washed with PBS and subjected to antigen retrieval by heating to 80 °C in 10 mM Sodium Citrate (Sigma Aldrich), pH 6 or Tris-EDTA pH 9(homemade) for 20 min. Once the slides had cooled to room temperature, they were washed with PBS and incubated with blocking/permeabilisation solution [Triton X100 (1% for nuclear antibodies and 0.1% for membrane and cytoplasmic antibodies), 1% BSA, 2% donkey serum, in PBS] for 2 h at room temperature. They were then stained with primary and secondary antibodies as described in section 2.9.6. Finally, after the final wash, they were mounted with Vectashield Mounting Medium (Vector Laboratories) and a cover slip was placed on each slide. IF stained slides were kept at 4 °C until imaging.

2.10 *In vitro* characterisation assays

2.10.1 Karyotyping

Organoids were split into a minimum of three wells and were allowed to expand for 24 h. hPOs were then incubated with 0.1 μg/ml KaryoMAX Colcemid solution in PBS (Gibco) for 24 h Afterwards, Colcemid was removed, 500ml of PBS was added and organoids were transferred to a 15ml tube whereby a further 10ml of PBS was added. Organoids were made into single cells as described in section 2.2.4, using PBS for the washing steps. After centrifugation, the supernatant was removed, leaving 100-200µl to re-suspend the pellet. Then, 1ml of 0.075M KCl (Fisher Chemicals) was added dropwise while shaking and incubated at 37°C for 10 min. A solution of 3:1 MeOH: Acetic Acid (VWR Chemicals) was made fresh for every karyotype assay and 1ml was added dropwise while shaking in order to fix the cells. The tube was centrifuged at 1500rpm for 5 min, the supernatant removed and a further 1 ml of MeOH: Acetic Acid was added after which the cells were incubated for 20min at RT. This was repeated for a further 20min incubation period, the cells were then re-suspended in 500µl, centrifuged at 1500rpm and the supernatant was removed leaving 200 µl. Using a 200µl pipette in the chemical safety fume hood, the solution was dropped onto Superfrost Microscope Slides (VWR) for chromosomes to spread. The slide was then allowed to dry and mounted with Vectashield-Dapi (Vector Laboratories) and a coverslip was added on each slide.

2.10.2 RNA isolation and qRT-PCR

2.10.2.1.Extraction of RNA from cultured cells and primary tissue

Primary tissue was either placed in RNAlater as described in 2.1.2 or snap frozen immediately on dry ice. Cultured organoids destined for RNA analysis, upon reaching confluency, were snap frozen in Buffer RLT (Qiagen)- 1 well was frozen in 350µl of Buffer RLT. For RNA extraction, primary tissue was homogenised on dry ice and was incubated with 350µl Buffer RLT and was snap frozen again to

allow lysis of cells. Organoids and tissue in Buffer RLT were thawed and RNA extraction was performed using the RNeasy Mini Kit (Qiagen) following the manufacturer's protocol. The RNA yield was measured using a Nanodrop spectrophotometer.

2.10.2.2.Reverse transcription (RT) of RNA samples

For each RT reaction, 200ng of RNA were used per sample. In cases that samples had not yielded enough RNA, the amount of RNA was reduced to a minimum of 50ng for each sample. The correct volume of RNA was then mixed with 2 µl of random primers (Promega) in an Eppendorf tube and the total mix was made up to 15 µl by the addition of water. The tube was incubated for 5 min at 70°C and quickly cooled to 4°C for a further 5 min. A further 5 µl of 5X Buffer (Promega), 1.25 µl of 10mM dNTP mix (Promega), 3.3 µl water and 0.4µl of M-MLV RT enzyme (Promega) were added to each tube to make a total reaction volume of 25µl. The mix was then incubated at room temperature for 10 min, then at 50°C for 50 min, then 70°C for 15 min and finally cooled to 4°C. The resulting cDNA was either immediately used for quantitative PCR or stored in -20°C for short-term storage until further analysis.

2.10.2.3.Quantitative PCR

All reagents were thawed and mastermix was made for each primer to be used. Hypoxanthine-guanine phosphoribosyltransferase (HPRT) was used as the reference gene and was added to each plate to allow comparison between samples and between plates. The primer mix was generated by adding 2μl of 10μM forward and reverse primers (Primers were generated by Sigma Aldrich and are listed in Appx. Table 6) and 7.5μl of iTaq Universal SYBR Green Supermix (2X; Bio-Rad) per reaction. This mastermix was added to each corresponding well. Then a second mix was created by adding 2 μl of cDNA to 3.5 μl of water for every reaction. The cDNA mix was then also added to each corresponding well. The plate was briefly centrifuged and run on a CFX96 Touch™ Real-Time PCR Detection System (Bio-Rad) with the following programme: 1 cycle at 95°C for 5 min, then 40 cycles of 95°C for 10 sec and 60°C for 30 sec, then 1 cycle at 95°C for 10 sec and 1 cycle at 65°C for 5 sec. Values are given relative to the expression of the housekeeping gene HPRT.

2.10.3 hPO co-cultures

2.10.3.1.hPO incubation with IFNγ

hPOs were expanded so as to allow for enough wells for technical replicates and collection of cells for both flow cytometry or qPCR analysis. Once enough wells had been obtained, hPOs were passaged and allowed to expand for 4 days. On the fourth day, fresh media supplemented with IFNγ (100 ng/ml) was added to the IFNγ wells while hPO-Opt.EM medium was added to the control wells. hPOs were

incubated with IFNγ supplemented media for 72 h, with fresh media added each day. Following the 72 h incubation, hPOs were collected for qPCR analysis as described in section 2.10.2.3 or for flow cytometry as described in section 2.10.4.

2.10.3.2.hPO-SpMC co-culture

hPOs were expanded to obtain enough cells for the multiple conditions outlined in section 5.2.2. 24 h prior to initiation of the co-culture, SpMCs from a different donor were thawed and activated using Dynabeads Human T-Activator CD3/CD28 (ThermoFisher Scientific) according to the manufacturer's protocol for a 24 h period. Following activation, the hPOs were fragmented and mixed in the ratios outlined in section 5.2.2, resuspended in BME 2 and overlaid with culture media which contained 50% basal media and 50% RPMI as well as all of the growth factors used in hPO-Opt.EM media. The co-culture was incubated for 72 h after which cells were collected for flow cytometric analysis.

2.10.4 Flow Cytometry

2.10.4.1.Preparation of mouse blood/spleen/BM for flow cytometry

Mouse spleens were collected and pushed through a 40µm filter to create a single cell suspension using a sterile syringe and flushing with RPMI. The cells were centrifuged at 300g for 7 min and the supernatant was discarded. The cells were resuspended in 600µl of red cell lysis buffer (RCLB) and incubated 4°C for 10 min. The cells were centrifuged at 300g for 7 min and the process was repeated up to 3 times so that all red blood cells were removed. Mouse blood was placed directly into Eppendorf tubes and was incubated with RCLB in a similar fashion to mouse spleens. Mouse bone marrow was extracted from the femur bones of culled mice and the marrow cells were isolated by repeated flushing of RPMI medium through the femur using a 27ga needle and 1 ml syringe. The bone marrow was then passed through the syringe and needle a few times to generate a single cell suspension after which the cells were treated with RCLB as described above. After the RCLB step, the cells were washed with staining buffer (PBS + 0.1% BSA + 0.1% Sodium azide; FACS Buffer) and were transferred to a U-bottomed 96 well plate for further washes and staining as described in section 2.10.3.2.

2.10.4.2.Single cell staining for flow cytometry

Single cell suspensions were placed in the appropriate pre-labelled wells in the 96 well plate and the plate was centrifuged at 450g for 4 min at room temperature. Each well of cells was resuspended with 50 µl of FcR block (1:20 dilution) and was incubated for 20 min at 4°C. For each staining session, a portion of cells was taken and incubated at 95°C for 5 min in order to generate a positive control for the live/dead stain. During the FcR block, an antibody mastermix was created whereby all the antibodies tested were mixed at the appropriate concentrations in FACS buffer. After the FcR block, wells were

washed once with FACS buffer and cells were stained appropriately with the mastermix solution including an unstained control, single stain controls and a live/dead control. The cells were stained for 20 min at 4°C after which they were washed 3 times with FACS buffer. The cells were then transferred to labelled FACS tube before further analysis.

2.11 Imaging and flow cytometry analysis

2.11.1 Brightfield and confocal imaging

Brightfield imaging of organoids was performed using a Leica M80 stereo microscope (Leica Microsystems) and a Leica DMIL LED microscope (Leica Microsystems). H&E images were taken using a Leica DM400B LED microscope (Leica Microsystems). Karyotypes and IF staining were imaged using a SP8 White Light inverted confocal microscope (Leica Microsystems) or with a Leica DMI3000 fluorescent inverted microscope (Leica Microsystems). Optical sections were acquired at 3 µm intervals. Images were acquired with Leica application suite X Software and processed using Fiji. Confocal microscope settings were determined according to negative and positive controls and were kept the same for each staining session. Post image acquisition analysis on Fiji was carried out with the same parameters for images taken in one staining and imaging session.

2.11.2 Flow cytometry analysis

Analysis of the stained single cells for flow cytometry was carried out using a 6- colour flow cytometer BD FACSCanto™ II linked to a computer equipped with BD FACSDiva™ software (BD Biosciences, version 6.1.3). For each analysis, unstained and single stain controls were included, and the automatic compensation options was performed. After acquiring the data, the files were exported and further analysed with FLowJo software. The gating strategies used are outlined for the relevant figures.

2.12 Statistical analyses

Statistical analysis was performed using GraphPad Prism software (version 8.4.3). Graphs which include datapoints from multiple donors are displayed as mean ± SD with each data point representing a separate donor. Graphs where technical replicates are illustrated, data is displayed as mean ± SEM. Two-tailed unpaired t-test (unless otherwise specified) was used for comparison of two groups. A one way or two-way ANOVA (analysis of variance) was used to compare three or more groups followed by Tukey's honestly significant differences (HSD) test (controlling for multiple comparisons) or Dunnett's test if groups were compared to a single control group. Results were considered statistically significant if the p-value ≤ 0.05.

2.13 Availability of data and materials

Whole genome sequencing data has been deposited in the European Genome-Phenome Archive under study accession EGAS00001002626.

CHAPTER 3. ESTABLISHMENT AND CHARACTERISATION OF hPOS

3.1 Introduction and aims

Since the advent of 3D organoid technology various studies have demonstrated the advantages of growing cells in a 3D environment over traditional 2D cell culture. Multiple groups have generated organoids from epithelial cells of different organs which have been used to either model cell biology and disease[80,120,123] or advance the clinical translation of cellular therapies[241]. Generation of the first pancreas organoid model was described by Huch *et al.*[121], which demonstrated the ability to expand mouse pancreas ductal cells *in vitro* as organoids. The study highlighted the efficacy of the system in allowing long-term expansion and maintenance of the ductal phenotype without the need for cell transformation, but more importantly, it highlighted the ability of adult pancreas ductal cells to differentiate towards an endocrine fate. This generated enormous potential for creation of a human pancreas organoid system that could be applied to model cell biology (healthy or diseased) or cell therapy for diabetes. Although previous studies were able to generate hPO systems, these suffer from several shortcomings: (1) they do not support the long-term expansion required to generate the necessary cell numbers[132], (2) the medium compositions are not chemically defined and require the addition of serum to the medium[123,131] and (3) the extracellular matrix (ECM) used, namely Matrigel, suffers from batch-to-batch effects and additionally, is derived from mouse tumours, which makes it difficult to produce under GMP compliant conditions [123,172].

In Section 3.2.1 I focus on establishing a culture protocol that would allow expansion of human pancreatic ductal cells as organoids while also aiming to generate a culture medium that allows long-term expansion of hPOs. With the understanding of the need to meet GMP criteria, I aimed to generate a culture-medium that was chemically defined and devoid of serum. Once the culture system was defined, it was used, as outlined in **section 3.2.2,** to explore its efficacy towards expansion of hPOs across multiple donors.

In order to address the potential needs of cryopreservation and transport of tissue to facilitate derivation of lines on a global scale, in **section 3.2.3** I investigate the ability to cryopreserve both at the primary tissue and organoid level and derive lines post cryopreservation. Importantly, in **section 3.2.4** I aim to characterise the hPOs on a histological and phenotypic expression level to understand the identity of the cells grown in the hPO system.

In line with the ability to translate the hPO system towards GMP production, in **section 3.2.5** I utilise novel biomimetic hydrogels to explore use of a chemically defined 3D matrix for expanding hPOs and compare the identity of the cells to those expanded in BME 2. Lastly, in order to explore whether the hPO culture system allows disease modelling, I demonstrate, in **section 3.2.6,** the ability to expand and characterise hPOs generated from patients with T2D.

3.2 Results

3.2.1 Generation of an optimised hPO media for long-term expansion

In order to establish a protocol to generate human pancreas organoids, I utilised existing lab knowledge based on mouse pancreas organoids (mPOs)[121] and worked with Daisy Harrison, a research assistant in our lab at the time. I obtained human pancreas tissue samples from deceased transplant organ donors, and, following enzymatic digestion, pancreatic ducts were seeded in Basement Membrane Extract Type 2 (BME 2) as extracellular matrix (ECM). Once the ducts were placed in BME 2 under the optimised culture conditions, they enlarged and formed a spherical organoid whereby each duct grew into one organoid (Fig 3.1).

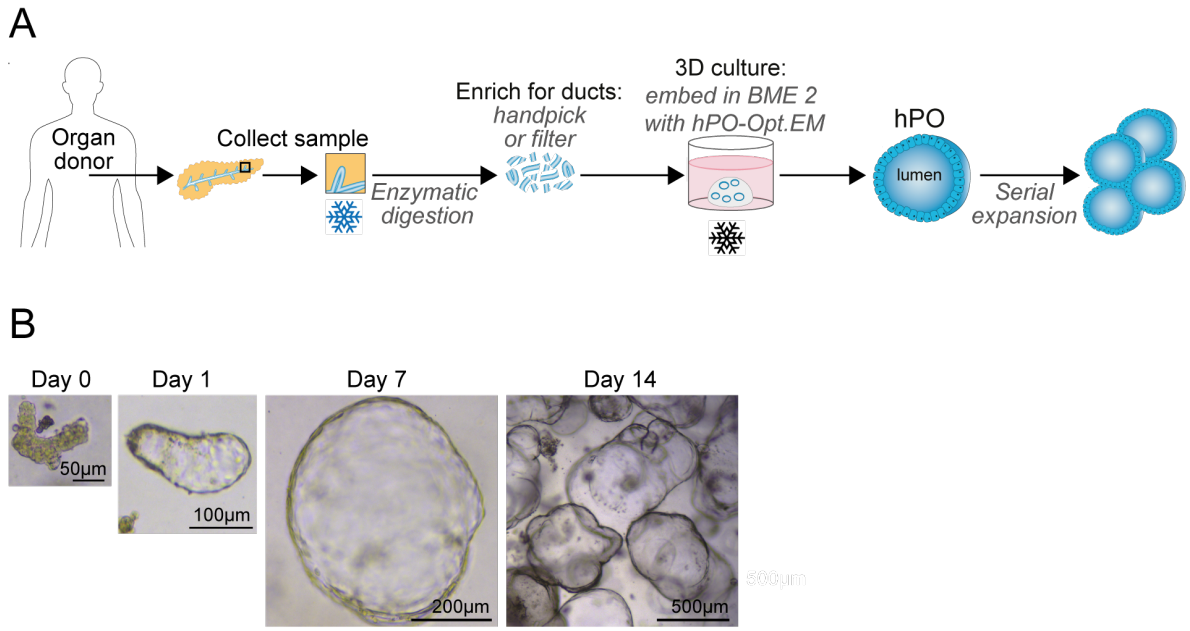

Figure 3.1 Pancreatic ducts expand *in vitro* as hPOs under defined culture conditions. (**A**)Schematic of hPO generation and expansion. Pancreatic tissue undergoes enzymatic digestion to release ductal fragments, which are subsequently enriched either by handpicking or filtration. Pancreas ductal fragments are then embedded in BME 2 as extracellular matrix and overlaid with the hPO-Opt.EM medium (see section 2.2.1; hPO-Opt.EM composition). Generated hPOs can be serially expanded by mechanical dissociation. Cryopreservation can be performed on the primary tissue for derivation at a later time (blue asterisk) or on the established hPOs (black asterisk). (**B**) Brightfield images of ductal fragments isolated from fresh human pancreatic donor tissue grown and expanded as hPOs.

To achieve an optimised culture media, a cocktail of growth factors and small molecule inhibitors were tested in different combinations and concentrations by Daisy Harrison, until a combination that would support the expansion of human primary pancreas ductal cells beyond passage 10 was achieved; The optimisation experiments and addition of key growth factors are summarised

	Optimisation Media							Other	hPC (tumour) Media	
No.	**1**	**2**	**3**	**4**	**5**	**6**	**7**	**8**	**9**	**10**
Condition Reference	mPO	mPO+ TGFβi	mPO+ TGFβ i+Wnt	mPO+ TGFβi+ Serum	mPO+ TGFβ i+Wnt + PGE2	hPO-Opt. EM+ Wnt	hPO-Opt. EM	Loomans *et al.*, 2018	IPMN	PDAC ITPN
EGNNF*	✓	✓	✓	✓	✓	✓	✓	✓	✓	✓
5% R-Spondin	✓	✓	✓	✓	✓	✓	✗	✓	✗	✗
TGFβi	✗	✓	✓	✓	✓	✓	✓	✓	✓	✓
Wnt (+serum)	✗	✗	✓	✗	✓	✓	✗	✗	✓	✓
Serum (3% FBS)	✗	✗	✗	✓	✗	✗	✗	✗	✗	✗
PGE2	✗	✗	✗	✗	✓	✓	✓	✗	✗	✓
FSK	✗	✗	✗	✗	✗	✓	✓	✗	✗	✗
10% R-Spondin	✗	✗	✗	✗	✗	✗	✓	✗	✓	✓
Expansion past Passage10	✗	✗	✗	✗	✗	✗	✓	✗	✗	✓
Related publications	Huch *et al.*, 2013				Boj *et al.*, 2015; Broutier *et al.*, 2016		Georgakopoulos *et al.*, 2020	Loomans *et al.*, 2018		

Table 1 Media compositions utilised for expanding hPOs and hPC derived organoids. Columns 1-7 demonstrate media compositions used to obtain an optimised, serum-free hPO media which allowed robust hPO expansion. Column 8 demonstrates the media composition used in Loomans *et al.* Columns 9-10 demonstrate the media utilised to expand hPC- organoids. Only medium number 7 allowed expansion of hPOs long term (past passage 10) while the other failed to support this expansion. (*EGF, Gastrin, Noggin,FGF-10,Nicotinamide). Optimisation media was designed and tested by Daisy Harrison.

below. In order to optimise the media, the established mPO media was used[121], which is composed of 'generic' organoid factors, epidermal growth factor (EGF), Rspo1 and Noggin derived from the original organoid protocol[118] , as well as gastrin, nicotinamide and FGF-10. Seeding of human pancreas ductal cells into mPO media (Table 3.1; media 1) allowed initial formation of organoids, but these quickly deteriorated (*data not shown*). TGFβ signalling inhibition has been utilised in the translation from mouse to human organoid cultures in tissues such as the liver, colon and stomach[120,242,243]. Addition of TGFβ inhibitor (TGFβi), A83-01 to the culture medium (Table 3.1) led to improved organoid generation with organoids forming hollow transparent spheres (healthy organoids) that could be passaged (Fig. 3.2). In mPO +TGFβi (Table 3.1; media 2) culture media, hPOs could be expanded to an average of 4.6 passages (Fig. 3.3), but the organoids lost their healthy phenotype as early as passage 4 (Fig. 3.2). Furthermore, Wnt condition media (Wnt3A-CM), to further activate the Wnt pathway, and PGE2, used in human gastric organoids, were added to the culture media[242] (Table 3.1; media 5). Media 5 reflected the culture media used by Broutier *et al.*[123] and Boj *et al.*[131] and generated similar expansion results to media 2 and did not confer a significant advantage (data not shown). Furthermore, Forskolin (FSK) works to increase cyclic AMP levels by activating adenyl cyclase and has been shown to increase

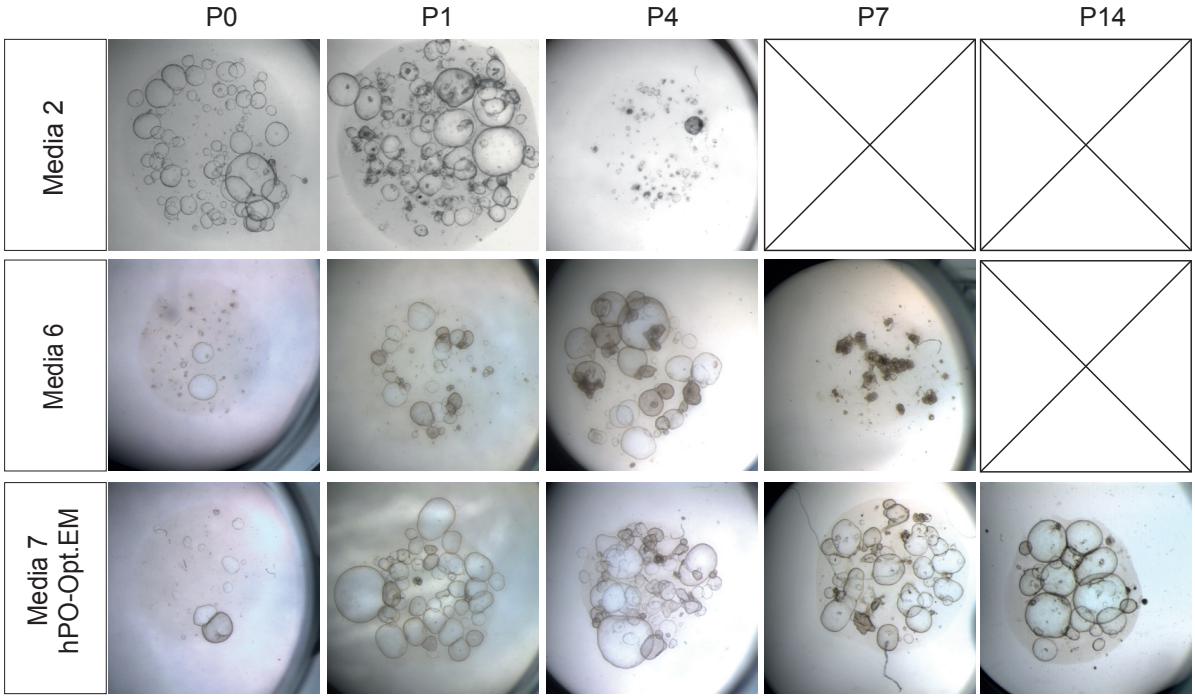

Figure 3.2 Optimised culture media allows expansion of hPOs. Brightfield images demonstrating hPOs expanded in media 2, 6 and 7 (hPO-Opt.EM). hPOs expanded in Media 2 (top row) began deteriorating as early as passage 4. Media 6 (middle row) showed significant improvement in expansion, but organoids deteriorated at passage 7. hPO-Opt.EM media (bottom row) allowed expansion of hPOs beyond passage 10, while also maintaining a healthy phenotype. (Images shown at 1x magnification. Data obtained in collaboration with Daisy Harrison.)

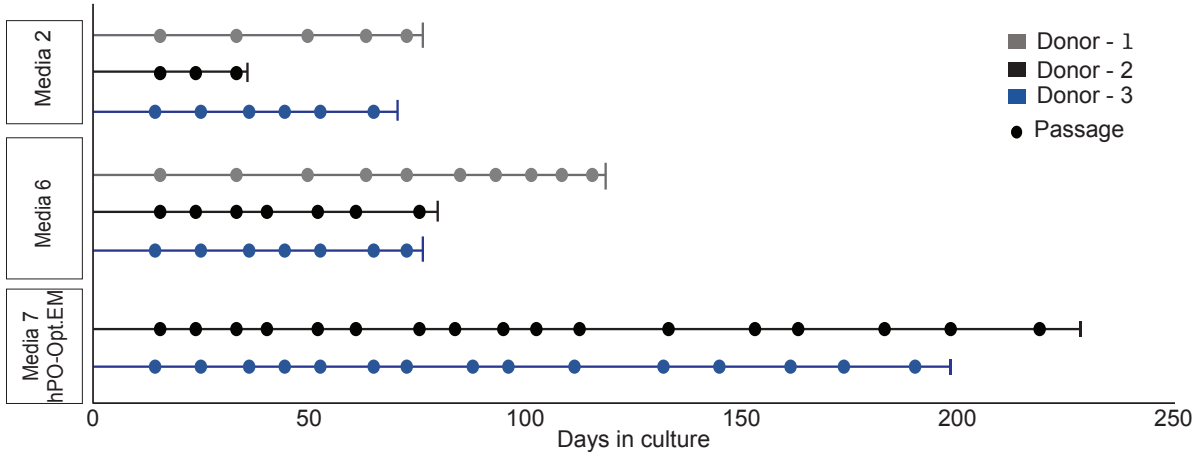

Figure 3.3 hPOs can be expanded long-term in optimised condition media. Graph demonstrates number of passages over time in culture in the different media (2,6, and 7). (n=3 independent donors; circle=passage; capped lines indicate deteriorated cultures). Testing of different media was performed by Daisy Harrison.

Wnt signalling by inactivating glycogen synthase 3 beta (GSK3β)[244] (Fig. 1.3). Notably, FSK was necessary for the long-term expansion of human liver organoids[120]. Addition of FSK to the media (Table 3.1; media 6) resulted in an improved culture time up to passage 8 (Fig. 3.2). In order to investigate whether the serum component of Wnt conditioned media had a negative effect on hPO growth, foetal bovine serum (FBS) was added instead of Wnt3A-CM (Table 3.1; media 4). This resulted in an average expansion of 3 passages which was similar expansion capacity to media 3 and worse than media 2. Therefore, Wnt3A-CM was removed from the media composition resulting in a medium which allowed increased expansion of hPOs. Furthermore, I suggested the use of 10% Rspo1 rather than 5% in Daisy's optimised medium, seeing that other human organoid lines in our lab utilised this percentage of Rspo1. This resulted in the final optimised media, hPO-Opt.EM (Table 3.1; media 7) which led to an improved expansion capacity of 16 passages (Fig. 3.3) with organoids maintaining their healthy morphology throughout expansion (Fig. 3.2). This optimised serum-free culture medium (hPO-Opt.EM), generated by Daisy Harrison, facilitates long-term expansion of hPOs beyond 180 days in culture compared with previous iterations and previously published protocols[121,123,131] (Fig. 3.3). I was able to utilise this optimised medium and contributed to its establishment by utilising it to generate multiple donor-derived hPO lines to demonstrate its efficiency among different donors and characterise the expansion kinetics of hPOs, as demonstrated in the following section.

3.2.2 Long-term *in vitro* expansion of hPOs

Ductal fragments can be isolated either by handpicking of ducts or by filtration of the digested tissue (refer to section 2.2.1). Handpicking of ducts results in a purer population of ductal organoid structures at P0; however, filtration is substantially faster (handpicking >30min vs. filtration ~5min) and yields more organoids (Fig. 3.4). Regardless of the ductal enrichment technique used, utilising hPO-Opt.EM, hPO derivation efficiency was greater than 90% (Appx. Table 1) and once seeded, ductal cells begin to proliferate and rapidly form cystic organoids by day 7, which are ready to passage by day 14-21 at a split ratio of (1:4-1:6) (Fig. 3.1b). Passaging of organoids was performed when hPOs reached confluency by mechanically dissociating organoids into ductal fragments and reseeding those fragments into fresh BME 2 (refer to section 2.2.1). Following dissociation, each fragment is capable of generating a new organoid (Fig. 3.5a) and the process is repeated to generate larger quantities of cells.

In this project, using the optimised medium, I derived lines from 27 out of 29 healthy human donors (i.e., donors without any known pancreatic disease) (Appx. Table 1) all of which could be robustly expanded up to 6 months while maintaining healthy spherical morphology (Fig. 3.5b). Donors had an age range of 24-79 years while successful hPO establishment was independent of the donor's sex, age or BMI (Appx. Table 1). Unsuccessful hPO isolations were due to technical reasons such as student training.

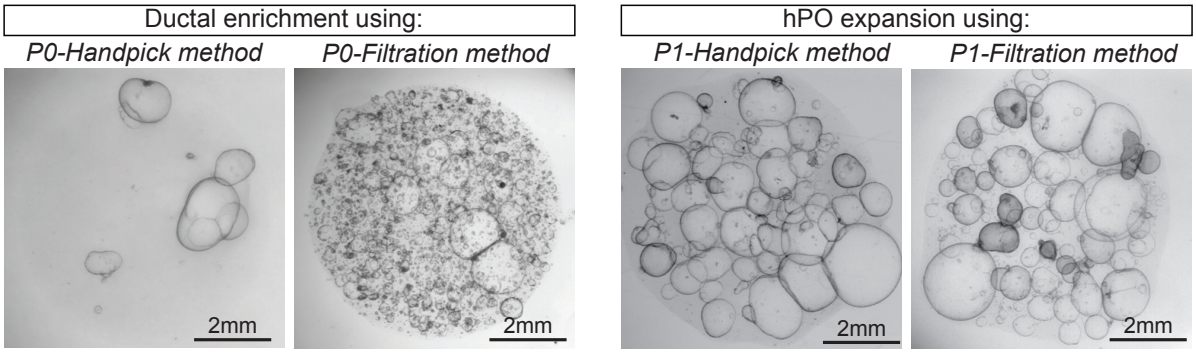

Figure 3.4 hPOs can be isolated using ductal enrichment via handpicking or filtration. Comparison of P0 (left images) and P1 (right images) cultures following ductal enrichment by handpicking (left) or filtration (right) (n = 5 independent donors)

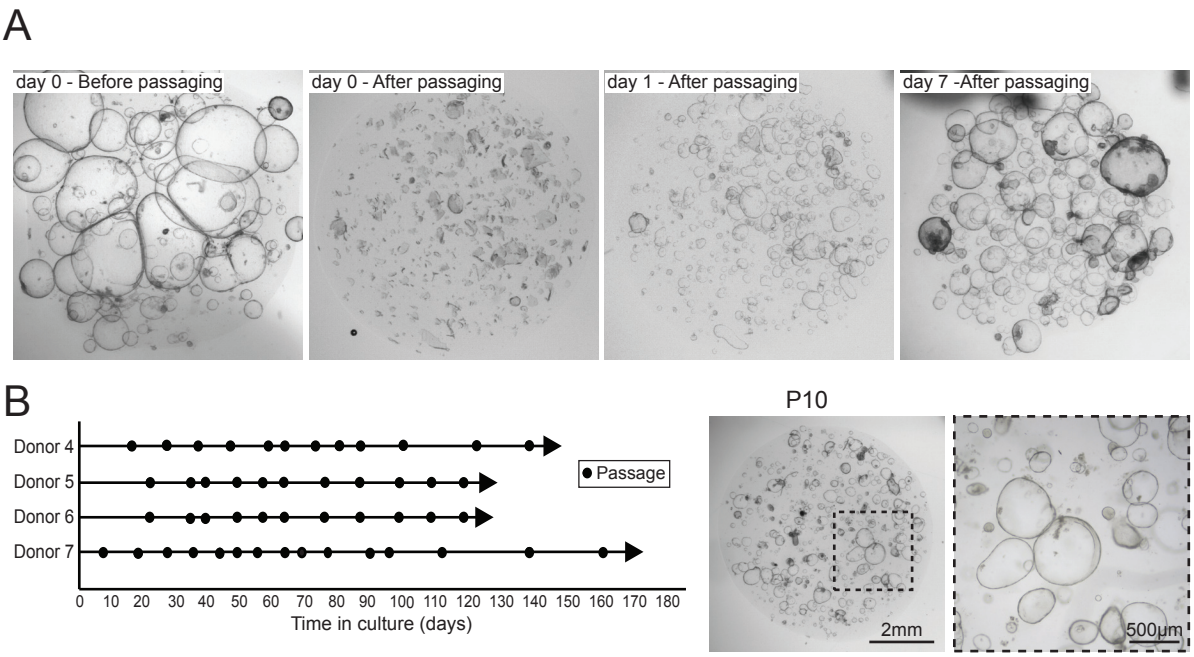

Figure 3.5 hPOs maintain expansion capacity and fragment reformation across multiple donors. (**A**) Following mechanical dissociation all organoid fragments are capable of forming a new organoid (passage) (**B**) hPOs can be passaged over many months in hPO-Opt.EM across multiple donors in a robust manner. (n = 4 independent donors; circle = passage)

While this project was ongoing, a report by Loomans *et al.*[132], described culture conditions that support hPO generation with a similar efficiency to hPO-Opt.EM. Comparison of the two media in 4 matched donors showed that duct to organoid formation efficiency was indeed similar within the two systems (Fig. 3.6a). However, hPOs cultured in the Loomans *et al.* medium begin deteriorating at passage 3 (Fig. 3.6b) and can be expanded to a maximum of 4 passages; therefore, long-term expansion is not sustained in this medium (Fig. 3.6c).

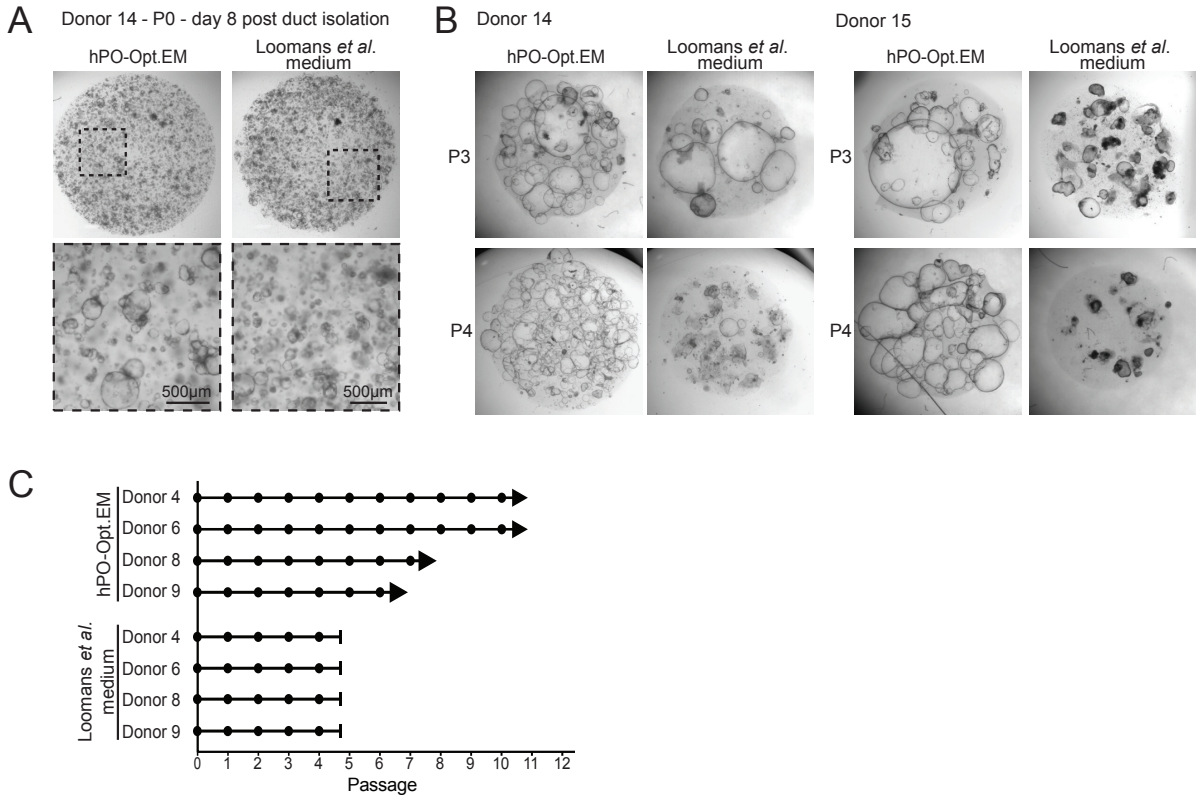

Figure 3.6 hPOs can be expanded more efficiently in hPO- Opt. EM when compared to published media. (**A-C**) Comparison of the hPO-Opt.EM medium to the hPO medium published by Loomans and colleagues during the course of this project[132]. Although both media enable the initial generation of hPOs, the hPO-Opt.EM medium supports long-term culture to a much greater extent than Loomans *et al.* medium[132]. (**A-B**) Representative images of hPO cultures derived from fresh pancreas tissue using hPO-Opt.EM medium or Loomans *et al.* medium[132] at (**A**) passage 0 (P0, 8-days post derivation; magnification in lower panels; n=3), or (**B**) at Passage 3 (top) and Passage 4 (bottom) in two independent donors. (**C**) Graph shows the expansion potential of hPOs cultured with the hPO-Opt.EM medium or the medium published by Loomans *et al.* medium[132] (arrows indicate ongoing cultures, capped lines indicate cultures that deteriorated; n=4 independent donors; work carried out in collaboration with Dr. Gianmarco Mastrogiovanni).

Contrastingly, the optimised culture system described in this project allows expansion of hPOs with high efficiency, exhibiting an initial doubling time of 78 hours which slows to 177 hours at later passages (Fig. 3.7a). Culture of hPOs in the optimised media maintains the pool of cells undergoing active proliferation as demonstrated by expression of proliferation marker Ki67 (Fig. 3.7b) with the proliferation status of hPOs remaining largely unchanged (not significantly different) until late passages (P10). Furthermore, hPO-Opt.EM allows derivation of organoids both from ductal fragments as well as from dissociated single cell suspensions with an average colony formation efficiency (CFE) of 1.7% at early passages. The colony formation efficiency from single hPO cells does not significantly decrease during long-term culture (Fig. 3.7c), and therefore single cells can be isolated at both early and late passages and cultured to generate expandable cystic organoids. The ability to expand from single cells opens up opportunities for genetic studies as well as genetic manipulation of the cultures (further explored in Chapters 4 and 5 respectively).

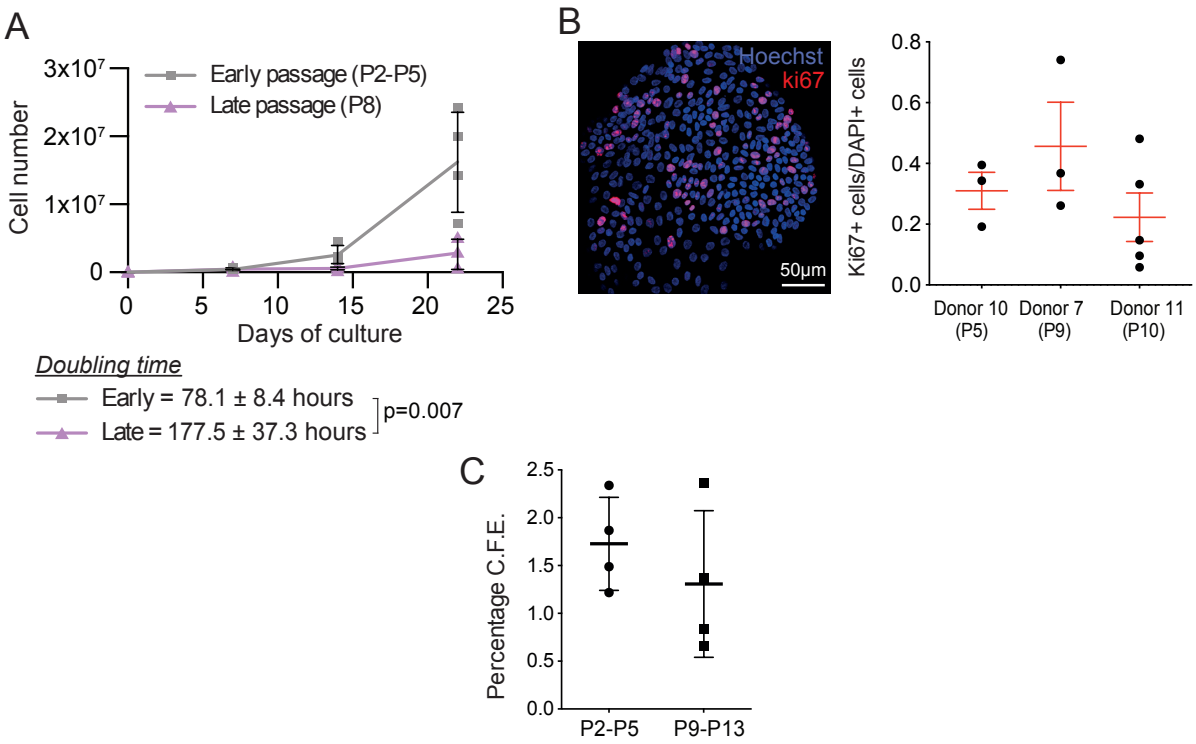

Figure 3.7 hPOs maintain doubling time, proliferation and colony formation efficiency over long term culture. (**A**)hPO growth curves indicate that hPOs expand exponentially even at late passages. Graph represents independent donors (early passage, grey n = 4; late passage, purple, n = 3) (**B**) Ki67 immunostaining demonstrates that hPOs retain pool of proliferative cells over time in culture (n>3 organoids). (**C**)The hPO culture system supports expansion from dissociated single cell suspensions, hPO cultures derived from single cells exhibit similar colony formation efficiency at early as well as late passages (n=4 independent donors). Data presented as mean± SD for **A, C** and mean ± SEM for **B**. Differences between groups for **A** and **C** were tested using a two-tailed t-test and one-way repeated measures ANOVA followed by Tukey's honestly significant difference (HSD)test for **B**. Significant differences are marked by asterisks. (Doubling time and C.F.E. data obtained in collaboration with Dr. Gianmarco Mastrogiovanni)

3.2.3 Derivation and expansion of hPOs from cryopreserved pancreas

A key benefit of many recent organoid systems is the ability to cryopreserve organoids at early passages and then thaw at later timepoints to re-establish cultures. This is key for establishing large organoid biobanks which encompass lines from hundreds of donors that can facilitate both HLA matching as well as shipping tissue to laboratories worldwide. Cryopreservation of organoids has been demonstrated in other types of organoid systems[120,121]. Unsurprisingly, hPOs can be cryopreserved by fragmenting-as in the protocol for passaging-, incubating them in a DMSO-based freezing solution followed by slow rate freezing. The hPOs can be thawed and the culture can be re-established and expanded as normal (Fig. 3.8a), thus allowing maintenance of multiple donor lines at various stages of expansion.

The ability to cryopreserve hPO cultures enables the sharing and storage of resources, yet it still requires hPO derivation to be conducted as quickly as possible following sample collection. By contrast, cryo-banking of primary tissue would further facilitate the workflow for global collection and subsequent distribution of tissue world-wide.

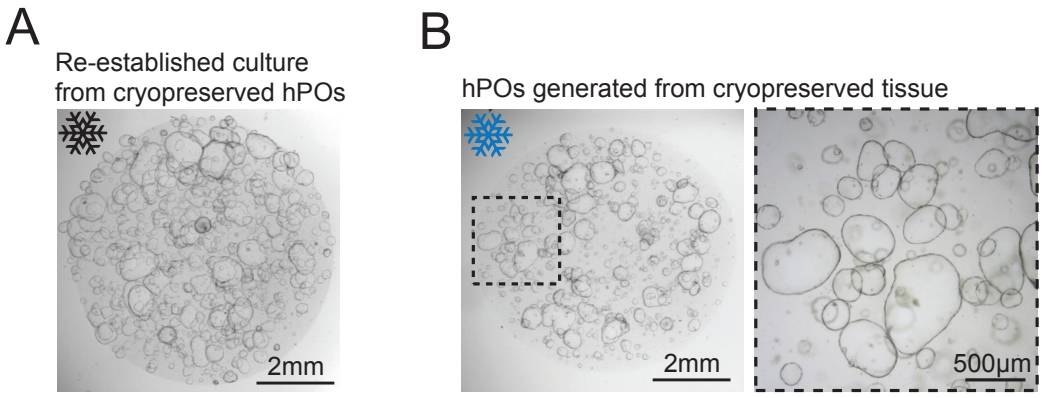

Figure 3.8 hPOs can be established from cryopreserved hPOs and primary pancreatic tissue. (**A**) hPO cultures can be cryopreserved as hPO fragments as described in section 2.2.3 and re-stablished by embedding the fragments in BME 2 and overlaid with hPO-Opt.EM. Representative image of a P4 culture obtained from a hPO culture cryopreserved at P0 and kept in liquid N2 for 3 months (n=9 independent donors). (**B**) hPOs can be generated from cryopreserved primary human pancreatic tissue (see section 2.2.2). Image shows hPOs derived from a pancreas tissue that had been cryopreserved for 3 weeks (n=3 independent donors).

Furthermore, experiments which utilise primary tissue can be initiated using retrospectively collected tissue. Hence, the ability to generate hPO cultures from cryopreserved tissue was tested. First, cryopreservation of the fresh tissue and subsequent organoid derivation from the frozen sample was optimised. Prior to cryopreservation, the primary tissue was mechanically minced to fine pieces utilising a tissue dissociator so that upon reconstitution in the freezing medium the tissue would be more uniformly suspended and cool in a more homogeneous manner than one large piece of tissue. The tissue was then stored at -80°C for 3 weeks. Upon thawing, tissue fragments were washed to remove any remaining freezing medium and subsequent derivation was performed as with fresh tissue. Organoid derivation efficiency was on average 10-fold lower from cryopreserved tissue compared with fresh tissue (Fig. 3.9a,b). However, in all cases, I was able to successfully generate hPOs from cryopreserved samples (Fig. 3.8b, Fig. 3.9a). hPOs generated from cryopreserved tissue displayed similar expansion efficiencies as cultures derived from freshly isolated pancreases (Fig. 3.9c). Using this methodology, donor material can be collected, cryopreserved and transferred to a recipient laboratory for derivation without time restrictions.

3.2.4 Characterisation of hPOs histology and markers

Pancreatic ducts are single cell-layered structures that are responsible for the collection and transfer of digestive enzymes produced by acinar cells to the duodenum. Smaller intercalated (or intralobular) ductules adopt a simple cuboidal epithelial structure and as the ducts become larger and are found interlobularly, the morphology becomes more columnar[2] (Fig. 1.1).

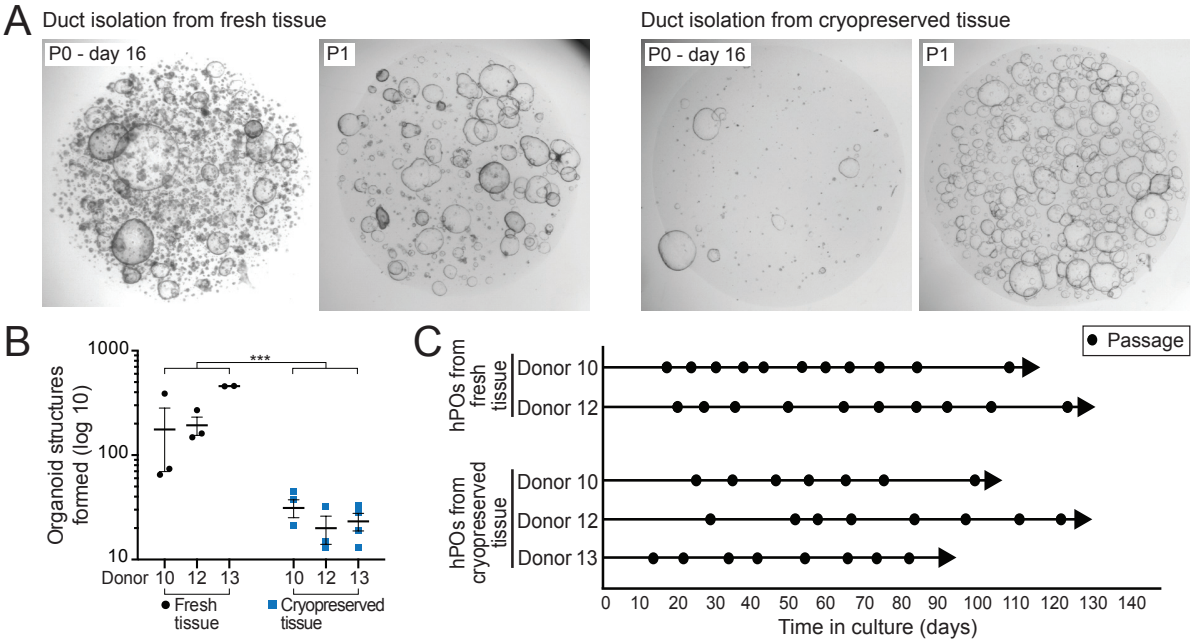

Figure 3.9 hPOs from cryopreserved tissue demonstrate lower isolation efficiency but similar expansion rates. (**A**) Organoid cultures derived from fresh tissue (left) or tissue cryopreserved at the time of collection (right). The organoid formation efficiency from cryopreserved tissue was reduced, yet in all cases, cultures exhibited similar expansion rate to hPOs derived from fresh tissue. Experiments were performed in n=3 independent donors, with similar outcomes. Representative images are shown. (**B**) Organoid formation from fresh tissue is more efficient than from cryopreserved tissue, the number of organoids formed following the isolation of ductal fragments from either fresh tissue (253 ± 58 organoids; black circles) or cryopreserved tissue (25 ± 3 organoids; blue squares) is shown. Ductal fragments were seeded in a 50µl BME 2 drop and quantified at P0. Data presented as mean ± SEM. Differences were tested by two-tailed t-test. Significant differences are marked by asterisks: *** $p \leq 0.001$ (**C**) hPOs derived from fresh or cryopreserved tissue expand at similar rates (circle=passage, arrows indicate ongoing or frozen cultures).

hPOs have a single cell structure organised as simple cuboidal or columnar epithelium recapitulating the architecture of the parental tissue, while also maintaining this morphology throughout long-term culture (Fig. 3.10a). Maintenance of apico-basal polarity is crucial for both tissue integrity as well as cellular functions such as protein transport, while loss of polarity is phenotypically observed in the transition to a cancerous state[245]. hPOs generate a lumen and demonstrate epithelial polarisation similar to the tissue of origin with polarisation of actin on the luminal (apical) side (Fig. 3.10b), similar to what has been demonstrated for human liver organoids[120].

In order to understand the identity of hPOs and whether the cells maintain the identity of the parental tissue, I carried out mRNA expression comparing hPOs with primary tissue. Comparison between hPOs and bulk pancreas tissue would have been inappropriate since the hPOs are ductal cell derived while the majority of pancreas parenchyma is composed of acinar cells. In order to collect the appropriate tissue type, I isolated the main pancreatic duct (as detailed in section 2.1.2), cleaned it of surrounding acinar tissue (Fig. 3.11) and froze it for subsequent RNA extraction.

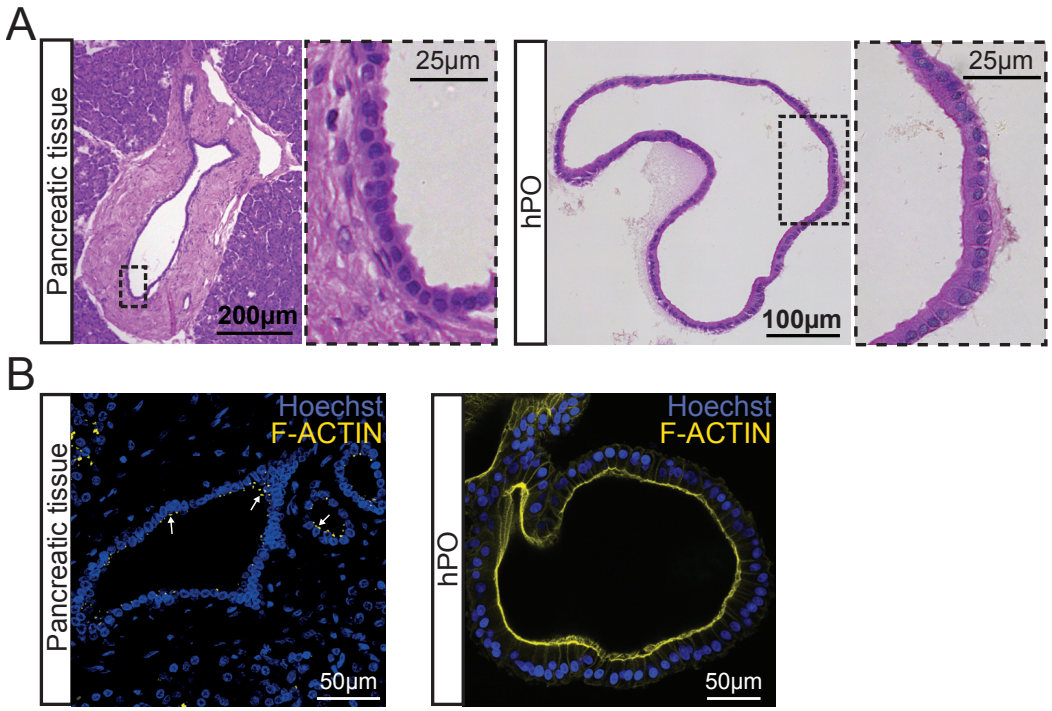

Figure 3.10 hPOs retain ductal architecture during *in vitro* culture and expand as a single cell-layer epithelium of ductal cells. (**A**)Representative images of H&E staining of human pancreatic ductal tissue and hPOs. Note that hPOs (right) expanded in culture retain the single-cell morphology exhibited by the pancreatic ductal tissue *in vivo* (left) (n = 6 independent donors). (**B**) Representative immunofluorescence staining of F-ACTIN (yellow) demonstrates that hPOs (right) maintain the epithelial cell polarity typical of ductal tissue (left) (nuclei counterstained with Hoechst, blue) (n = 6 independent donors)

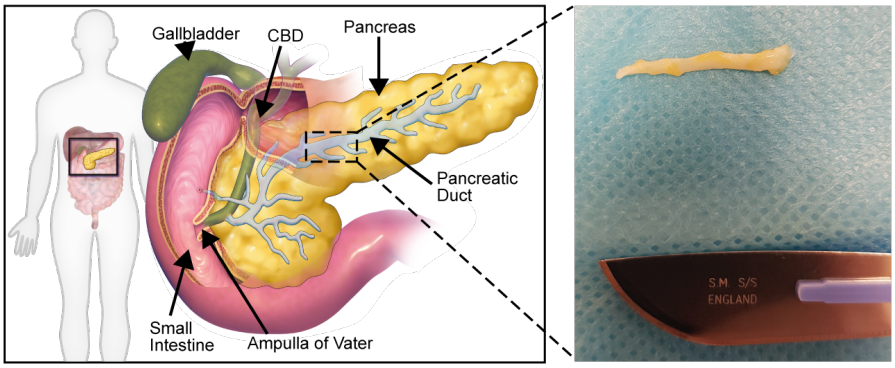

Figure 3.11 Obtaining a biopsy of true pancreatic duct from deceased donor pancreases. In order to achieve this, pancreases that were allocated for research were used and were dissected in our laboratory. The common bile duct (CBD) was separated from surrounding tissue and followed towards the ampulla of Vater where it connects to the primary pancreatic duct. The primary pancreatic duct was then separated from surrounding tissue and a segment was isolated. Image adapted from Blausen Medican Library.[12]

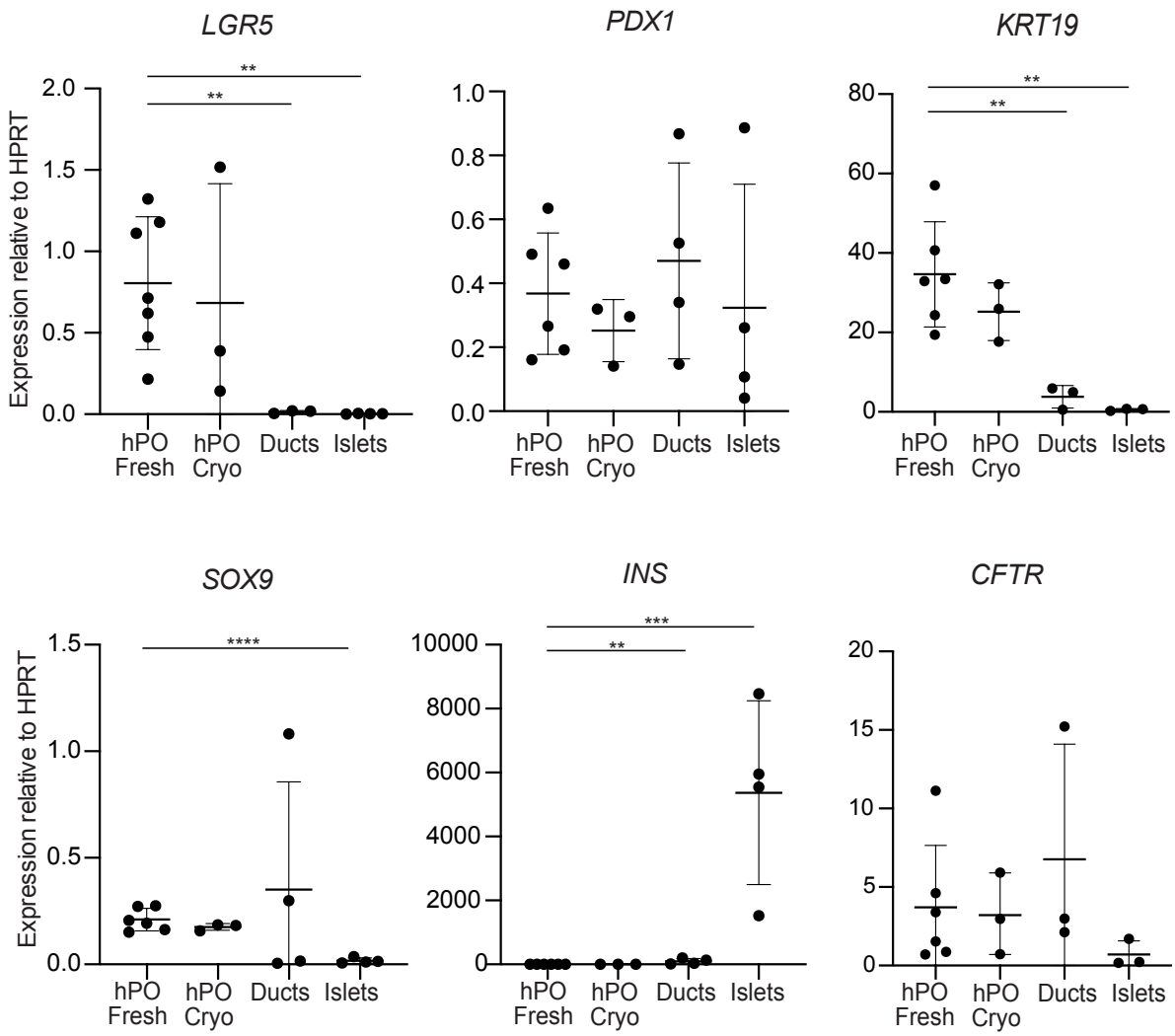

Figure 3.12 mRNA analysis of key markers of stem cell biology and ductal epithelium. mRNA expression analysis of genes involved in stem cell biology (*LGR5*), pancreatic fate (*PDX1*), ductal fate (*SOX9* and *KRT19*), β-cell function (*INS*) and ductal function (*CFTR*) in hPOs derived from fresh tissue (hPO Fresh, n ≥ 6), cryopreserved tissue (hPO Cryo, n = 3), isolated primary ducts (n = 3-4) and isolated islets (n = 4) Each dot represent an independent donor. Data presented as mean ± SEM. Differences were tested by two-tailed t-test. Significant differences are marked by asterisks: * p ≤ 0.05, ** p ≤ 0.01, *** p ≤ 0.001, **** p ≤ 0.0001

Furthermore, in order to assess whether hPOs obtain an endocrine identity as a result of culture, or whether endocrine cells are propagated in this culture system, islets were also collected for RNA analysis. Islets were obtained from the Scottish National Blood Transfusion Service (SNBTS) Islet Isolation Centre following allocation to research; these islets are initially isolated for the purpose of transplantation into diabetic patients and are therefore a very pure population. mRNA expression analysis of hPOs (derived from either fresh or cryopreserved tissue), isolated primary ducts and isolated islets (Fig. 3.12) reveals that hPOs express increased levels of the adult stem cell marker *LGR5*[246]. hPOs, isolated ducts and islets all express similar levels of the pancreatic progenitor and beta-cell marker

PDX1. Contrastingly, hPOs express increased levels of ductal markers *KRT19* and *SOX9*, when compared to isolated islets (Fig. 3.12). However, while difference of expression of *SOX9* is not statistically significant between hPOs and isolated ducts, hPOs retain higher levels of *KRT19* expression when compared to isolated ducts (Fig. 3.12). This may be due to KRT19+ cells being favourably expanded in the hPO-Opt.EM media or due to hPOs being a highly pure population of ductal cells. These findings suggest hPOs maintain a pancreatic ductal identity during *in vitro* culture. This is further supported as hPOs and isolated ducts express significantly less insulin mRNA than islets (Fig. 3.12). It should be noted that some insulin expression was detected in the ductal preparation. It is hypothesised that this is likely due to an artefact of the isolation method used for primary ducts, which although enriches for ductal cells, may also include other contaminating acinar and endocrine tissue. Furthermore, ductal cells in the pancreas secrete bicarbonate and chloride ions into the lumen, a process largely governed by channels such as CFTR[17](Fig. 1.1). hPOs show expression of *CFTR* which is similar to expression levels in isolated ducts. However, although numerically higher, *CFTR* expression was not significantly different between hPOs and islets (Fig. 3.12).

Furthermore, I carried out immunofluorescent staining of hPOs and primary pancreas tissue which demonstrated that hPOs maintain expression of PDX1 (pancreas marker) as well as KRT19, SOX9, EpCAM and HNF1β (ductal markers) at the protein level during long term culture (Fig. 3.13, Supp Fig. 1). These markers are homogeneously expressed among all cells of the organoids while expression is maintained throughout long-term culture. In primary pancreas tissue, ductal cells express KRT19 in a homogeneous manner while PDX1 is expressed by both ductal and non-ductal cells and SOX9 expression is restricted to KRT19+ cells confirming that hPOs preserve ductal identity (Fig. 3.13). Of note, similar expression patterns and tissue architecture were observed from hPOs derived from cryopreserved tissue as compared to hPOs derived from freshly isolated tissue from the same donor (Figs. 3.12. 3.14, 3.15).

Therefore, the chemically defined, optimised pancreas organoid medium developed in this project supports the long-term expansion of human pancreatic tissue as ductal epithelial cells from both fresh and cryopreserved donor tissue.

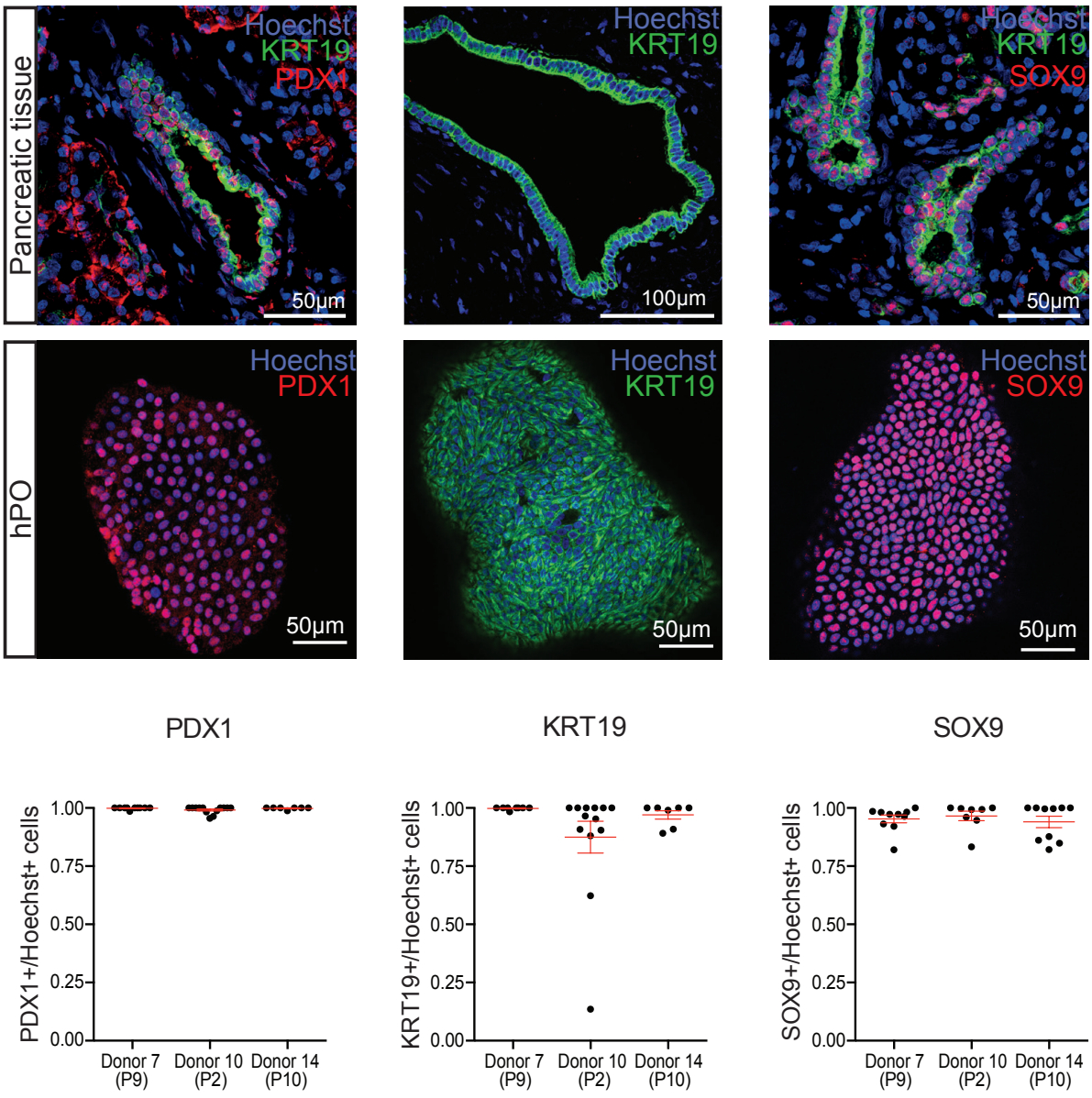

Figure 3.13 hPOs retain protein expression of key ductal epithelium markers. Immunofluorescence staining of primary tissue and hPOs (upper panel) and quantification of positive cells (lower panels) of nuclear PDX1 (red), cytoplasmic KRT19 (green) and nuclear SOX9 (red) protein in hPOs. Graphs represent number of positive cells for the corresponding marker (≥7 organoids counted per donor). Graphs show mean ± SEM. Differences were tested by one-way repeated measures ANOVA followed by Tukey's honestly significant difference (HSD) test. Significant differences are marked by asterisks.

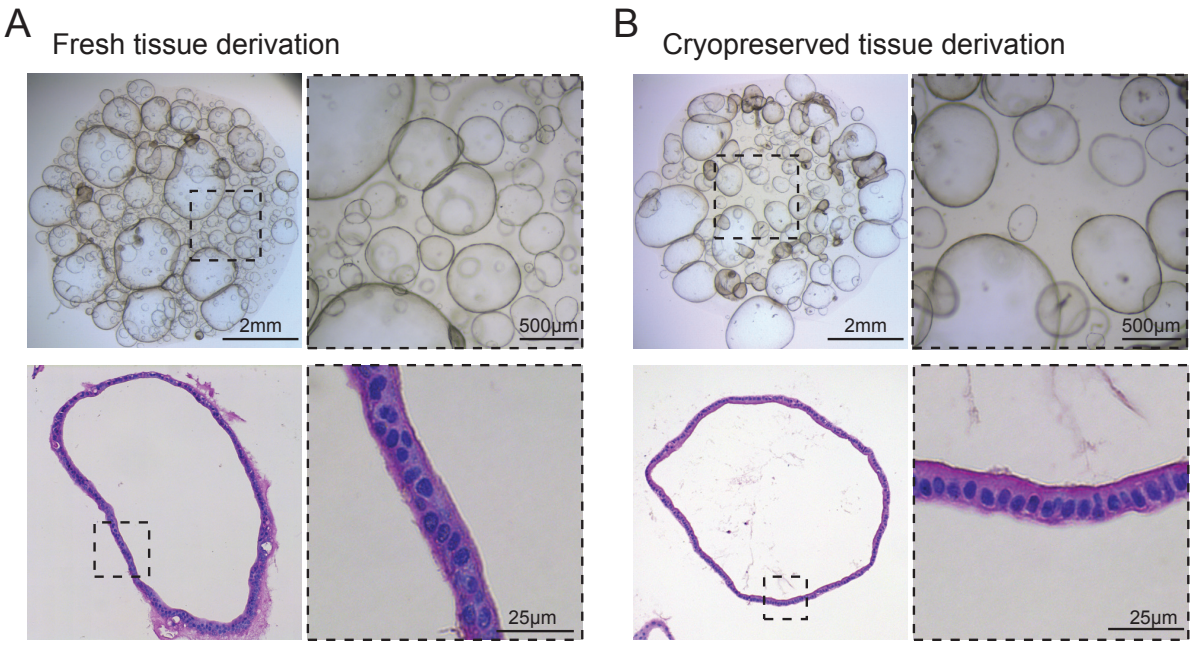

Figure 3.14 hPOs derived from fresh and cryopreserved samples expand as a single cell-layer epithelium of ductal cells and are phenotypically indistinguishable. Comparison of hPOs derived from (**A**) fresh tissue (collected at P3) or (**B**) cryopreserved tissue (collected at P2) from the same donor. Brightfield images (upper panels) indicate that hPO cultures expand efficiently as cystic structures regardless of whether the original tissue is fresh (**A**) or cryopreserved (**B**). H&E stainings reveal that hPOs derived from cryopreserved tissue maintain the single cell-layer epithelial architecture seen in the original donor tissue and in hPOs derived from fresh tissue (lower panels).

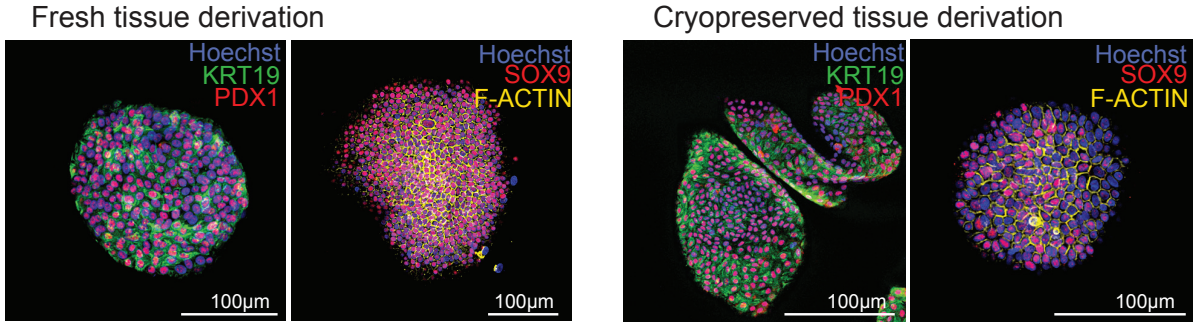

Figure 3.15 hPOs derived from fresh and cryopreserved samples show similar expression patterns of key ductal and pancreatic markers. Comparison of hPOs derived from fresh tissue (collected at P3) or cryopreserved tissue (collected at P2) from the same donor. Immunofluorescence stainings demonstrate that hPO cultures maintain ductal identity (KRT19 and SOX9), cellular polarisation (F-ACTIN) and express PDX1 regardless of the original tissue being fresh (left) or cryopreserved (right).

3.2.5 Culture of hPOs with a chemically defined, biomimetic ECM

A vital requirement for *in vitro* studies focused on understanding basic principles of human cellular biology (e.g. cell-cell communication, role of mechanical and physical forces or intracellular communication) as well as disease modelling and cell therapy is the ability to manipulate not only the cells and the medium, but also the ECM in which the cells are cultured. Furthermore, a requirement for a potential cell therapy is the ability to expand cells under GMP conditions. However, the majority of current organoid protocols use Matrigel and BME 2, which cannot be manipulated to change their chemical and/or physical properties (e.g. stiffness). Additionally, these matrices are not appropriate for clinical use due to their xenogeneic origin (Engelbreth–Holm–Swarm mouse sarcoma), which risks pathogenic contamination and immunogenicity complications, as well as batch-to-batch differences, hindering scalability and reproducibility[172]. Hence, in collaboration with a commercial partner, Cellendes, a chemically defined, adjustable, scalable and biomimetic hydrogel was developed in which hPOs could be established and expanded.

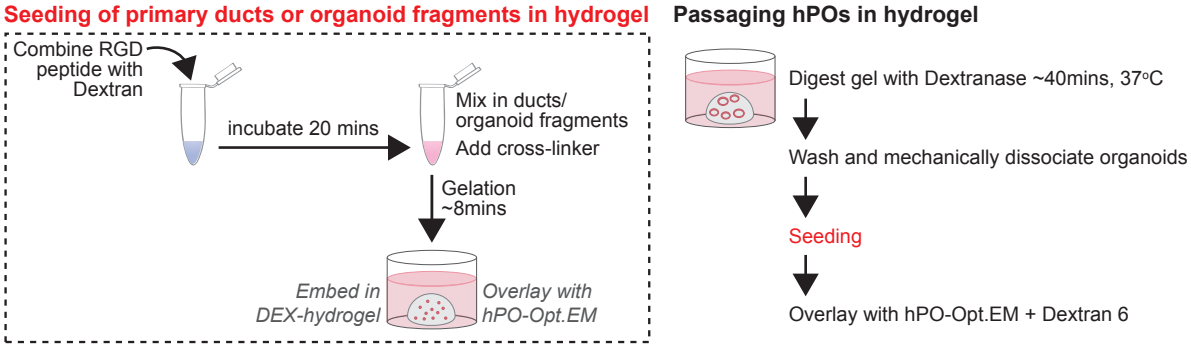

Figure 3.16 Novel protocol for the use of a chemically defined biomimetic hydrogel to culture hPOs. Schematic showing the workflow to use DEX-hydrogel as ECM when seeding ductal fragments for hPO culture initiation or organoid fragments during passaging (left panel). During passaging, dextranase is used to digest the hydrogel and Dextran 6 is added to the culture medium thereafter to prevent hydrogel breakdown (right panel), see section 2.4 for details.

In this project, through my collaboration with Cellendes, we found that dextran polymers modified with a peptide containing the RGD cell adhesion motif covalently crosslinked with hyaluronic acid in the presence of organoid fragments, in a cell-compatible chemical reaction, supported organoid formation and maintained the epithelial morphology of the organoids (Fig. 3.16). Hyaluronic acid was chosen as a crosslinker because it has been shown to support the undifferentiated state of human embryonic stem cells *in vitro*[247]. Importantly, this hydrogel (DEX-hydrogel) is amenable to digestion by Dextranase, which facilitates passaging and expansion of the hPOs (Fig. 3.16). I was able to isolate pancreatic ducts and seed them in DEX-hydrogel; culture with hPO-Opt.EM gave rise to hPO structures in a comparable manner to BME 2 (Fig. 3.17a).

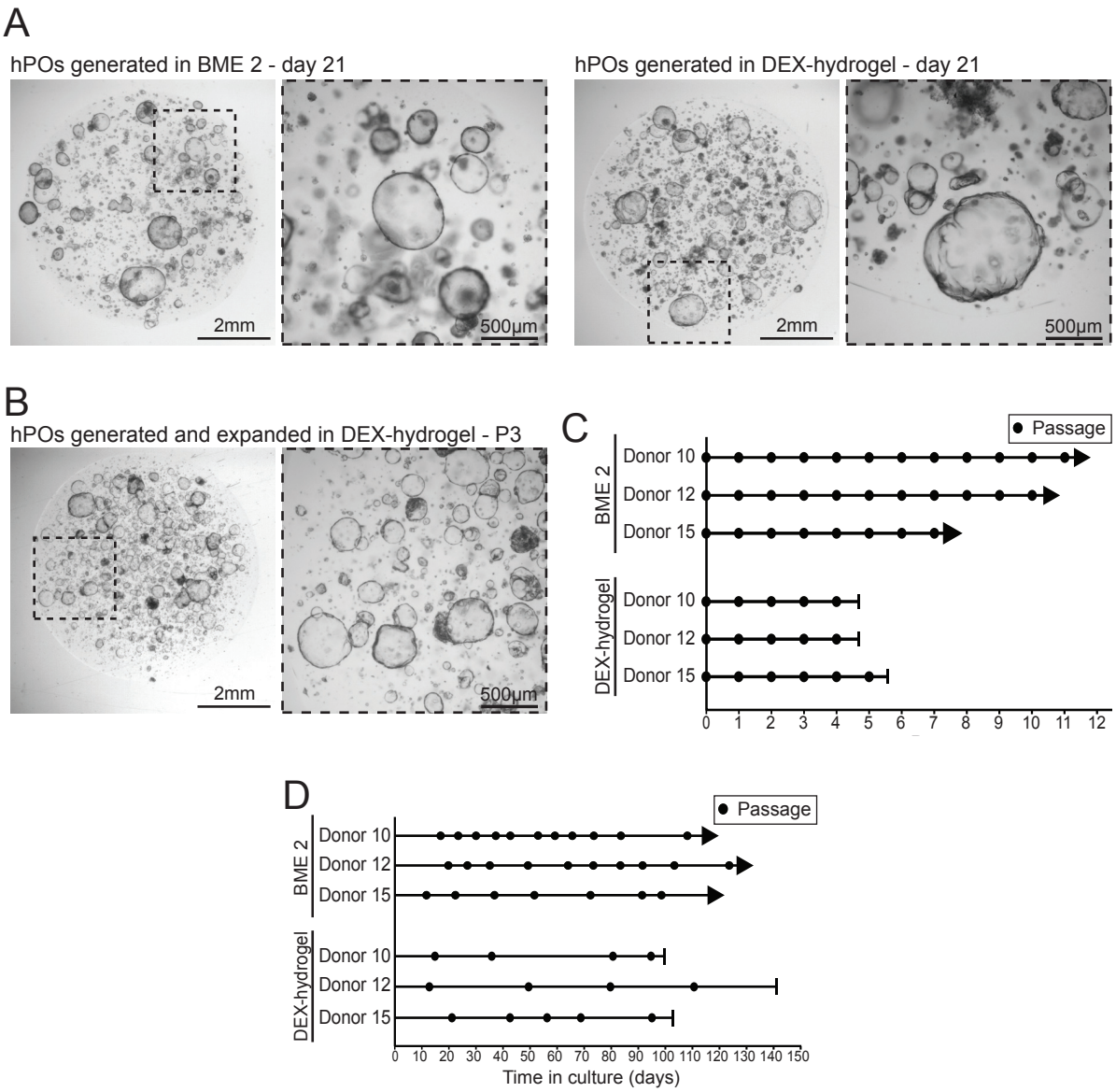

Figure 3.17 A chemically defined Dextran-based hydrogel supports hPO growth. (**A**)Representative images of hPO cultures derived from freshly isolated human pancreas tissue and initiated in BME 2 (left) or DEX-hydrogel (right). Pictures were taken 21 days after seeding. (**B-D**) hPOs can be passaged up to passage 4 when cultured in DEX-hydrogel. Note that, hPOs in DEX-hydrogel expand to a lesser extent than those with BME 2 and cultures begin to deteriorate after P4. (**B**) Representative images of hPOs in DEX-hydrogel at P3 (n = 3). (**C-D**) Graph represents the expansion potential of independent donors cultured with BME 2 or DEX-hydrogel. (circle = passage, arrows indicate ongoing cultures, capped lines indicate cultures that deteriorated)

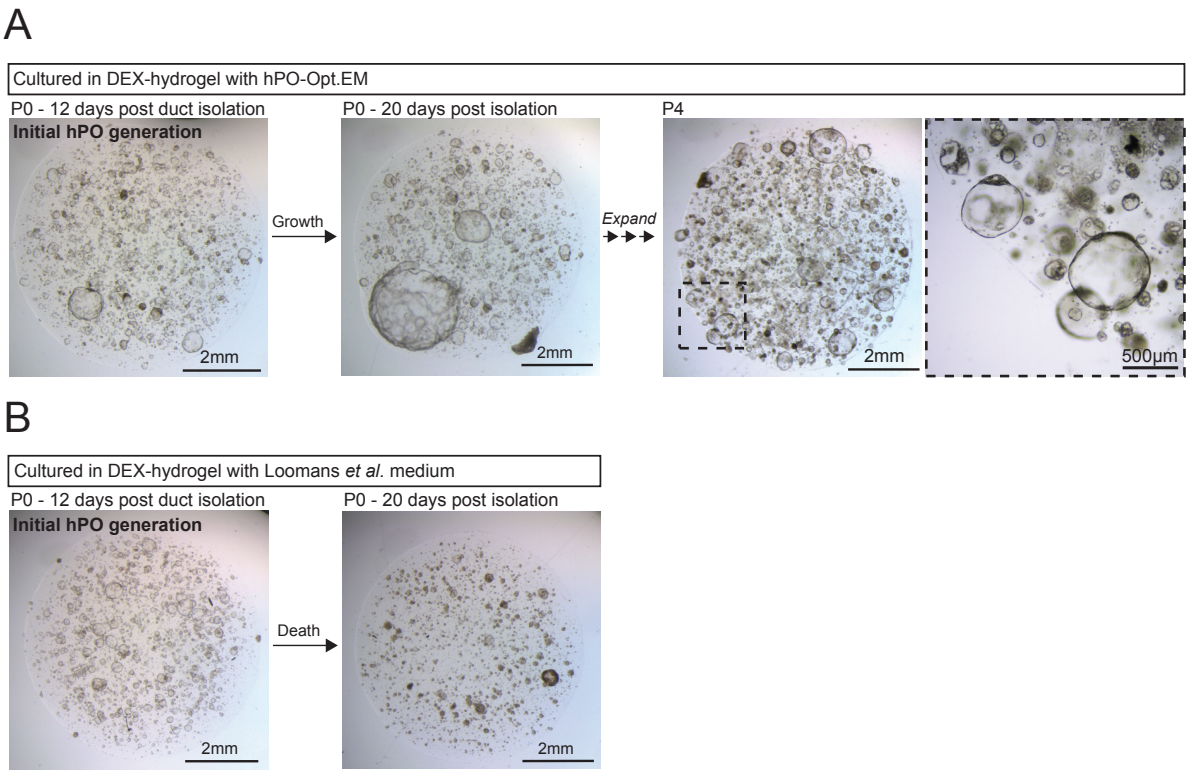

Figure 3.18 hPOs cultured in optimised hPO-Opt.EM medium grow in a chemically defined hydrogel. (**A-B**) Comparison of hPO cultures in the chemically defined dextran-based hydrogel (DEX-hydrogel) initiated from freshly isolated ducts overlaid with either (**A**) hPO-Opt.EM medium or (**B**) the medium published by Loomans and colleagues[132]. Both media support the formation of cystic structures, however, organoids in Loomans *et al.* medium[132] quickly deteriorated and could not be passaged. In contrast, organoids formed with the optimised hPO-EM medium could undergo expansion up to P4, after which they deteriorated. Experiments performed in n=1 donors.

hPOs could be expanded and several passages could be performed (up to P4) in the DEX-hydrogel culture system (Fig. 3.17b,c), yet these organoids expand more slowly and can only be passaged at smaller ratios (1:2-1:3; Fig. 3.17d) when compared to BME 2 grown hPOs. Notably, this chemically defined DEX-hydrogel did not support expansion of hPOs when using a previously published medium by Loomans *et al.*[132], with initially formed organoids deteriorating 14 days after seeding and before the structures could be passaged (Fig. 3.18).

Characterisation of hPOs generated with either DEX-hydrogel or BME 2 showed that both ECMs supported hPO cultures that expressed similar levels of *PDX1* mRNA (Fig. 3.19). However, the expression of *KRT19* and *SOX9* mRNA in hPOs cultured with DEX-hydrogel was 2-fold lower than in hPOs grown in BME 2 (Fig. 3.19), potentially underlying the reduced expansion capacity seen with the DEX-hydrogel.

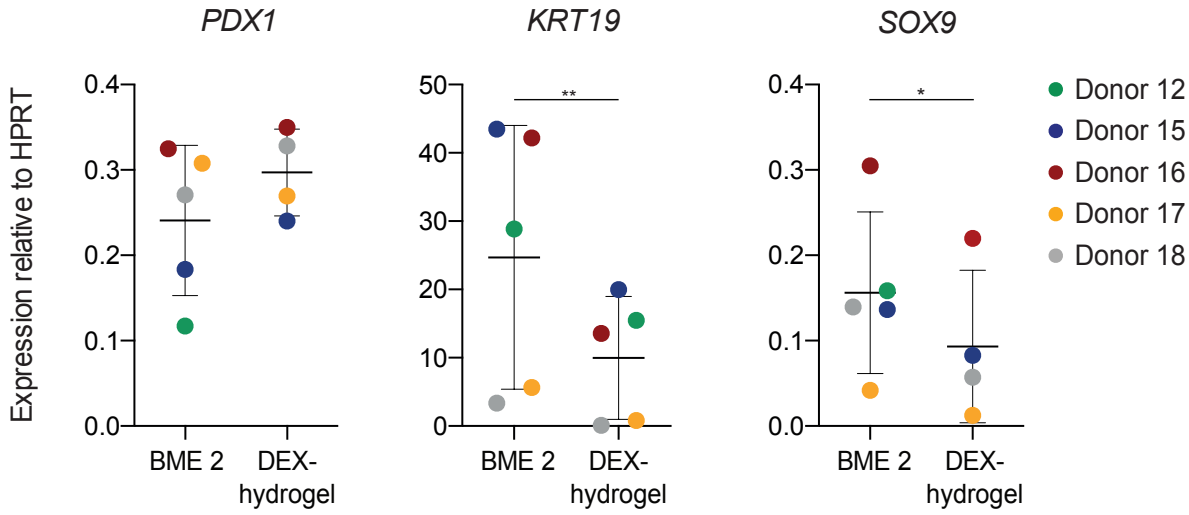

Figure 3.19 hPOs grown in DEX-hydrogel express key pancreatic and ductal markers at the mRNA level. mRNA expression analysis of hPO cultures (P1-P4) reveals that organoids grown with DEX-hydrogel retain the expression of ductal and pancreatic genes although *KRT19* and *SOX9* are at a lower level than those cultured with BME 2. Graphs show mean ± SD. Differences were tested by paired two-tailed t-test. Significant differences are marked by asterisks: *≤0.05, ** p ≤ 0.01

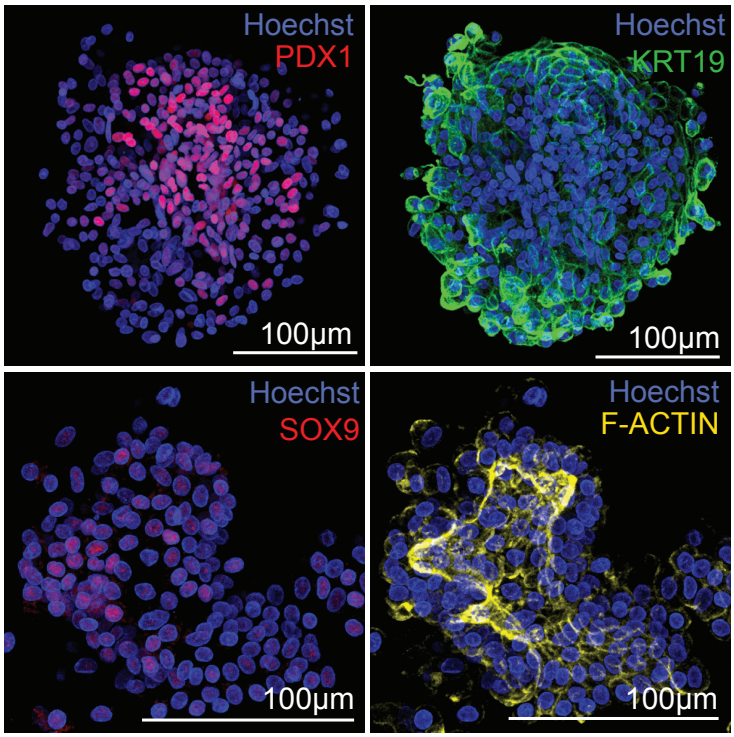

Figure 3.20 Immunofluorescent staining of DEX-hydrogel grown hPOs shows irregular expression pattern. Immunofluorescent staining of hPOs generated in DEX-hydrogel at passage 1. (PDX1-red; KRT19-green; SOX9-red; F-ACTIN- yellow; Nuclei were counterstained with Hoechst-blue. Experiments were performed in n=1 donors.

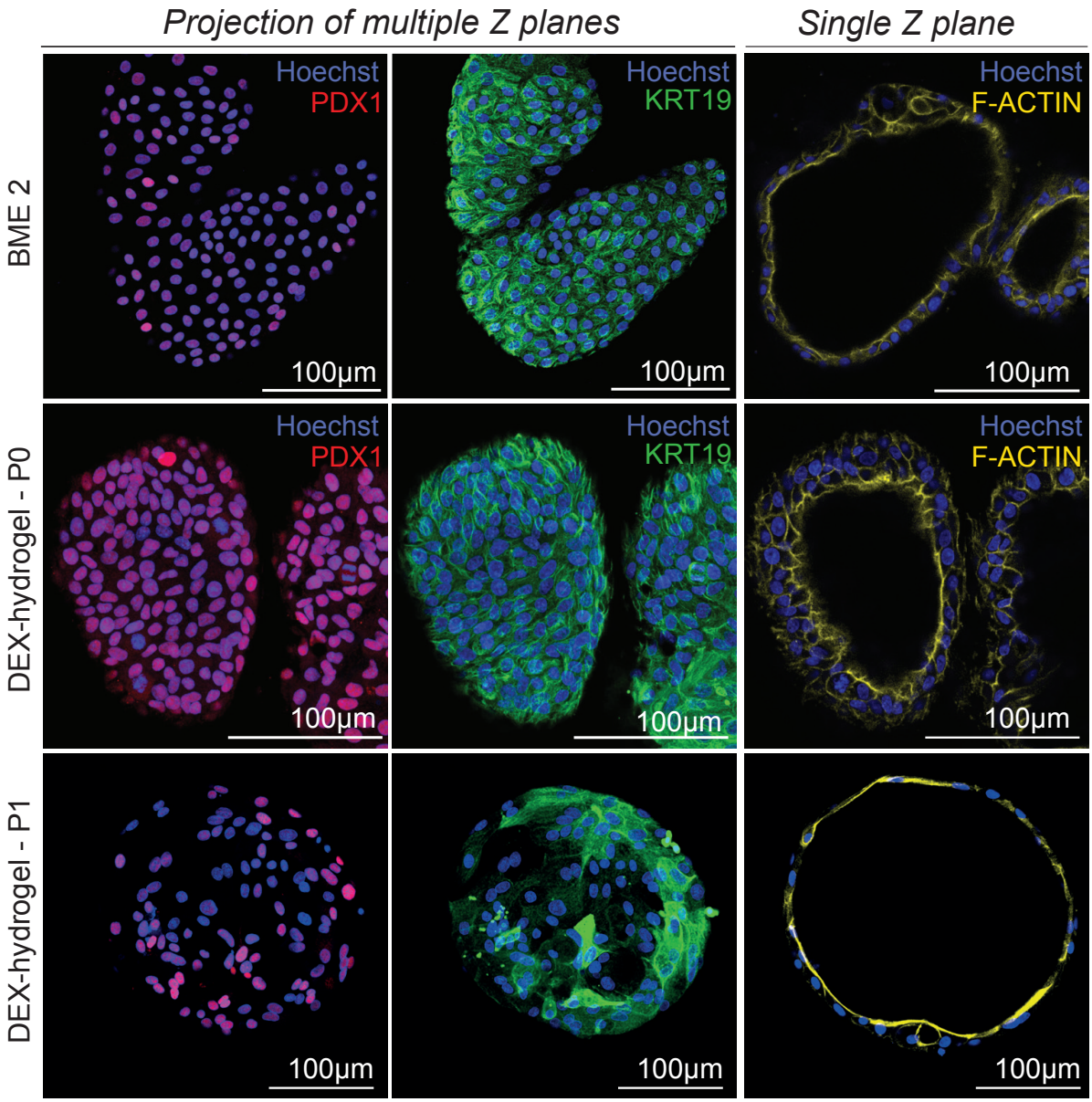

Figure 3.21 Immunofluorescence staining of DEX-hydrogel hPOs. Immunofluorescence of hPOs in DEX-hydrogel at passage 0 and 1 compared to hPOs generated in BME 2. (PDX1 - red; KRT19 - green; F-Actin - yellow; Nuclei were counterstained with Hoechst - blue). Experiments were performed in n=2 independent donors

Immunofluorescent staining using the original protocol (see section 2.9.3.1) which mimicked the one used for hPOs grown in BME 2 (i.e., removal of hPOs from the hydrogel followed by fixation) demonstrates that hPOs grown in DEX-hydrogel expressed PDX1, KRT19 and SOX9 at the protein level (Fig. 3.20). However, the expression pattern was notably different to that of hPOs grown in BME 2 (Fig. 3.13), with non-ubiquitous expression of the three markers and PDX1 localised in the centre of the organoids while KRT19 was expressed on the periphery of the organoids (Fig. 3.20). Furthermore, the structure of the organoids was severely affected with some loss of polarity as demonstrated by F-ACTIN staining (Fig. 3.20). This therefore raised the question of whether the irregular expression

pattern was an effect of expanding organoids in DEX-hydrogel or whether this was artefact of the staining procedure. Since DEX-hydrogel needed to be degraded through incubation with Dextranase, this meant that prior to fixation, the organoids spent a period of up to 40 min without being attached to an ECM. To test whether the staining protocol was causing this expression pattern observed, I fixed hPOs grown in DEX-hydrogel with formalin while still embedded in the hydrogel, after which the hydrogel was degraded with dextranase. This optimised protocol demonstrated that at P0, hPOs grown in DEX-hydrogel had a similar expression pattern of PDX1 and KRT19 protein with correct polarisation and epithelial arrangement (Fig. 3.21). While this was promising, even with the optimised staining protocol, hPOs grown in DEX-hydrogel demonstrated an irregular expression pattern of PDX1 and KRT19 with some cells having lost expression of either markers following 1 passage. While F-ACTIN remained polarised to the lumen, hPOs grown in hydrogel adopted a simple squamous epithelium contrasting the cuboidal or columnar epithelium of hPOs grown in BME 2 (Figs. 3.21, 3.10).

Optimisation of the chemically defined hydrogel culture system

When passaging hPOs grown in DEX-hydrogel, a necessary step is the degradation of the hydrogel by enzymatic digestion through incubation with Dextranase. hPOs in DEX-hydrogel are incubated with dextranase up to 1.5 hrs leaving them for a significant amount of time without attachment to an ECM. This may therefore have an additive effect on organoids with the accumulation of passages which may underlie the decreased expansion capacity of the DEX-hydrogel system. Furthermore, despite extensive washes post enzymatic incubation, minute amounts of dextranase carry over into the newly seeded wells. In order to combat unwanted digestion of the DEX-hydrogel, Dextran 6 is added into the expansion medium to act as a competitive inhibitor, with the medium refreshed every day for the first 3 days post passage. Nevertheless, the DEX-hydrogel can be degraded leading to increased adhesion of organoids to the plate and subsequent loss of the culture (Supp. Fig. 2). To combat this degradation hPOs were expanded and passaged in DEX-hydrogel without use of dextranase, as detailed in section 2.4.3. This led to an increase in expansion capacity allowing hPOs to reach passage 6 while maintaining ductal morphology (Fig. 3.22).

While my project progressed, Cellendes generated a new version of the hydrogel for further improvement of the hPO culture system. The RGD-binding motif used in DEX-hydrogel has been useful both in the culture of hPOs within the context of this project as well as other culture systems such as intestinal stem cell organoids[173]. RGD (Arginine-Glycine-Aspartate) is the amino acid sequence found within fibronectin and has been utilised to replace or mimic full-length fibronectin in synthetic ECMs[173,175]. However, organoid formation was only stimulated after addition of full-length laminin to the RGD based hydrogel[173]. Furthermore, in the culture system presented here, the DEX-hydrogel severely limits expansion of hPOs when compared to those expanded in BME 2. As a result, a new hydrogel was developed within this project which replaced RGD with the peptide GFOGER (referred to as GFOGER-hydrogel) which is found in collagen, a major component of Matrigel[172].

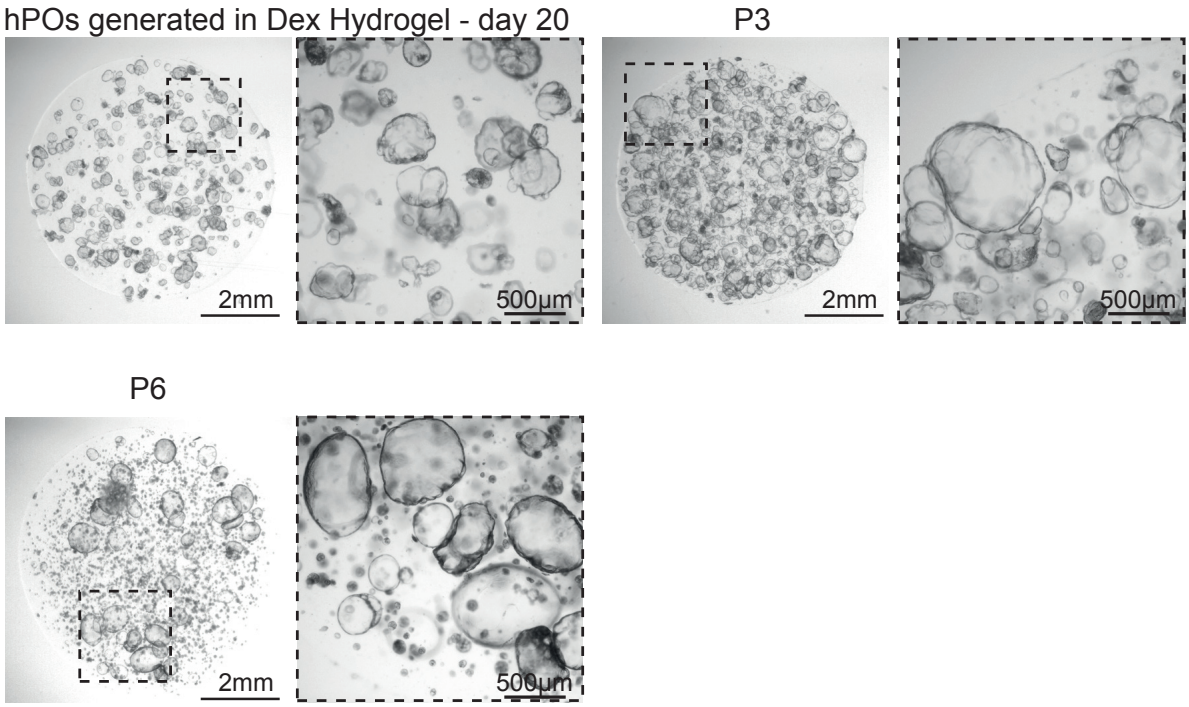

Figure 3.22 Removal of Dextranase in the passaging of hPOs in hydrogel allows for increased expansion time. Representative brightfield images of hPOs generated in DEX-hydrogel expanded for 20 days and passaged up to passage 6 without the use of dextranase to degrade the DEX-hydrogel in between passages. Experiments were performed in n=1 donors.

I isolated hPOs and expanded them in GFOGER-hydrogel with a large number of organoids generated at P0 (Fig. 3.23a). Through utilisation of the optimised passaging protocol (i.e., without use of dextranase), hPOs could be expanded to passage 8 while retaining ductal and organoid morphology (Fig. 3.23a) similar to hPOs grown in BME 2. Of note, hPOs grown in GFOGER-hydrogel did demonstrate some loss of spherical shape and increased invaginations although this was difficult to quantify (Fig. 3.23a). Nevertheless, the aim was to expand hPOs until the cultures failed, but due to the shutdown of our laboratory as a result of the restrictions imposed in response to the spread of the SARS-CoV-2 virus, expansion of Donor 17 hPOs in GFOGER-hydrogel was stopped and the organoids were cryopreserved (Fig. 3.23b). Notably, when hPOs were expanded in GFOGER-hydrogel with the use of dextranase, this resulted in the limited expansion capacity of hPOs to a maximum of 4 passages (Fig. 3.23b). Nevertheless, expansion of hPOs in GFOGER-hydrogel led to an increase in passage numbers while time in culture was similar to hPOs expanded in DEX-hydrogel (with or without use of dextranase; Fig 3.23b). Furthermore, hPOs in GFOGER-hydrogel reached confluency and could be passaged in a similar time manner as compared to BME 2 (Fig. 3.23).

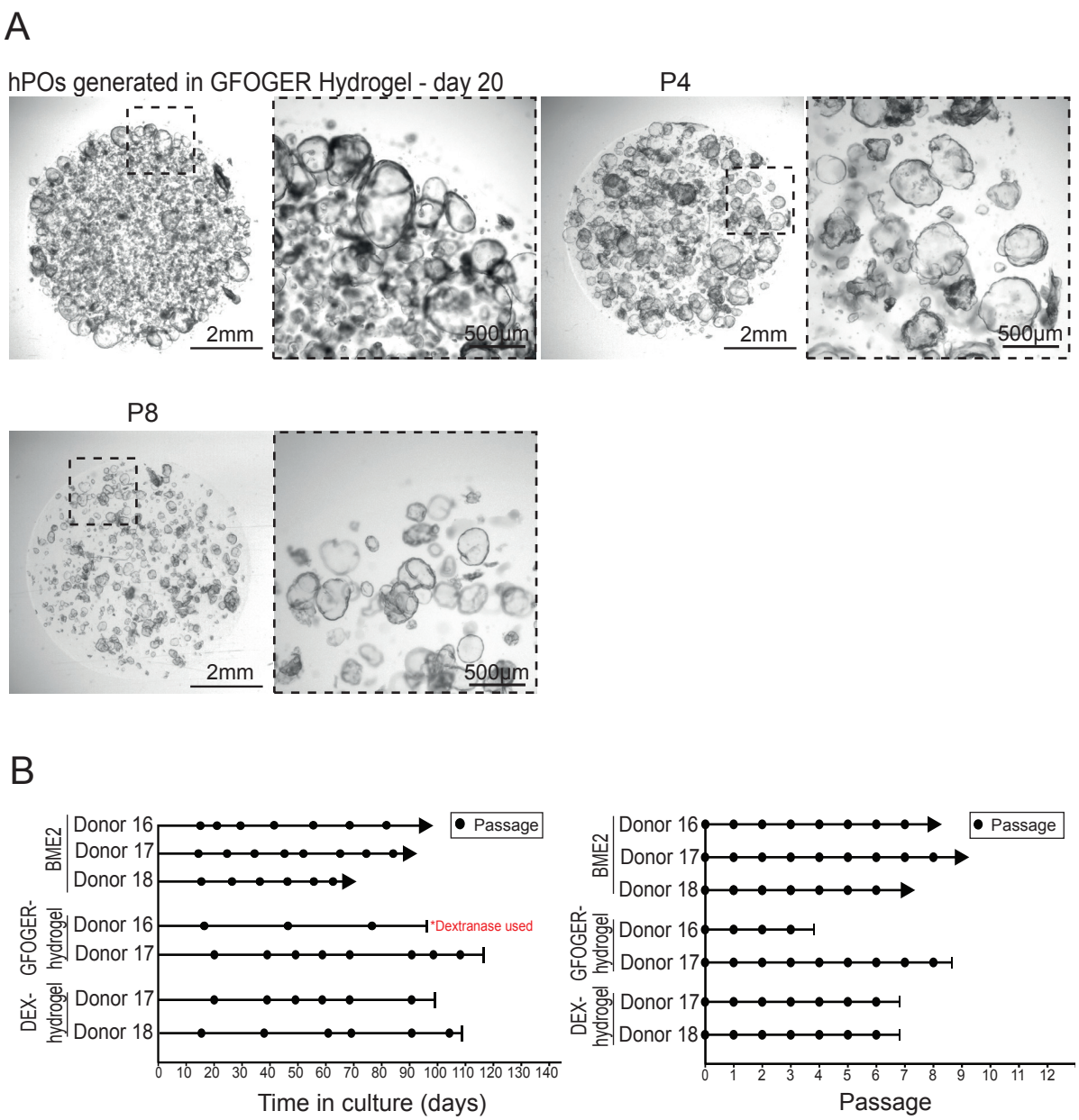

Figure 3.23 An optimised hydrogel (GFOGER) shows modest increase in expansion capacity of hPOs. (**A**)Representative images of hPO cultures derived from freshly isolated human pancreas tissue and initiated in GFOGER-hydrogel demonstrating expansion up to passage 8 (n=1 donor expanded to passage 8). (**B**) Graph represents the expansion potential of independent donors cultured with BME 2, DEX-hydrogel or GFOGER-hydrogel. (circle = passage, arrows indicate ongoing cultures, capped lines indicate cultures that deteriorated)

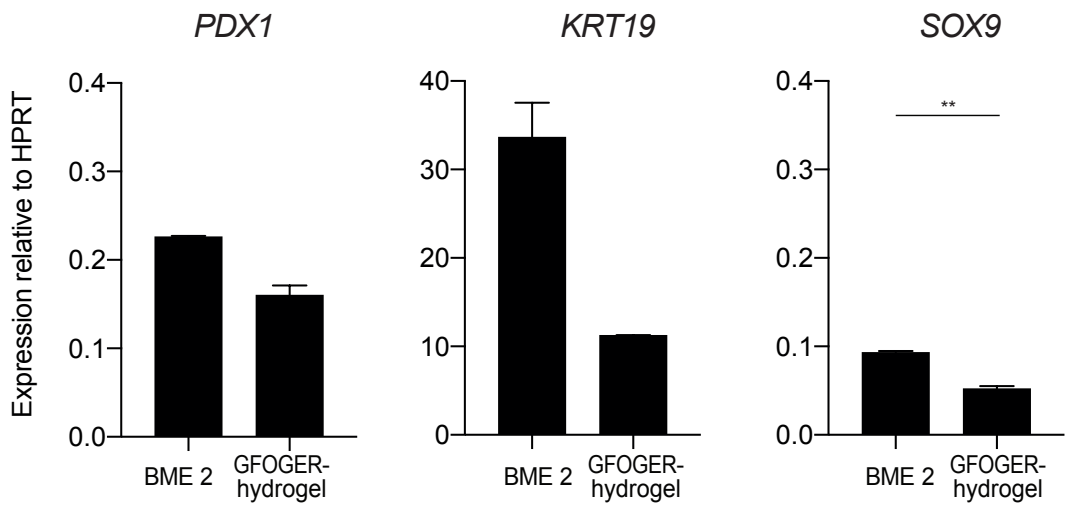

Figure 3.24 GFOGER-hydrogel grown hPOs retain expression of key pancreatic and ductal markers at the mRNA level. mRNA expression analysis of hPO cultures (passage 2) generated in BME 2 or GFOGER-hydrogel reveals that organoids grown with GFOGER-hydrogel retain expression of pancreatic and ductal markers *PDX1, KRT19,* and *SOX9*. Graphs show mean ± SEM. Differences were tested by paired two-tailed t-test. Significant differences are marked by asterisks: *p≤0.05. Experiments were performed in n=1 donor; n=2 technical replicates shown.

Characterisation of hPOs generated and expanded in either BME 2 or GFOGER-hydrogel demonstrated that *PDX1* (pancreatic), *KRT19* and *SOX9* (ductal) markers are expressed at the mRNA level, with expression levels of all three markers being numerically lower in hPOs expanded in GFOGER-hydrogel, with only SOX9 reaching statistical significance (Fig. 3.24). Furthermore, immunofluorescent staining of hPOs from the same donor expanded in BME 2, DEX-hydrogel or GFOGER-hydrogel demonstrates that expression of PDX1, KRT19 and SOX9 is maintained as late as passage 4 at the protein level in all three conditions (Fig. 3.25). However, when compared to BME 2, the expression pattern of these three markers in either chemically defined hydrogel is different with multiple cells demonstrating complete lack of expression (Fig. 3.25). Furthermore, while hPOs grown in either DEX- or GFOGER-hydrogel maintain a single cell epithelial structure, the cellular organisation is clearly affected while polarisation of F-ACTIN towards the lumen is less prominent than hPOs expanded in BME 2 (Fig. 3.25). However, both DEX-hydrogel and GFOGER-hydrogel allow expansion of hPOs in a comparable manner to BME 2.

In summary, these results demonstrate the development of a chemically defined, tuneable, reproducible and scalable biomimetic hydrogel which, through use of the optimised medium hPO-Opt. EM, supports hPO growth and initial expansion although long-term expansion is yet to be achieved.

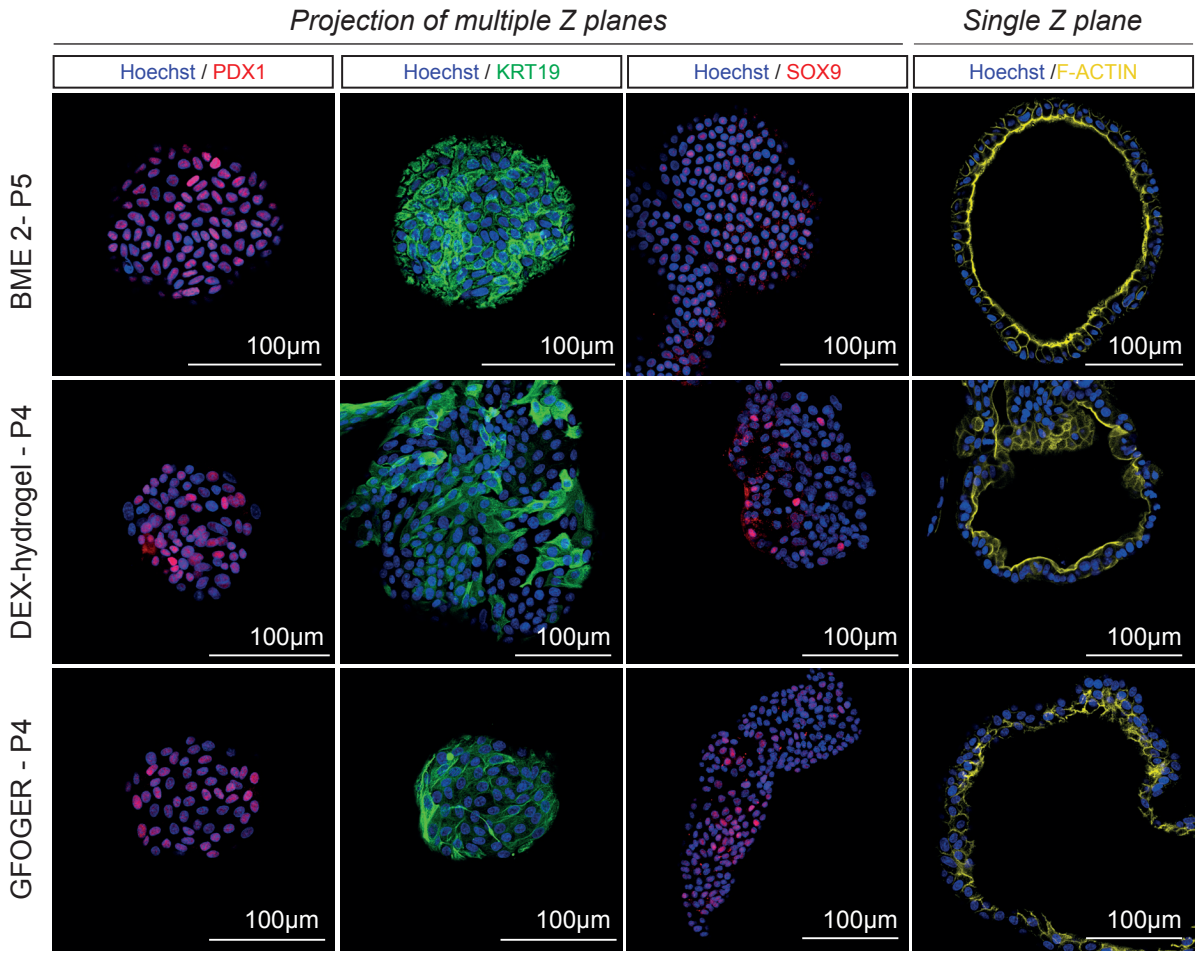

Figure 3.25 Immunofluorescence staining of pancreatic and ductal markers on mid-passage hPOS in hydrogels without use of dextranase. Immunofluorescence of hPOs in GFOGER-hydrogel at passage 4 compared to hPOs generated in DEX-hydrogel or BME 2 from the same donor. (PDX1 - red; KRT19 - green; SOX9-red; F-Actin - yellow; Nuclei were counterstained with Hoechst - blue). Experiments were performed in n=1 independent donor, n≥3 organoids imaged per condition.

3.2.6 Expansion of hPOs from donors with Type 2 Diabetes (T2D)

In vitro models that faithfully recapitulate normal as well as diseased cell biology are powerful in both understanding the progression to a diseased state, as well as for the discovery of novel therapeutics. While some pancreatic diseases like cancer have been modelled *in vitro*[131,137,248], modelling diabetes remains challenging due to the difficulty of both acquiring fresh diabetic tissue as well as the propagation of β-cells, the main cell type affected in diabetes. Furthermore, in order to generate a cellular therapy for diabetes that can be administered to patients in a personalised and autologous manner, it is necessary to be able to expand tissue from the diabetic patient.

In this project, tissue was procured from three patients who were diagnosed with T2D in various stages of progression (Appx. Table 1). Donor 19 was diagnosed with T2D which was controlled by medication (insulin glargine, metformin, gliclazide), while there was also a history of heavy alcohol use, smoking, hypertension, pulmonary disease and cardiac disease.

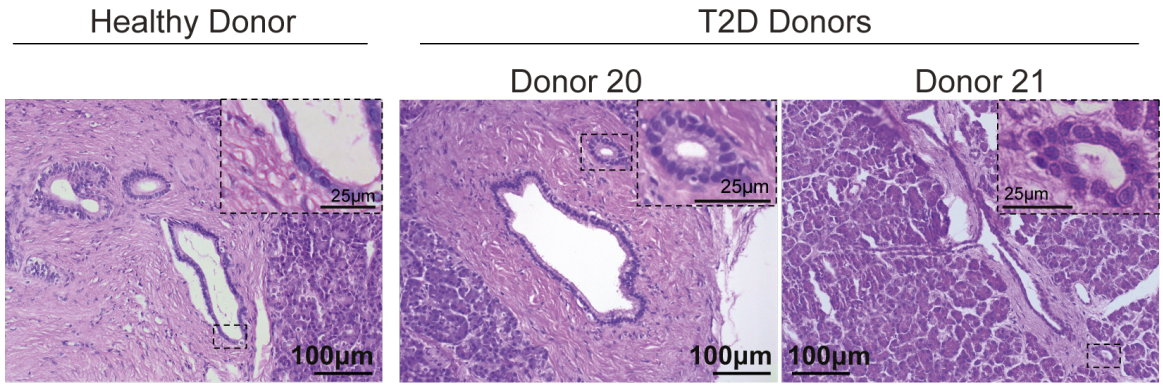

Figure 3.26 Pancreatic ductal histological architecture is indistinguishable between healthy and T2D donors. Representative images of H&E staining of human pancreatic ductal tissue from a healthy donor (left) and two donors with T2D (right). Note that the ductal cells look similar between the two types of donors without obvious morphological differences.

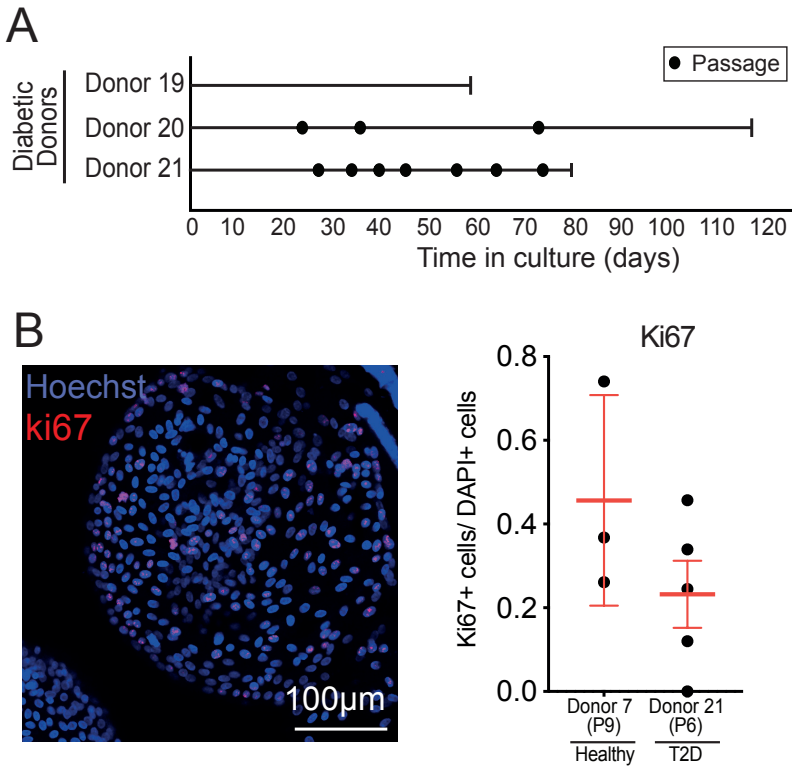

Figure 3.27 hPOs from T2D retain proliferative capacity but show a marked decrease in expansion potential. (**A**) Expansion graphs demonstrating that hPOs from T2D donors can be expanded *in vitro* but have increased times between passages and cultures are lost early. (**B**) Quantification of immunofluorescent staining of proliferative marker Ki67 on healthy and T2D hPOs shows that T2D donor derived hPOs maintain their proliferative pool of cells. Data presented as mean ± SEM. Differences were tested using a two-tailed t-test. Significant differences are marked by asterisks.

Donor 20 was classified as "borderline diabetic" without use of medication to treat diabetes while there was also history of heavy alcohol consumption. Furthermore, Donor 21 was diagnosed with Type 2 diabetes which was diet controlled without need of medication while the donor had been on medication for hypertension and cholesterol (Appx. Table 1). Histological comparison of primary tissue from the three T2D patients with healthy tissue showed no obvious morphological or architectural differences in the ductal compartment (Fig. 3.26). However, when ductal tissue from these T2D donors was expanded under the defined culture conditions outlined in this project using hPO-Opt.EM medium, the three donors expanded with marked difference. While Donor 19 was not able to be expanded *in vitro*, both Donor 20 and 21 were expanded to varying degrees (Fig. 3.27a). hPOs from Donor 20 quickly developed an unhealthy phenotype (Supp. Fig. 3), with passage times that were considerably longer than healthy hPOs (Fig. 27a). Donor 21, while it initially expanded in a similar manner to healthy hPOs, the cultures began to deteriorate at P6-P7 and could not be expanded beyond that (Fig. 3.27a, Supp. Fig. 3). Of note, Donor 21 culture deteriorated despite retaining a proliferative pool of cells at similar levels to those of healthy hPOs (Fig. 3.27b). H&E staining of Donor 21 organoids at passage 7 demonstrated a change in architecture with profound loss of ductal epithelial organisation and increased attachment to the plate, underlying a potential epithelial-to-mesenchymal transition (EMT; Fig. 3.28, Supp. Fig. 3). Immunofluorescent staining of Donor 21 hPOs shows that many organoids lack

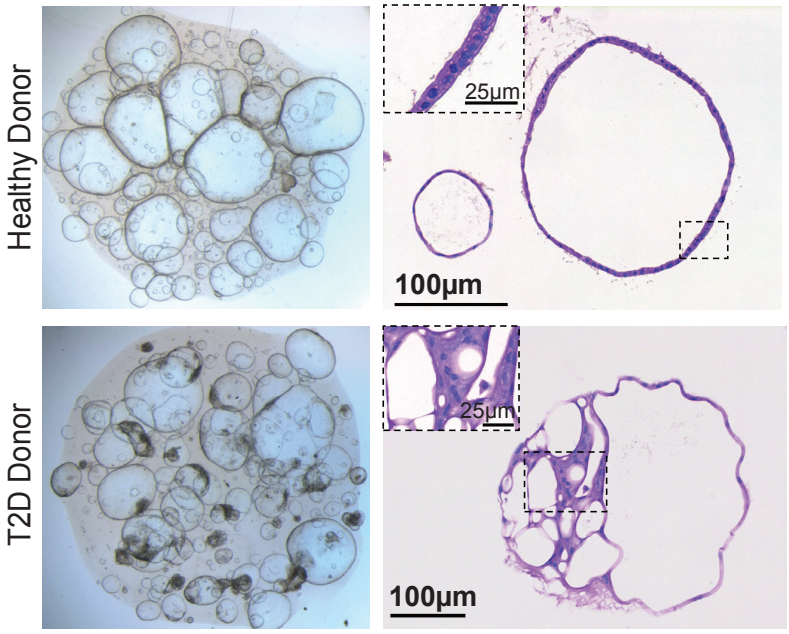

Figure 3.28 hPOs from T2D are phenotypically different to hPOs derived from healthy tissue. Representative brightfield and H&E images from healthy (upper panels) and T2D donor derived hPOs (lower panels). Note that healthy maintain normal morphology and single cell epithelial organisation while T2D donor hPOs have increased attachment to the plate and a disorganised architecture.

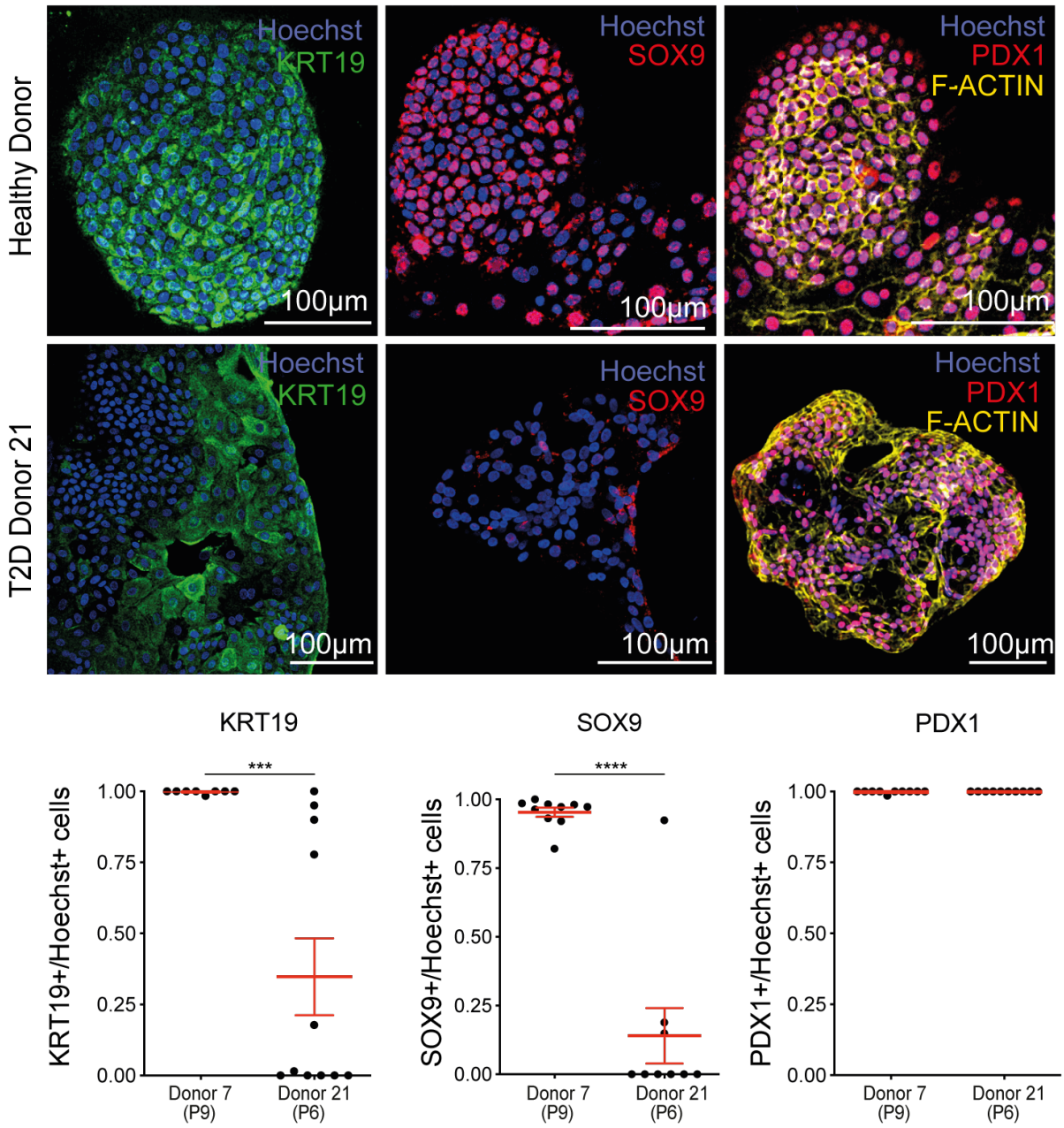

Figure 3.29 hPOs from T2D are phenotypically different to hPOs derived from healthy tissue. Immunofluorescence staining of healthy and T2D donor hPOs (upper panels) and quantification of positive cells (lower panels) of cytoplasmic KRT19 (green) and nuclear SOX9 (red), nuclear PDX1 (red), and F-Actin (yellow). Note the actin disorganisation in hPOs derived from T2D donors (5/9 organoids). Graphs represent number of positive cells for the corresponding marker (≥8 organoids counted per donor). Graphs show mean ± SEM. Differences were tested using a two-tailed t-test. Significant differences are marked by asterisks. *** $p \leq 0.001$, **** $p \leq 0.0001$

expression of KRT19 (Fig. 3.29; 6/11 organoids) while the expression pattern is markedly different to that of healthy hPOs. SOX9 is equally downregulated among Donor 21 hPOs organoids (8/9) while PDX1 is unaffected and is similarly expressed between T2D and healthy hPOs (Fig. 3.29). Moreover, Donor 21 hPOs often demonstrated loss of polarity and lack of organisation as demonstrated by expression of F-ACTIN (Fig. 3.29; 5/9 organoids). This pattern was also reflected in Donor 20 hPOs which had two phenotypes of F-ACTIN expression with some loss of KRT19 and SOX9 expression (Supp. Fig. 4). This illustrates that hPOs derived from T2D donors can be expanded using the defined culture conditions and optimised medium for healthy hPO growth.

3.3 Discussion

3.3.1 Refinement of the hPO culture system

Recently, organoid culture systems have emerged as a promising technology to bridge the gap between cell lines and *in vivo* tissue[108]. Pancreas organoids derived from adult mouse pancreatic ducts recapitulate the ductal epithelium structure and physiology in culture. However, healthy human pancreas tissue has proven more challenging to recreate and expand in culture. While three protocols describe the establishment of human pancreatic ductal organoids *in vitro*[123,131,132], these suffer from a limited capacity for expansion, use of serum-containing, and chemically ill-defined media. These limitations hamper their use in studies of pancreas duct cell biology and genetics as well as for disease modelling of the exocrine compartment and potential cell therapy approaches.

In this project, I contributed to developing and characterising an improved culture medium which allowed long-term expansion of human pancreatic ductal cells without the need of cell transformation such as cell immortalisation via viral gene integration. The success of the optimised medium was a result of the addition of growth factors TGFβi, PGE2, and FSK as well as the removal of Wnt3A conditioned medium, and an increase of Rspo1 from 5% to 10%. The dependence of hPOs on Rspo1 suggests that the Wnt pathway is involved (refer to Fig. 1.3) and plays a significant role in the generation and expansion of the organoids. However, removal of Wnt3A led to increased expansion thereby contradicting the involvement of the Wnt pathway. Interestingly, a recent report in which liver cholangiocyte organoids were generated, demonstrated use of Rspo1 and Dickkopf-related protein 1 (DKK-1; Wnt inhibitor) in the culture medium explaining that non-canonical Wnt signalling (planar cell polarity; PCP pathway) rather than canonical Wnt signalling is important for the expansion of cholangiocyte organoids[241] (Fig. 1.3). Importantly, Wnt3A is a conditioned medium which contains serum[123] and it was demonstrated in section 3.2.1 that addition of serum alone was damaging to the expansion of hPOs. Therefore, further experiments with the use of recombinant Wnt protein and DKK-1 would help elucidate whether Wnt is required and can increase hPO expansion or whether hPO growth is driven by non-canonical Wnt signalling.

While this project identifies, for the first time, a medium that is chemically defined, serum-free and allows expansion of pancreas organoids beyond 180 days, the expansion is not unlimited such as in the case of mouse pancreas organoids[121]. This may be due to inherent species differences or could outline a potential limitation of the culture system and a need to further optimise the culture medium. Use of automated assays whereby hundreds of growth factors can be assessed in multiple combination matrices would be useful in uncovering novel molecules that can increase the expansion capacity of the culture system.

Nevertheless, the success of organoid generation was very high while passage times and expansion longevity remained consistent among 29 donors with ranging demographics. While it was suspected that age of the organ donor may have an impact on subsequent derivation, no such pattern emerged. Furthermore, organoids were generated from pancreases that had undergone an average of 24 hours of cold ischaemic time (CIT) with successful organoid generation from organs with CIT of up to 80 hours. This removed time restrictions for collection of tissue as the biopsies could be procured late at night and organoid generation could be initiated the following morning without impacting the success rate. It would however be interesting to explore how long pancreas tissue can be preserved in hypothermic conditions before organoid generation becomes severely impacted.

Another aim of this project was to achieve efficient cryopreservation at the tissue level. This would not only allow the ability to capture donors without the need for immediate organoid derivation but would also have significant implications in the generation of biobanks and shipment of viable tissue world-wide. Albeit the initial organoid formation was reduced, the protocol in this project allowed derivation of hPOs after 3 weeks of tissue cryopreservation. While this is an important achievement, 3 weeks is a short amount of time and it is expected that future biobanks would need to be able to freeze the tissue for months if not years. Therefore, it would be necessary to explore the maximum time that tissue can be effectively cryopreserved utilising the protocol in this project as well as generating cryopreservation media and protocols tailored for long-term cryopreservation of human pancreas tissue. Equally, the ability to assess the quality of a cryopreservation protocol requires a functional assessment, usually in comparison with the corresponding fresh tissue. Therefore, the efficiency of hPO derivation could be used as a functional criterion to assess future cryopreservation protocols.

Interestingly, the question remains as to whether other factors can impact the derivation success and longevity of the cultures. While Loomans *et al.* reported expansion of human pancreas ductal cells up to passage 10, recapitulation of their culture conditions in this project led to a rapid decline and failure of cultures with a maximal passage number of 4. This could be due to the expansion of different cell populations or minor differences in the culture methods which could not be reproduced. Indeed, reproducibility is an ongoing issue among the greater scientific community[249] while the culture system developed in this project has been successfully reproduced by Dossena and colleagues in order to generate a GMP-compliant process of hPO production[250]. Their GMP-compliant process involved three additions to the protocol in this project: 1) use of islet depleted tissue with subsequent manual

dissociation to bypass the hand-picking and enzymatic digestion stage; 2) use of recombinant Rspo1; 3) a hPO cryopreservation protocol which included control-rate freezing. In this project it has also been demonstrated that hPO generation can occur through use of either manual handpicking of ducts or filtration through a 100μm filter following dissociation with a MACS dissociator, but enzymatic digestion is a requirement. However, while pancreas biopsies are utilised in the protocol described in this project, Dossena *et al.* utilises islet depleted tissue which by definition would have required an enzymatic step during islet isolation[39] and hence introduction of an enzyme in the protocol may not reduce GMP compatibility. Furthermore, hPO-Opt.EM media contains Rspo1 conditioned media which although does not contain serum, the growth medium for the 293T-HA-RSPO1-Fc cell line needed to produce Rspo1 does contain foetal bovine serum (FBS). Therefore, depending on GMP guidelines, recombinant Rspo1 rather than Rspo1 conditioned medium may be required. Furthermore, the cryopreservation protocol within this project utilises a cryopreservation chamber, not a control rate freezer, however this would be easy to implement within the protocol. Therefore, this project demonstrates a culture system that with minimal changes may be translated to a GMP-compliant environment.

3.3.2 Understanding the identity of hPOs

The developmental pathway of the pancreas is a complicated process which relies on the correct sequential maturation of pancreatic progenitors which is partly driven by activation or inhibition of signalling pathways from secreted molecules[1]. Importantly, numerous studies, along with advanced PSC differentiation protocols, have been crucial at mapping the developmental steps of the pancreatic cell subtypes (Fig.1.2) [1,96,97]. However, in the mature human pancreas most studies have centred around uncovering the identity and complexity of islet cells, largely due to the implications for diabetes[68,69]. Therefore, surprisingly little is known about the cell heterogeneity that may exist in adult the human pancreatic ductal system. While the existence of a human pancreatic ductal progenitor has been suggested[84] and evidence exists to support its existence in the mouse[79,81,82,121], robust evidence in the human setting is still lacking. Furthermore, organoids that have been developed from various parts of the human biliary tree are contrastingly deemed both bona fide stem cells[120] or fully mature cells[241].

In this project, it has been demonstrated that hPOs recapitulate the architecture and polarity of pancreatic ductal cells while also express key pancreas ductal markers KRT19, SOX9, EpCAM, HNF1β and CFTR at the gene and/or protein level. Interestingly, hPOs upregulate expression of adult stem cell marker LGR5 when compared to primary tissue while also retaining a proliferative pool of cells and a stable colony formation efficiency over time in culture. Furthermore, they express PDX1, which although it is normally expressed in cells of the adult pancreas[129,251], its expression in development marks the specification of the pancreatic endoderm[1] (Fig. 1.2) and has been implicated to mark an adult progenitor pool[129]. This data brings forth the question of whether a progenitor pool is driving the

proliferative capacity observed in hPOs. Indeed, this would complement the theory that the eventual loss of hPO culture is driven by a continuously reducing population of progenitors. Studies have demonstrated in the mouse that the LGR5+ pool of cells serve as an adult stem cell population that under normal or damaged scenarios can repopulate the ductal compartment[80,116,117], while in the human, organoid generating cells with stem cell characteristics (self-renewal and bi-potency)express *LGR5* mRNA[120]. However, this has not been demonstrated within this project for hPOs and no direct evidence exists to support a need or dependence on LGR5 function. Similarly, the true identity and maturity of hPOs is not elucidated. A recent study by Rimland *et al.* performed principal component analysis on sc-RNAseq data from human pancreas tissue and organoids and demonstrated that while organoids correlated to their corresponding tissue for one component (PC1), they were a distinct population on the other component (PC2). Furthermore, 5,594 genes were differentially expressed between tissue and organoids and the authors stated that the culture conditions promoted a progenitor profile[252]. Moreover, the same study indicated that culture conditions played an important role in whether the organoids remained similar to the tissue of origin or acquired a stem/progenitor fate[252]. This highlights the idea that culture conditions may play an important role in either promoting expansion of specific cell populations or reverting adult cells into a progenitor state.

Further investigations such as sc-RNAseq of hPOs will allow better understanding of the heterogeneity within hPOs. It would also allow understanding of whether hPOs are reverting towards a progenitor state and thereby acquiring features of other cell types such as endocrine cells. Although hPOs do not express insulin at the mRNA level, it would be relevant whether other earlier markers of endocrine differentiation such as MAFA, NGN3, or Chromogranin A are expressed at any stage of the culture. For this, comparison to a pure cell population from primary tissue is needed. While the islets used for qPCR were obtained from an islet isolation centre and were a very pure population, one limitation in this characterisation was the ductal tissue collected for qPCR studies. The pancreatic duct was isolated through surgical dissection and while the tissue was cleaned, some acinar tissue remained which could not be removed. Cell sorting of primary ductal cells using ductal markers (e.g. EpCAM) could result in improved purity of cells. Moreover, in this project, expression of LGR5 in hPOs was not demonstrated at the protein level and it is unclear whether the qPCR results are reflective of the protein being translated. Immunohistochemistry staining for LGR5 is needed to demonstrate if it is expressed and at which stage of the cell culture process it is expressed. Furthermore, identification of proliferative cells was carried out by Ki67 staining. However, these experiments require more donors at the early, medium and late stages of culture while use of other assays such as EdU incorporation can be used to strengthen understanding of the proliferative nature of hPOs *in vitro*.

Moreover, while histology and immunohistochemistry were used to assess whether hPOs are healthy and recapitulate the tissue of origin, no functional analyses were carried out in this project which is a very important aspect to demonstrate that hPOs recapitulate the physiology of ductal cells. However, functional assessment of exocrine pancreatic organoids is challenging. Pancreatic ductal cells

regulate fluid and ion secretions into the ductal system via the CFTR ion channel in order to maintain pH and secretory volume for proteins secreted by the acini[16] (Refer to Fig. 1.1). Currently, the gold-standard CFTR functional test is the forskolin induced swelling assay in which addition of forskolin increases cAMP activity which regulates the CFTR anion channel to increase fluid secretion into the lumen, leading to an increase of the volume of the organoids, demonstrated in studies by Dekkers *et al.*[253] and Sampaziotis *et al.*[241] for small intestine and liver biliary ductal organoids, respectively. However due to the presence of forskolin in the hPO-Opt.EM media composition, this assay cannot be used to evaluate the functionality of the CFTR channel. Therefore, future studies will need to focus on assessing the functionality of hPOs.

Despite these limitations, the data demonstrate that hPOs can be used to model pancreatic ductal cells *in vitro* and investigate ductal cell identity, progenitor status and ductal cell biology.

3.3.3 Evaluation of the chemically defined ECM for hPO expansion

Another important aspect in tissue and disease modelling is the ECM, which is a crucial component in all tissues, and provides a scaffold and physical sites for cells to attach. Interactions between cells and the ECM have been implicated in many biological processes, including establishment of stem cell niches and cellular differentiation. Additionally, abnormal ECM dynamics are often associated with disease[254]. Recent advances in the generation of *in vitro* organoid systems with ECM have provided a new opportunity to investigate these interactions; however, the use of ECMs such as Matrigel and BME 2 is suboptimal due to their xenogenic origin, inability to modulate the ECM components and batch-to-batch variability. A fully chemically defined hydrogel has been shown to be able to support growth of human intestinal organoids[255] but as yet, fully chemically defined hydrogels have not been able to support human liver or pancreas organoid culture[174].

In this project, I present the first culture system able to support generation and expansion of hPOs in a fully chemically defined hydrogel. While the original hydrogel protocol presented allowed expansion of hPOs up to passage 4, further optimisation improved expansion up to passage 8. While this is a very important step towards replacement of animal derived ECMs, several limitations as well as areas to be optimised can be identified in this study.

In both original and optimised protocols, the expansion capacity in terms of passage number is reduced when compared to hPOs grown in BME 2 and therefore, further optimisation of the culture conditions is needed in order to recapitulate the results seen in BME 2. Furthermore, optimisation of the chemically defined hydrogel culture system consisted of two components: 1) removal of dextranase during passaging and 2) use GFOGER instead of RGD peptide in the hydrogel mixture. However, only one donor line was expanded in GFOGER-hydrogel without use of dextranase while also grown in DEX-hydrogel and BME 2 in parallel (Donor 17). Therefore, it remains unclear as to whether addition of GFOGER peptide contributed significantly to the increase of passage numbers. Furthermore,

removal of dextranase from the protocol meant that 'old' hydrogel fragments remained attached to hPO cells and potentially carried over to the new cell-hydrogel composition. This may have induced a stiffening of the gel which further caused a reduced spherical morphology and increase in invagination observed in hPOs expanded in DEX- and GFOGER-hydrogel.

Therefore, experiments need to be repeated with more donor lines expanded in the three types of ECMs, allowing for the expansion of hPOs until the cultures fail in order to understand whether GFOGER-hydrogel allows for improvement of the *in vitro* expansion time of hPOs. Assays to assess gel stiffness would be informative to understand whether the gels are growing stiffer with time and to what extent this differs from BME. Furthermore, assays such as colony formation efficiency, doubling time, and immunostainings for markers of proliferation would be useful in understanding the impact in growth kinetics both as a result of culture in chemically defined hydrogels, as well the impact of specifically adding the GFOGER peptide.

Importantly, when assessing the efficiency of the chemically defined hydrogels, BME 2 was used for comparison and an assumption was made that hPOs grown in BME 2 represent the optimal cell type and model. As such, hPOs grown in DEX-hydrogel demonstrated statistically significant lower levels of *KRT19* and *SOX9* mRNA expression. However, primary ducts similarly showed reduced levels of *KRT19* mRNA when compared to hPOs grown in BME 2 (refer to Fig. 3.12); however due to large inter-donor variability, this was not recapitulated in the expression of SOX9 in primary ducts. This may illustrate that hPOs grown in BME 2 are a uniform KRT19+ population of cells and/or gain a stem/progenitor identity, while hPOs grown in DEX-hydrogel maintain an identity closer to the primary ducts. However, this theory is largely unsupported by immunostainings which show that hPOs in DEX-hydrogel have uniform expression of PDX1 and KRT19 at passage 0, but this is severely altered after just one passage with many cells downregulating expression of both markers. Of note, ductal cells in the pancreas tissue uniformly express KRT19, PDX1, and SOX9 at the protein level as demonstrated in this and other studies[129]. Therefore, downregulation of these markers in hPOs grown in DEX-hydrogel may underlie the progressive loss of the cultures. Furthermore, this phenotype was not rescued neither by removal of dextranase from the cultures nor by the replacement of RGD with GFOGER and hPOs grown in either condition demonstrated significant downregulation of KRT19, PDX1, and SOX9 as well as alterations in actin organisation. Notably, cells *in vivo* interact with the ECM through integrin molecules which in turn are attached to actin microfilaments or keratin filaments[256]. Furthermore, different integrin subunits bind to different receptors such as $\alpha1\beta1$ binding to GFOGER (collagen) receptors, $\alpha V\beta3$ binding RGD (fibronectin) receptors or $\alpha3\beta1$ binding laminin receptors[256]. It has also been shown that keratins act as modulators of the mechanosensing processes in hepatic cells and play a key role in the alteration of cell structure in response to increased rigidity through reorganisation of the actin cytoskeleton[257]. Therefore, it is perhaps unsurprising that changes in KRT19 expression coincide with alterations of the actin cytoskeleton in hPOs grown in the chemically defined hydrogel.

Use of monoclonal antibodies to uncover the specific integrin subunits expressed in hPOs could assist in understanding which ECM component is necessary for hPO growth. Interestingly, the synthetic hydrogels which allowed growth of epithelial organoids (including pancreas) generated by Broguiere *et al*.[174], utilised a fibrin (human derived) and laminin-111 mixture, therefore pointing to laminin as the next potential candidate to be trialled for improvement of the chemically defined hydrogel presented in this project.

Despite the need for optimisation, data from these experiments demonstrate that hPOs can be generated and grown in a fully chemically defined hydrogel thereby facilitating the GMP translation of hPOs while also paving the ways of future studies interrogating the interaction between ductal cells and the ECM.

3.3.4 Modelling diabetes and its effects in the pancreatic ductal system

Disease modelling is a crucial aspect for most *in vitro* culture systems as it allows understanding of the pathways involved in the progression of the disease, as well as generation of novel therapies. Organoid models are increasingly used to model diseases ranging from congenital disorders such as Alpha-1 antitrypsin (A1AT) deficiency in the liver modelled with liver organoids and Cystic Fibrosis with intestinal organoids, to acquired diseases such as cancer[107]. In the field of pancreas research however, generation of a β-cell line has been difficult thereby hampering *in vitro* research into the progression of diabetes. While Ravassard and colleagues generated a human β-cell line, this required use of human foetal tissue, transformation of the cells and transplantation into mice in order to generate insulinomas from which to derive the β-cell line[258] which raises the question of the extent that this line recapitulates β-cell physiology. Moreover, while it is clear that T1D is mediated by autoimmune destruction of the β-cells and causes general inflammation in the pancreas, less is known about its effects in other pancreatic cell types. The effect of T2D on other pancreatic cell types is equally poorly understood.

One of the initial aims of this project was to generate hPOs from diseased tissue and specifically from T1D patients. However, tissue from such patients is extremely rare, since due to concomitant complications, T1D patients rarely become organ donors. Nevertheless, pancreatic tissue from three patients with T2D was procured for this project and hPOs were generated with varying success. Interestingly, hPOs from the donor with the most severe form of T2D could not be expanded. However, hPOs from Donor 21, who was clinically diagnosed with T2D (albeit diet-controlled) grew for a longer time period than hPOs from Donor 20 who was diagnosed as “border-line” diabetic. Diabetes is a progressive disease whereby in most cases, it has initiated years prior to the clinical and definitive diagnosis. Furthermore, a somewhat arbitrary number of fasting plasma glucose concentration ≥ 7.0 mmol/l is the cut off point for being diagnosed with T2D[259]. However, severity of the disease is multifactorial and is dependent on each person while blood glucose levels can alter depending on many factors. Therefore, it is difficult to understand which donor had more severe T2D and more importantly,

the time that the pancreas had been exposed to a potential destructive environment based on the clinical diagnosis. Furthermore, Donor 20 had a history of alcohol consumption while Donor 21 had a history of hypertension and high cholesterol. Therefore, it remains difficult to discern which pathology contributed to the effects seen *in vitro* and whether the results presented for the T2D donors are representative of the effects of T2D on the ductal cells or rather the effects of long-term damage caused by other pathologies. Indeed, a limitation in this study is the low number of T2D donors used to expand hPOs. A greater cohort of samples would be required in order to understand the effects of T2D on the generation and expansion of T2D organoids. Furthermore, a better clinical marker such as glycated haemoglobin (HbA1c; which measures blood glucose levels over three months[259], as well as histologically assessed levels of fibrosis should be used to understand the extent of diabetes progression and correlate any *in vitro* effects to severity of the disease. Nevertheless, it remains likely that the *in vitro* observations for Donors 19, 20 and 21 are linked to T2D since other donors from which hPOs were derived had histories of alcohol consumption, hypertension, medication etc. with no obvious effects on the expansion times of hPOs.

Interestingly, the primary ductal tissue from the T2D donors seemed identical to that of a healthy pancreas with no obvious damage or inflammation. While this needs to be confirmed by a clinical histopathologist, it is interesting that hPOs could initially form for 2/3 donors but eventually collapsed suggesting that cellular damage may exist which cannot be detected through histological assessment. The significant downregulation of KRT19 and SOX9 in T2D hPOs, coupled with actin disorganisation is reminiscent of the phenotype observed in hPOs grown in the chemically defined hydrogels and points towards an inappropriate interaction of T2D hPOs with the ECM. In murine models of diabetes, it has been shown that many of the cell-cell, cell-matrix, vascular and ductal communications are lost or impaired. Fibrosis is associated with T2D which is driven by ECM remodelling due to activation of metalloproteases (MMPs) and increased collagen deposition from pancreatic stellate cells[260]. Therefore, it is possible the ductal cells from T2D patients have been exposed to a different ECM composition (compared to healthy pancreases) as a result of the disease progression and hence cannot generate appropriate connections to the BME 2- based ECM and undergo EMT as demonstrated by the results of this project. Interestingly, SOX9 downregulation in hPOs was concomitant with a disorganised F-ACTIN pattern. Studies have shown that SOX9 is activated as a result of Canonical Wnt pathway activation whereas genes activated from non-canonical Wnt pathway such as DKK-1 can inhibit canonical Wnt and in turn inhibit Wnt target genes such as SOX9. Furthermore, YAP/TAZ transcriptional co-activators, which are part of the Hippo signalling pathway, are activated as a result of non-canonical Wnt signalling[261]. It is known that the Hippo signalling pathway integrates diverse stimuli including mechanical and cytoskeletal cues, cell adhesion, apico-basolateral polarity, and mitogens to control cell growth and organ size[261]. Furthermore, SOX9 can also be inactivated from actin polymerisation as demonstrated in chondrocytes[262]. While the message is unclear, a relationship might exist between ECM attachment, SOX9 activity and cell

viability/proliferation which are mediated through Wnt and Hippo-YAP/TAZ signalling pathways. Further investigation to unravel such relationships would be an interesting development in understanding the effects of T2D in ductal cells of the pancreas.

An interesting study demonstrated an increase in pancreatic duct proliferation in individuals with obesity and/or T2D. Furthermore, it proposed that this increase in proliferation might underlie the increased risk of pancreatic cancer in obese and diabetic individuals[62]. However, Ki67 immunostaining on Donor 21 hPOs did not show an increase in proliferation and in fact demonstrated a trend towards decreased proliferation. However, this was only performed on one donor line and for one passage (passage 6) and therefore more donor lines would be needed to understand the differences in proliferation from T2D donor derived hPOs. Furthermore, the decrease in proliferation may be a response of T2D hPOs to the culture conditions and therefore early and late passage hPOs as well as primary tissue should be used for immunostaining to understand whether hPOs start with high proliferative rates compared to healthy tissue and organoids, that eventually decline over time in culture. In addition, further characterisation assays such as the ones performed for healthy hPOs as well as RNA sequencing (either bulk or single cell) would be crucial to understand whether T2D hPOs can maintain the identity of primary derived pancreatic ductal cells.

These results highlight that hPOs can be generated from pancreases with conditions such as T2D and can potentially be used to model diabetes and explore the pathology of the disease. Moreover, the ability to generate organoids from diseased individuals opens up the possibility of autologous treatment. For example, this could be applied to T1D whereby organoids can be derived from the patients, differentiated *in vitro* towards insulin producing cells, and transplanted into the patient therefore potentially bypassing an immune reaction.

3.4 Conclusion

In this chapter, I have demonstrated that pancreas organoids can be generated from the ducts of the human pancreas and can be expanded long-term using a chemically defined, serum free medium. Importantly, the primary tissue as well as the derived organoids can be cryopreserved for subsequent derivation without loss of expansion rates. Both fresh and frozen tissue derived hPOs recapitulate the pancreatic ductal cells both in histoarchitecture and biomarker expression. Furthermore, the ability to expand hPOs in a chemically defined biomimetic hydrogel paves the way towards translation in a GMP environment. Finally, preliminary data has been shown supporting the ability to use hPOs to model ductal cells in a diabetic scenario therefore opening up the possibility of their use to model other diseases and be used for generation of novel therapies.

CHAPTER 4. *IN VITRO* AND *IN VIVO* SAFETY ASSESSMENT OF hPOs

4.1 Introduction and aims

Cellular therapies aim to revolutionize the field of personalised medicine with the hopes of one day replacing treatments such as organ transplantation or treating genetic diseases by delivery of the appropriate cell type with a correct form of the gene. However, translation into the clinic not only means adhering to GMP standards of production, it also means demonstrating that the end product is safe and will not cause unwanted effects to the patient. However, as cellular therapies are still novel, the regulatory framework is still in development and guidelines remain vague as to the types of assays to be used for demonstrating safety of cell therapy products[147]. One important concern, partly due to the potential use of pluripotent cells (ESCs/iPSCs), is the risk of tumour formation as a result of contaminating undifferentiated cells or due to the malignant transformation of cells from oncogenic mutations[263]. This has in part stigmatised the field of ESCs/iPSCs and has significantly slowed the translation into the clinic. Despite this, studies utilising ESCs have persevered, making it to clinical trials and successfully treating patients with macular degeneration[264,265]. While adult organoids are expected to be less problematic in terms of the risk of tumorigenicity, since they are not reverted to a pluripotent state, it is expected that the same proof of safety as PSCs will be required for their clinical translation. As such, the organoid field can learn from studies that have paved the way for safety assessment of other cell therapy products[266,267].

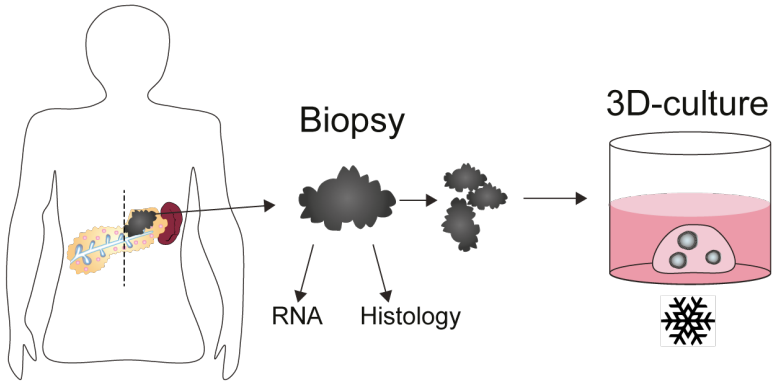

Figure 4.1 Obtaining pancreas cancer biopsies for tumour organoid isolation. Schematic of human pancreas cancer (hPC) organoid generation. Pancreatic cancer tissue undergoes enzymatic digestion (6-12 h) to release tumour cells which are embedded in BME 2 and overlaid with tumour media. Generated hPC organoids can be expanded and passaged depending on the tumour of origin.

In this chapter I aimed to assess the safety of hPOs. Therefore, **section 4.2.1** focuses on establishing a 3D *in vitro* model of pancreatic cancer which is used in subsequent studies of safety as a positive control. In order to assess both the chromosomal stability and genomic integrity of hPOs grown long-term *in vitro***, section 4.2.2** focuses on karyotype analyses of healthy and tumour derived organoids as well as Whole Genome Sequencing (WGS) of clonally derived cultures aiming to understand mutational burden, and copy number variations that may be caused by the culture process. With the understanding that the *in vitro* findings need to be translated to an *in vivo* model, **section 4.2.3** focuses on assessing safety of the hPO culture system *in vivo*. This includes optimisation of the transplantation techniques to allow for long-term engraftment, as well as generation of an assessment panel to evaluate safety of healthy hPOs.

4.2 Results

4.2.1 Development of human pancreas cancer (hPC) organoids

To assess the safety of hPOs, namely, transformation/tumorigenic formation capacity after long-term culture, the establishment of a positive control was an important aspect. This would allow the scrutinization of the sensitivity of subsequent *in vitro* and *in vivo* safety assays. In order to achieve this, patients with a ductal derived pancreas cancer that were scheduled to undergo pancreatic resections (either in the form of partial or total pancreatectomy or Whipple's procedures) were identified by liaising with medical personnel and surgeons. In the course of this study, three individuals with suspected pancreatic ductal adenocarcinomas (PDACs) were identified (Appx. Table 1) and after undergoing the surgical procedure, the removed gland was transported to the Clinical Histopathology department whereby a consultant histopathologist assessed the tumour and provided a biopsy for the study. Interestingly, although not confirmed at the time of initiating cultures, the tumours had differing diagnoses; the first sample procured (hPC-IPMN) was diagnosed as extensive main duct intraductal papillary mucinous neoplasm (IPMN), with high grade dysplasia, branch ductal involvement and focal invasive mucinous adenocarcinoma. Perineural infiltration (invasion of surrounding space including a nerve) was identified with no lymphovascular invasion. The second sample procured (hPC-PDAC) was diagnosed as a 25mm PDAC with both lymphovascular and perineural invasion; nodal metastasis was confirmed in 5/11 lymph nodes collected. The third sample procured (hPC-ITPN) was diagnosed as primary malignant intraductal tubulo-papillary neoplasm (ITPN), a rare tumour type[268], with invasive morphology, perineural infiltration and vascular invasion but no nodal metastasis.

In order to generate organoids from the tumour biopsies, I utilised and adapted published protocols that have been used for establishing liver cancer[269] or pancreas cancer[131] organoids. Similarly to hPOs, pancreas cancer tissue was digested, and the digest was placed directly in culture with no filtration or manual duct-picking step (Fig. 4.1).

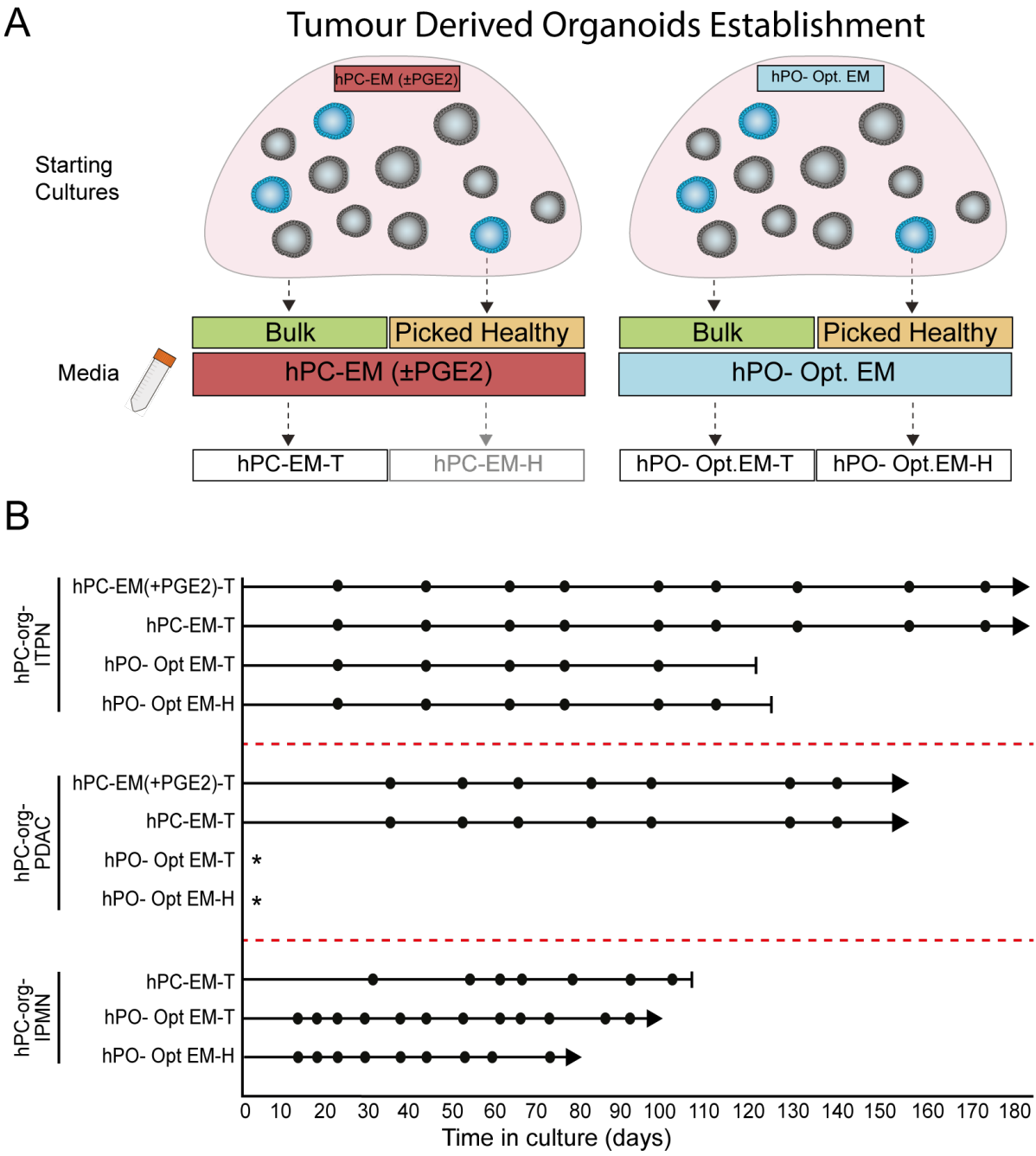

Figure 4.2 hPC organoids derived from different pancreatic cancer subtypes expand in tumour defined media. (**A**)Schematic depicting experimental design for generation of a tumour organoid line without healthy organoid contamination. (**B**) Expansion diagrams demonstrating growth of the three tumour organoid lines expanded in either tumour media (hPC-EM) or healthy hPO expansion media (hPO-Opt.EM) for either tumour cells (**T**) or handpicked healthy cells (**H**) i.e., "hPO-Opt.EM-H" denotes tumour organoids with healthy phenotype expanded in the hPO-Opt.EM media. Starting cultures with freshly isolated tumour cells were seeded in hPC-EM media with or without addition of PGE2, and healthy hPO expansion media (hPO-Opt.EM). Organoids with a healthy phenotype were handpicked out and cultured separately while cancer cells were cultured in bulk to allow maintenance of the heterogeneity of the tumour population. Note that the aggressive tumour PDAC organoids cannot expand in healthy medium while the more benign cancer (IPMN, ITPN) derived organoids can.

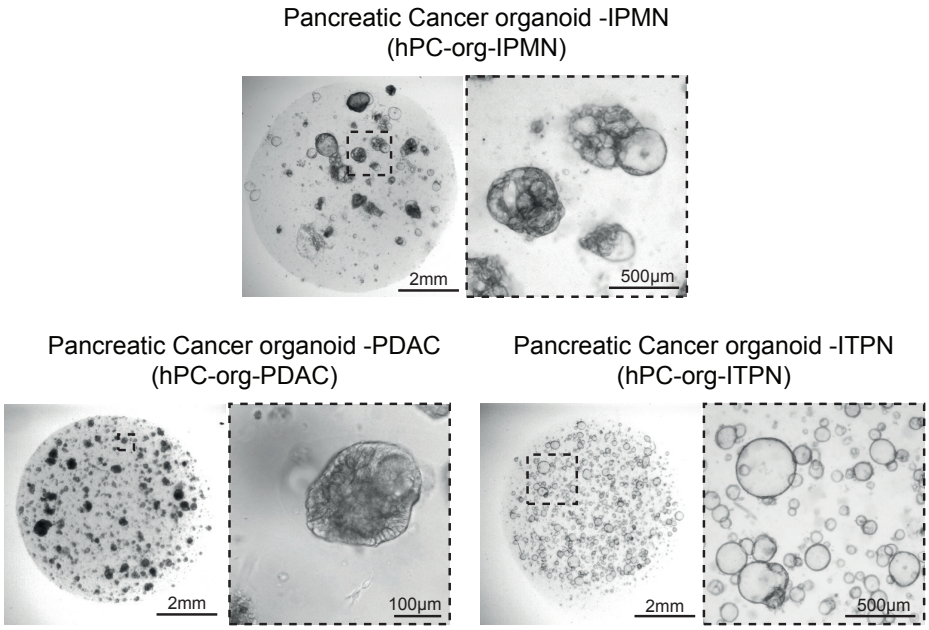

Figure 4.3 Establishing human pancreas cancer organoids from cancer resection biopsies. Representative brightfield images showing hPC organoids derived from intraductal papillary mucinous neoplasm (IPMN; upper panel), pancreatic ductal adenocarcinoma (PDAC; lower left panel), and intraductal tubulopapillary neoplasm (ITPN; lower right panel).

This is due to a low amount of tissue that is usually provided with these types of biopsies. In order to maximise the likelihood of deriving a line, as well as to capture both healthy and tumour populations, the digested tissue was cultured in either hPO-Opt. EM media or tumour media (Table 1). The tumour media used was a similar media composition to the one used by Boj. *et al.*, (media 10) while also removal of PGE2 was trialled (media 9) to further restrict the medium and reduce chances of healthy contamination. Furthermore, in order to produce a pure population of tumour organoids, organoids that at the seeding stage adopted a healthy phenotype were handpicked and removed, and the remaining tumour organoids were expanded separately in either tumour media or hPO-Opt. EM (Fig. 4.2a). Interestingly, the two pre-malignant tumour derived organoids, namely hPC-org-IPMN and hPC-org-ITPN, both generated cultures when seeded in hPO-Opt.EM media. However, hPC-org-PDAC organoids, from the more aggressive and malignant tumour, failed to expand in hPO-Opt. EM (Fig. 4.2b, Supp. Fig. 5). hPC-org-IPMN organoids expanded with similar efficiency to healthy hPOs in hPO-Opt.EM media with no slowing down at passage 12, but in the tumour media, grew slower and the cultures eventually collapsed at passage 7 (Fig. 4.2b). hPC-org-ITPN expanded in both hPO-Opt. EM media and tumour media (with or without PGE2) but cultures eventually collapsed in hPO-Opt.EM media while they expanded in tumour media indefinitely. Furthermore, hPC-org-PDAC organoids, which were generated and expanded only in tumour media, expanded in the same manner with or without addition of PGE2 (Fig. 4.2b). Furthermore, hPC-org-PDAC and hPC-org-ITPN lines have been expanded for studies outside the scope of this project and have continued to expand and be passaged

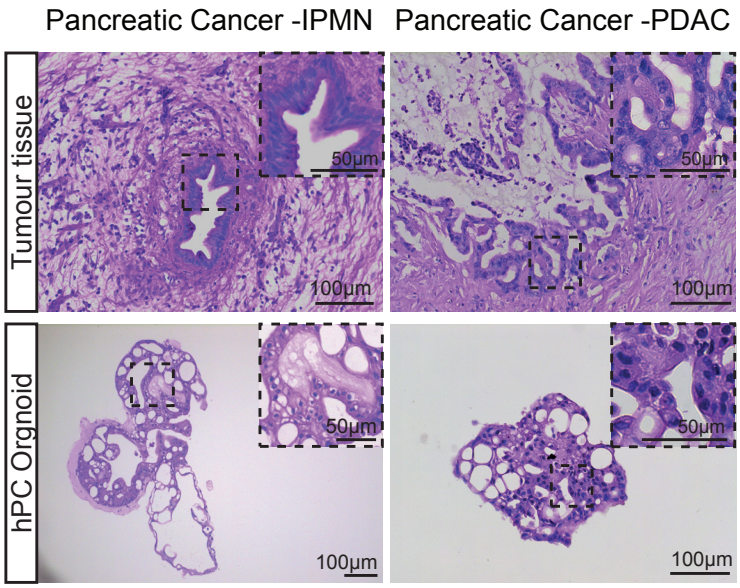

Figure 4.4 hPC organoids maintain the histological architecture of the parental tumour. Representative H&E staining of human pancreatic tumour tissue (upper panels) and organoids derived from the tissue (lower panels). Note the lack of epithelial organisation that is maintained between the parental tumour and the derived organoid. (n>6 organoids imaged per donor). Please compare with Figure 3.10 with healthy organoids expanded in hPO-Opt.EM.

without signs of slowed growth rate (data not shown). Importantly, since the purpose of hPC organoid generation was to obtain a positive control for comparison to healthy organoids, hPC organoids (inclusive of hPC-PDAC, hPC-IPMN and hPC-ITPN organoids) expanded in tumour media (hPC-EM+PGE2) were used for subsequent analysis and comparison (unless stated otherwise).

Utilising these culture conditions, three human pancreas cancer lines were established. Each line presented a markedly different morphology: hPC-org-IPMN demonstrated a multi-cystic or budding-like phenotype with a compact organisation while hPC-org-PDAC presented a complete loss of lumen formation with compact structure that appeared dark under the brightfield microscope (Fig. 4.3). hPC-org-ITPN generated structures similar to hPOs however, the cysts generated a more uniform round structure and did not swell like hPOs (Fig. 4.3). Additionally, healthy hPOs from a healthy donor line were also expanded in tumour media to test whether any of the phenotypes presented were a result of the media conditions rather than the tumourigenic nature of the line. Healthy hPOs placed in tumour media from passage 6 quickly deteriorated after just one passage (Supp. Fig. 6).

Histological assessment of the primary cancer tissue and derived organoids through H&E staining demonstrated that hPC-organoids had a complete loss of organisation, no single-cell epithelium as well as no lumen formation with some instances of small lumen-like structures (Fig. 4.4). However, apart from the loss of epithelial organisation, it is uncertain to what extent these tumour derived organoids recapitulate the architecture of the primary tumour as these are yet to be assessed by a clinical

histopathologists. Additionally, due to the restrictions imposed in response to the SARS-CoV-2 virus, H&E staining of hPC-org-ITPN organoids and the correlating tissue have not yet been generated.

Furthermore, in order to elucidate whether hPC organoids maintained expression of biomarkers at the same level as the parental tissue, I carried out mRNA analysis. hPC organoids from IPMN and PDAC tissue (expanded in tumour media) demonstrated higher KRT19 levels than the parental tissue (Fig. 4.5). Interestingly, hPC-ITPN organoids generated in tumour media showed reduced levels of KRT19 while organoids generated from the adjacent tissue demonstrated significantly increased levels of KRT19 compared to the parental tissue (Fig. 4.5). Interestingly, the clinical histopathology report noted low KRT19 staining in the tumour biopsy which is in concordance with mRNA levels of the tumour derived organoid but not the organoids derived from the adjacent tissue. Furthermore, all hPC organoids maintained expression of SOX9 with IPMN and ITPN organoids showing increased expression while PDAC organoids had lower levels of SOX9 compared to primary tissue.

In order to assess whether these hPC-organoids are proliferative *in vitro*, I performed Ki67 immunostaining demonstrating that they maintained proliferation. This was similar to hPOs expanded *in vitro* (0.35 ± 0.07 and 0.32 ± 0.05 Ki67/DAPI cells, respectively; Fig. 4.6a), demonstrating that proliferation rates among hPC-org-PDAC and hPOs were indistinguishable. Furthermore, mRNA analysis of key ductal markers KRT19 and SOX9 revealed no clear differences between healthy and cancer derived organoids (Fig. 4.6b).

Nevertheless, this data demonstrates that pancreas tumour-derived organoid lines can be generated and utilised to establish criteria of tumour growth *in vitro*.

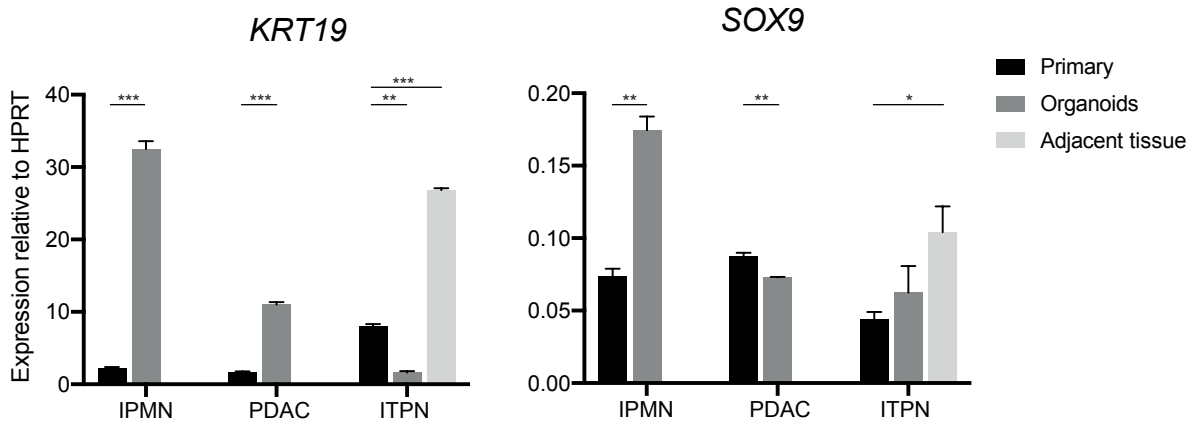

Figure 4.5 mRNA analysis of pancreas cancer primary tissue and organoids. mRNA expression analysis of pancreatic ductal genes KRT19 and SOX9 in primary tumour tissue, derived tumour organoids and adjacent tissue organoids (available only for the ITPN tumour). Data presented as mean ± SEM. Differences were tested by paired t-test. Significant differences are marked by asterisks: * $p \leq 0.05$, ** $p \leq 0.01$, *** $p \leq 0.001$.

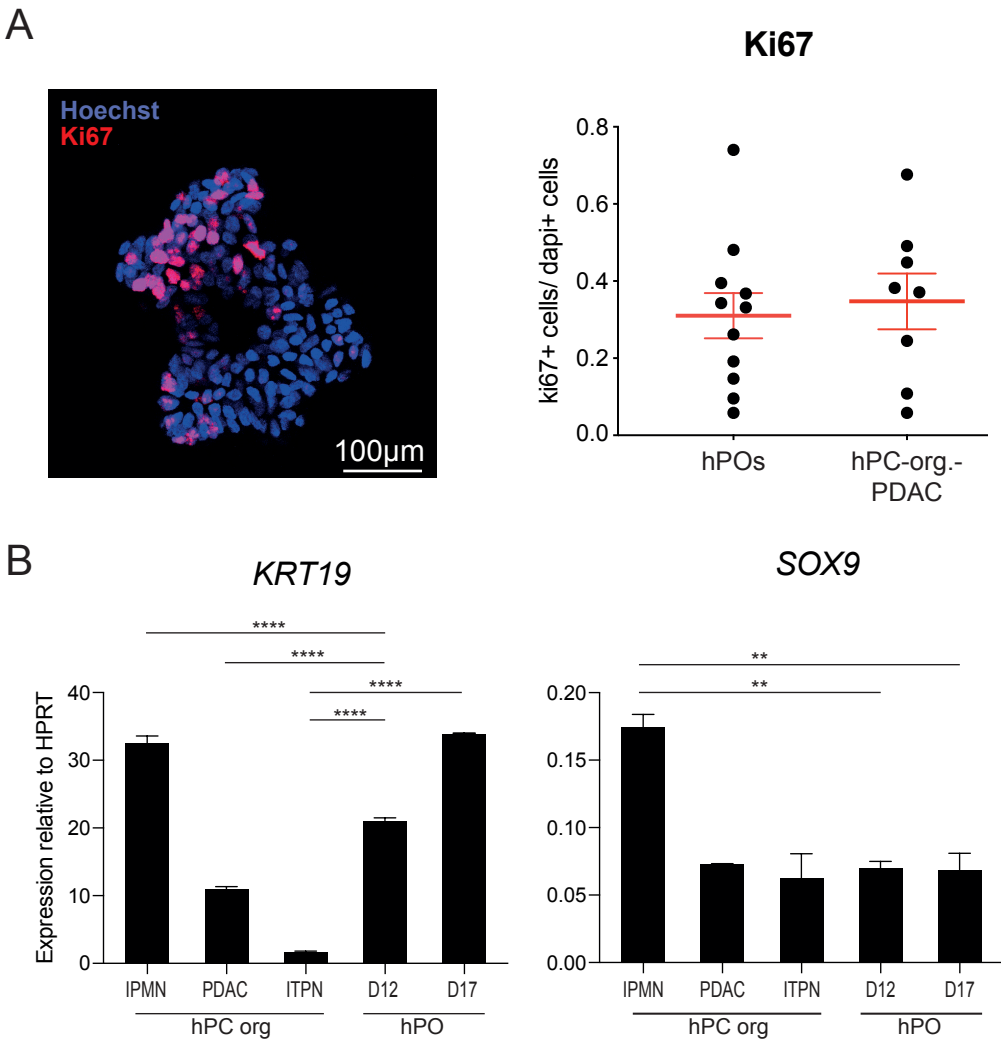

Figure 4.6 Proliferation and marker expression between healthy and cancer derived organoids. (**A**) Representative image of Ki67 immunostaining of hPC-org-PDAC organoids and Ki67 quantification of healthy hPOs and hPC-org-PDAC. (**B**) mRNA expression analysis of pancreatic ductal genes *KRT19* and *SOX9* in hPC derived organoids and hPOs. Data presented as mean ± SEM. Differences were tested by two tailed t-test for (**A**) and one-way repeated measures ANOVA followed by Tukey's honestly significant difference (HSD) test for (**B**). Differences shown between hPC organoids and hPOs. Significant differences are marked by asterisks: * $p \leq 0.05$, ** $p \leq 0.01$, *** $p \leq 0.001$, **** $p \leq 0.0001$.

4.2.2 Genomic stability of hPOs

Somatic mutations and chromosomal abnormalities accumulate spontaneously throughout the lifetime of an individual, and while most are harmless, others act as driver mutations which increase the likelihood of cell transformation and tumorigenesis[162]. For accurate disease modelling as well as use as a cell therapy, it is vital that the cells used do not show an increased susceptibility to accumulate genetic aberrations upon time in culture, which could interfere with the conclusions obtained from the disease model or cause tumour formation in the recipient patient if used as a cell therapy.

4.2.2.1.Karyotype analysis

Aneuploidy in normal cells is uncommon since chromosome segregation during mitosis is tightly regulated and mis-segregation events occur at rates below 1% in normal cells[270]. Cancer cells are more commonly aneuploid due to chromosomal instability either due to mis-segregation or due to structural aberrations such as translocations, deletions and duplications, which can affect parts or the whole of the chromosome leading to gains or losses of whole-chromosomes[270].

Karyotyping allows detection of large chromosomal aberrations and is a useful method to determine whether cultured cells still maintain a normal diploid karyotype after a certain number of passages or cell divisions, thus providing a rough indicator of genetic stability[147]. Furthermore, guidelines from the FDA and EMA state that karyotype analysis is to be performed for cell therapy products or for establishing a biobank[168,169].

Karyotype analysis usually entails the assessment of chromosomal numbers as well as chromosomal arms. I performed karyotype analysis on hPOs which included the former but not the latter. The number of chromosomes in both early- and late-passage hPOs was analysed to evaluate their genomic stability over time in culture. As a positive control, the number of chromosomes in all three human pancreas cancer lines, hPC-org-IPMN, -PDAC, -ITPN were also analysed (Fig. 4.7a). As expected, abnormal chromosomal numbers were found even at early stages in hPC-org cultures, with more than 50% of the cells exhibiting chromosomal numbers greater than 46, with the most severe chromosomal number changes detected in organoids derived from the more aggressive PDAC tissue (Fig. 4.7b). In contrast, karyotype analysis of two donors in the early (P3-5) and late (P10-12) stage expanded in BME 2 did not demonstrate numbers greater than 46. Notably, hPOs generated and expanded in the chemically defined GFOGER-hydrogel also showed normal ploidy (Fig. 4.7b). This therefore demonstrates that hPOs maintain stable chromosomal numbers over long-term culture unlike their malignant counterparts.

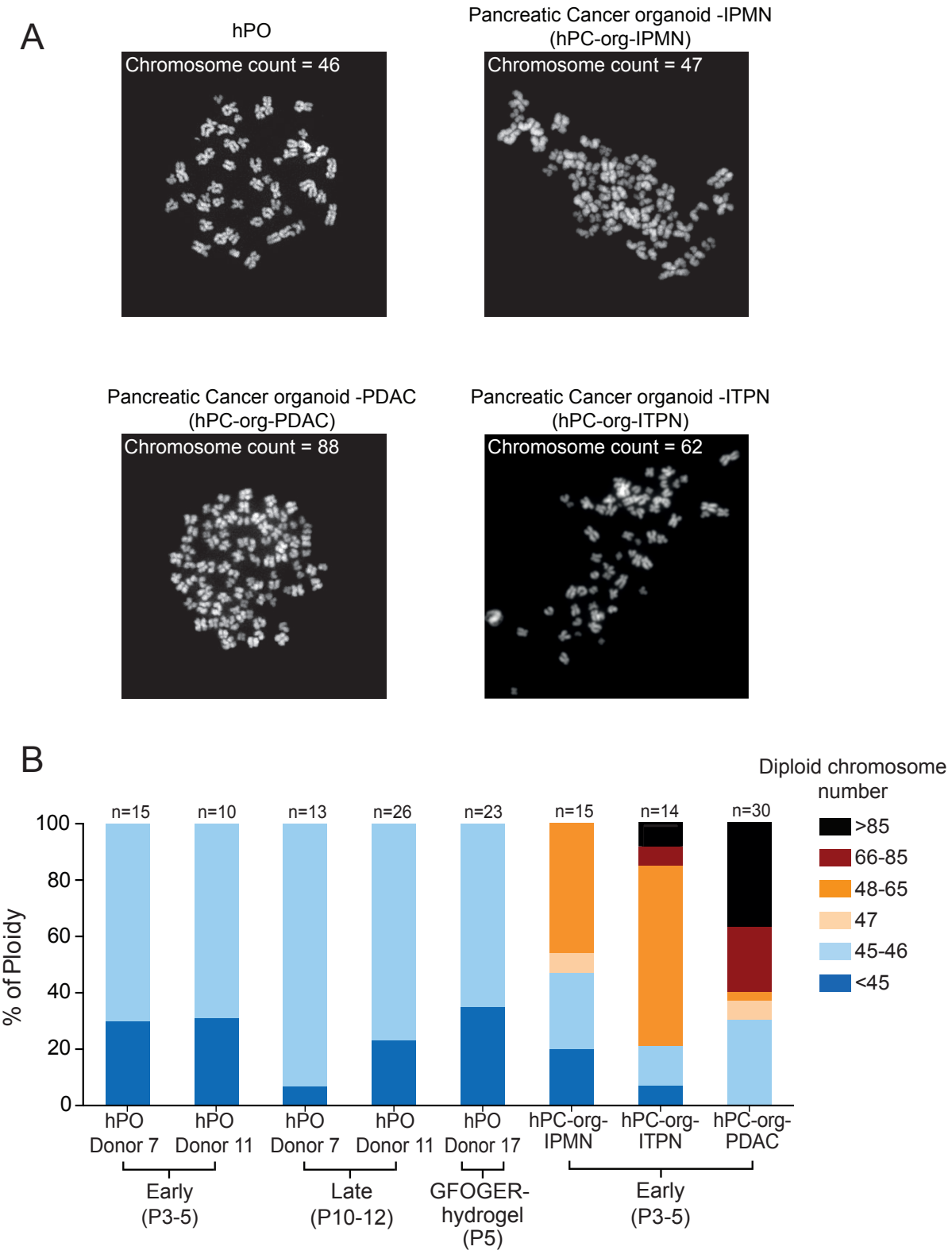
A
hPO
Chromosome count = 46
Pancreatic Cancer organoid -IPMN
(hPC-org-IPMN)
Chromosome count = 47
Pancreatic Cancer organoid -PDAC
(hPC-org-PDAC)
Chromosome count = 88
Pancreatic Cancer organoid -ITPN
(hPC-org-ITPN)
Chromosome count = 62
B
Diploid chromosome number
>85
66-85
48-65
47
45-46
<45
% of Ploidy
100
80
60
40
20
0
n=15
n=10
n=13
n=26
n=23
n=15
n=14
n=30
hPO Donor 7
hPO Donor 11
hPO Donor 7
hPO Donor 11
hPO Donor 17
hPC-org-IPMN
hPC-org-ITPN
hPC-org-PDAC
Early (P3-5)
Late (P10-12)
GFOGER-hydrogel (P5)
Early (P3-5)

Figure 4.7 Human pancreatic organoids (hPOs) expanded long-term in culture maintain chromosomal stability over time. (**A**) Representative images of chromosome spreads used for counting from healthy human pancreas derived organoids (hPO) and pancreas cancer derived organoids (generated from pancreatic tumour tissue; Intraductal Papillary Mucinous Neoplasm (hPC-org-IPMN) and Pancreatic Ductal Adenocarcinoma (hPC-org-PDAC) and Intraductal Tubulopapillary Neoplasm (hPC-org-ITPN) . (**B**) Chromosome spreads were prepared and counted from early (P3–5) and late (P10–12) passage cultures. Note that hPOs generated from healthy donors (expanded in BME 2 or GFOGER-hydrogel) do not display increased chromosomal counts (above 46) indicating hPOs maintain normal chromosome numbers during *in vitro* culture, whilst this is not the case for pancreas cancer organoids, as previously reported (Boj *et al.*[131]). The number of chromosome spreads counted per condition is detailed above the graph.

4.2.2.2. Whole genome sequencing (WGS) of hPOs

Karyotype analysis is a useful tool in understanding whether gross chromosomal changes have occurred, but it lacks the sensitivity to detect mutations that have taken place across the genome. Therefore, this project aimed to investigate the mutations that occur as a result of *in vitro* culture of hPOs to understand the mutational burden and potential oncogenic transformation risks. Since cells of a bulk non-clonal culture would have a high amount of mutational differences between them owed to somatic mutations accumulated throughout the lifetime of the individual, clonal cultures were generated for WGS in order to detect mutations that have arisen in the duration of the culture (Fig. 4.8a). To achieve this, dissociated pancreatic ducts from Donor 14 were seeded in BME 2 and allowed to generate organoids. At this stage, the organoids were made into single cells and seeded in a sparse manner and single cells (that were manually tracked) that formed organoids were handpicked out and allowed to expand for DNA collection. Then, a subsequent second clonal step was performed at the 2-month timepoint after the first clonal step, in order to generate subclones. The subclones were also allowed to expand and were collected at approximately 4 months after initiation of the culture. Clones, subclones and matched nonclonal reference sample were subjected to WGS (Fig. 4.8a) Of note, clones were generated from a second donor, Donor 10, but generation of sub-clones was not possible as the cells did not expand following the second single-cell step. This was likely due to expansion capacity difference of the hPO line associated with the donor. Library preparation, sequencing, sequence read alignment, variant calling, copy number calling, and variant filtering were performed by Alex Cagan in the Martincorena lab, Wellcome Sanger institute as detailed in section 2.5. Graphs were generated in collaboration with Alex Cagan following multiple discussions on the design of the filtering, use of the outputted data, exclusion of contaminated samples etc.

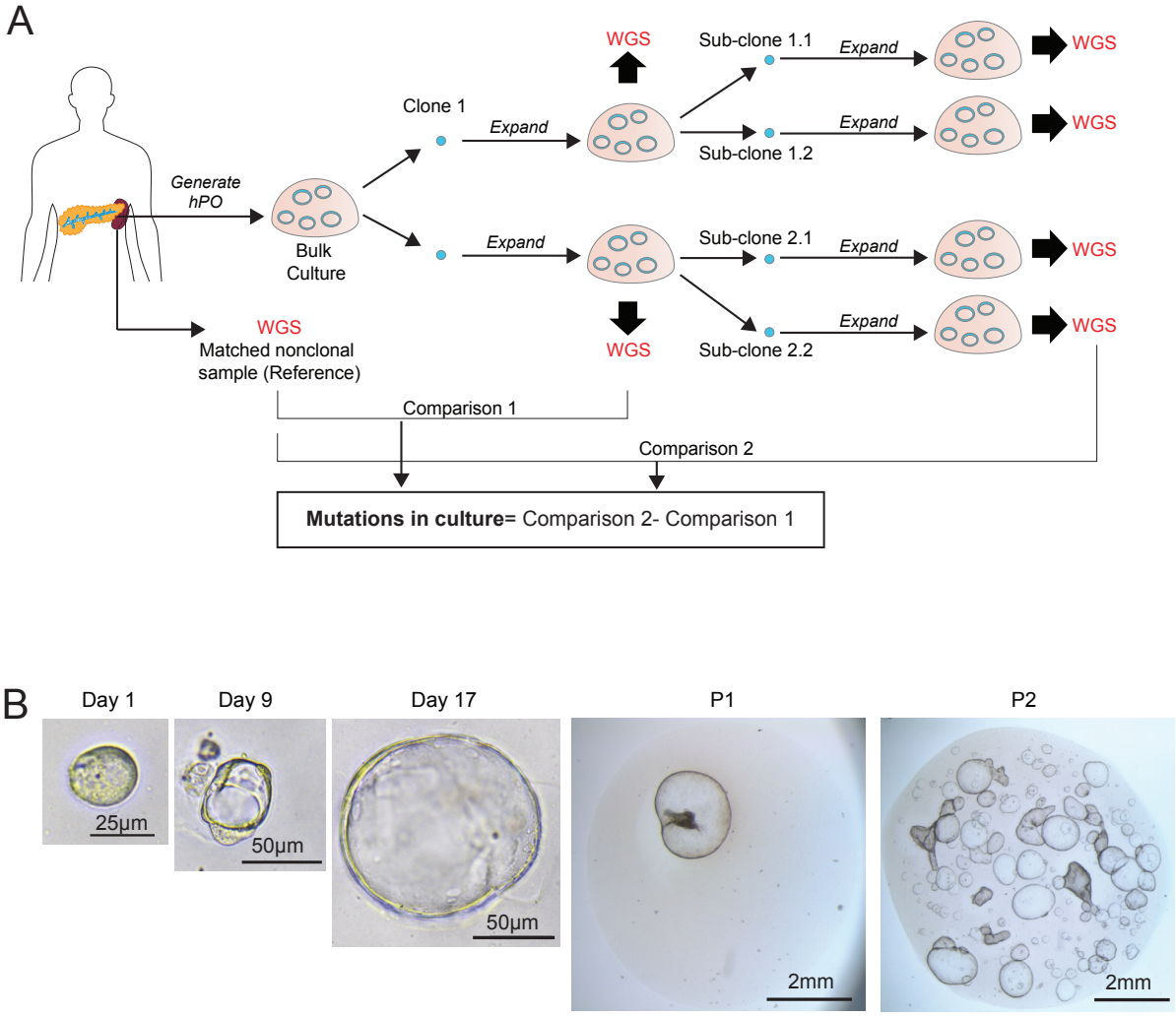

Figure 4.8 Generation of hPO clones and subclones for WGS. **(A)** Schematic illustrating generation of clones and subclones from pancreatic ductal tissue. Pancreatic ducts are seeded and allowed to expand into organoids. The organoids are made into single cells and are seeded in low cell density. Single cells that grow into organoids (**B**) are picked out and grown separately to generate clonal cultures. At 2 months, the single-cell step is repeated to generate subclones. Clones, subclones and matched reference samples (i.e., splenocytes) are submitted for WGS. Germline mutations are removed using the matched normal sample and mutations in culture are calculated by subtracting the clonal variants from the subclonal variants. (**B**) Representative images of a single cell expanding into an organoid after 17 days. Once the organoid is large enough, it is hand-picked out and grown in a different well.

4.2.2.3.Mutational burden of in vitro culture on hPOs

In order to understand the mutational burden of hPO culture, we derived the following strategy. Germline variants would be removed following matching the clone variants to the matched reference sample. Furthermore, variants which were likely due to PCR errors would be filtered out bioinformatically. Then, the variants found in clones would be subtracted from the variants found in subclones to provide with the number of mutations that have arisen solely during the time of *in vitro* culture between the two steps (Fig. 4.8a).

As the organoids were derived from single cells, we expected the majority of somatic variants to be present as heterozygotes in all cells in the organoid. Such variants would have a variant allele frequency (VAF) distribution centred around 0.5, with noise due to sampling. To confirm the clonality of the organoids we plotted their VAF distributions (Fig. 4.9a). We noted that the majority of samples have a VAF distribution centred around 0.5, confirming that the organoids are clonal and therefore likely to be derived from a single cell. A few samples (Clone 4, Clone 5) show an additional small peak of variants with low VAF (< 0.2). This could represent PCR errors introduced during library preparation or subclonal mutations acquired during culture (Fig. 4.9a).

However, following the application of bioinformatic filters for contamination, we identified four samples where contamination levels were >5%, exceeding the cut-off point and therefore removed from further analysis. The four samples included the 4/6 subclones included in the analysis (Appx. Table 3). Notably, these samples had spent longer in culture and underwent a second clonal step, suggesting that this may be connected to higher risk of exposure to contamination from human cells not derived from the donor, though this is purely speculative. Therefore, the samples that could be used for further analysis were Clones 1, 4, 5 and 5.5 (clones 5 and 5.5 were expanded from the organoid fragments of a single clonal organoid and are representative of 1 clonal cell) as well as subclone 5-4 (daughter of clone 5) and subclone 5.5-3 (daughter of clone 5.5; Fig. 4.9b). A heatmap of the shared variants among the samples shows that clones 1 and 4 group closer together, while clones 5, 5.5 and subclones 5-4 and 5.5-3 group closer together, which is in agreement with their lineage (Fig. 4.9b). Starting with the raw variants of these samples, in order to accurately and comparably call mutations in these samples and avoid the risk of calling mutations that are either artefacts or sequencing errors, we first applied bioinformatic algorithms to genotype mutations found in these samples in all other samples to minimise risk of missing mutations due to lower coverage. Any mutations seen across all samples were excluded as likely to be artefacts or germline SNPs. For the remaining set of mutations, we called the mutation in a sample if there were at least two supporting reads in that sample (4.9c). To alleviate problems of comparison caused by differences in coverage across samples, we filtered out mutations that did not have at least 10x coverage in all of the samples from Donor 14 (Fig. 4.9c). Subtracting the variants found for the clonal samples from their subclones it can be deduced that hPOs accumulate on average

A

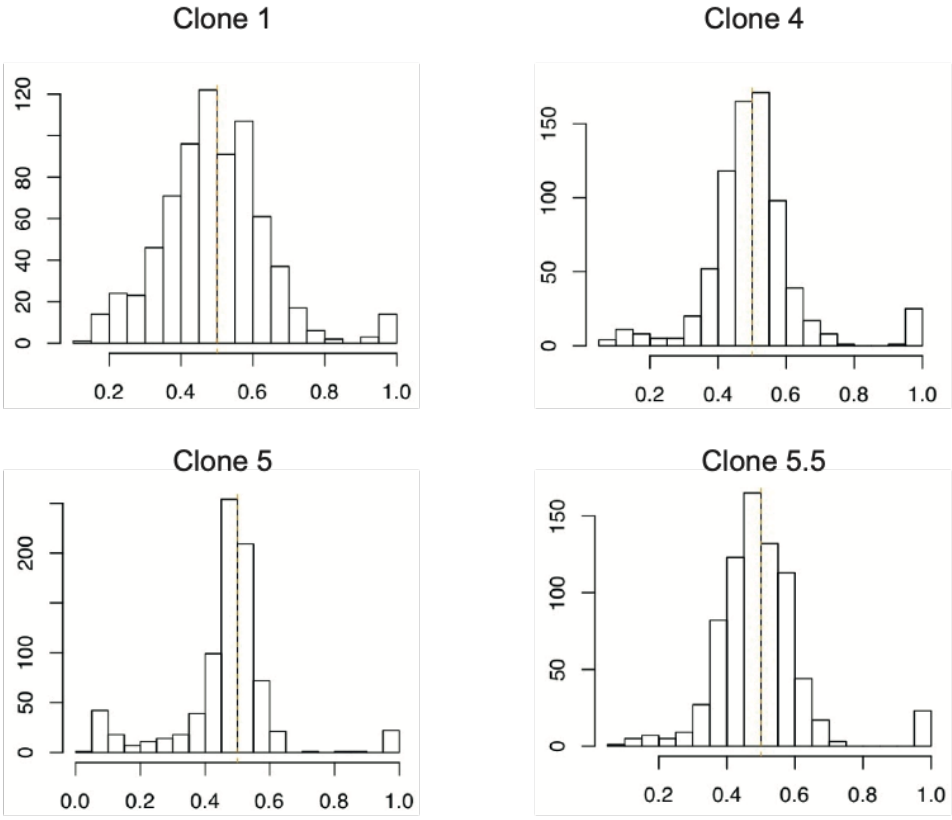
Clone 1
Clone 4
Clone 5
Clone 5.5

B

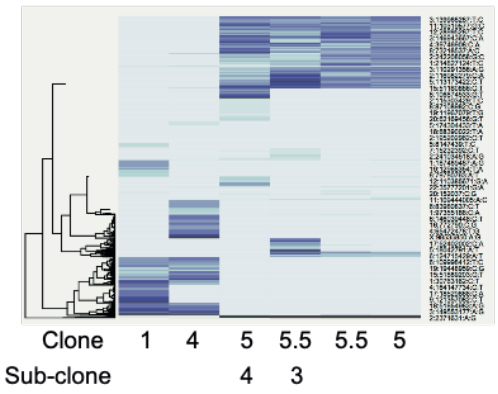
Clone 1 4 5 5.5 5.5 5
Sub-clone 4 3

C

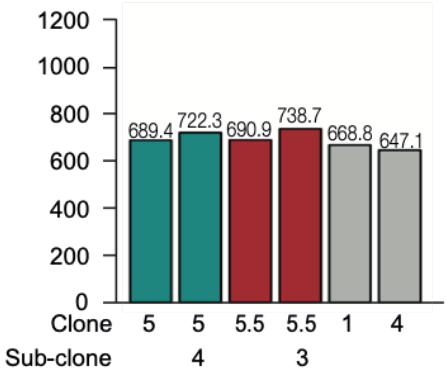
689.4
722.3
690.9
738.7
668.8
647.1
Clone 5 5 5.5 5.5 1 4
Sub-clone 4 3

D

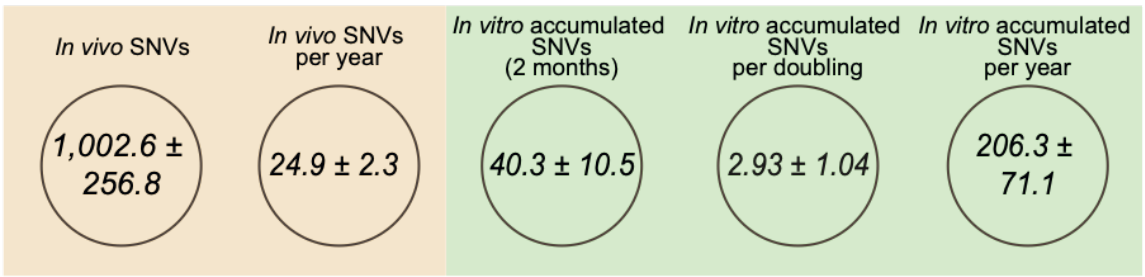
In vivo SNVs
1,002.6 ± 256.8
In vivo SNVs per year
24.9 ± 2.3
In vitro accumulated SNVs (2 months)
40.3 ± 10.5
In vitro accumulated SNVs per doubling
2.93 ± 1.04
In vitro accumulated SNVs per year
206.3 ± 71.1

Figure 4.9 Variant allele frequencies plots of clonal hPOs and variant accumulation during *in vitro* culture The variant allele frequency (VAF) of single nucleotide variants was assessed using genome sequencing data from cultures derived from single cells as described in Figure 4.8a, in all cases the VAF was close to 0.5, confirming clonality of these cultures. Graphs show clones 1,4,5 and 5.5 from Donor 14. Of note, clones 5 and 5.5 were derived from the same organoid that was split into two fragments and are therefore representative of the same clone. (**B**) Heatmap showing variant sharing among clones and subclones for Donor 14. (**C**) Graph demonstrating number of variants following use of bioinformatic filters set for at least 2 supporting reads and a minimum coverage of 10x for each variant. (D) Calculations made from variant data to show accumulation of variants in the donor tissue as well as during *in vitro* culture of clonal hPOs.

40.3 ± 10.3 SNVs in approximately 2 months of culture (time between first and second clonal step; Fig. 4.9d). Furthermore, in section 3.2.2 I calculated that the doubling time for hPOs is 78 and 177 hours for early and late passage hPOs. Taking the average of the two values, i.e., 128 hours, seeing as how the clonal organoids were expanded from P0 until late passage, it is calculated that hPOs accumulate approximately 2.93 ± 1.04 SNVs per population doubling.

Furthermore, the values can also be extrapolated to illustrate that hPOs could accumulate 206.3 ± 71.1 SNVs in a year of *in vitro* culture (Fig. 4.d). While this is indeed very interesting, the data can be compared with that of the *in vivo* mutation accumulation, i.e*.,* mutations that have arisen in the donor tissue. The SNVs found in the clones only, following filters to remove potential PCR or sequencing errors, equate to the SNVs found in the donor. Therefore, looking at the SNVs in the clones of both Donor 14 and 10, there is an average of 1,002 SNVs among 7 different clones (Appx. Table 3). This points to the possibility that a single ductal cell acquires approximately 1,000 SNVs in 41 years (average age of Donors 14 and 10; Fig. 4.9d). Taking the average SNVs per year for each donor, it can be said that pancreas ductal cells obtain 24.9 ± 2.3 SNVs per year (Fig. 4.9d). This shows that hPOs accumulate approximately 8-fold higher SNV numbers *in vitro* than their *in vivo* counterpart over a year.

4.2.2.4.Functional mutations in hPOs

Looking further into the data of Donor 14 it is possible to scrutinise the WGS data to understand whether the mutations were in gene-coding regions and whether they already existed in the donor tissue or if they were generated during culture. To look for putatively functional mutations acquired during culturing for each organoid we selected the variants with frequency > 0.3 VAF. This removed very low frequency variants likely to be enriched for sequencing errors. These variants were annotated according to their putative function (Fig. 4.10). The overwhelming majority, 98.6%, of mutations fall within non-coding regions, mostly in intergenic or intronic regions, and are unlikely to impact cellular function (Fig. 4.10).

For the variants that were within gene coding regions (1.4%), they were classified as non-synonymous, stop-gain or stop-loss or synonymous mutations (Fig. 4.11). Interestingly, the subclonal samples did not show an increase in numbers of gene-coding mutations compared to their parent clones.

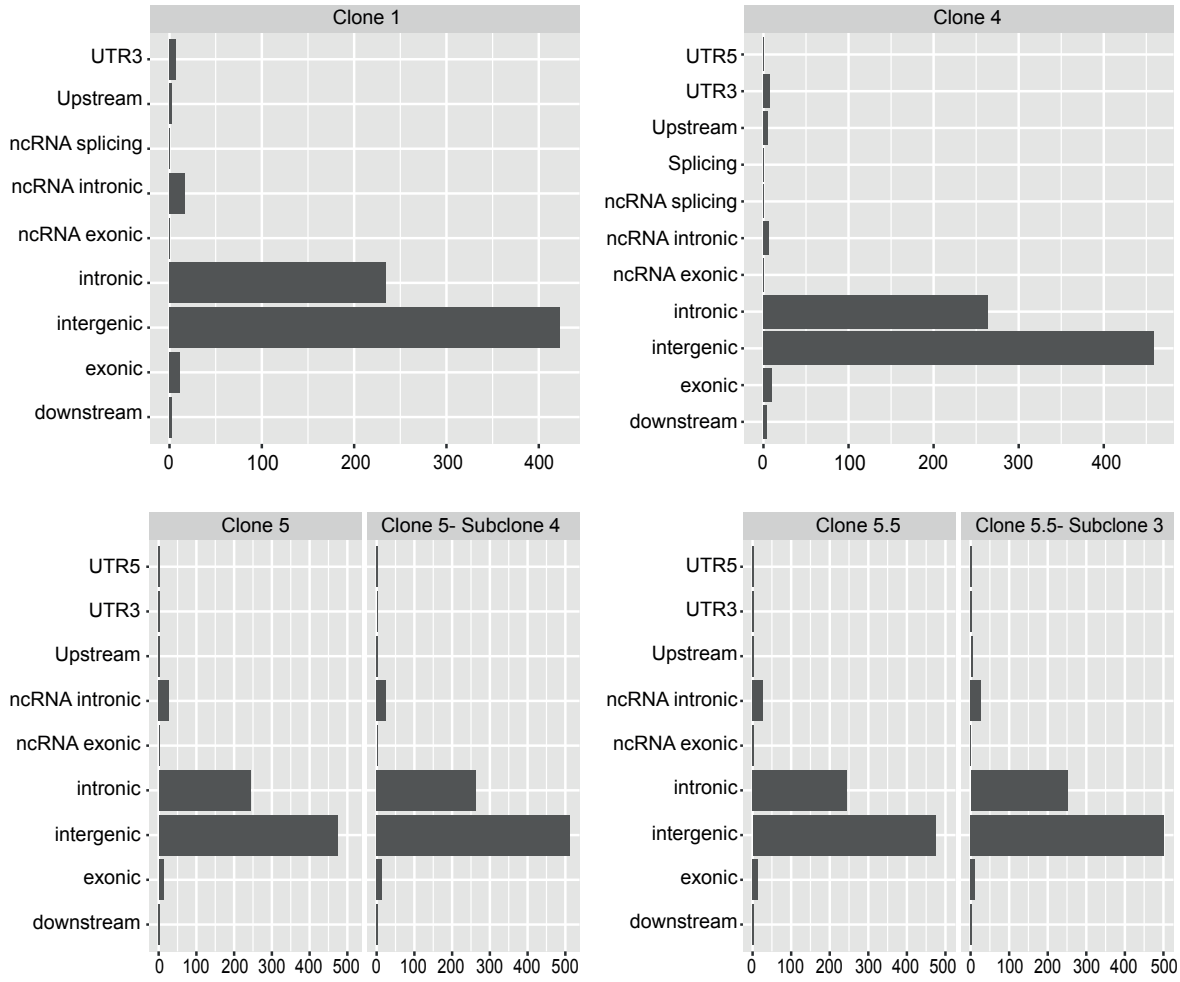

Figure 4.10 Genomic location of SNVs in hPOs. Graphs demonstrating the genomic location of SNVS for clonal and subclonal samples from Donor 14. Note that the vast majority of variants fall in non-gene coding regions and are therefore less likely to have deleterious effects.

However, I was able to identify a mutation in the alpha-actinin-3 (*ACTN3*) gene found in subclone 5-4 and not in its parent clone. However, this same variant was found in clone 1 suggesting that this variant existed in the donor and was perhaps not detected in clone 5. A synonymous mutation was identified in the PR/SET Domain 11 (*PDRM11*) gene for subclone 5.5-3 which could not be found any of the other samples, meaning that this may be a novel variant that has arisen during culture. However, as it is a synonymous mutation, the gene's function would not be affected.

For the putatively functional variants in coding regions (non-synonymous, stop-gain or stop-loss) we checked whether there was any overlap with known cancer driver mutations. First, we tested whether any of the mutations occurred in genes in a list of 369 genes previously identified as being under selection in human cancers[161] and validated them as driver genes. We identified a loss of function (stop-gain) mutation in the Neurofibromin 1 (*NF1*) gene that was shared by two clones (Clone 1 and 4)

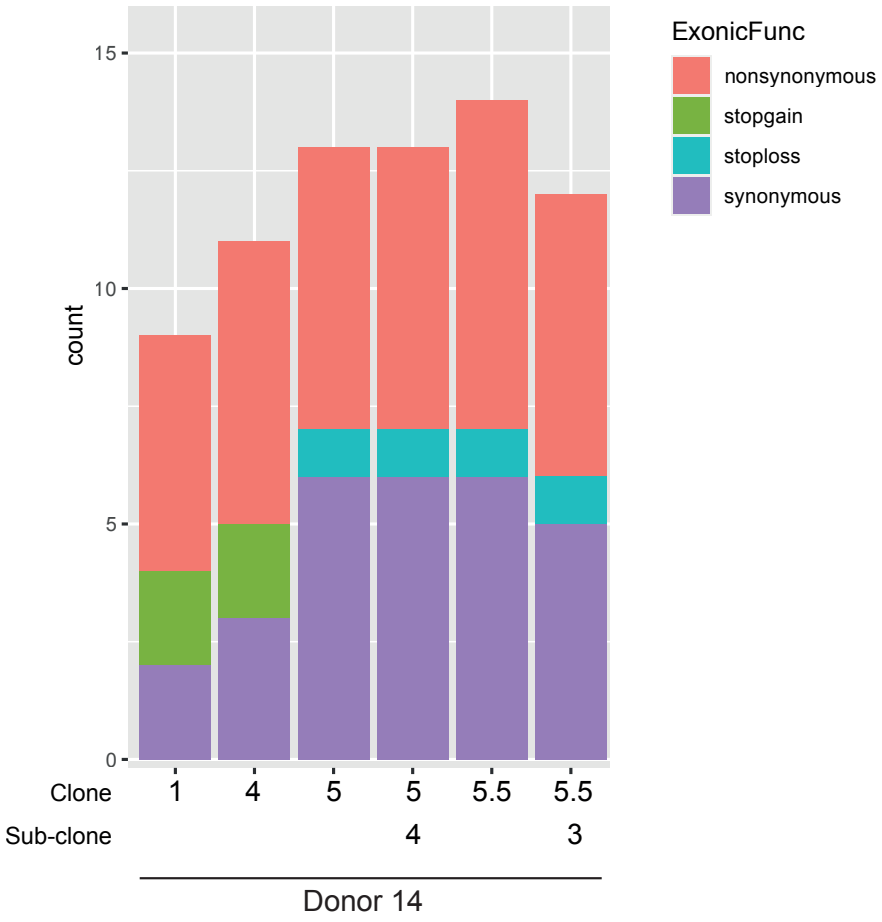

Figure 4.11 Functional variants in gene-coding regions. Variants were filtered for VAF>0.3 to, removing variants that were likely detected due to sequencing errors. Variants were then annotated as synonymous and non-synonymous mutations and further into stop-gain or stop-loss mutation. Notably, subclones had either the same or a smaller number of variants in gene-coding regions than their parental clones.

from Donor 14. However, the variant was found to be present in all three subclones of Clone 4. Although these subclones were excluded from the analyses due to their high levels of contamination these results suggest that this variant was present in the duct before culturing began and persisted in the organoid throughout culturing.

4.2.2.5.Copy number variations (CNVs) in hPOs

The allele-specific copy number analysis of tumours algorithm (ASCAT)[239] was then used to call copy-number changes. ASCAT makes use of both read depth and the ratio of heterozygous SNPs to determine allele-specific copy number. The results reveal no evidence of large-scale chromosomal differences in any of the clones derived from Donor 14 and 10 (Fig. 4.12). Furthermore, the CNV plots look equally stable for subclone 5-4, however there appear to be some CNVs in subclone 5.5-3 (Fig. 4.12). Although there is no agreed definition as to what accounts as a large structural variation, the

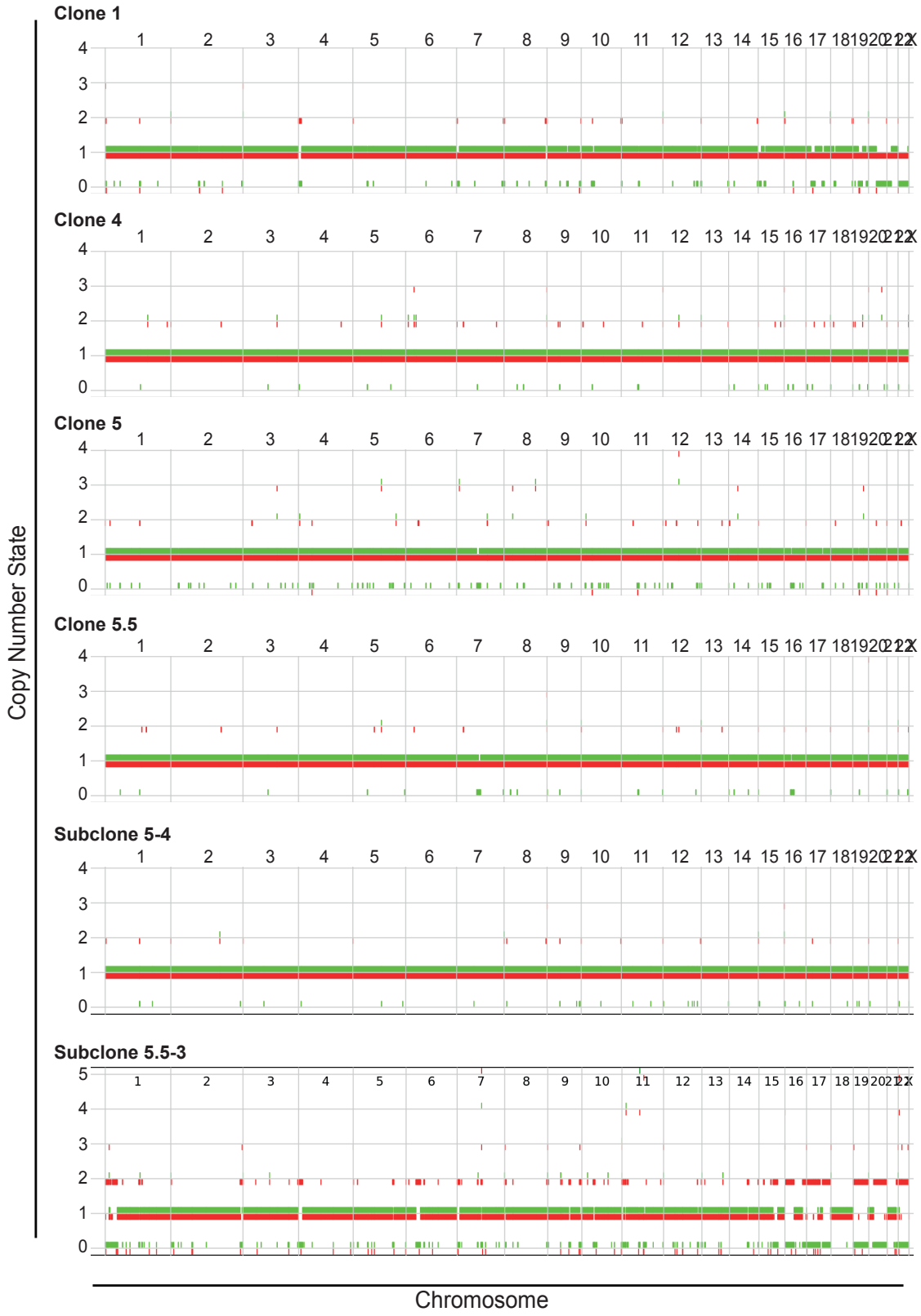

Figure 4.12 Copy number variations in clonal and subclonal hPOs. ASCAT copy number plots of three clonal hPO cultures show that hPOs do not exhibit loss of chromosomes or large structural rearrangements during *in vitro* culture (clonal expansion of 5 weeks). The copy-number state for each chromosome is shown on the Y-axis, with one allele coloured in red and the other in green. Chromosomes are labelled along the top of the graphs

CNV plot of subclone 5.5-3 is markedly different than the other samples particularly in chromosomes 16,17, 19,20 and 22 (Fig. 4.12). Notably, this sample had relatively lower sequencing coverage (Appx. Table 3) which may result in noisier CNV calls giving false positives. Deeper sequencing would be required with use of further bioinformatic tools to map the exact breakpoints of the duplications or deletions and further understand their potential impact. Moreover, the analysis was performed on only 2 subclones from 1 donor and further donors would be required to understand the prevalence of CNVs among long-term cultured subclones and/or whether the CNVs in subclone 5.5-3 are donor specific. Importantly, all clones assessed showed no chromosomal aberrations which support the data form the karyotype analysis.

4.2.3 *In vivo* safety assessment of hPOs

For a successful cell therapy, cells need to persist long-term in the body without giving rise to tumours or teratomas. Furthermore, mutations that have arisen during culture may or may not result in tumour formation and this risk needs to be interrogated thoroughly *in vivo*. The time of engraftment needs to be long enough to allow for potential development of tumours and thereby increase the sensitivity of the assay. Previous studies that have performed xenografts using healthy human pancreatic organoid cells have reported a low engraftment efficiency (12.5% of xenografts resulted in cells that could be recovered within the 1-month timepoint, and no xenografts recovered at later timepoints)[131]. Therefore, the ability of hPOS to engraft and be maintained long-term (beyond the reported 1-month limit) was tested as well as their potential tumorigenicity *in vivo*.

Prior to the initiation of this project, previous experiments had demonstrated subcutaneous injections of ductal organoids did not result in engraftment (data not shown). Therefore, this site was avoided, and the kidney capsule was chosen as an injection site owing to its vascularisation and accessibility as well as it being a site commonly used to assess engraftment or functionality of human cells in the mouse[271].

hPOs were generated, expanded and transplanted under the kidney capsule of NSG mice at the early passage (P6; 60 days of expansion) and late passage (P14; 135 days of expansion) stage. Early passage hPOs were able to engraft to a maximum of 2 weeks with an engraftment rate of 50% (2/4 mice) while late passage hPOs engrafted up to 4 weeks with an engraftment rate of 25% (2/8; Fig. 4.13). Non-engraftment was characterised by the inability to recover hPOs after thorough sectioning and staining. Subsequent efforts to engraft hPOs from 2 different donor lines resulted in no engraftment at any of the recovered timepoints. This meant that when accounting all the animals engrafted with hPOs in the kidney capsule using this early protocol, there was an overall very poor hPO engraftment of 20% within a 1-month timepoint (4/20 animals) and 0% engraftment beyond 1 month in the kidney capsule (0/23 animal; Table 2;Appx. Table 2). Nevertheless, hPOs that had engrafted retained ductal

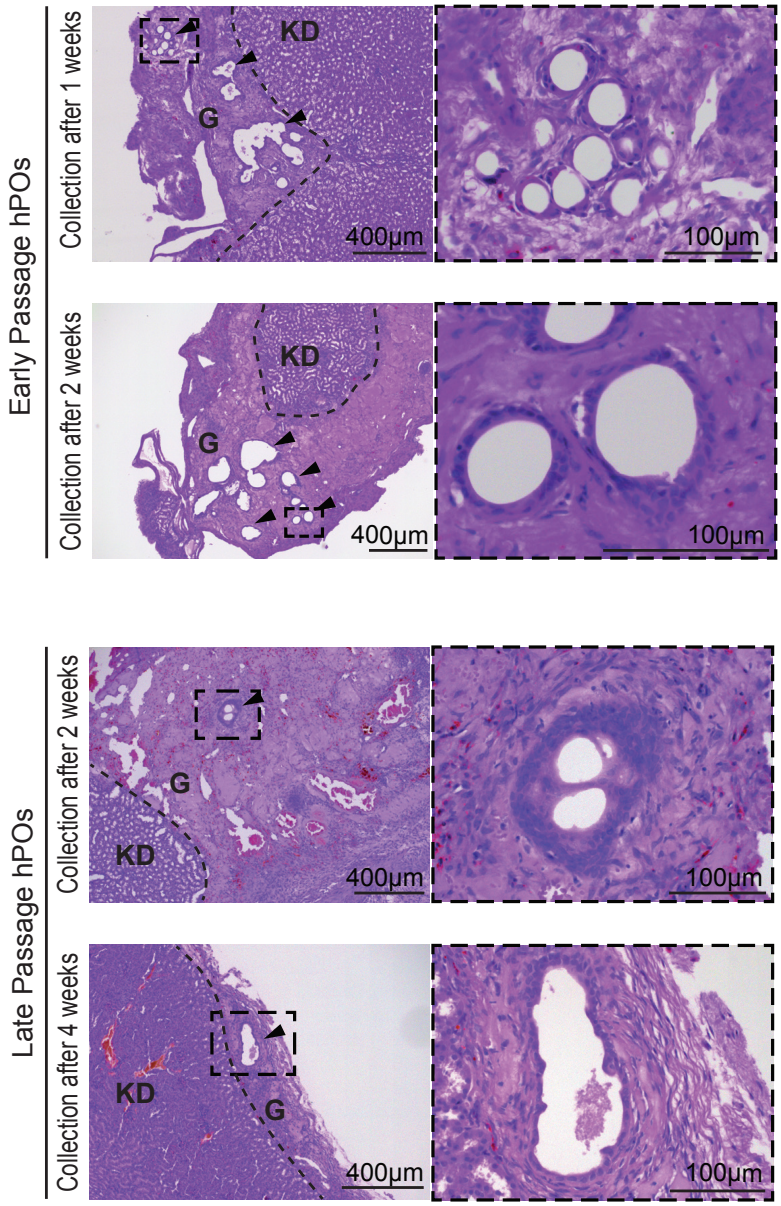

Figure 4.13 Early and late passage hPOs can be transplanted in the kidney capsule of NSG mice and survive up to 4 weeks. Representative images of early passage (60 days expansion) and late passage (135 days expansion) hPOs transplanted under the kidney capsule of NSG mice. (Refer to Appx. Table 2 for further details)

architecture (Fig. 4.13) and maintained expression of human specific KRT19 (Fig. 4.14) for both early and late passage hPOs.

However, in order to assess tumorigenicity of hPOs *in vivo*, consistent as well as long-term engraftment needs to be achieved. I aimed to improve the transplantation protocol by investigating multiple sites of transplantation to increase engraftment success and longevity. I developed a method to ensure I could identify the transplanted cells consistently. I generated mouse pancreas organoids (mPOs) from the ROSA^{nTnG} (ROSA26-nuclear-tdTomato-nuclear-EGFP) mouse. This mouse carries

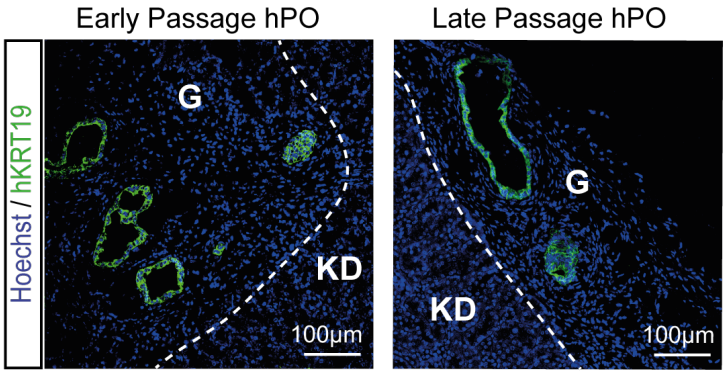

Figure 4.14 Engrafted hPOs maintain ductal architecture and key ductal marker (hKRT19). Representative immunofluorescence images of human specific antibody for ductal marker KRT19 (green). Both early passage hPOs and late passage hPOs maintain expression of KRT19 and a single cell epithelial organisation.

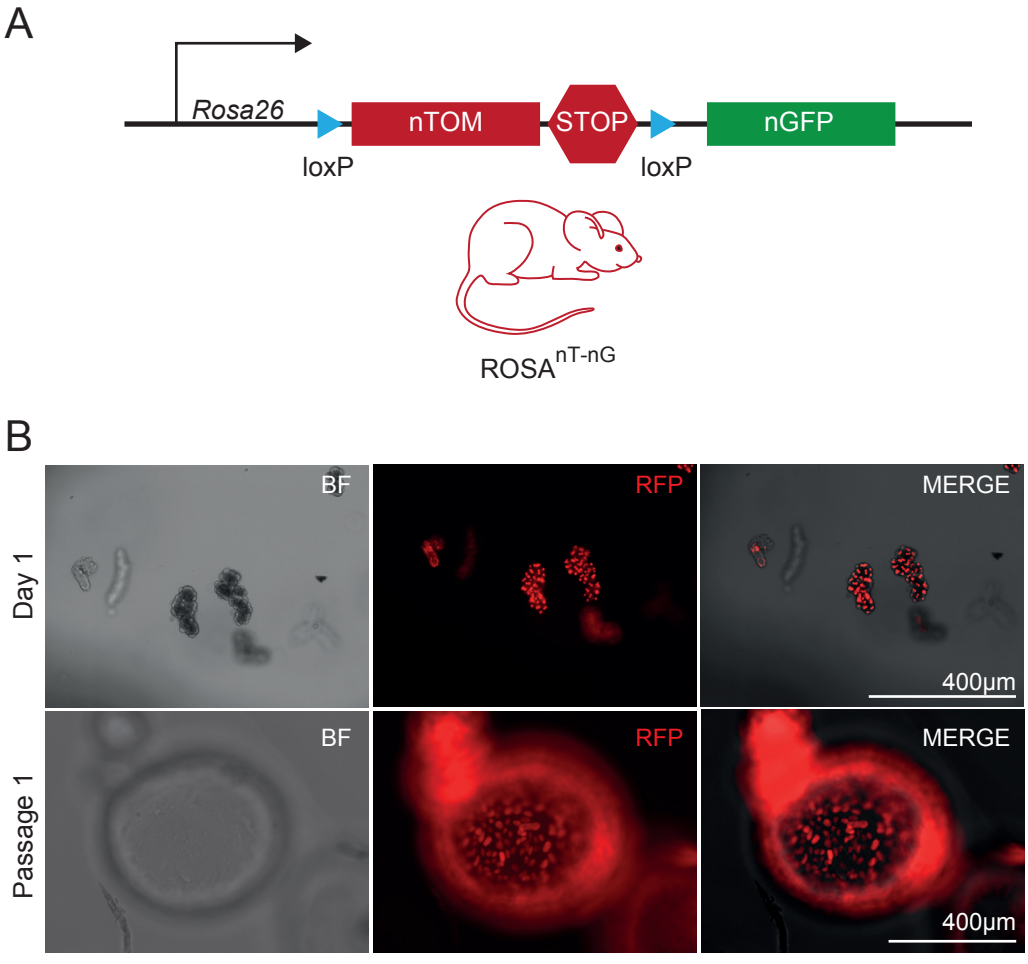

Figure 4.15 mPOs established from the ROSA-nTnG mouse. (**A**)Gene construct of the ROSA^{nTnG} mouse showing that RFP is constitutively expressed under the *Rosa26* locus. (**B**) Ducts derived from the nTnG mouse express RFP and expand normally into organoids which also maintain RFP expression.

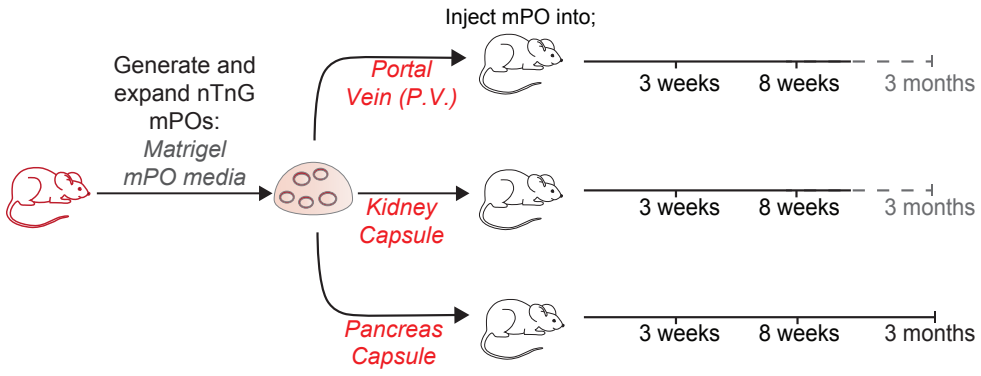

	Collection timepoint		
	3 weeks	8 weeks	3 months
P.V. (engraftment)	0/1	0/1	N.A
Kidney (engraftment)	2/2	2/2	N.A
Pancreas (engraftment)	2/2	2/2	3/3

Figure 4.16 nTnG mPO transplantations into the portal vein, kidney capsule and pancreas capsule of NSG mice. Schematic showing nTnG mPO transplantations into the various locations. Engraftment of nTnG mPOs into the portal vein (PV) or kidney capsule was not assessed at the three-month time point (grey dashed lines). Table (lower panel) shows summary of engraftment across the three locations in the mouse.

the ROSA$^{nT\text{-}nG}$ allele that consists of a CMV enhancer/chicken beta-actin core promoter, a loxP-flanked nT cassette, and a nG cassette, all inserted into the Gt(ROSA)26Sor locus[272] (Fig. 4.15a). The nonessential ROSA26 gene on chromosome 6 is ubiquitously expressed and when edited with ROSA$^{nT\text{-}nG}$ and in the absence of Cre-recombinase, tdTomato fluorescent protein is expressed (Fig. 4.15a). Since the ROSA26 gene is expressed in all cells, mPOs generated from this mouse maintained nuclear expression of fluorescent tdTomato in culture and after expansion (hereafter referred to as nTnG-mPOs; Fig. 4.15b). In order to investigate a favourable site for long-term engraftment, nTnG-mPOs were transplanted into the portal vein, kidney capsule or pancreas capsule and for the latter two sites, diluted (30%) Matrigel was used as opposed to 100% BME 2 utilised in the initial transplantations. The portal vein was chosen as it is the site of islet transplantation in the clinic[39]. The pancreas was chosen on the premise that mPOs/hPOs may survive better in their native/orthotopic environment while other studies have also demonstrated that orthotopic transplants can support the engraftment of pluripotent stem cell (PSC) or adult stem cell (AdSC) organoids[131,273]. Following transplantation, no nTnG mPOs could be recovered from the portal vein injections (Supp. Fig. 7). However, at the 3-week and 8-week timepoints, nTnG-mPOs engrafted in a similar manner in the kidney and pancreas (Fig. 4.16; Supp. Fig. 7; Appx. Table 2). In the pancreas, mPOs were retained within the Matrigel bubble and did not seem to engraft onto the pancreas parenchyma (Fig. 4.17 a,b,c). Furthermore, mPOs engrafted in the pancreas were also

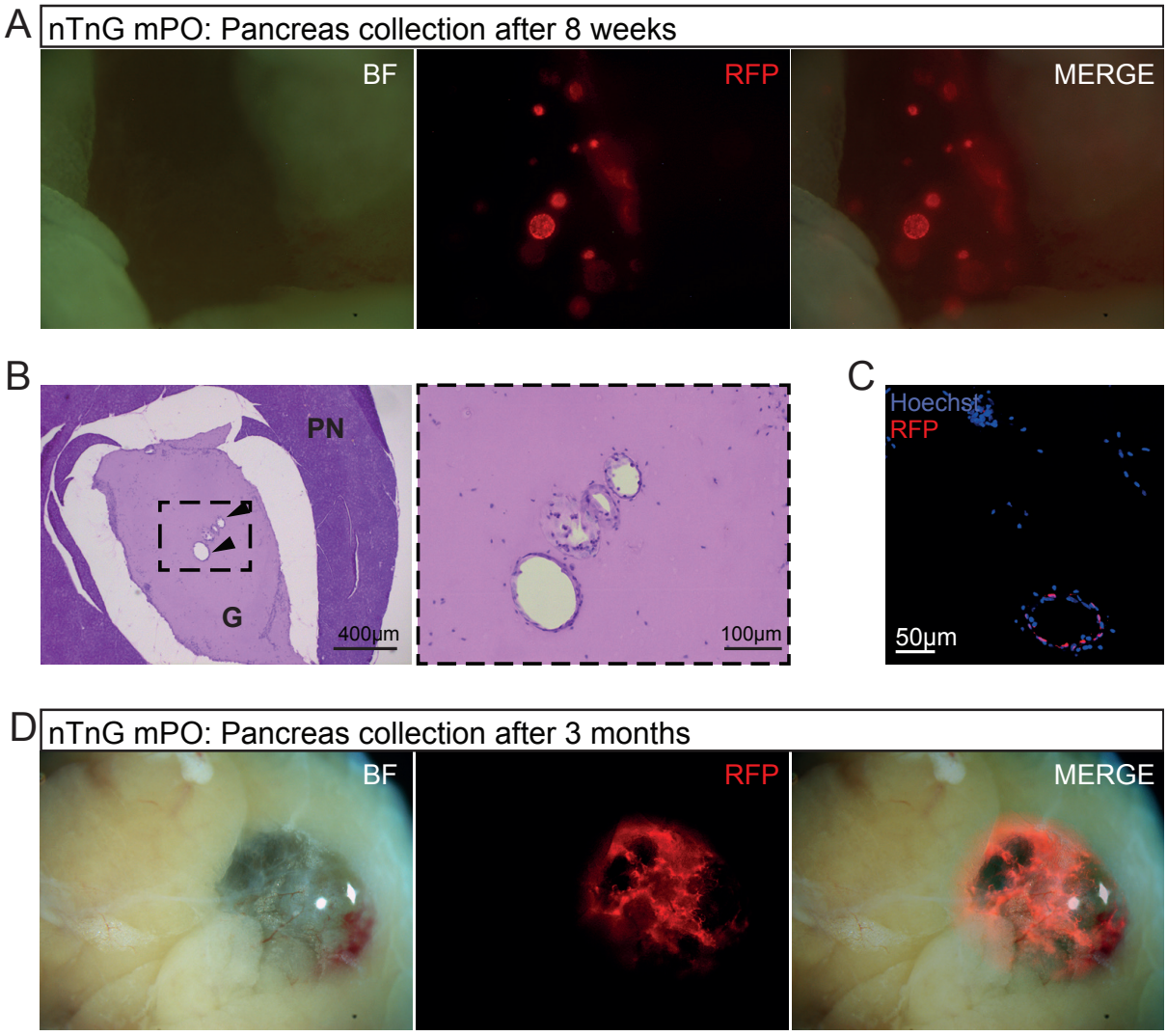

Figure 4.17 nTNG mPOs can be transplanted into the mouse pancreas and survive up to 3 months. (**A**) Representative wholemount images of nTnG mPOs transplanted into the pancreas of NSG mice and recovered after 8 weeks. Note that the organoids are in between the pancreas parenchyma and retain their cystic morphology. This is confirmed by H&E staining (**B**), and immunofluorescent staining for RFP protein (**C**). (D) Representative images showing nTnG mPOs engrafted into the pancreas of NSG mice after 3 months.

collected and at the 3-month timepoint while fluorescent microscopy demonstrated that the cells had survived (Fig. 4.17d). Assessment of other organs including the liver, spleen and small intestine and the 3- and 8-week timepoints did not show engraftment of nTnG-mPOs in these organs demonstrating that the cells are retained in the site of transplantation (Supp. Fig. 8). This data therefore demonstrated that the pancreas capsule is a suitable site for transplantation which allows long-term engraftment of mPOs while the procedure is also well tolerated by the mice.

In order to achieve long-term (3 month) engraftment of hPOs in immunodeficient mice, I tested multiple injection protocols by combining different ECMs, injection sites (namely kidney and pancreas capsule), as well as the addition of several growth factors and media to act as an injection vehicle (Table

Condition	K-0	K-1	K-2	P-1	K-3	P-2	P-3	P-4
Location	Kidney	Kidney	Kidney	Pancreas	Kidney	Pancreas	Pancreas	Pancreas
Matrix type	BME 2	BME 2	BME 2	BME 2	Matrigel	Matrigel	Glycosil Hyaluronic Acid	Matrigel
Matrix (%)	100	100	30	100	30	30	50	30
VEGF	✗	✗	✓	✗	✓	✗	✓	✓
Rho Kinase inhibitor	✗	✓	✓	✓	✓	✓	✓	✓
hPO-Opt.EM Medium	✗	✗	✗*	✗	✓	✗*	✓	✓
Engraftment Success (1 month)	4/20	2/3	2/3	3/3	1/3	3/3	1/1	1/1
Engraftment Success (3 months)	0/23	NT	NT	NT	NT	NT	3/3	3/3
Time of *in vitro* expansion	35 mice- 60 days 8 mice- 135 days	60 days			60 days		40 days	

Table 2 Summary of hPO transplants in NSG mice. Table outlining engraftment conditions and engraftment success rates of hPO xenografts conducted with a combination of injection medium compositions and injection sites in order to achieve long-term survival of hPOs *in vivo* (NT – not tested). *PBS was used for the dilution of the ECM.

2, Appx. Table 2). Injections were performed using either Matrigel (a commonly used yet ill-defined xenogenic ECM), BME 2 (a variant of Matrigel with a higher tensile strength and lower batch-to-batch variability) or Glycosil Hyaluronic Acid (G-HA, a chemically defined ECM). hPOs were therefore injected either in the kidney or pancreas capsule of NSG mice in the various injection conditions (Table 2, Fig. 4.18a). As mentioned, my initial attempts to engraft hPO cells using 100% BME 2 in the kidney capsule resulted in poor engraftment (20% of animals) within the 1-month timepoint (Table 2; K-0). Addition of VEGF, Rho Kinase inhibitor and hPO-Opt.EM medium as a vehicle for the cells, as well as a dilution of the ECM to 30%, improved engraftment efficiency after 1 month in the kidney capsule (56%; 5 out of 9 mice) (Table 2 and Fig. 4.18b; K-1,K-2,K-3). Interestingly, injection to the pancreas capsule resulted in 100% engraftment at 1 month regardless of ECM dilution or vehicle supplementation with VEGF and hPO-Opt.EM medium (Table 2 and Fig. 4.18b; P-1, P-2). This led me to further investigate the ability of the pancreatic niche to support hPO cell survival at 3 months; 100% engraftment of cells was observed when using either Matrigel or the chemically defined G-HA (Fig. 4.18b; P-3, P-4). Overall, transplants of hPO cells into the pancreas capsule resulted in 100% engraftment at 1 and 3 months (6/6 and 8/8 mice, respectively) while only 46% of transplants into the kidney capsule (among all conditions) could be recovered at 1 month (16 out of 35 mice, Appx. Table 2) with none surviving past the 1-month timepoint (0 out of 23 mice) (Figs. 4.18c, Table 2). Together these results indicate that mixing cells with growth factors, dilution of the ECM and injection to the pancreatic niche have a positive effect on the engraftment capability of hPOs.

Importantly, hPOs which have engrafted long-term in the mouse pancreas maintain the single cell-layered, epithelial organisation characteristic of healthy pancreas ductal tissue and retain

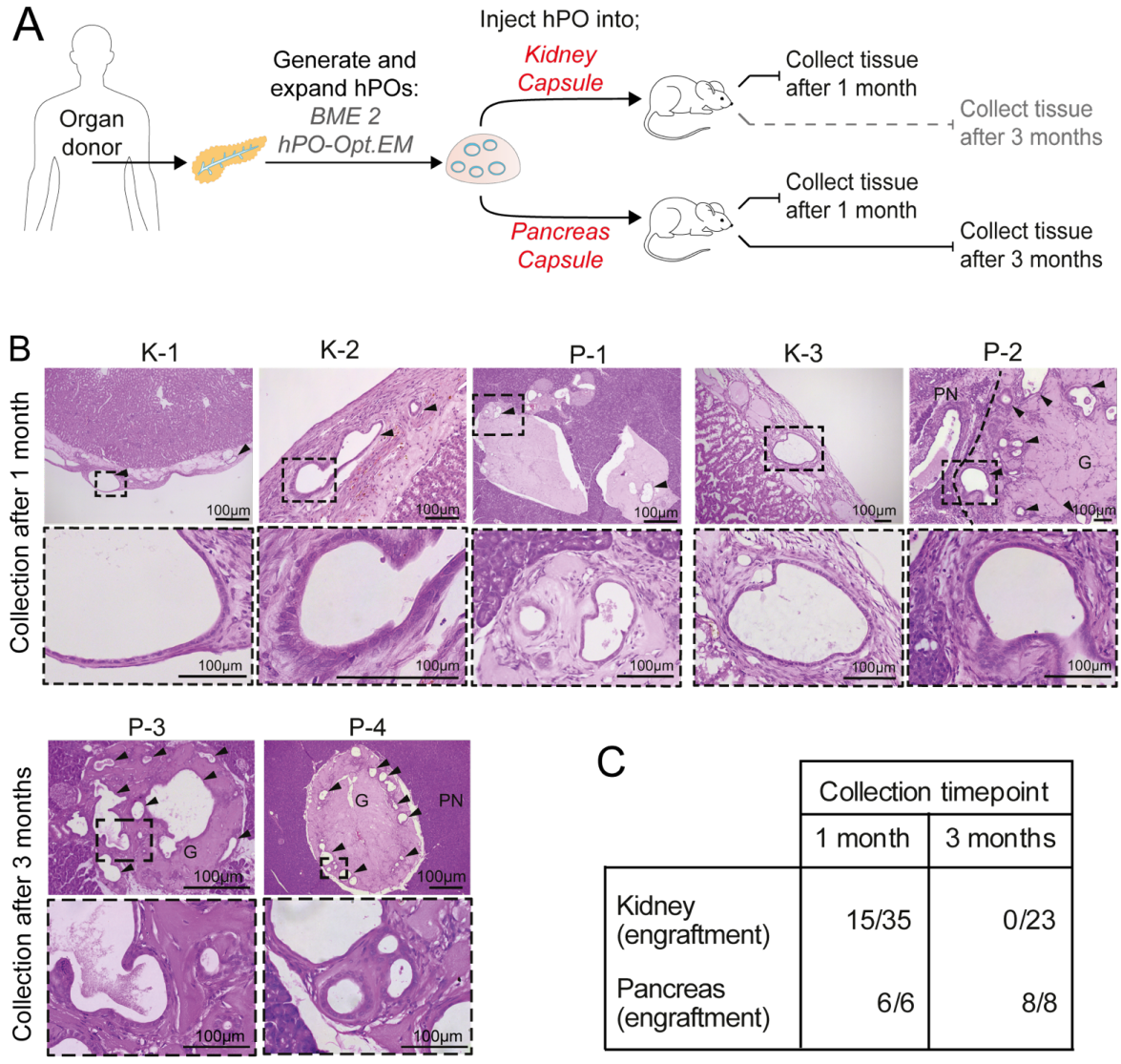

Figure 4.18 Optimisation of hPO transplantation leads to long-term (3 months) engraftment. (**A**) Experimental design. Following hPO generation and expansion with BME 2 and hPO-Opt.EM, hPOs were transplanted into either the kidney capsule or pancreas capsule of NSG mice; tissues were collected after 1 month or 3 months. (**B**) Representative H&E images of engrafted hPO cells at 1 month (upper panels) or 3 months (lower panels) show engrafted cells form ductal-like structures *in vivo* (G-graft, PN-pancreas). (**C**) Summary of engraftment success after 1 month or 3 months for all hPOs injected, including multiple injection compositions of ECMs and growth factors (For full details refer to Table 2 and Appx. Table 2).

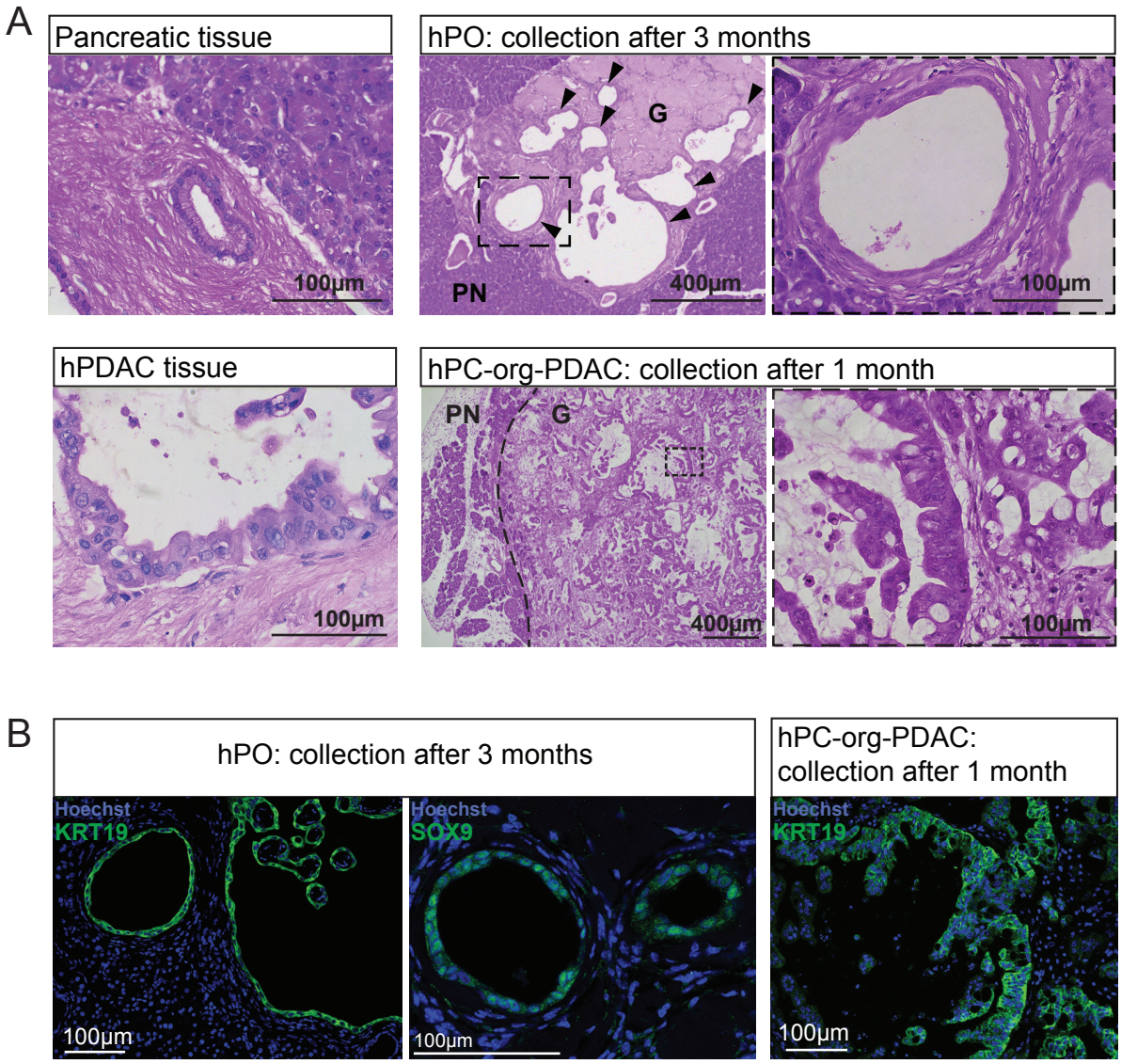

Figure 4.19 Expanded human pancreatic organoids (hPOs) do not show signs of transformation following long-term engraftment. (**A**) H&E staining demonstrates survival of hPOs (G-Graft) after 3 months in the mouse pancreas (PN-pancreas) and shows engrafted hPOs are formed by a single cell-layered epithelium recapitulating the ductal tissue structure of a healthy pancreatic tissue (n=6). Xenografts of pancreas cancer organoids (hPC-org-PDAC) obtained after 1 month resulted in aberrant ductal morphology reminiscent of the tumour of origin, as expected (n=2). (**B**) The human origin of the engrafted cells in the mouse pancreas is confirmed by expression of human-specific KRT19 (green) while both KRT19 and SOX9 (green) demonstrate the ductal nature of xenografted hPOs, nuclei counterstained with Hoechst (blue)(n=6). Of note hPC-org-PDAC xenografts also maintain expression of KRT19 (green).

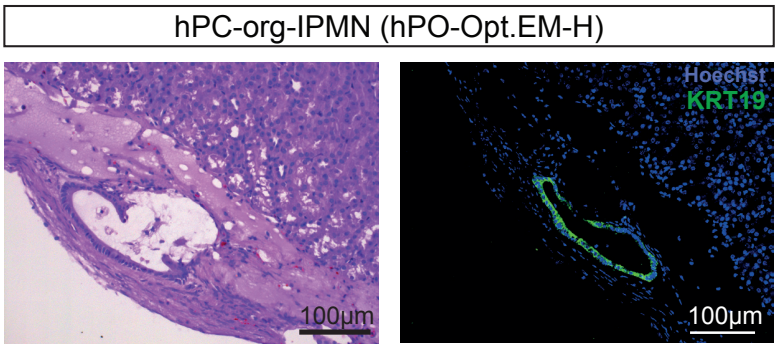

Figure 4.20 Xenotransplantation of hPO-org-IPMN expanded in hPO-Opt.-EM medium. Representative H&E staining images of hPC-IPMN derived organoids with a healthy phenotype (H) expanded in hPO healthy media (hPO-Opt.EM) transplanted under the kidney capsule of immunodeficient mice recovered after 1 month. hPC-org-IPMN xenografts maintain expression of ductal marker KRT19 (green) and a single cell epithelial organisation (n=4 mice transplanted, n=1 mouse for recovered graft) (hPO-Opt.EM-H denotes the media used for expansion i.e., hPO-Opt.EM and the phenotype of the organoids i.e., Healthy (H)).

expression of KRT19 and SOX9 (Fig. 4.19a, b). As a positive control, I performed xenografts of human cancer hPC-org-PDAC organoid. Injection of hPC-org-PDAC resulted in engraftment and subsequent generation of neoplastic tissue, with ductal cells organised into PanIN structures reminiscent in morphology of the original PDAC tumour (Fig. 4.19a). Interestingly, organoids derived from hPC-IPMN with a healthy phenotype, that had been expanded in hPO-Opt.-EM-H ('H' refers to healthy phenotype organoids handpicked and expanded) conditions (refer to Fig. 4.2) were transplanted in mice and upon engraftment, generated ductal structures with a single cell layered epithelium (which was positive for KRT19) similar to transplanted hPOs (Fig. 4.20). However, a graft could only be recovered from 1 mouse of the 4 injected, therefore more mice would be needed to confirm this statement. Of note, karyotype analysis of hPC-org-IPMN expanded in hPO-Opt.EM-H showed abnormal chromosome counts with more than 37% and 21% of cells exhibiting numbers greater than 46 at the early and late passage stage, respectively (Supp. Fig. 9).

Although at the histopathological level, engrafted hPOs appeared healthy and normal, I generated a more stringent assessment panel to evaluate whether hPOs had undergone malignant transformation or presented signs that could increase the risk of tumour formation. While hPOs presented similar rates of proliferation *in vitro*, Ki67 immunostaining demonstrated that engrafted healthy organoids were significantly less proliferative than engrafted hPC-PDAC organoids both at the 1-month and 3-month timepoints with very low overall proliferative cell percentages of 2% and 0.6% respectively (Fig. 4.21).

Furthermore, mucins are a family of high-molecular-weight glycoproteins characterized by the presence of a heavily O-glycosylated tandem repeat region (TRR) that is rich in proline, threonine and serine residues (called PTS sequences) which are divided into two categories: secreted and membrane bound. They serve to form a mucus layer which acts as a barrier to foreign pathogens[274]. Healthy

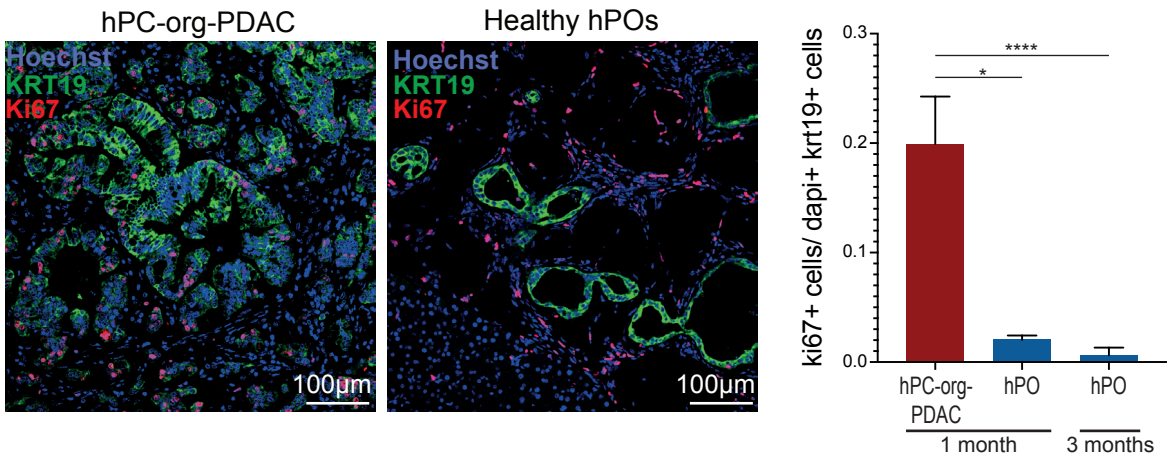

Figure 4.21 Healthy hPOs show reduced proliferation following xenotransplantation. Immunofluorescence staining for proliferation marker Ki67 of hPC-PDAC organoids and healthy hPOs following transplantation under the pancreas capsule (left images). Note the Ki67+ cells around the healthy hPOs. Quantification (right graph) of the Ki67 staining for xenografts of hPC-org-PDAC and hPOs and 1 month and xenografts of hPOs at 3 months (n=2 mice for hPO xenografts at 1 month, n=6 mice for hPO xenografts at 3 months, n=2 mice for hPC-org-PDAC xenografts).Data presented as mean ± SEM. Differences were tested by two tailed t-test. Significant differences are marked by asterisks: * $p \leq 0.05$, ** $p \leq 0.01$, *** $p \leq 0.001$, **** $p \leq 0.0001$.

pancreatic ductal cells are either devoid of or weakly express mucins while pancreatic cancer is characterised by aberrant expression of mucins[274]. I assessed antibodies against four types of mucins for their specificity against tumour but not healthy pancreas. These included secreted mucins MUC2 and MUC5AC which are not expressed in healthy pancreas as well as membrane bound mucins, MUC1- which is expressed in normal pancreas but overexpressed in cancer and MUC4 which is exclusively expressed in pancreas cancer and not healthy tissue[274,275]. Initial immunohistochemistry staining demonstrated that antibodies either bound to both healthy and tumour tissue (MUC1, MUC4[1G8]) or were not specific for either (MUC2, MUC5AC; Fig. 4.22). Further investigation into different antibodies as well as opting for immunofluorescent staining rather than DAB based IHC (which has previously shown reduced levels of background staining in my experience) demonstrated the specificity of MUC5AC (Clone 45M1; Supp. Fig. 10). However, despite studies demonstrating high specificity of MUC4 antibody (Clone 8G7), immunostaining in this project demonstrated reactivity in healthy pancreases (3/5 healthy donor pancreases; Supp Fig. 11). Therefore, MUC5AC was used as a specific biomarker to assess malignant transformation in engrafted hPOs. Immunostaining of the 3-month engrafted hPOs confirmed lack of expression of the cancer-specific MUC5AC (Fig. 4.23a). As expected, and as previously reported for transplanted PDAC-derived organoids[131], expression of MUC5AC was detected in the engrafted cells (Fig. 4.23a). Furthermore, primary tissue hPC-PDAC showed expression of MUC4, however neither hPC-org-PDAC organoids nor healthy pancreas tissue or engrafted hPOs demonstrated MUC4 expression (Fig. 4.23b).

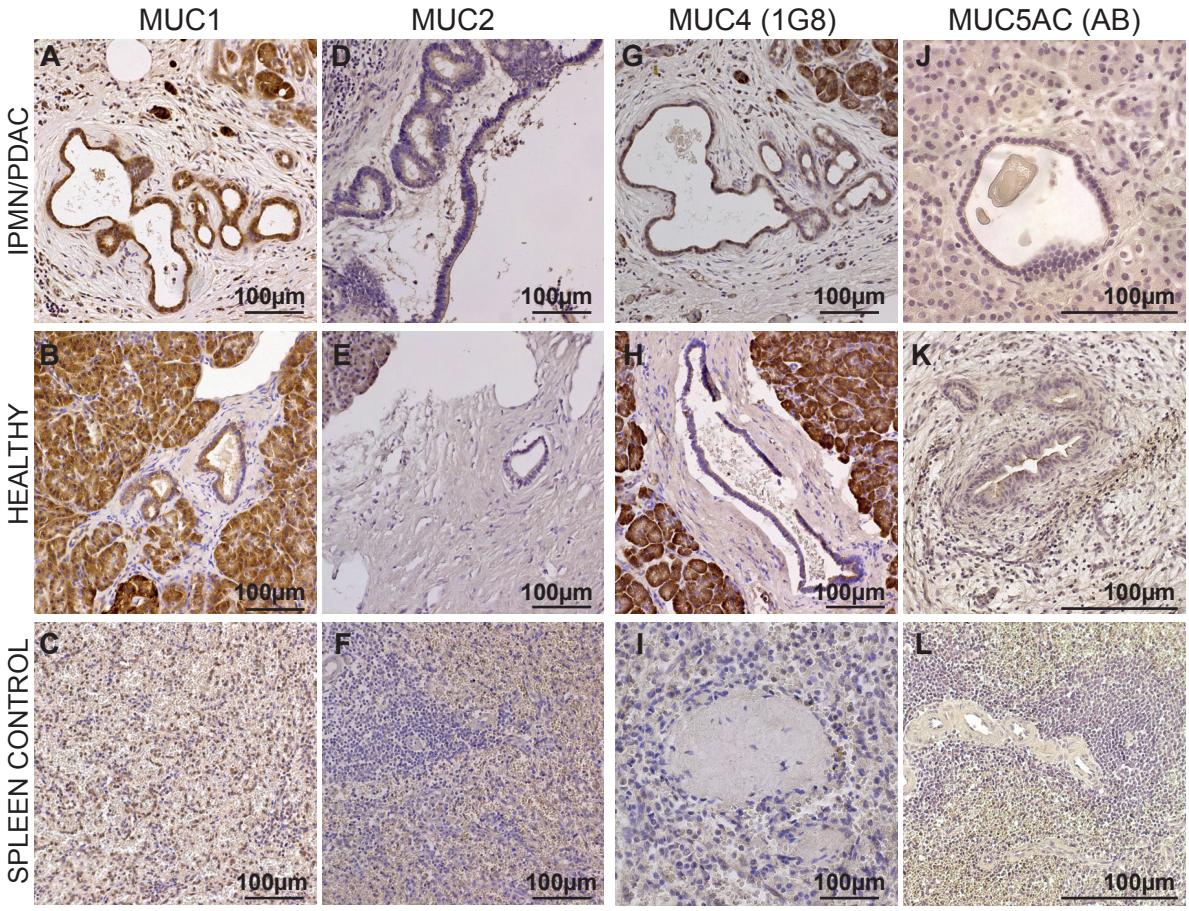

Figure 4.22 Mucin antibody screening and staining optimisation. Representative immunohistochemistry images demonstrating trial of multiple mucin antibodies against cancerous, healthy and spleen control tissue. (**A-C**) Show expression of MUC1, (**D-F**) MUC2, (**G-I**) MUC4 (1G8) and (**J-L**) MUC5AC in IPMN/PDAC, healthy pancreas and spleen tissue. Note that all antibodies fail to specifically mark tumour tissue and are either detected on healthy pancreas tissue or not detected in either healthy nor tumour tissue.

Thus, the morphology of the engrafted cells and lack of pancreatic cancer marker expression indicate that hPOs do not undergo neoplastic transformation *in vivo*.

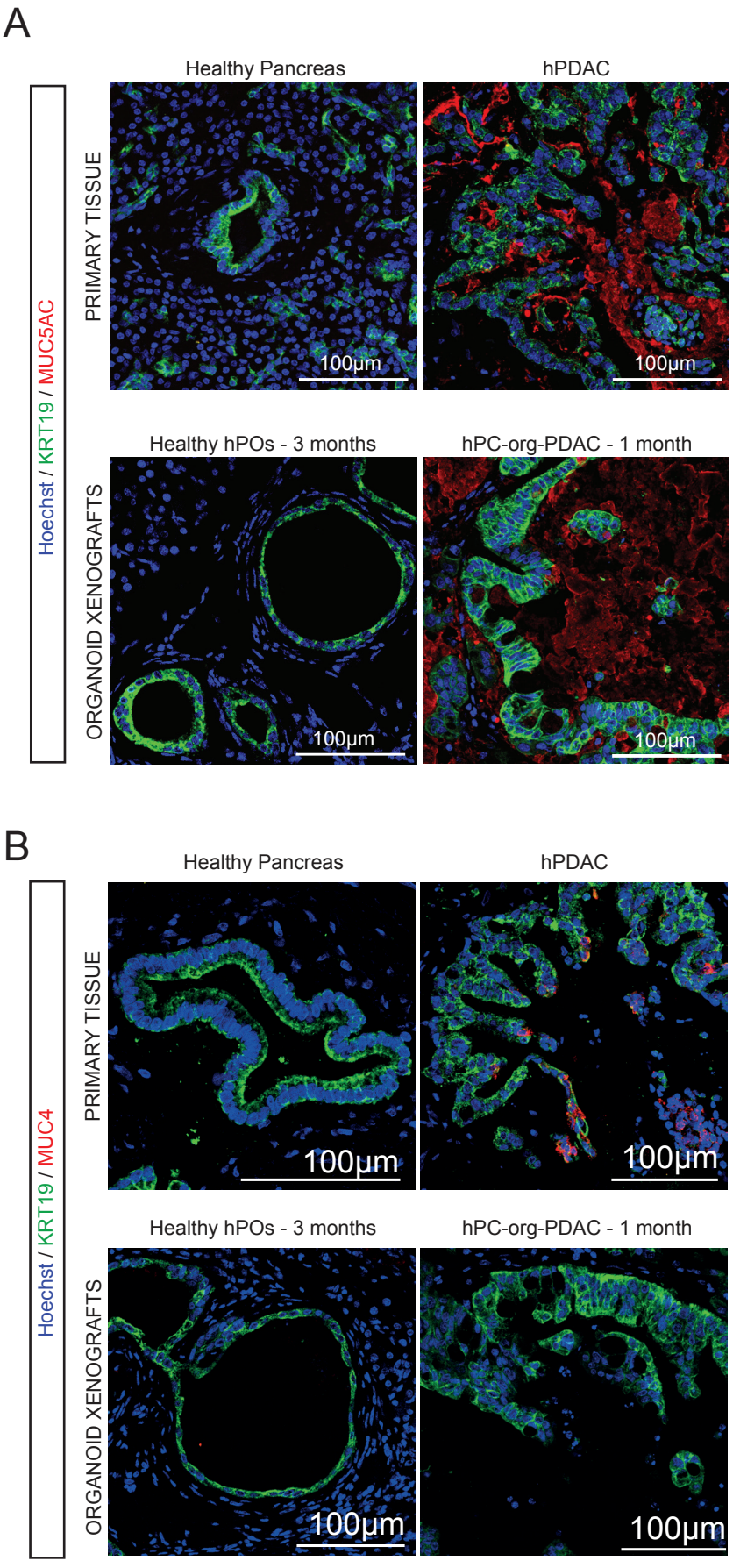
A
Healthy Pancreas
hPDAC
PRIMARY TISSUE
Hoechst / KRT19 / MUC5AC
100µm
100µm
Healthy hPOs - 3 months
hPC-org-PDAC - 1 month
ORGANOID XENOGRAFTS
100µm
100µm
B
Healthy Pancreas
hPDAC
PRIMARY TISSUE
Hoechst / KRT19 / MUC4
100µm
100µm
Healthy hPOs - 3 months
hPC-org-PDAC - 1 month
ORGANOID XENOGRAFTS
100µm
100µm

Figure 4.23 Long-term engrafted hPOs do not express key cancer markers. (**A**) Analysis of primary tissue shows expression of the cancer marker MUC5AC (red) only in tissue from a PDAC tumour resection and not in healthy tissue (n = 4 independent donors). Of note, MUC5AC is absent in xenografts from organoids derived from healthy donors (n = 6 mice), even at 3 months, while it is strongly expressed in xenografts derived from hPC-org-PDAC organoids already after 1 month (n = 2 mice) (**B**) MUC4 expression in the same groups as for MUC5AC. MUC4 was detected in primary tissue from PDAC tumour resection but not in the derived tumour organoids (hPC-org-PDAC) nor in the healthy tissue or healthy organoids.

4.3 Discussion

4.3.1 Assessment of hPC organoids

The organoid culture system has been utilised to model not only healthy tissue but also diseases such as cancer[106]. Recent publications have demonstrated both potential of this technology in its ability to recapitulate the architecture and heterogeneity of the disease[139,269] and the translational applications such as drug screening and personalised medicine[137,140,269]. A wide variety of solid tissue tumour organoid systems have already been developed[276] including from pancreas cancer, and more specifically pancreatic ductal adenocarcinoma (PDAC)[131,137,277,278]. Faithful models of pancreas cancer, aside from their clear benefit in drug screening and clinical applications, can also serve in the generation of novel biomarkers as well as a positive control for safety validation of healthy cellular therapies. Interestingly, this has been highlighted as an issue with mesenchymal stromal cell (MSC)-derived therapies whereby immortalised rather than transformed cells are used as a positive control[279]. Therefore, establishing an appropriate positive control will play an important role in the safety assessment criteria of future cell therapy products.

In this project, I have demonstrated the generation of both aggressive (PDAC) and pre-malignant benign tumour (IPMN, ITPN) derived organoids. The derivation protocol utilised is an adaptation from the ones previously reported[131,269] and the hPO culture protocol demonstrated in this project. By serendipity, a rare type of pancreatic tumour, ITPN, was captured for this project and an organoid line from this tumour was generated; this is the first time that an ITPN organoid line is reported. However, this type of tumour involves less than 1% of all pancreatic exocrine neoplasms and was only officially recognised as a distinct tumour type in 2010[268]. Therefore, it is possible that previous hPC organoid models have captured similar tumour types, but these were mis-classified as IPMNs.

Interestingly, for all three tumour organoids, the expansion rates were slower when compared to hPOs with average passage times of 10-14 days compared to 7-10 days in hPOs. Of interest was the marked difference in expansion of the tumour cells in either healthy or tumour media. While both IPMN and ITPN derived organoids (either bulk or handpicked) could be expanded in hPO-Opt.EM, the more aggressive malignant PDAC organoids could not be expanded. This highlights that the hPO culture system is optimised for expansion of healthy cells rather than tumour ones. Furthermore, karyotypes of hPC-IPMN organoids expanded in hPO-Opt.EM medium (i.e., not tumour medium), showed overall lower numbers of cells containing chromosome counts above 46 when compared to organoids expanded in tumour media from the same tissue in line with the idea of an increase in the healthy population. It is therefore likely that when two populations exist (healthy and tumour) the healthy organoids outcompete the cancer ones and overtake the culture, an observation that has previously also been reported[131,278].

In line with this notion, previous studies have demonstrated that PDAC derived organoids have different dependencies on niche factor requirements with some lines demonstrating a Wnt3A and Rspo1

dependency while others were able to grow in absence of such factors[278]. Indeed, this variance in Wnt3A/Rspo1 was only identified in a large-scale study by Seino *et al.* as a result of deriving organoids from 39 samples, while the first group to generate PDAC organoids, namely Boj and colleagues, reported a strong dependency of exogenously added Wnt in their organoids[131,278]. Seino *et al.* also demonstrated that driver-gene alterations dictated requirements for growth factors in the culture media and demonstrated that lines independent of EGF, Noggin, A83-01 (TGFβi), or Nutlin3 (p53 inhibitor) in the media correlated with mutations in KRAS, SMAD4, TGFBR2 and TP53 genes respectively[278]. However, dependency on Wnt3A and Rspo1 did not correlate to Wnt signalling mutations in a similar manner; some PDAC organoids were completely independent of Wnt signalling while others self-secreted Wnt and were therefore independent of exogenously added Wnt3A[278]. It is therefore likely that hPC-PDAC organoids fall into the category of exogenous Wnt dependent PDACs and are not able to self-secrete Wnt. Although it is outside the scope of this project, it would be interesting to perform similar growth factor exclusion studies as well as targeted sequencing of the primary tissue and hPC organoids to understand the different type of mutations that may be governing the growth of pancreatic tumours. This would be particularly interesting in the ITPN organoids as it may help uncover key driver mutations in this newly characterised pancreatic cancer.

Nevertheless, while in this project I have shown that healthy hPOs cannot grow in tumour media, largely due to the presence of Wnt3A conditioned media and the restriction of growth factors, the converse is not the same for tumour derived organoids. It is clear from this and other studies that the more benign tumour derived organoids as well as certain subtypes of PDAC derived organoids can still be expanded in hPO-Opt.EM, albeit in a slower manner to healthy hPOs, and therefore future protocols requiring healthy organoids cannot rely on the ability of healthy ductal cells to outcompete cancer cells *in vitro*. Therefore, stringent safety assessment protocols are required to ensure the expansion of a non-malignant population of cells.

However, hPC organoids generated in this project recapitulated the architecture of the parental tumour, maintained the expression pattern of ductal markers *KRT19* and *SOX9* while also showing aneuploidy during *in vitro* expansion. Taking all data into consideration, hPC organoids are a suitable positive control to assess the safety of hPOs. What is perhaps surprising is that neither *KRT19/SOX9* mRNA expression, nor proliferation rates *in vitro* were able to distinguish between healthy and tumour cells. Therefore, it is also uncertain whether expression of biomarkers, either at the RNA or protein level, can be the only assessment tool to confirm lack of malignant cells in the culture. However, only a limited number of markers (i.e., Ki67, KRT19, and SOX9) were used for *in vitro* comparison of healthy and tumour organoids in this project and therefore more markers are required to understand whether biomarker analysis can be used to certify a healthy population of cells in the culture. Current ongoing work aims to investigate cancer specific markers such as mucins (i.e., MUC4, MUC5AC) as well as the clinically used CA19-9 protein[280] and their use to specifically mark hPC organoids and not healthy hPOs.

In summary, in this project I have demonstrated the ability to generate hPC derived organoids and have shown the establishment of a novel hPC-ITPN organoid line. These hPC organoids can serve as a tool to establish novel biomarkers of pancreatic cancer but can also be used as a positive control to assess tumorigenicity of hPOs.

4.3.2 Mutational landscape of hPOs

Cellular therapies hold the potential to offer a cure for diseases for which there are limited treatment options, or which rely on donor material which is scarce. However, as with all clinical products, safety of these therapies needs to be illustrated before their use in the clinic. One aspect of determining safety is the assessment of genomic integrity of the cells which includes assessing for gross chromosomal rearrangements or duplication/deletion events or for particular mutations that have taken place which can be impactful. In this project, I have utilised karyotyping to assess whether hPOs maintain stable chromosomal numbers. Indeed, assessment of 2 separate donor derived hPO lines showed that hPOs maintain chromosomal numbers that do not surpass 46 even after long-term culture. This was demonstrated for hPOs expanded in BME 2 and in GFOGER-hydrogel showing that hPOs maintain chromosomal numbers across different ECMs. Furthermore, the data are supported through the use of hPC organoids serving as positive controls. hPC-organoid lines showed high numbers of aneuploidy, while higher numbers of aneuploidy correlated with the more aggressive tumour type, i.e., hPC-PDAC. However, the karyotype analysis performed in this project presents some limitations. Firstly, the technique only allows for chromosomal counting and does not have enough resolution to visualise the specific chromosomal arms. As such, it is impossible to tell whether there have been any large-scale events such as translocation/deletion/insertion etc. of chromosomal segments. Furthermore, it can be noted that in Fig. 4.7, there are cells which contain chromosome numbers below 46. The method used in this project, and as has been used previously[131], has limitations as during the procedure when dropping the cell solution onto the slide, chromosomes can be 'lost'. For this reason, chromosome counts less than 46 are not necessarily due to chromosomal abnormalities. Conversely, it is not possible to gain an extra chromosome and therefore chromosome counts above 46 are evidence of polyploidy.

While the chromosomal counting reassuringly demonstrated that hPOs maintain normal ploidy even after long-term culture, it was important to understand the mutational burden of the culture system and any associated risk of the acquired mutations towards transformation of the cells. This was determined through the whole genome sequencing (WGS) of clonal and sub-clonal organoids.

Previous studies have performed similar experiments in adult stem cell derived liver organoids[120,171] and colon organoids[171] and pluripotent stem cells. The earlier study by Huch *et al.*[120] demonstrated that liver organoids accumulated 63-139 mutations in 3 months of culture (or 67 mutations in 2 months, taking the median between 63-139). Interestingly, hPOs accumulate on average 40 mutations in approximately 2 months of culture which is roughly 30 mutations less than liver

organoids. It is therefore reassuring that hPOs have similar, if not less, mutations than previously reported models. Furthermore, Kuijk *et al.*[171], performed similar analysis in liver and colon organoids and found that they accumulate 8.3 and 7.2 SNVs per population doubling. Comparably, I found that hPOs have an average of 2.93 ± 1.04 SNVs per population doubling. Moreover, while Kuijk and colleagues[171] reported that liver and colon organoids accumulate 40-fold higher numbers of mutations *in vitro* when compared to *in vivo* (in the donor tissue), I demonstrated that hPOs accumulate only 8-fold higher numbers of mutations per *in vitro* year than in the donor tissue. Remarkably, this shows that hPOs potentially accumulate less mutations than what is reported for other organoid systems in two separate studies[120,171]. Moreover, Kuijk and colleagues[171] reported that their iPSC lines had less SNVs compared to the liver and colon organoid lines which has contrasted previous thoughts on the accumulation of mutations in pluripotent lines particularly when compared to adult liver stem cell organoids[120,281]. Surprisingly, hPOs accumulate less mutations per doubling compared to iPSCs (3.5 ± 0.5). The low mutation rate observed could be reflective of the pancreas' low proliferative capacity or due to the hPO culture not inducing an excessive amount of mutations.

Furthermore, through analysis performed by Alex Cagan, we were able to obtain the genomic location of each mutation and understand whether they fell within gene coding regions or not. Reassuringly, the overwhelming majority of mutations fell in non-coding regions such as introns. However, some mutations did in fact fall in gene coding regions. However, there were no non-synonymous mutations found specifically in subclones, i.e., arising during *in vitro* culture, nor any mutations affecting known cancer driver genes.

Notably, there were no CNVs in any of the clonal samples from either Donor 14 or 10. This is important as it indicates with certainty that in 2 months of culture, from organoid derivation to the first sample collected for WGS, there are no gross chromosomal aberrations. However, some CNVs were detected in 1 out of the 2 subclones analysed, which was collected 4 months after culture, while further work is required to map the CNVs and understand their impact further. Moreover, this was only found in 1 subclone, and could indeed be due to the fact that the subclone received lower sequencing coverage than the rest of the samples. Sequencing of more clone/subclone pairs could elucidate whether hPO culture leads to CNV accumulation.

Indeed, the low numbers of clones/subclones sequenced correlates to the design of the experiments which has some limitations. The necessity for clonal populations and the need for two single-cell steps, resulted in significant cellular stress and impacted the capacity of single cells to form organoids. As such, it was difficult to obtain large numbers of clones that could be expanded further. Moreover, single cells needed to be seeded in a cell density that would allow organoid formation, as there is a 'community' effect for organoid generation[109]. However, this meant that duplicate cells or cells which had fused and formed a single organoid could have been selected. Whilst clonal samples could be confirmed through their variant allele frequency distributions, centred around 0.5, some organoids which were submitted indeed were not clonal and were removed from analysis, further

reducing the numbers of organoids analysed. To add to this, 4/6 of the subclones showed evidence of contamination. Therefore, there were only two subclones remaining that could be analysed. While this would have in theory sufficed as previously reported[120], the subclones were derived from clones 5 and 5.5 which were essentially expanded from organoid fragments from the same clone. Therefore, results of this analysis are based on low numbers of clones and will therefore need to be repeated with further samples from multiple donors in order to draw definitive conclusions.

While this data is important in understanding the mutational burden of the hPO culture and to outline either gross chromosomal changes, or specific genomic regions which may be affected, it is difficult to understand which *in vitro* observations classify cells as safe or not safe for us in the clinic. Clearly aneuploid lines or cells which harbour functional mutations in oncogenes would not be chosen for a cell therapy. However, there are genetic variations (CNVs, SNVs) that are not associated with disease and may never impact the integrity of the cell. Therefore, it is important to couple genomic data with other assays including i*n vivo* tumorigenicity assays.

4.3.3 *In vivo* platform for tumorigenicity assays

Tumorigenicity testing is a requirement for many regulatory body guidelines when developing a cell therapy product. It is important to note that considerations for regulatory guidelines have largely centred around the use of PSC derived cell therapies with particular concern around their propensity to form teratomas. Therefore, although the risk may at least in theory be lower for primary tissue or adult stem cell derived therapies, it is fair to assume that such cell therapy products will fall under the same category. Tumorigenicity testing aims to "detect either residual undifferentiated cells or transformed cells in the final product…both of which are considered "contaminants" or "impurities" to the final differentiated CTP"[147]. Whilst hPOs do not undergo a differentiation process and it is yet unclear as to how precisely they will be translated into the clinic, it is of value to understand the risk of tumorigenicity in this stage. Of course, with the hPOs reported in this project, the risk source is potentially transformed cells rather than contaminating undifferentiated cells. However, in the scenario whereby hPOs are differentiated, for example towards insulin producing cells, if there is no tumorigenicity risk from the undifferentiated population, less stringent testing will be needed to ensure a fully differentiated final product. Furthermore, establishing a safety assessment pipeline at this stage will allow easy implementation in a later stage product.

Animal studies for tumorigenicity testing are often debated as the translation of the results is not always clear largely due to the species difference between rodents and humans. However, as it is the only alternative, careful consideration is needed with regards to animal models chosen, number of cells to be inoculated, study duration, controls used, as well as site of transplantation.

Initial transplantations of hPOs into the kidney capsule of NSG mice demonstrated that they could engraft at both the early and late passage stage while maintaining ductal morphology and KRT19

expression. However, the rates of engraftment were very low, and a key aim of this project was to ensure engraftment of hPOs long-term for an accurate assessment of tumorigenicity. The three sites of investigation included the classically used kidney capsule, the liver via portal vein injections and the pancreas. One of the criteria for tumorigenicity assessment is the choice of the site of transplantation in the animal model as this would need to reflect the site in the human setting. Furthermore, the microenvironment plays a key role since it has been implicated in tumour progression[282]. Whilst it is uncertain which site will be used in humans for an hPO-based cell therapy product, certainly the liver is an option especially when considering a treatment for diabetes, given that islets are transplanted in the liver via portal vein infusion[39]. However, the mouse portal vein injections proved to be technically challenging due to the size of the portal vein and the risk of a vein rupture given that the needle gauge size needed to be large enough to allow release of organoid fragments. Furthermore, despite use of a fluorescently labelled mPO line, recovery of these cells was difficult since no distinct transplantation site could be identified. However, this site remains of interest for future studies and the transplantation protocol requires optimisation with the use of a potentially larger animal model to allow infusion of larger quantities of cells.

The pancreas was chosen as it was the orthotopic site for hPOs and could perhaps provide niche growth factors that allowed the long-term survival of hPOs. Indeed, previous studies have used the pancreas as a site for transplantation of normal and cancer derived organoids[131] while for PSC derived, transplantation into the pancreas allowed exocrine and endocrine lineages[273]. However, despite the orthotopic site, Boj *et al.*[131] reported low engraftment rates and organoids did not survive beyond the 1-month time limit. Therefore, the pancreas was used as a site of investigation while also investigating various injection vehicles and media composition. One possible medium of injection would have been PBS or saline, but due to the soft and diffuse nature of the mouse pancreas, it was anticipated that the cells would leak from the site of injection. As such, Matrigel, which is used to grow mPOs, was used in 30% dilution which allowed for enough Matrigel to form a gel. As a result of the success of the nTnG-mPO transplants, Matrigel was used in the optimisation for long-term engraftment of hPOs. Importantly, the transplants with nTnG-mPOs demonstrated that the pancreas site was accessible, did not result in significant damage to the organ (from the use of Matrigel or the surgical procedure) and allowed survival of mPOs until 3 months.

Interestingly, an improvement of engraftment of hPOs in mice was observed from either the addition of vascular endothelial growth factor (VEGF), use of Rho kinase inhibitor, supplementation of the injection media with hPO-Opt.EM and/or dilution of the matrix irrespective of site of injection at the 1-month stage. Although during sectioning, more ductal structures appeared in the pancreas sites, this was difficult to accurately quantify as it would have required sections throughout the whole organ to objectively compare survival between the kidney and the pancreas. Nevertheless, the pancreas always resulted in 100% engraftment at both the 1-month and 3-month timepoints while the data demonstrates that the injection medium was also important in the successful engraftment of the hPOs.

It is difficult to discern which factors could be secreted by the mouse pancreas that allow long-term survival of hPOs. It is possible that this is a result of the correct ratios and/or concentrations of stem cell-promoting growth factors such as Wnt agonists, BMP antagonists or FGF signalling activators provided by the mouse pancreas. Furthermore, Yamaguchi and colleagues reported pancreatic ductal glands (PDGs) to be sites of proliferative ductal cells in the mouse and human pancreas while in the mouse, they have stem-cell properties and can migrate and integrate to the ductal epithelium in response to damage[283]. Indeed, I observed numerous Ki67+ cells which were KRT19- in the grafts following hPO transplantation in the pancreas (Fig. 4.21). Therefore, the sustained survival of hPOs in the mouse pancreas could be a result from the activation of *in situ* ductal progenitors, their migration to the graft site, and provision of pro-survival factors although this is speculation.

Importantly, in this project I demonstrate use of assessment criteria for the robust characterisation of safety and lack of tumorigenicity of hPOs. Although proliferation rates *in vitro* are similar between healthy and cancer hPOs, proliferation was significantly lower for hPOs transplanted in the pancreas compared to hPC organoids. Indeed, a lower proliferative nature reduces the risk of teratoma formation. Furthermore, cancer specific markers such as MUC5AC and MUC4 were absent from transplanted hPOs which also highlights the importance of the use of biomarkers for the assessment of cell transformation. Notably, this type of screening may add further sensitivity for detecting cell transformation which may not be detected from histopathology assessment of the tissue. This is further highlighted by the normal morphology of hPC-IPMN organoids (grown in hPO-Opt.EM) following transplantation into the mouse kidney capsule. However, mucin staining was not performed for these sections and hence it would be interesting to assess whether these normal-like cells indeed produce cancer specific mucins.

Limitations of the in vivo hPO tumorigenicity assays

Although the data demonstrates that hPOs maintain their ductal healthy morphology after long-term *in vivo* orthotopic transplants, and do not show signs of transformation or tumorigenicity, several limitations of the model exist which would need to be addressed in future experiments. The orthotopic transplants were vital for allowing long-term engraftment of hPOs, and also provided the right microenvironment equivalent to the human setting in order to allow growth of any potential malignant cells. However, it is unlikely that hPOs would be transplanted in the pancreas of humans. Furthermore, hPOs were transplanted long-term using either Matrigel or the chemically defined Glycosil Hyaluronic-Acid (HA). However, injection of a hydrogel into a solid tissue may cause damage due to inflammation, disruption of the tissue's structural integrity, or embolism caused by a detached piece of hydrogel. Interestingly, when HA-human blood hydrogels were transplanted into rat hearts, the rats could only survive for a few hours[284]. Therefore, it is unlikely that future cell therapy products will be injected in hydrogels even with chemically defined one such as HA. Furthermore, use of hydrogels, either Matrigel

or HA did not allow integration of hPOs with the surrounding parenchyma even after 3 months. Therefore, use of an easily degradable hydrogel could allow better integration of hPOs with the surrounding tissue and may allow either improved engraftment or push the differentiation of hPOs. Indeed, it has been reported that differentiation of human ductal derived pancreas organoids occurs only after transplantation into the kidney capsule of mice[132]. Although hPOs were negative for insulin after a 3-month engraftment (data not shown), they were not screened for expression of early markers of endocrine differentiation.

Indeed, if a cell therapy product is generated from hPOs, it is likely that it will include insulin producing cells for the treatment of diabetes (explored further in Chapter 6), owing to the successful differentiation of mouse pancreas organoids and the reported differentiation of human pancreas ductal organoids[121,132]. As such, the easiest integration into the clinic would be to mimic the pathway of islet transplantation. Therefore, it would be logical for future hPO tumorigenicity experiments to be performed in the liver of mice (or larger animal models) via portal vein injection.

The tumorigenicity assays performed in this project had a maximal timeline of 3 months. While this is a novel and important achievement for hPOs, other studies, including ones for assessing the safety of ESC cell therapy products have assessed tumorigenicity *in vivo* for 7 months and have also performed cell titrations[267]. Achieving such timepoints would be a crucial step for assessing the safety of hPOs while cell titrations would need to be performed to understand if transplanting more cells could result in increased risk of tumorigenicity. Interestingly, on average, 400,000 islets are transplanted per individual which is approximately 6,700 islets/kg[285] which in turn is approximately $6x10^6$ β-cells[286]. Assuming a mouse has an average weight of 25g, approximately $1.5x10^5$ hPOs would need to be transplanted into the mouse to achieve a clinically relevant number. Indeed, between 5-$10x10^5$ hPO cells were injected into NSG mice for the xenografts performed in this project which is higher than the clinically relevant number and reassuringly no tumour was formed. Nevertheless, it would be of interest to demonstrate what would occur if higher numbers of hPOs were to be transplanted.

While the lack of MUC5AC and MUC4 expression in 3-month engrafted hPOs is encouraging, further markers are needed to generate conclusions. Importantly, the MUC4 antibody utilised in this project did not demonstrate specificity against tumour tissue and was reactive against healthy organ donor derived pancreas tissue. Therefore, a more specific antibody is needed while also addition of markers such as CA19-9, which is clinically used to diagnose pancreatic cancer, would be needed in order to establish a robust screening panel to rule out transformation of hPOs. Furthermore, whilst hPOs survived for 3 months in the mouse pancreas maintained, a healthy ductal architecture with a single cell layer epithelium, while also maintaining expression of a ductal markers, further assessment from a clinical histopathologist would be required to definitively determine whether the engrafted cells present indications of tumour formation. Lastly, while potential migration of engrafted cells was analysed for nTnG-mPOs, this was not recapitulated for long-term engrafted hPOs. Organs have been collected from these mice and current ongoing work aims to assess whether hPOs are present in organs such as the

lung, spleen and liver of these animals. This would indeed be crucial in assessing the safety of hPOs and removing concerns regarding their tumorigenicity risk in a human transplant setting.

4.4 Conclusion

In summary, the data from this chapter demonstrate that organoids can be generated from multiple types of pancreas cancer and can be used to assess the safety of healthy cells across multiple assays. Importantly, hPOs maintained stable chromosomal numbers following long-term culture and when compared to a positive cancer control. Moreover, hPOs do not accumulate an excessive amount of mutations during *in vitro* culture and potentially deleterious mutations do not arise during this time. When transplanted *in vivo*, hPOs do not show any signs of tumorigenicity, even after a long-term (3 month) engraftment timepoint and maintain expression of healthy pancreas ductal markers. Therefore, hPOs are a potentially safe source of adult stem cells which hold great promise for future regenerative medicine approaches with potentially less obstacles towards their introduction into the clinic.

CHAPTER 5. ANTIGENICITY AND IMMUNOGENICITY OF hPOs

5.1 Introduction and aims

Translation of a cellular therapy product to the clinic requires investigation of the risk of immune rejection upon transplantation into the patient. Allograft rejection in a transplant setting is largely governed by T and B cells. T cells primarily recognise either foreign HLA molecules or foreign peptides bound on self-HLA molecules, resulting in cytotoxic destruction of the target cell. B cells have important roles in antigen presentation and also produce antibodies targeted to foreign molecules which can trigger antibody-mediated cell cytotoxicity. Autologous cell therapies are in theory non-immunogenic since no foreign HLA molecules should exist to drive the immune response. However, it was shown that autologous hiPSC cells could elicit an immune response in a humanised mouse setting due to expression of specific antigenic proteins[208]. Furthermore, whilst autologous derived cell therapies may still be non-immunogenic, or at least less immunogenic, compared to allogeneic cells, there are significant financial and logistical challenges in setting up autologous cellular therapies for each patient[179]. Therefore, since allogeneic therapies may be more desirable, rejection of cell therapies due to HLA mismatch or antigenic protein expression requires investigation.

Transplantation of solid organs (or islets) initiates an inflammatory environment whereby immune cells such as CD4+ T cell subsets, upon activation, release cytokines including TNFα, INFγ and IL-1β[31,189]. Importantly, IFNγ can cause the upregulation of HLA molecules on all nucleated cells including non-professional antigen presenting cells (APCs) such as islets and exocrine cells[209,214]. HLA upregulation by IFNγ is mediated by the JAK/STAT signalling pathway, which is initiated by the binding of IFNγ to the dimeric IFNγ receptor at the cell surface membrane resulting in upregulation of downstream signalling targets[287]. Importantly, it has been shown that human ESCs express low levels of HLA in the undifferentiated state while this can be upregulated upon differentiation or in the presence of IFNγ[204]. Moreover, similar results are demonstrated with adult mesenchymal stem cells (MStCs) after incubation with cytokines such as IFNγ[288]. Therefore, it is possible that hPOs pose a risk for immune rejection, particularly when placed in an inflammatory environment and therefore warrant investigation into whether they express immunogenic antigens and whether they can elicit an immune response in an autologous or allogeneic setting.

In this chapter I investigate the immunogenicity of hPOs by assessing the expression of antigenic molecules and their ability to generate an immune response *in vivo*. In **section 5.2.1** I focus on studying whether hPOs express HLA Class I and II under normal and inflammatory conditions simulated by addition of IFNγ. In order to understand whether the findings translate in more physiologically relevant conditions, in **section 5.2.2**, hPOs are co-cultured with splenocyte mononuclear cells (SpMCs) and assessed for upregulation of HLA molecules. In order to understand

whether hPOs are rejected by the human immune system, hPOs are transplanted in SpMC and haematopoietic stem cell (HSC) humanised mice or human immune system (HIS) mice in **section 5.2.3**. Lastly, in order to further optimise the tracking of survival, engraftment and immune rejection of hPOs transplanted in mice, in **section 5.2.4** I show preliminary data for generation of Luciferase+ hPO lines which allow the use of bioluminescent imaging (BLI) to track hPOs *in vivo*.

5.2 Results

5.2.1 hPOs upregulate HLA Class I/II upon IFNγ stimulation

Although expression of HLA molecules differs among cell types, it is generally understood that nucleated cells express HLA Class I while professional antigen presenting cells (APCs) express both HLA Class I and II and hence activate both major subsets of T cells (CD4+ and CD8+). However, evidence exists that non-APCs can upregulate HLA Class I and II as well as other co-stimulatory molecules and can activate lymphocyte populations. However, little is known as to the expression of such molecules in primary cell derived organoid systems and whether indeed these cells present an opportunity for a less immunogenic cellular therapy.

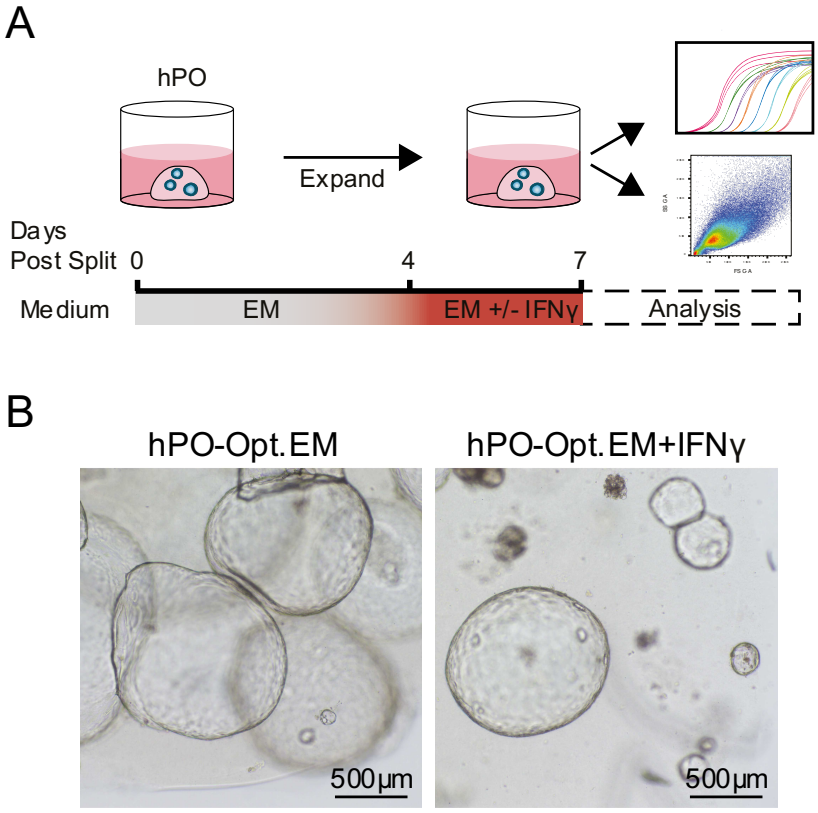

Figure 5.1 hPOs can be cultured under inflammatory conditions. (**A**) Schematic of hPO culture with the inflammatory cytokine IFNγ to assess HLA expression of hPOs under *in vitro* inflammatory conditions. hPOs are allowed to expand for 4 days post passage and are the incubated with IFNγ for 3 days after which they are collected for subsequent analysis. (**B**) Representative brightfield images demonstrate that hPOs maintain healthy phenotype following incubation with IFNγ.

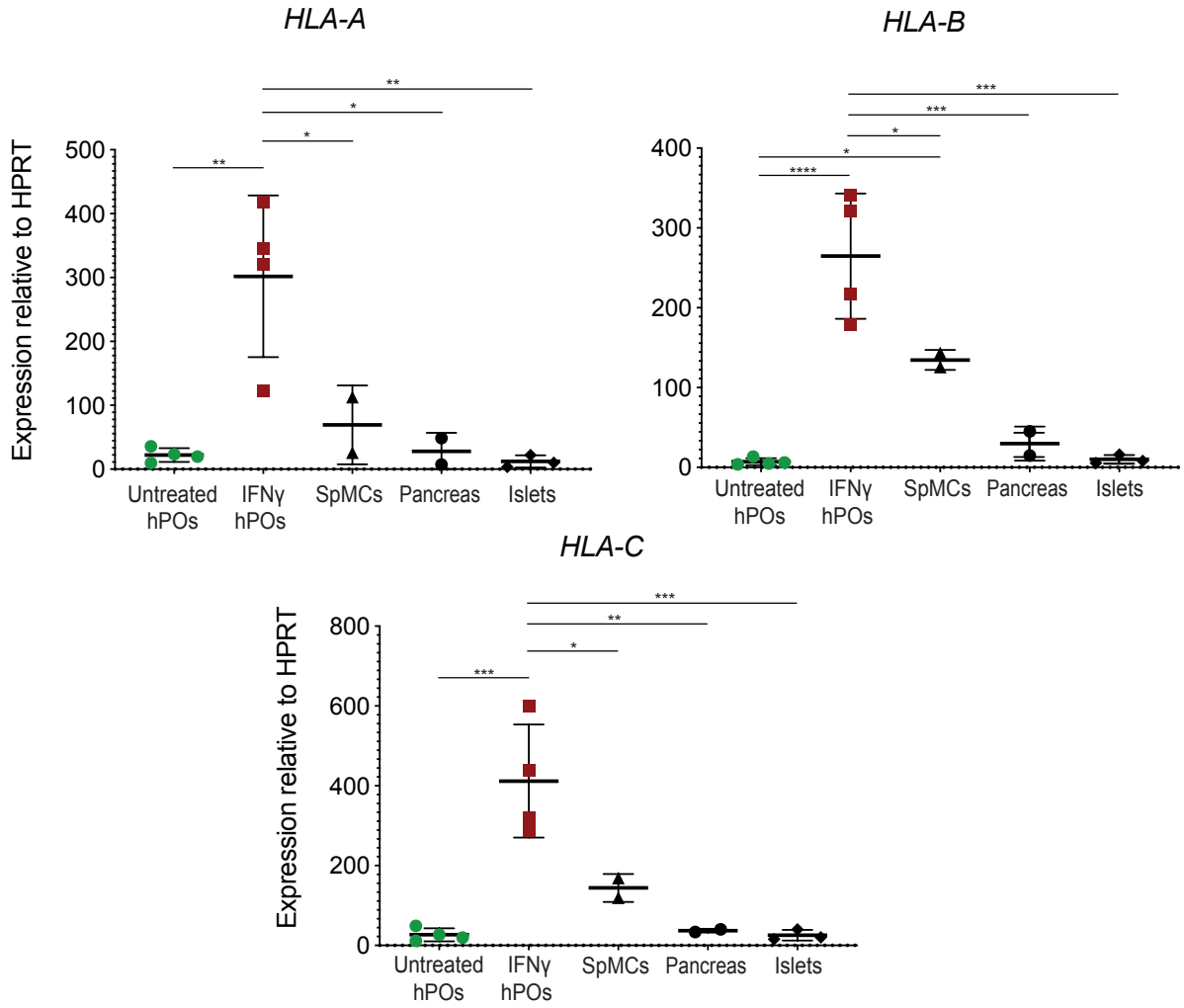

Figure 5.2 MHC Class I expression in hPOs under normal and IFNγ-inflammatory conditions. Graphs demonstrating expression of HLA Class I molecules (*A, B, C*) in hPOs cultured under untreated conditions (hPO-Opt.EM media) or inflammatory conditions (IFNγ) and compared to primary SpMCs, pancreas tissue and islets. Graphs represent technical (separate wells) replicates for n=2 independent donors (Donors 8 and 22) for "Untreated" and "IFNγ" conditions and n≥2 independent donors for SpMCs, pancreas and islets. Data presented as mean ± SD. Differences between groups were tested using one-way repeated measures ANOVA followed by Tukey's honestly significant difference (HSD) test. Significant differences are marked by asterisks: * $p \leq 0.05$** $p \leq 0.01$.*** $p \leq 0.001$, **** $p \leq 0.0001$. Differences between untreated hPOs and SpMCs are not significant for HLA-A and -C.

In order to understand whether hPOs can upregulate HLA molecules under inflammatory conditions, I cultured hPOs with an inflammatory cytokine. Previous experiments in our lab had demonstrated that culture of liver cholangiocyte organoids with pro-inflammatory cytokines such IFNγ or IL-6 demonstrated a significant upregulation of HLA molecules compared to control conditions. Hence, I designed a straightforward experiment whereby hPOs were expanded in culture, passaged on 'Day 0', allowed to expand for 4 days after which they were cultured for 72 hours in IFNγ supplemented hPO-Opt.EM media so as to allow sufficient time for the effects of IFNγ without impacting the health

of the organoids (Fig. 5.1). Indeed, brightfield images demonstrated that hPOs retained their healthy phenotype after the 72-hour incubation period (Fig. 5.1). After the incubation period, hPOs were collected for subsequent qPCR analysis or flow cytometric analysis.

I analysed mRNA expression of HLA Class I and II of hPOs incubated in hPO-Opt. EM+IFNγ or hPO-Opt.EM (untreated) and compared to positive control primary SpMCs, as well as primary pancreas tissue and isolated islets. For all HLA Class I molecules *(A, B,* and *C*), mRNA expression was lowest for hPOs expanded in hPO-Opt.EM (untreated) conditions and while numerically lower than all primary tissue types, it was not significantly different, with the exception of *HLA-B* whereby hPOs demonstrated significantly lower mRNA levels compared to SpMC controls (Fig. 5.2). Importantly, for all HLA Class I molecules, mRNA levels of IFNγ-treated hPOs were significantly higher than controls hPOs and also pancreas, islets, and SpMCs (Fig. 5.2). In order to investigate expression of HLA Class II mRNA, I analysed mRNA levels of *HLA-DP, -DQ, -DR*, in the same samples as for HLA Class I. mRNA expression of HLA Class II in hPOs grown in hPO-Opt.EM (untreated) was not detected while it was significantly increased in IFNγ-treated hPOs, with the exception of *HLA-DQ* (Fig. 5.3). Interestingly, mRNA expression of both *HLA -DP* and *-DR* by IFNγ-treated hPOs was similar to SpMCs and significantly higher than primary tissue pancreas and islets. However, *HLA-DQ* mRNA levels demonstrated a more modest increase in IFNγ-treated hPOs (Fig. 5.3). These results demonstrate that hPOs can increase mRNA expression of HLA Class I and II to levels similar to professional APCs upon INFγ stimulation.

In order to understand whether HLA Class I and II expression was dependent on time in culture, hPOs were collected at an early passage (P1-5) or late passage (P8-11). mRNA levels of HLA Class I under untreated conditions was similar between early and late passage hPOs (Fig. 5.4a). Interestingly, HLA Class I levels for IFNγ-treated hPOs was numerically higher in late passage hPOs, but the difference reached statistical significance for *HLA-B* only (Fig. 5.4a). In the case of mRNA expression of HLA Class II molecules, mRNA levels were similar between early and late passage hPOs for both untreated and IFNγ-treated conditions (Fig. 5.4b). This data show that mRNA expression levels of HLA Class I may be partly dependent on duration of culture, with prolonged culture periods resulting in an increase in HLA Class I expression.

Although expression of HLA molecules is expected to be the dominant driver of immunogenicity, expression of other antigens has also been demonstrated to cause an immune rejection. For example, two proteins Hormad1 and Zg16 were reported to cause immune rejection of autologous derived hiPSCS in mice[208]. Furthermore, type 1 diabetes is characterised by expression of autoantibodies which react against known antigens such as GAD65 and IA-2[218]. Therefore, I analysed mRNA expression of these two known T1D autoantigens in hPOs expanded under untreated or IFNγ-treated conditions. Again, SpMCS, primary pancreas and islets were used as primary tissue controls. hPOs did not express GAD65 or IA-2 mRNA in untreated or IFNγ-treated conditions, in contrast with

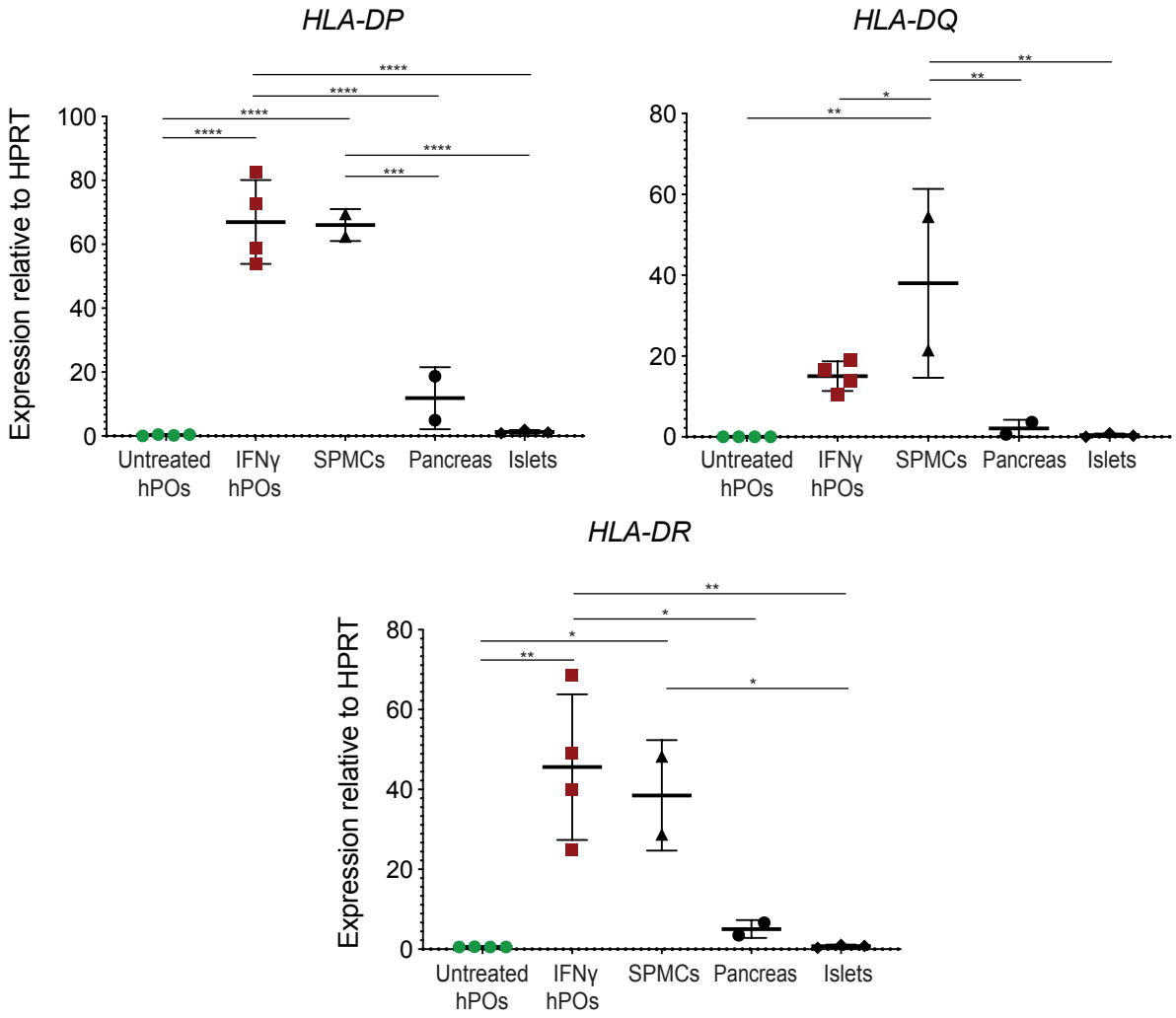

Figure 5.3 MHC Class II expression in hPOs under normal and IFNγ-inflammatory conditions. Graphs demonstrating expression of HLA Class II molecules (*DP, DQ, DR*) in hPOs cultured under untreated conditions (hPO-Opt.EM media) or inflammatory conditions (IFNγ) and compared to primary SpMCs, pancreas tissue and islets. Graphs represent technical (separate wells) replicates for n=2 independent donors (Donors 8 and 22) for "Untreated" and "IFNγ" conditions and n≥2 independent donors for SpMCs, pancreas and islets. Data presented as mean± SD. Differences between groups were tested using one-way repeated measures ANOVA followed by Tukey's honestly significant difference (HSD)test. Significant differences are marked by asterisks: * $p \leq 0.05$** $p \leq 0.01$.*** $p \leq 0.001$, **** $p \leq 0.0001$

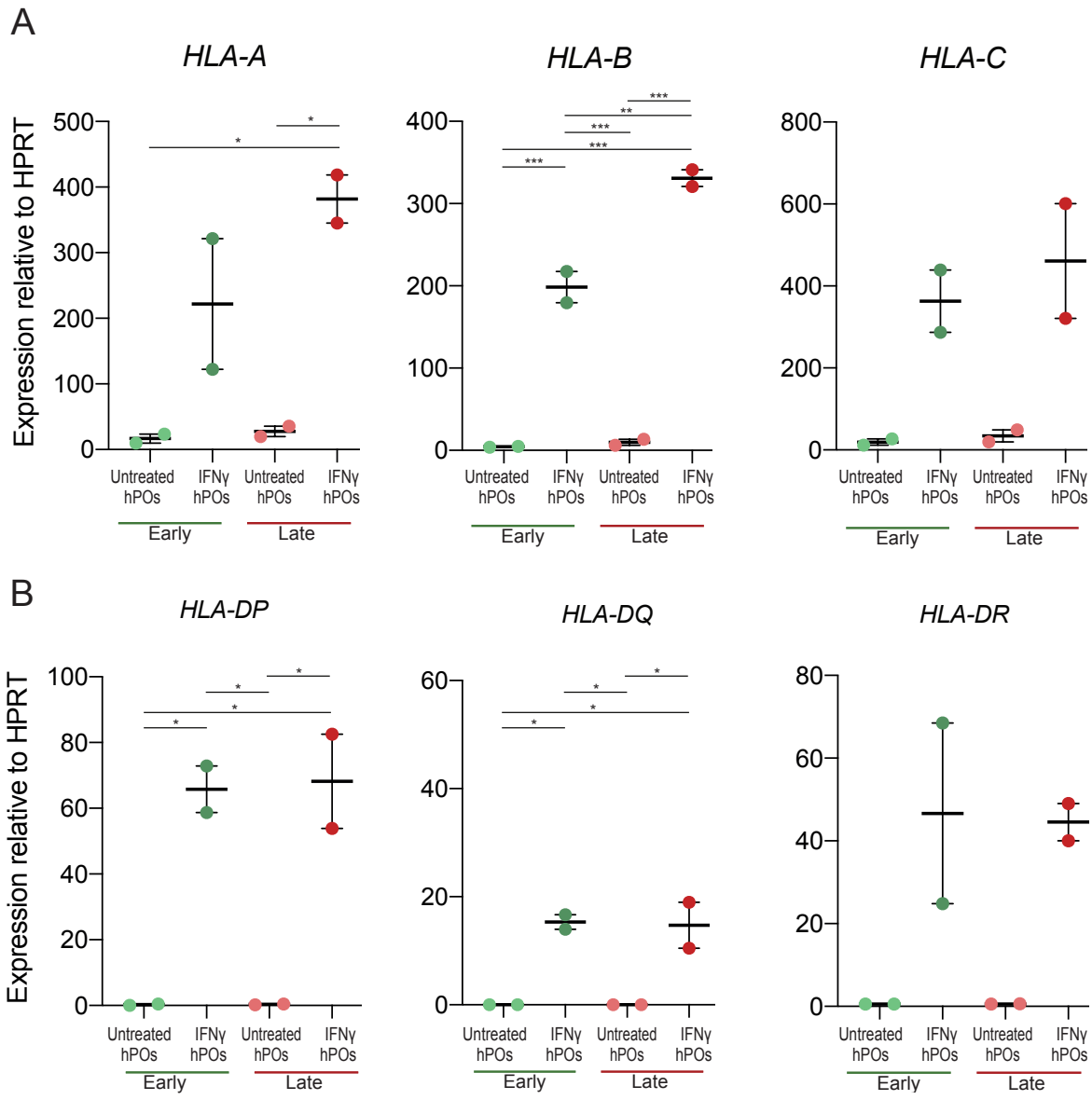

Figure 5.4 MHC Class I/II expression in early and late passage hPOs under normal and IFNγ-treated culture conditions. Graphs demonstrating expression of HLA Class I molecules (*A,B,C*) (**A**) and HLA Class II molecules (*DP, DQ, DR*) (**B**) in hPOs cultured under normal conditions (hPO-Opt.EM media) or inflammatory conditions (IFNγ) at the early (P1-5) and late (P 8-15) passage for n=2 independent donors (Donor 8 and 22). Data presented as mean ± SD. Differences between groups were tested using paired two-tailed t-test. Significant differences are marked by asterisks: * $p \leq 0.05$** $p \leq 0.01$.*** $p \leq 0.001$. Differences are not significant for HLA-C and HLA-DR.

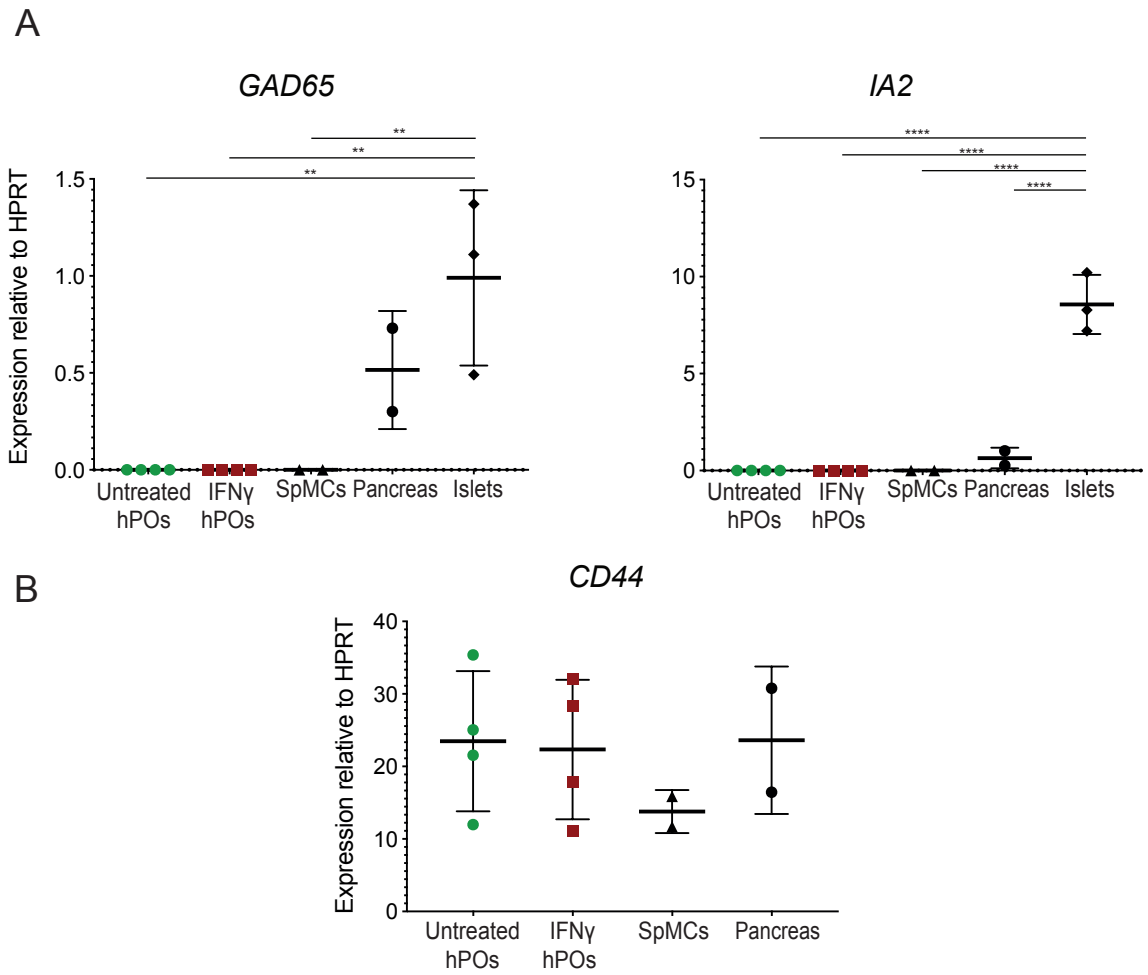

Figure 5.5 Alloantigen expression in hPOs under normal and IFNγ-treated culture conditions. (**A**)Graphs demonstrating gene expression of known autoantigens *GAD65* and *IA-2* associated with development of Type 1 Diabetes. (**B**) Graphs demonstrating gene expression of Wnt target gene *CD44* which has a role in lymphocyte recruitment. Expression levels were assessed for hPOs under normal (hPO-Opt.EM media), inflammatory (IFNγ) conditions as well as in primary SpMCs and pancreas tissue. Graphs represent technical (separate wells) replicates for n=2 independent donors for "Normal" and "IFNγ" conditions and n≥2 independent donors for SpMCs, pancreas and islets. Data presented as mean ± SD. Differences between groups were tested using one-way repeated measures ANOVA followed by Tukey's honestly significant difference (HSD) test. Significant differences are marked by asterisks: * $p \leq 0.05$** $p \leq 0.01$.*** $p \leq 0.001$, **** $p \leq 0.0001$.

islets which demonstrated significantly higher levels of expression under untreated conditions (Fig. 5.5a). Notably, both molecules were expressed in primary pancreas, although not significantly higher than hPOs, likely due to the existence of islet cells in the primary pancreas tissue (Fig. 5.5a). Furthermore, mRNA levels of known Wnt target gene CD44 were assessed, which also has a role in attachment to the ECM and lymphocyte recruitment in response to inflammation[289]. While CD44 mRNA is expressed in hPOs, mRNA levels were similar between hPOs expanded in untreated conditions and IFNγ treated conditions, as well as SpMCs and primary pancreas tissue (Fig. 5.5b). Therefore, while hPOs do not express known autoantigens involved in the progression of T1D, they do express CD44, a molecule potentially important in lymphocyte recruitment and activation.

In addition to mRNA analysis, I performed flow cytometry analysis of hPOs following the same experimental design (Fig. 5.1) to investigate protein expression. Following optimisation of the experiment to achieve the best flow cytometric parameters, including an appropriate gating strategy (Fig. 5.6), hPOs were analysed for their expression of HLA Class I (antibody recognising HLA A,B and C molecules), and HLA Class II (antibody recognising HLA-DP, DQ, DR) as well as CD44 (Figs. 5.6, 5.7). Interestingly, while the proportion of cells expressing HLA Class I was similar in hPOs expanded in untreated or IFNγ-treated conditions, histogram analysis of protein expression intensity showed that IFNγ-treated hPOs had a higher intensity of HLA Class I staining (Fig. 5.7a, b). Furthermore, protein expression of HLA Class II, quantified as a percentage of positive cells, was significantly higher in IFNγ-treated hPOs compared to both hPOs expanded in hPO-Opt.EM (untreated) and to SpMCs (Fig. 5.7b). However, the increase in HLA Class II expression in IFNγ-treated hPOs compared to SpMCs could be due to hPOs being a purer population as SpMCs also contain a variety of cells from the human spleen not all of which may express HLA Class II (Fig. 5.7). Interestingly, CD44 protein levels mirrored results from the mRNA analysis and remained similar between hPOs expanded in hPO-Opt.EM media (untreated) or treated with IFNγ (Fig. 5.7). In summary, this data illustrates that in an induced inflammatory scenario, hPOs can increase expression of HLA Class I and II. Therefore, HLA matching, much like in the scenario of solid organ transplantation, may be required for an hPO-based cell therapy product.

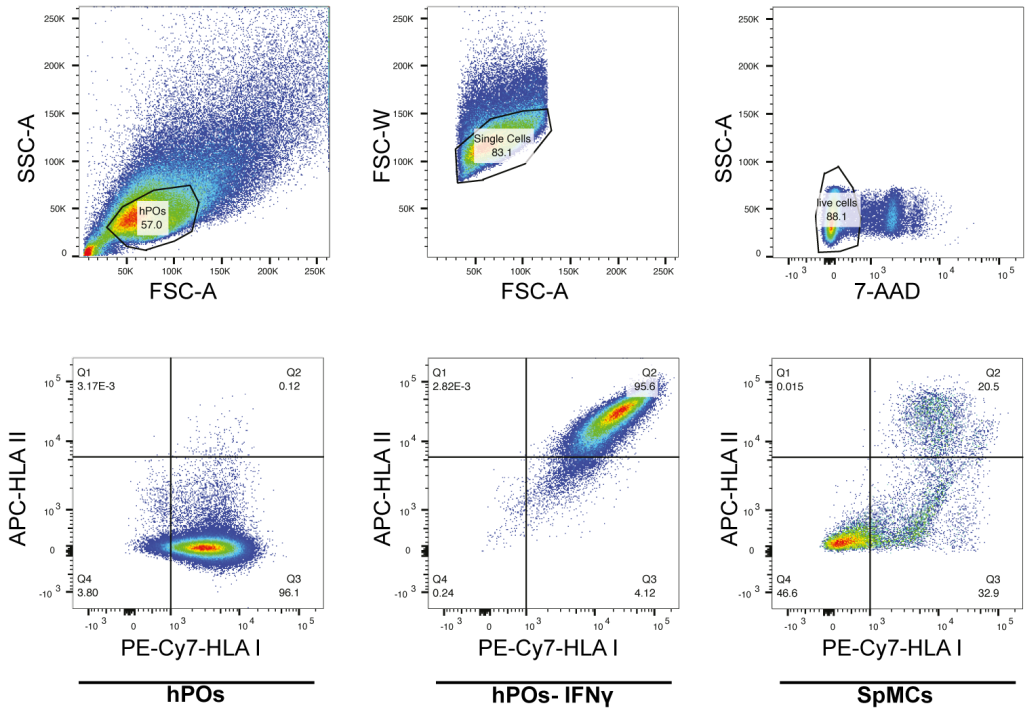

Figure 5.6 Gating Strategy for normal vs IFNγ treated hPO *in vitro*. Representative flow cytometry plots showing gating strategy for HLA I/II flow cytometric analyses, gating on hPOs, then single cells, then live cells (dead cell exclusion) followed by HLA I or HLA II positive cells. Bottom plots show representative HLA I and HLA II population in hPOs under normal or inflammatory conditions or in SpMCs.

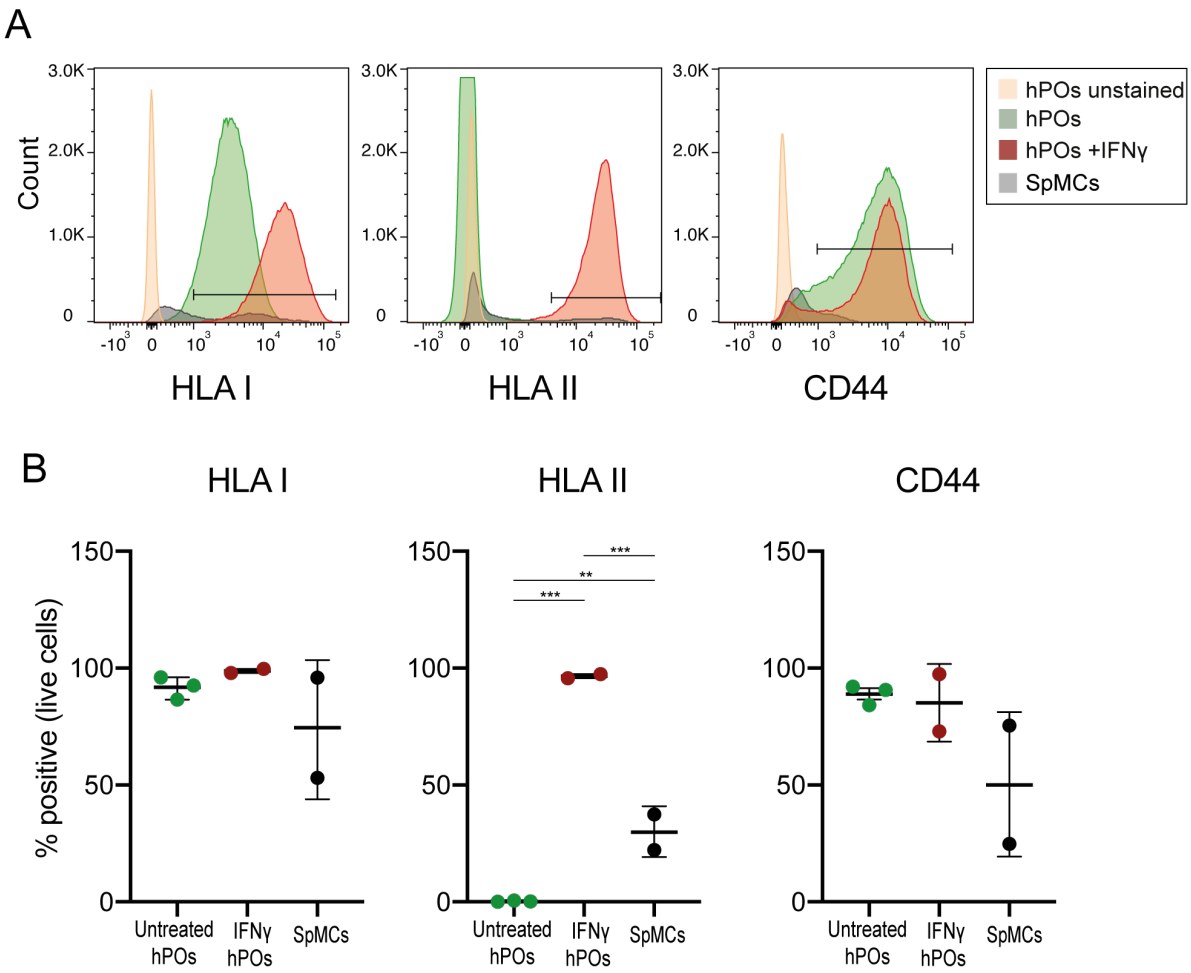

Figure 5.7 hPOs upregulate HLA I and II under IFNγ induced inflammatory conditions. Flow cytometric analysis showing staining intensity (**A**) and percentage of positive cells (**B**) for HLA Class I and II as well as CD44 in unstained negative control hPOs (cream), hPOs cultured in untreated conditions (green), hPOs cultured under inflammatory conditions (IFNγ; red), or in SpMCs (grey) for n≥2 independent donors. Data presented as mean± SD. Differences between groups were tested using one-way repeated measures ANOVA followed by Tukey's honestly significant difference (HSD)test. Significant differences are marked by asterisks: ** $p \leq 0.01$.*** $p \leq 0.001$.

5.2.2 hPO co-culture with SpMCs

It has been reported that following solid organ transplantation as well as pancreatic islet transplantation, there is production of donor-specific anti-HLA antibodies as well as allograft specific T cells by the recipient which target the graft, thereby significantly impacting the graft's survival[290]. These antibodies and T cells are reactive against both HLA Class I and II, meaning that due to the pro-inflammatory environment and interaction with lymphocytes, cells such as the endocrine cells in islets which do not typically express HLA Class II, can potentially start expressing these molecules. While I have demonstrated that hPOs can increase expression of HLA Class I and II after exposure to IFNγ, it is important to understand whether this will occur as a result of interacting with lymphocyte populations.

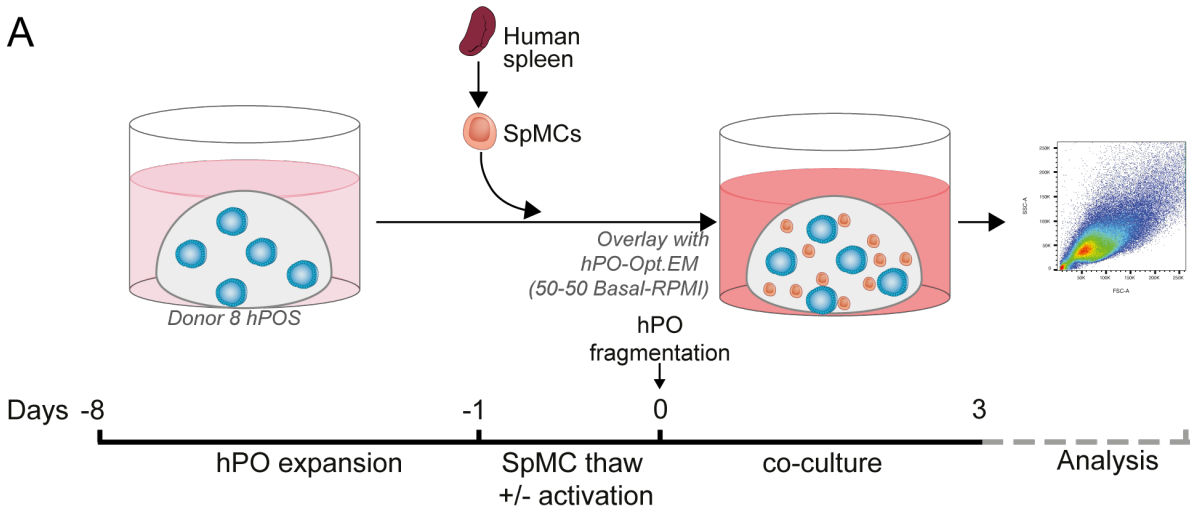
A
Human spleen
SpMCs
Donor 8 hPOS
Overlay with hPO-Opt.EM (50-50 Basal-RPMI)
hPO fragmentation
Days -8
-1
0
3
hPO expansion
SpMC thaw +/- activation
co-culture
Analysis

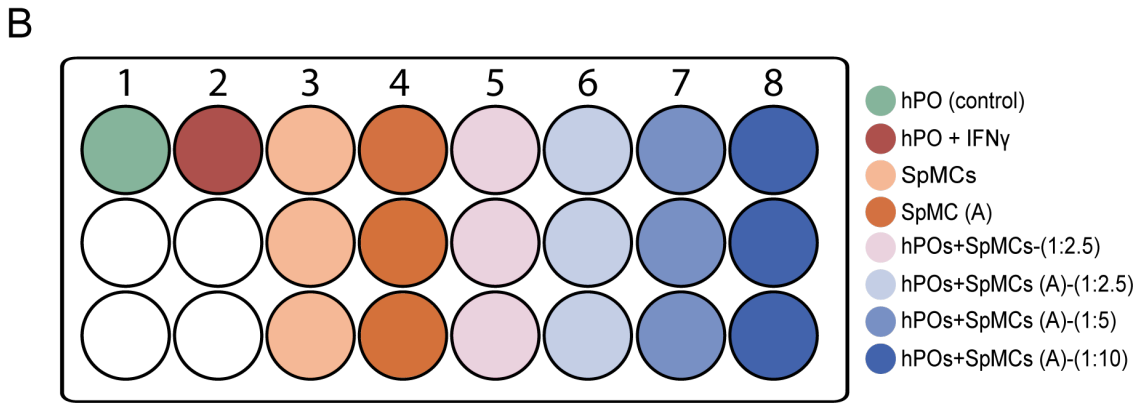
B
1 2 3 4 5 6 7 8
hPO (control)
hPO + IFNγ
SpMCs
SpMC (A)
hPOs+SpMCs-(1:2.5)
hPOs+SpMCs (A)-(1:2.5)
hPOs+SpMCs (A)-(1:5)
hPOs+SpMCs (A)-(1:10)

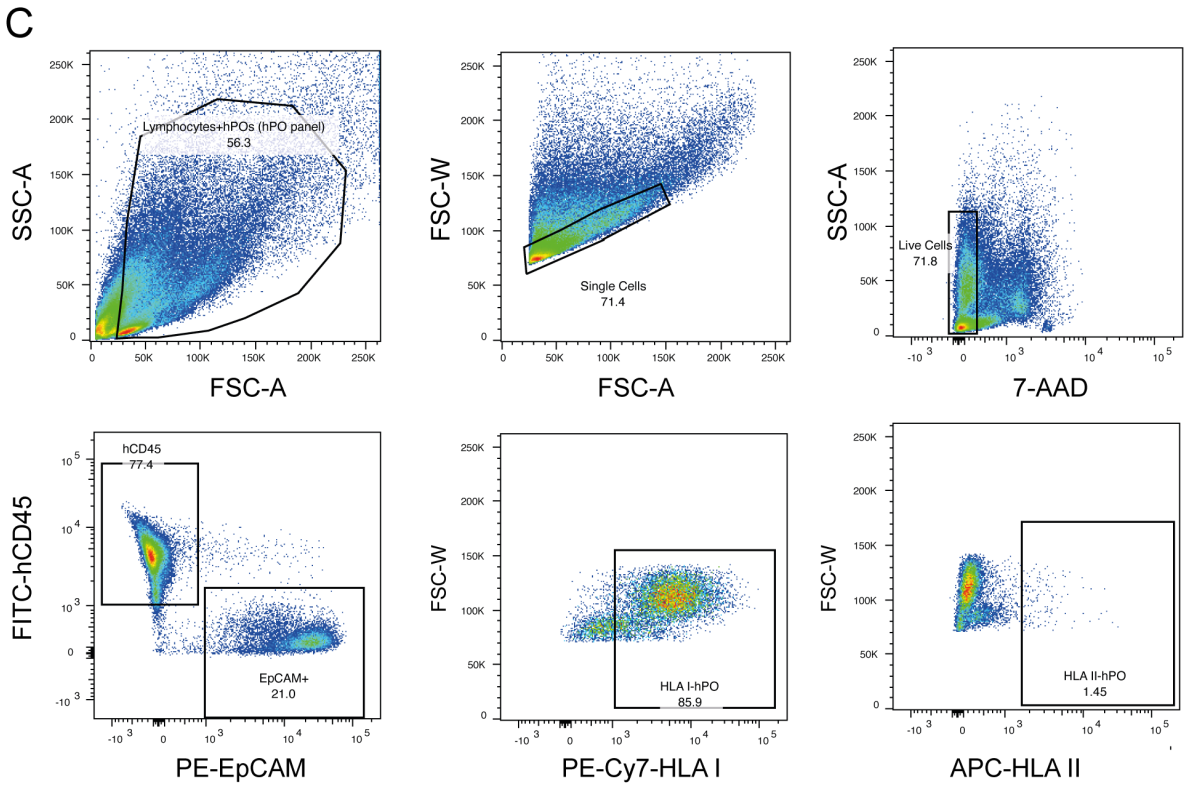
C
SSC-A
FSC-A
Lymphocytes+hPOs (hPO panel)
56.3
FSC-W
Single Cells
71.4
Live Cells
71.8
7-AAD
FITC-hCD45
hCD45
77.4
EpCAM+
21.0
PE-EpCAM
HLA I-hPO
85.9
PE-Cy7-HLA I
HLA II-hPO
1.45
APC-HLA II

Figure 5.8 Experimental design for co-culture of hPOs with SpMCs. (**A**) Schematic showing experimental design for culture of hPOs with SpMCs. hPOs are expanded to sufficient numbers to allow for all the experimental groups outlined in (**B**). 24 h prior to initiation of the co-culture, SpMCs are thawed, counted and incubated with CD3/CD28 dynabeads to allow for activation of the T cell population. On day 0, hPOs are fragmented as for the method of passaging and are mixed with SpMCs at the appropriate ratios, embedded in BME 2 and overlaid with 50% basal media and 50% RPMI as well as all of the growth factors used in hPO-Opt.EM media (see section 2.10.3.2 for further details. hPOs are incubated with the co-culture for 72 h after which they are collected for flow cytometric analysis. (**B**) Schematic to demonstrate the conditions for the co-culture experiment. hPOs were mixed at a ratio of 1:1.25 with non-activated SpMCs and increasing numbers with activated SpMCs. (**C**) Representative flow cytometry plots showing gating strategy for EpCAM and HLA I/II flow cytometric analyses, gating initially on lymphocytes and hPOs, then single cells, then live cells (dead cell exclusion), then on EpCAM positive cells to select hPOs and then finally gating on HLA I and II populations.

I therefore established a co-culture system to model the interaction of hPOs with activated lymphocytes in order to understand whether this interaction and the resulting pro-inflammatory environment is sufficient to cause upregulation of HLA molecules particularly HLA Class II in hPOs.

In order to achieve this, I thawed hPOs and expanded them to sufficient numbers for the multiple conditions outlined below. 24 hours prior to the initiation of co-culture, SpMCs were thawed from a different donor to that of the hPO line (allogeneic) and were activated using CD3/CD28 activation beads. The SpMC-bead mix was cultured at 37°C in RPMI media until the following day (Fig. 5.8a). After this, hPOs were fragmented and mixed with SpMCs in the following conditions (Fig. 5.8b):

1. hPO control
2. hPOs incubated with IFNγ
3. SpMCs only (not activated)
4. SPMCS only (activated)
5. hPOs+ SpMCs (not activated; ratio 1:2.5)
6. hPOs +SpMCs (activated; ratio 1:2.5)
7. hPOs +SpMCs (activated; ratio 1:5)
8. hPOs +SpMCs (activated; ratio 1:10)

Cells were collected for flow cytometric analysis after 72 hours in culture, following a similar timepoint as for the IFNγ stimulation experiments. Following a gating strategy which allowed to gate on the hPO and SPMC populations and to exclude doublets and dead cells, I was able to assess the expression of HLA Class I and II on EpCAM+ cells (EpCAM is a ductal cell marker and is not expressed on lymphocytes; Fig. 5.8c). In order to quantify T cell populations in the various conditions, cells were also stained with pan lymphocyte marker hCD45, T cell marker CD3, T helper cell marker CD4, cytotoxic T cell marker CD8 and T cell activation marker CD25. Unsurprisingly, percentage of lymphocyte (CD45+) populations were highest in SpMC only conditions (3 and 4) and were

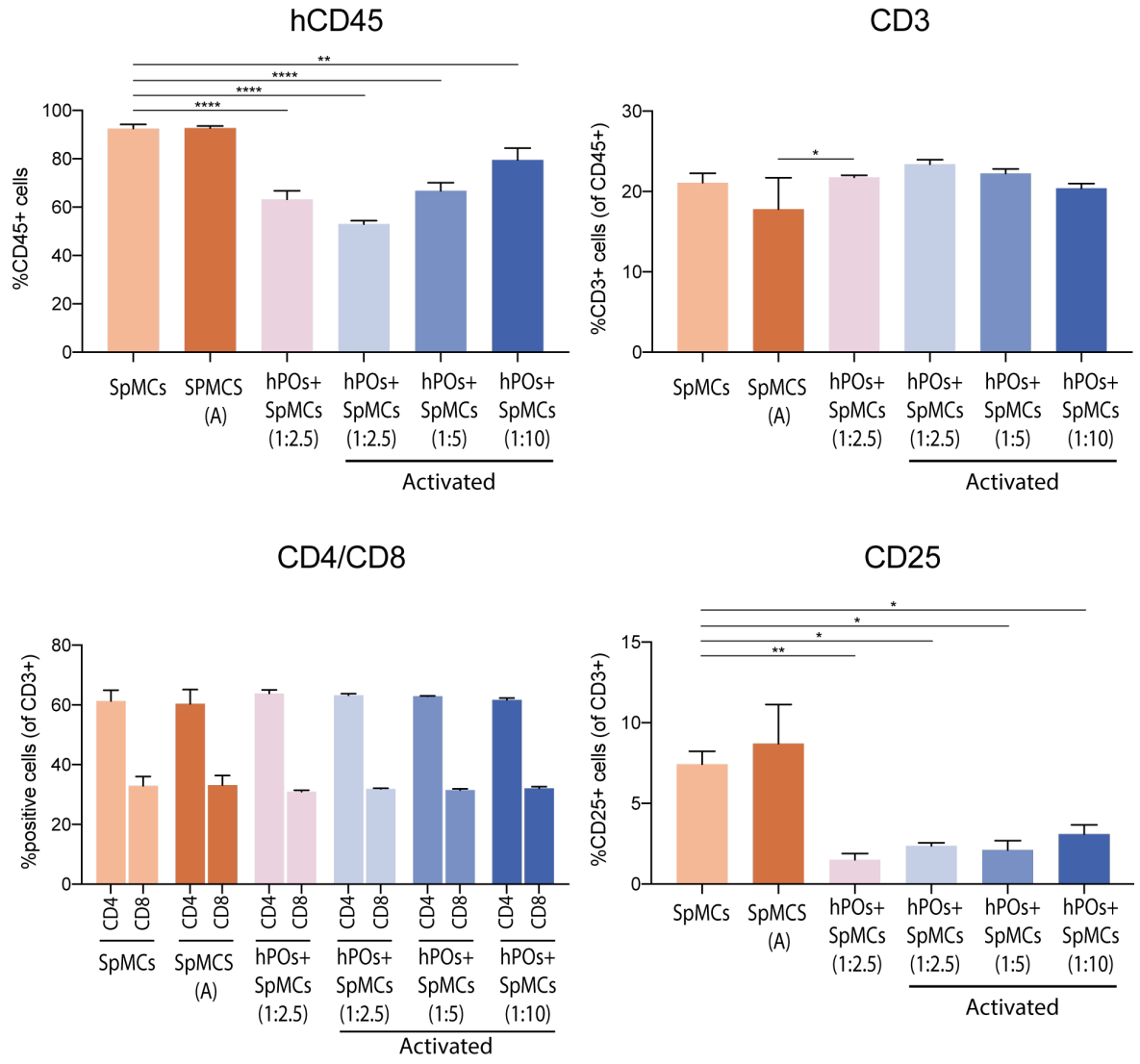

Figure 5.9 T cell activation levels following co-culture of hPOs with SpMCs. Graphs showing levels of CD45, CD3, CD4/CD8 cells and activated T cells (CD25+) in the lymphocyte population of control non activated SpMCs, activated SpMCs, SpMCs with hPOs or activated SpMCs with hPOs in the outlined ratios following flow cytometric analysis. Note the low level of CD25+ cells in the co-culture conditions indicating that activation of T cells did not occur at sufficient levels. Experiments were carried out for n=1 hPO donor and n=1 SpMC donor. Data presented as mean± SEM. Differences between groups were tested using one-way repeated measures ANOVA followed by Dunett's honestly significant difference (HSD)test as groups were compared to SpMCs. Significant differences are marked by asterisks: * $p \leq 0.05$,** $p \leq 0.01$.*** $p \leq 0.001$,**** $p \leq 0.0001$.

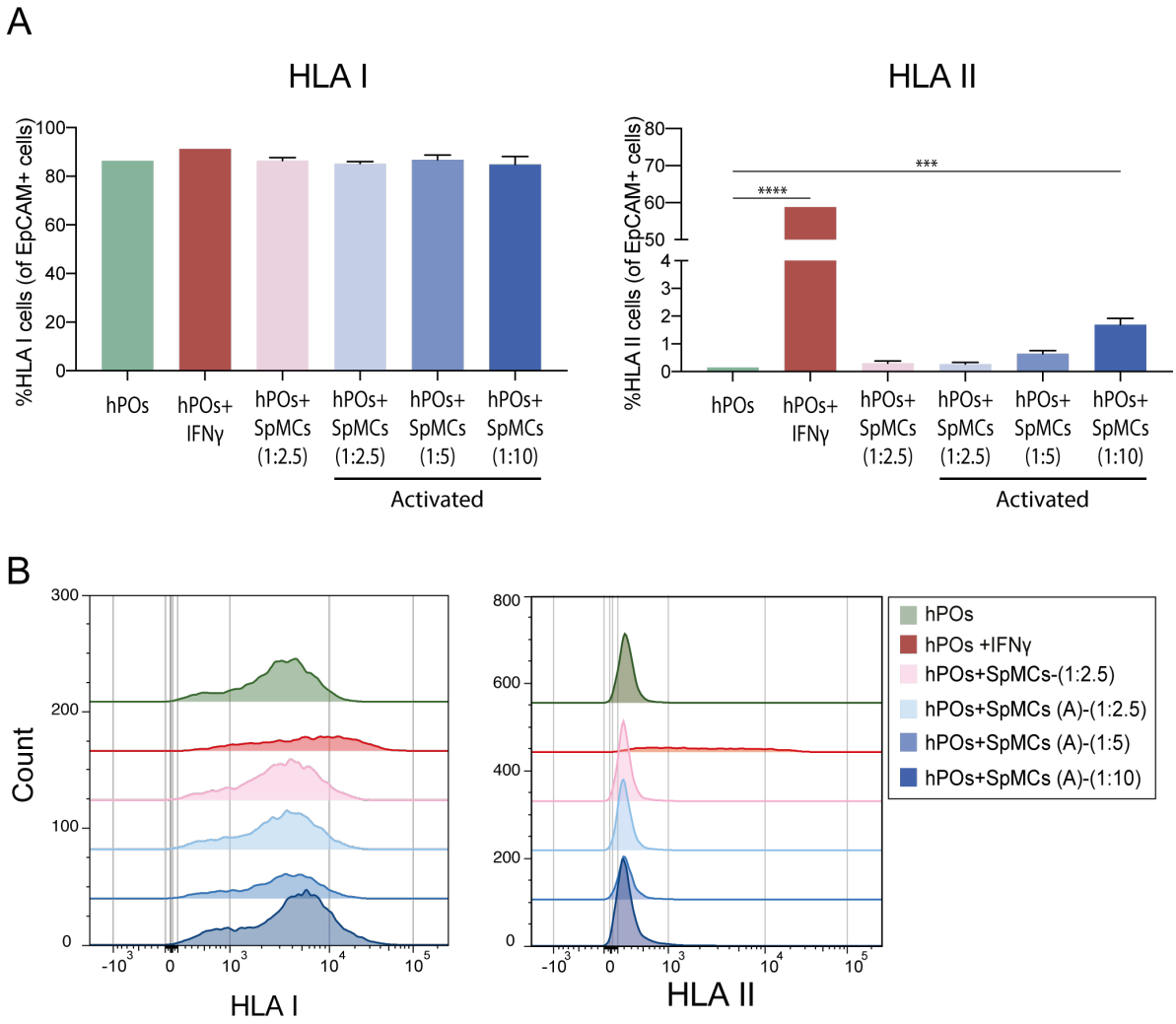

Figure 5.10 hPOs increase expression of HLA II following co-culture with SPMCs. (**A**)Graphs showing percentages of positive cells for HLA I (left) and HLA II (right) of hPOs (EpCAM+ population) in either control conditions, or following incubation with either IFNγ, or with SPMCs as indicated by the graphs. (**B**) Graphs showing staining intensity counts following flow cytometric analysis in the same groups as for graph A. Experiments were carried out for n=1 hPO donor and n=1 SpMC donor. Data presented as mean ± SEM. Differences between groups were tested using one-way repeated measures ANOVA followed by Dunett's honestly significant difference (HSD)test as groups were compared to SpMCs. Significant differences are marked by asterisks: *** $p \leq 0.001$, **** $p \leq 0.0001$.

significantly reduced in the co-culture conditions 5-8 (Fig. 5.9). However, percentage of CD3+ cells of hCD45+ cells remained constant among all conditions, with only SpMCs (Activated; condition 4) showing a reduced CD3+ cell percentage (Fig. 5.9). Furthermore, CD4+ and CD8+ populations remained constant between all conditions. Interestingly, activation of T cells was low, at 8.7% for activated SpMCs (condition 4) compared to control (conditions 3) which was 7.4% (Fig. 5.9). Furthermore, in the co-culture conditions, levels of CD25+ cells were significantly lower than the control, non-activated condition 3, signifying that T cells were not sufficiently activated by the beads or by the potential interaction with hPOs (Fig. 5.9). After gating on the EpCAM+ population, all conditions, either hPOs alone (1 and 2) or co-cultures (5-8) showed similar proportion of HLA Class

I+ cells (Fig. 5.10a). However, similar to the results demonstrated in section 5.2.1, hPOs incubated with IFNγ (condition 2) showed a marked upregulation of HLA Class II with 58.8% positive cells (Fig. 5.10a). Contrastingly, hPOs co-cultured either with non-activated SpMCs (condition 5) or activated SpMCs in a ratio of 1:1.25 (condition 6) or 1:5 (condition 7) showed slightly higher percentages of HLA Class II+ cells compared to control, but this difference was not statistically significant. A significant increase in HLA Class II expression was only detected in the final condition, 8, wherein hPOs were co-cultured with activated SpMCs in a ratio of 1:10 (Fig. 5.10a). Furthermore, intensity of staining of HLA Class I or II remained similar between all conditions except the IFNγ treated group (5.10b). In summary, this data shows that co-culture of hPOs with SpMCs can indeed lead to an increase in HLA Class II expression, although at much lower levels to those observed upon IFNγ stimulation of hPOs.

5.2.3 Autologous and allogeneic rejection of transplanted hPOs in HIS mice

Thorough assessment of the immunogenicity of potential cellular therapies is essential prior to their use in the clinic. Furthermore, as discussed in section 1.6.7, future cellular therapies might be derived in an allogeneic manner due to both logistical and cost implications. As such, it is important to assess whether the human immune system will reject either autologous or allogeneic derived cellular therapies and whether strategies to ameliorate the immune response, such as immunotherapies or HLA matching, are required. While I have demonstrated that hPOs have the potential to be immunogenic as they can upregulate expression of both HLA Class I and II following culture with either IFNγ or SpMCs, it is unclear whether this would translate to an immune rejection event *in vivo*. Moreover, testing of cellular therapies in a human setting is difficult particularly for those that are in early stages of development. Humanised mouse models or human immune system (HIS) mice are a tool that offer a way to study immunogenicity of cellular therapies in the context of a human immune system. They are defined as "immunodeficient mice that have been engrafted with human primary haematopoietic cells and tissues that generate a functional human immune system" [227]. In the Saeb-Parsy group, we utilise two types of humanised mouse models, the first being the human SCID repopulating cell (Hu-SRC) model which we generate through introduction of human bone marrow derived haematopoietic stem cells (HSCs) into the mouse. In this project I refer to this model as HSC-HIS mice. The second HIS mouse model is the human peripheral blood lymphocyte (Hu-PBL) model which we generate through introduction of splenocyte mononuclear cells (SpMCs) from the spleen of a human donor; therefore, this model will be referred to as SpMC-HIS mice. Importantly, during collection of pancreatic tissue from organ donors in the operation theatre, I was also able to collect samples of bone marrow and spleen. Therefore, this allowed generation of HIS mice from SpMCs or HSCs from the same donors that hPOs were generated from, thus allowing investigation of both autologous and allogeneic settings.

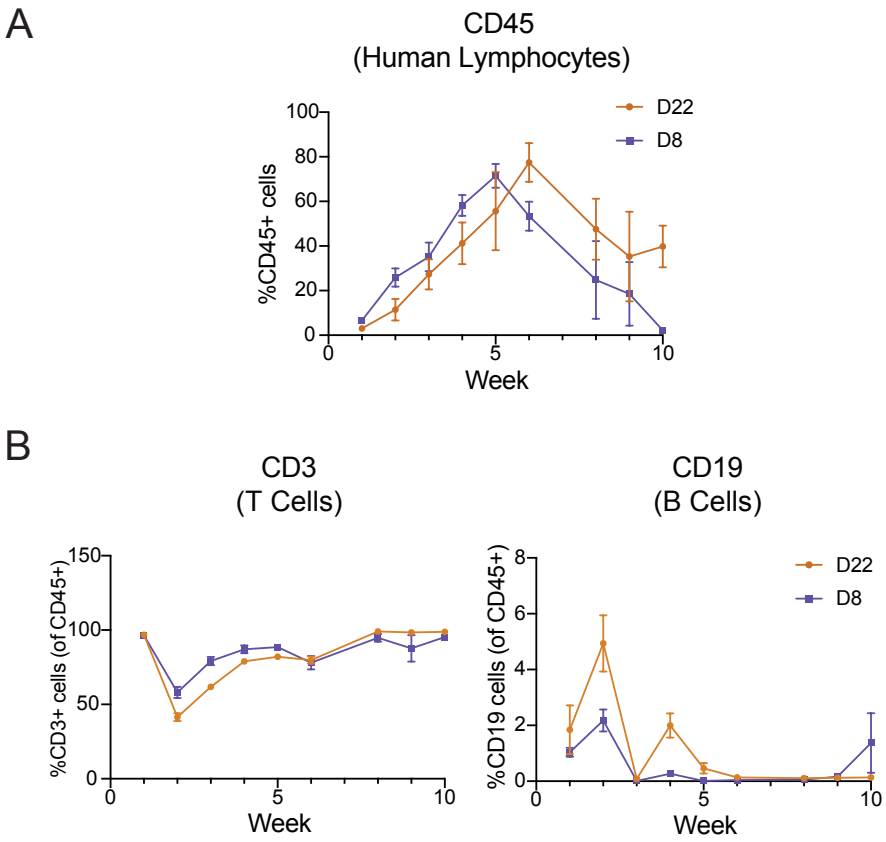

Figure 5.11 Lymphocyte engraftment time course in SpMC-HIS mice. Graphs showing time course for the engraftment of CD45+, CD3+, and CD19+ cells in the peripheral blood of NSG-dKO mice, as measured by flow cytometry, following I.P. injections with SpMCs from Donor 22 and 8. Note that these mice did not receive hPO transplants as they were used as controls to assess humanisation levels in order to plan future experiments. (**A**) Graph shows levels of human lymphocytes (CD45+ cells) in the peripheral blood of NSG-dKO mice across 10 weeks. (**B**) Graphs show levels of T cells (CD3+) and B cells (CD19+) in the peripheral blood of NSG-dKO mice. Each line represents a donor, n=3 mice were used per donor. Data presented as mean ± SEM.

Use of SpMC-HIS mice to study rejection of hPOs

I first aimed to study rejection of hPOs using the SpMC-HIS model, as it has a shorter timescale than the HSC-HIS mouse model. This model elicits a strong CD3+ T cell response that can effectively reject allogeneic grafts[227]. However, the level and efficiency of humanisation varies among different donors and there is a risk of utilising cells that do not engraft well in the mice. Contrastingly, if the CD3+ T cell response is too strong, it can lead to rapid graft *vs* host disease (GvHD) thereby confounding assessment of hPO rejection. Therefore, utilising SpMCs from Donors 8 and 22, from which hPOs were used to investigate HLA expression *in vitro* (Section 5.2.1-2), I humanised 6 NSG-dKO mice (3 mice per donor) in order to obtain a time course of engraftment (Fig. 5.11). The mice were bled weekly and humanisation was assessed through flow cytometric analysis and quantification of the levels of human lymphocytes (CD45+ cells) in mouse blood. Both groups were maintained for 10 weeks, with only one mouse showing signs of GvHD in the second week post-humanisation. SpMC-

HIS mice from Donor 8 reached levels of humanisation greater than 20% at week 2 while mice with Donor 22 SpMCs reached similar levels at week 3 (Fig. 5.11). The maximum average level of humanisation was 71% at week 5 for Donor 8 and 77% at week 6 for Donor 22. Furthermore, levels of T (CD3+) and B (CD19+) cells were assessed weekly. As expected, the majority of the cells in both groups of mice were T cells, with a low number of B cells maintained until week 4, after which either no or extremely low numbers (<1%) of B cells could be detected (Fig. 5.11). Interestingly, while the two donors showed similar engraftment kinetics, Donor 22-engrafted mice maintained levels of CD45+ cells at an average of 40% even at the final cull point (week 10) while Donor 8-engrafted mice had very low levels (<5%) in the same timepoint (Fig. 5.11). Most importantly, this experiment allowed the understanding of the engraftment kinetics of SpMCs from Donors 8 and 22, allowing high levels of humanisation without appearance of GvHD, and informed the design of subsequent SpMC-HIS mouse experiments.

In order to investigate rejection of hPOs in an autologous and allogeneic setting, I designed a "crossover" experiment with cells from Donors-8 and -22. Eight NSG-dKO mice were transplanted with hPOs from Donor-8 and 8 mice with hPOs from Donor-22 using the same protocol as described in section 4.2.3, i.e*.,* pancreas capsule injections. hPOs were allowed to engraft for 2 weeks after which 4 mice from each group received SpMCs from Donor-22 and 4 mice from Donor-8, thereby resulting in 2 autologous groups and 2 allogeneic groups from 2 donors (Fig. 5.12). For clarity purposes, the groups will be referred to by the donor from which they received SpMCs, followed by "autologous" or "allogeneic" to signify the donor from which they received hPOs, i.e., D22-autologous. The mice were maintained for 3 weeks to allow humanisation levels to reach approximately 20%, as similar levels have previously been used to assess allograft rejection[291]. Once mice were culled, the pancreas, liver and spleen were collected for histological assessment, while the blood, spleen, and bone marrow were used for flow cytometric analysis.

Weekly bleeding of the mice, from week 2 post humanisation, demonstrated that D22-autologous and D22-allogeneic had levels of 27% and 24% CD45+ cells in the blood respectively, while D8-autologous and D8-allogeneic had 37% and 30% respectively (Fig. 5.13). Interestingly, although the initial humanisation levels were reflective of the donor used, rather than autologous versus allogeneic, the autologous groups demonstrated a decrease in humanisation levels from week 2 to 3 while both allogeneic groups showed an increase in humanisation levels. Although it is difficult to draw conclusions, partly due to the variability in humanisation levels across both mice and donors, one explanation for the contrasting changes of humanisation levels is that in the allogeneic groups, lymphocytes are getting activated at higher levels due to the interaction with allogeneic cells. This could result in stimulating proliferation, while in the autologous groups, the human lymphocytes do not receive similar interactions. Interestingly, the same pattern was not observed for T cells (CD3+) and B cells (CD19+). Both D22 and D8 groups showed a decrease in T cell populations, while the D22 groups

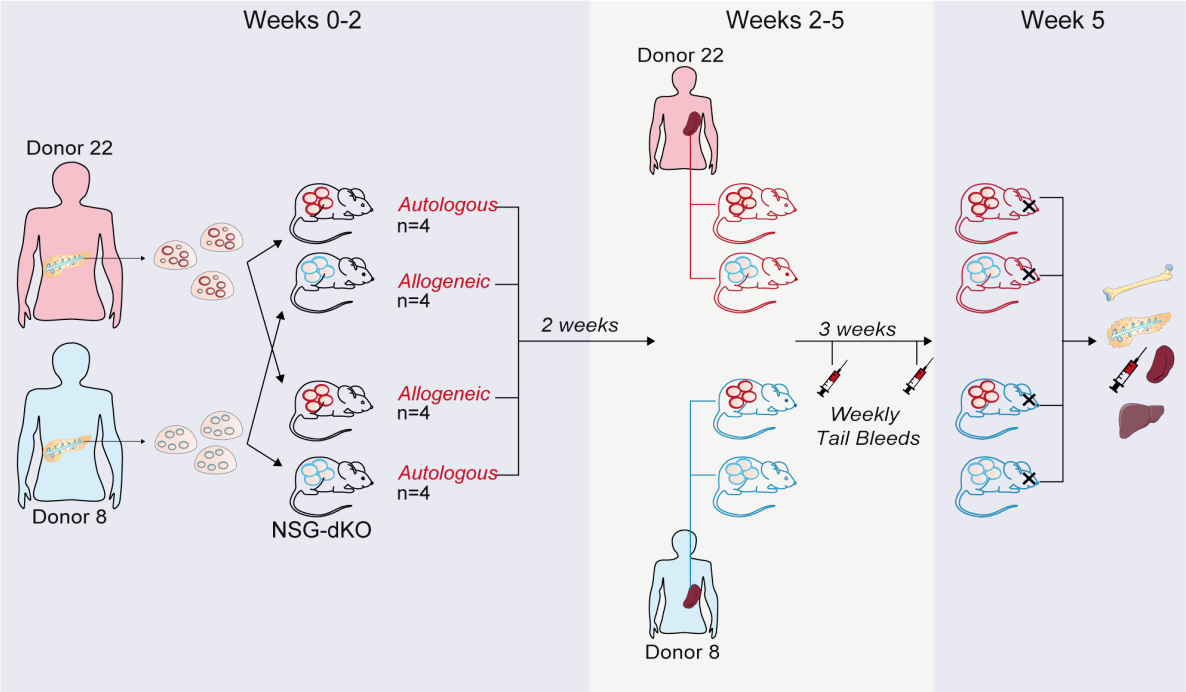

Figure 5.12 Assessment of allograft rejection of hPOs in the SpMC-HIS mouse model. Schematic showing experimental design for generation of SpMC human immune system mice in order to assess rejection of engrafted hPOs in autologous and allogeneic conditions. Initially, hPOs from 2 donors (Donor 22 and Donor 8) are transplanted into the pancreas capsule of 16 NSG-dKO mice (8 mice per donor) and are allowed to engraft for 2 weeks to ensure stabilisation of the graft. Then, the mice are humanised with SpMCs isolated from Donor 22 and Donor 8 in a manner allowing investigation of autologous and allogeneic rejection (i.e., SpMCs from Donor 22 are injected into mice engrafted with hPOs from Donor 22 and Donor 8 and the same is performed for SpMCs from Donor 8). The humanised mice with the engrafted hPOs are kept for a period of 3 weeks, after which they are culled, and organs are collected for flow cytometric analysis (to assess humanisation levels and lymphocyte populations) and staining (H&E, immunofluorescence) to assess infiltration of the graft by human lymphocytes.

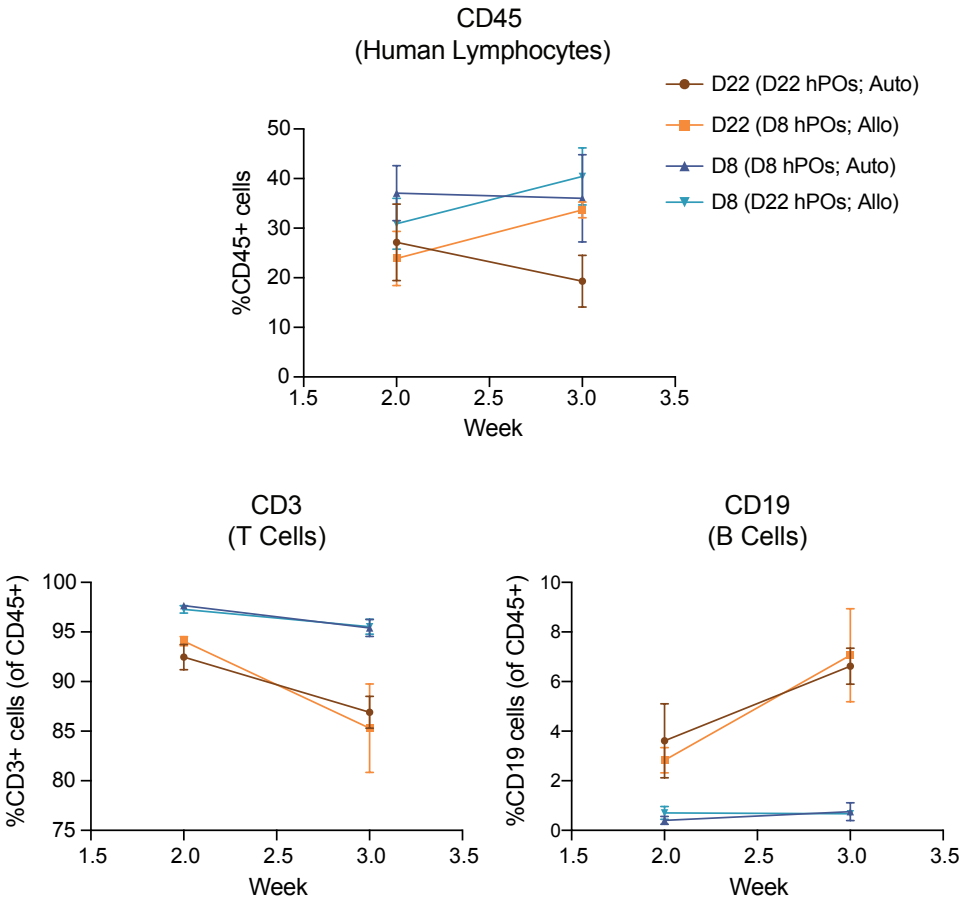

Figure 5.13 Assessing immune rejection of hPOs in an autologous and allogeneic environment in SpMC-HIS mice. Graphs showing percentage of human lymphocytes (CD45+ cells; top graph), T cells (CD3+ cells) and B cells (CD19+ cells; bottom graphs) in peripheral blood of NSG mice following humanisation with CD3 depleted human HSCs. Data is shown as mean ± SEM.

showed an increase in B cells from week 2 to week 3. However, in either week, CD45+ were still predominantly T cells, as expected, while levels of T and B cells reflected the donor of humanisation, rather than the experimental group. (Fig. 5.13). Once the animals were culled, I analysed the blood, bone marrow and spleen for levels of CD45+ cells, T and B cell subsets, as well as subsets of T cells (CD4+ and CD8+ cells; Fig. 5.14). In the peripheral blood, levels of CD45+ cells in autologous and allogeneic groups were similar and were also not statistically significant from the control group (week 3 timepoint of the non-transplanted SpMC-HIS mice; Fig. 5.14). Interestingly, the proportion of CD3+ cells was significantly higher in both autologous and allogeneic groups compared to the control group while CD19+ levels were the same among control, autologous and allogeneic groups. In the bone marrow, CD45+ cells were at levels of 5% and 6% in the autologous and allogeneic groups, respectively, which were not significantly different. Furthermore, both CD3+ and CD19+ cells were detected in the bone marrow, while a higher percentage of CD19+ cells resided in the bone marrow than in the peripheral blood, although levels were not different between autologous and allogeneic

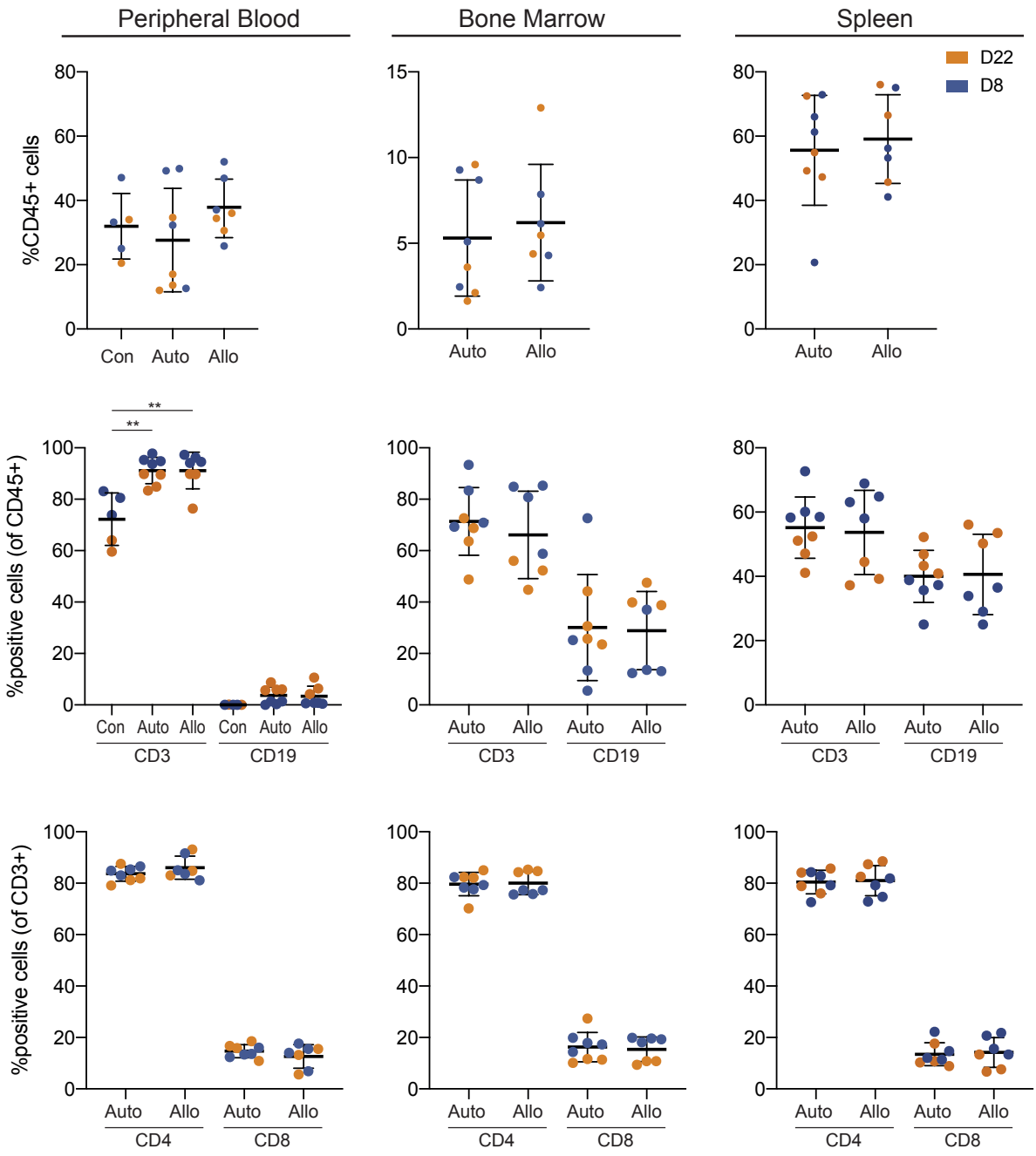

Figure 5.14. Lymphocyte infiltration in peripheral blood, bone marrow and spleen of SpMC-HIS mice. Graphs represent levels of human lymphocyte populations in the peripheral blood, bone marrow and spleen of NSG-dKO mice. The mice were transplanted with hPOs for 2 weeks after which they were humanised with SpMCs from donors 22 or 8 as illustrated in Figure 5.12. Control mice (Con) did not receive hPO transplants. Top graphs demonstrate levels of human lymphocytes (CD45+ cells), middle graphs show levels of T cells (CD3+) and B cells (CD19+) as a proportion of CD45+ cells and bottom graphs show levels of T cell subsets CD4+ cells (T-helper cells) and CD8+ cells (Cytotoxic T cells). Experiments were performed on n=3 mice per donor for the Control group and n=4 mice per donor per condition (autologous and allogeneic), with a total of 22 mice. Each dot represents a single mouse. Data is shown as mean± SD. Differences between groups were tested using one-way repeated measures ANOVA followed by Tukey's honestly significant difference (HSD)test for the 'Peripheral blood" graphs and a paired two-tailed t-test for the remaining graphs. Significant differences are marked by asterisks: ** $p \leq 0.01$.

groups (Fig. 5.14). Additionally, levels of CD4+ and CD8+ were similar in the bone marrow to those detected in the peripheral blood and were also similar between autologous and allogeneic groups. The highest levels of CD45+ cells were found in the spleen of the mice with levels of 55% and 59% in the autologous and allogeneic groups, respectively, which were not significantly different (Fig. 5.14). This is perhaps unsurprising since the spleen functions as a filter for blood, while both T and B cells can reside within the spleen. Interestingly, SpMC-HIS mice display splenomegaly (data not shown), likely owed to the increased storage of human cells. This might also explain the higher percentage of B cells found in the spleen of both autologous and allogeneic groups. Furthermore, the proportions of CD4+ and CD8+ cells remained similar and reflective of what was detected in the peripheral blood and bone marrow (Fig. 5.14).

While levels of T and B cells between autologous and allogeneic groups remained similar, the fact that the allogeneic groups presented higher levels of overall humanisation, i.e., CD45+ cells could be reflective of an active allograft rejection. However, as this in theory is T cell mediated, differences in levels of T cells would also be expected. Furthermore, HLA typing data from the two donors confirmed that they were indeed a complete mismatch for all HLA Class I and II molecules (Appx. Table 4). This further supports the idea that the allogeneic hPOs should be rejected more aggressively than the autologous ones. However, this rejection may be happening at the local, graft, level and may not be able to be detected on a global scale, i.e., the mouse peripheral blood.

In summary, this data shows that SpMC mice can be used to assess rejection of hPOs in a short time scale in a model largely governed by CD3+ T cells. Interestingly, humanisation levels are higher in the allogeneic group than the autologous group potentially pointing to a decreased rejection of autologous cells. However, CD45+ cell subtypes were similar between both groups. Current work is ongoing to perform histological analysis of the grafts to understand whether lymphocyte infiltration of the graft was different between the two groups, and therefore quantify the level of rejection that is taking place in either group.

Use of HSC-HIS mice to study rejection of hPOs

While the SpMC-HIS mouse model allows for assessment of allograft rejection from mature CD3+ T cells, it does not allow efficient engraftment of cells other than T cells, with B cells only surviving in the spleen of mice. However, the HSC-HIS mouse model can support the engraftment of a wider variety of human immune cells, including B cells, NK cells and macrophages and rarely develops GVHD within the time frame of a typical experiment[225,227]. Therefore, I designed a "crossover" experiment using the HSC-HIS mouse model in a similar manner as with the SpMC-HIS mouse model, to allow investigation of graft rejection at the autologous and allogeneic level using the same donors, 8 and 22, which I had also established were complete HLA-mismatched (Appx. Table 4). The NSG mice were first injected with CD3 depleted HSCs (refer to section 2.8 for details) and were allowed to engraft

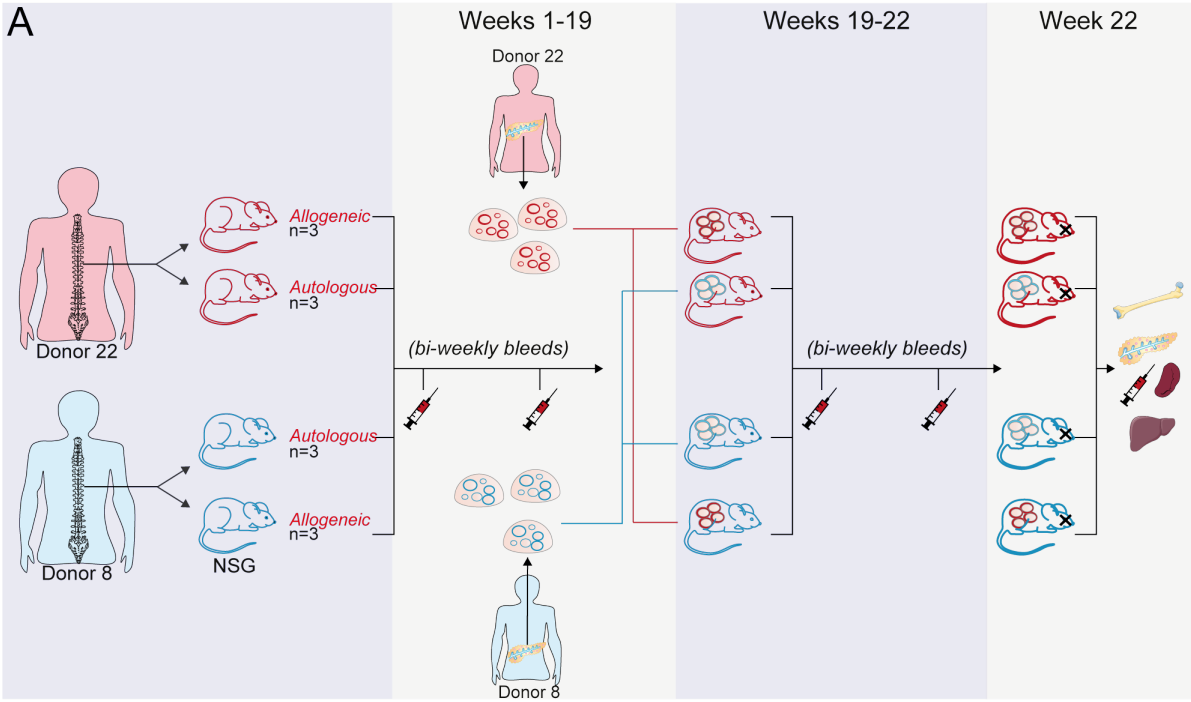
A
Weeks 1-19
Weeks 19-22
Week 22
Donor 22
Allogeneic
n=3
Autologous
n=3
Donor 22
(bi-weekly bleeds)
(bi-weekly bleeds)
Autologous
n=3
Allogeneic
n=3
Donor 8
NSG
Donor 8

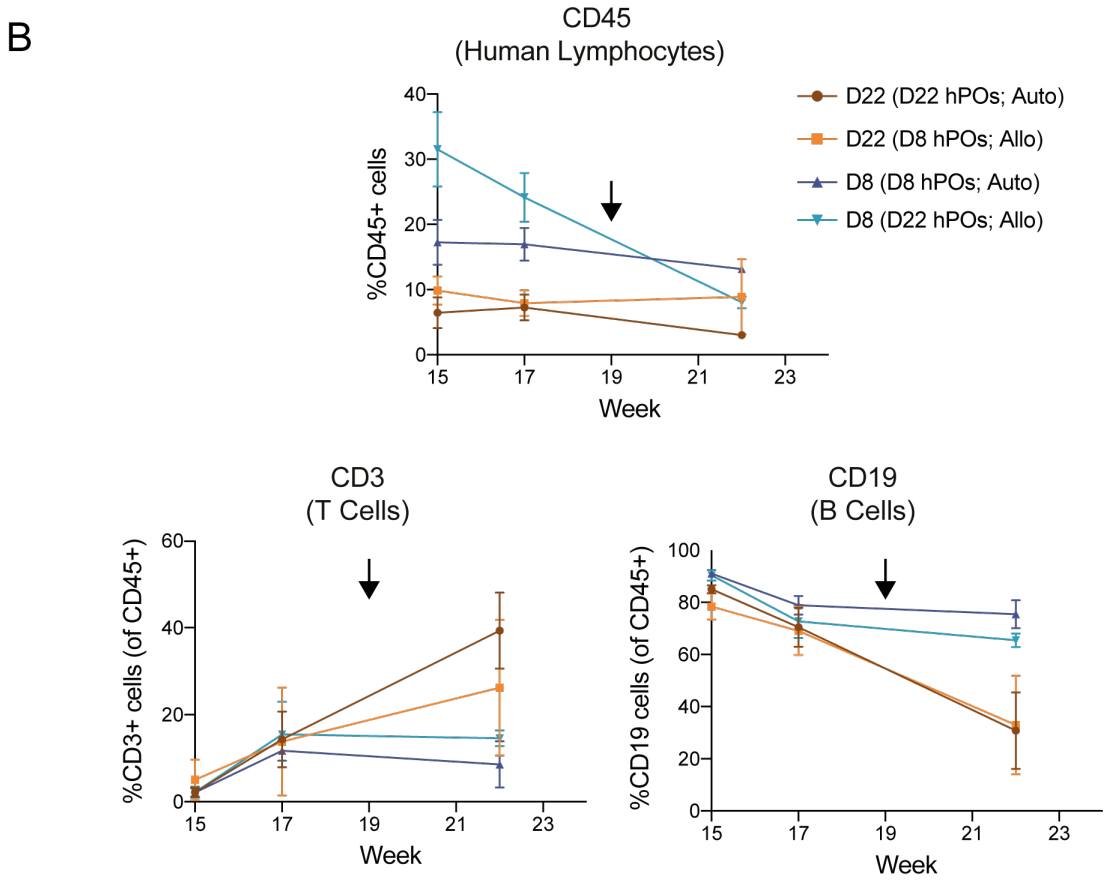
B
CD45
(Human Lymphocytes)
%CD45+ cells
Week
D22 (D22 hPOs; Auto)
D22 (D8 hPOs; Allo)
D8 (D8 hPOs; Auto)
D8 (D22 hPOs; Allo)
CD3
(T Cells)
%CD3+ cells (of CD45+)
Week
CD19
(B Cells)
%CD19 cells (of CD45+)
Week

Figure 5.15 Assessing immune rejection of hPOs in an autologous and allogeneic environment in HSC-HIS mice. (**A**) Schematic showing experimental design for generation of HSC human immune system (HIS) mice in order to assess rejection of engrafted hPOs in autologous and allogeneic conditions. Mice are first subjected to sublethal radiation to completely eradicate the immune system and they are then subjected to I.V. injections with HSCs which have undergone CD3 depletion. For this experiment, 6 NSG mice were injected with HSCs from Donor 22 and 6 mice from Donor 8. Mice are maintained for a period of 15-19 weeks and are monitored for level of humanisation. After humanisation has been established, the mice are transplanted with hPOs from Donors 22 and 8 so as to allow investigation of immune rejection under autologous and allogeneic settings. Namely, NSG mice humanised with Donor 22 HSCs receive hPOs from Donor 22 and 8 (3 mice from each donor), while the same is performed with mice humanised with Donor 8 HSCs. Once hPOs are transplanted, the mice are maintained for 3 weeks after which they are sacrificed and the organs are collected for flow cytometric analysis (to assess humanisation levels and lymphocyte populations) and staining (H&E, immunofluorescence) to assess infiltration of the graft by human lymphocytes. (**B**) Graphs showing percentage of human lymphocytes (CD45+ cells; top graph), T cells (CD3+ cells) and B cells (CD19+ cells; bottom graphs) in peripheral blood of NSG mice following humanisation with CD3 depleted human HSCs. Data is shown as mean ± SEM. Arrow indicates time of hPO transplantation.

for a period of 19 weeks. Once the mice were humanised and *de novo* T cells began to be detected, the mice were transplanted with hPOs. The mice were then maintained for 3 weeks and were sacrificed, for a total time scale of 22 weeks, and their organs collected for further processing as described for the SpMC-HIS mice (Fig. 5.15a).

Due to the shutdown of our laboratory as a result of the restrictions imposed in response to the spread of the SARS-CoV-2 virus, the earliest timepoint that the mice could be bled for monitoring of humanisation was at 15 weeks. At this point however the mice were showing adequate levels of humanisation. D8-autologous and D8-allogeneic mice had levels of CD45+ cells in the blood of 17% and 32% respectively, while D22-autologous and D22-allogeneic had 6% and 10% respectively (Fig. 5.15b). This interestingly shows that variability of the levels of humanisation in this model exists not only between donors, but also between mice. Levels of CD45+ cells continued to decrease among all groups after week 15 despite the transplantation of hPOs at week 19. However, the proportion of T cells increased after week 15 and was on average at 14% among all groups at week 17, while there was a notable amount of variability (Fig. 5.15b). D8-autologous and D8-allogeneic reached final levels of T cells of 9% and 15% respectively, while D22-autologous and D22-allogeneic groups were 40% and 26% respectively. Furthermore, while all groups started with high levels of B cells in the peripheral blood (>75%), D8-autologous and D8-allogeneic maintained levels at 75% and 65% respectively while levels in D22-autologous and D22-allogeneic dropped to 31% and 33% respectively (Fig. 5.15b).

Following the final cull point, comparison of autologous and allogeneic groups in terms of levels of CD45+ cells in the blood, bone marrow and spleen shows that while peripheral blood had lower levels of CD45+ cells compared to the other two compartments, levels were overall similar between the allogeneic and autologous groups (Fig. 5.16). Peripheral blood showed lower levels of CD3+ cells than CD19+ B cells in both groups while the difference was more marked in bone marrow and peripheral blood. Furthermore, differences between autologous and allogeneic were not significant

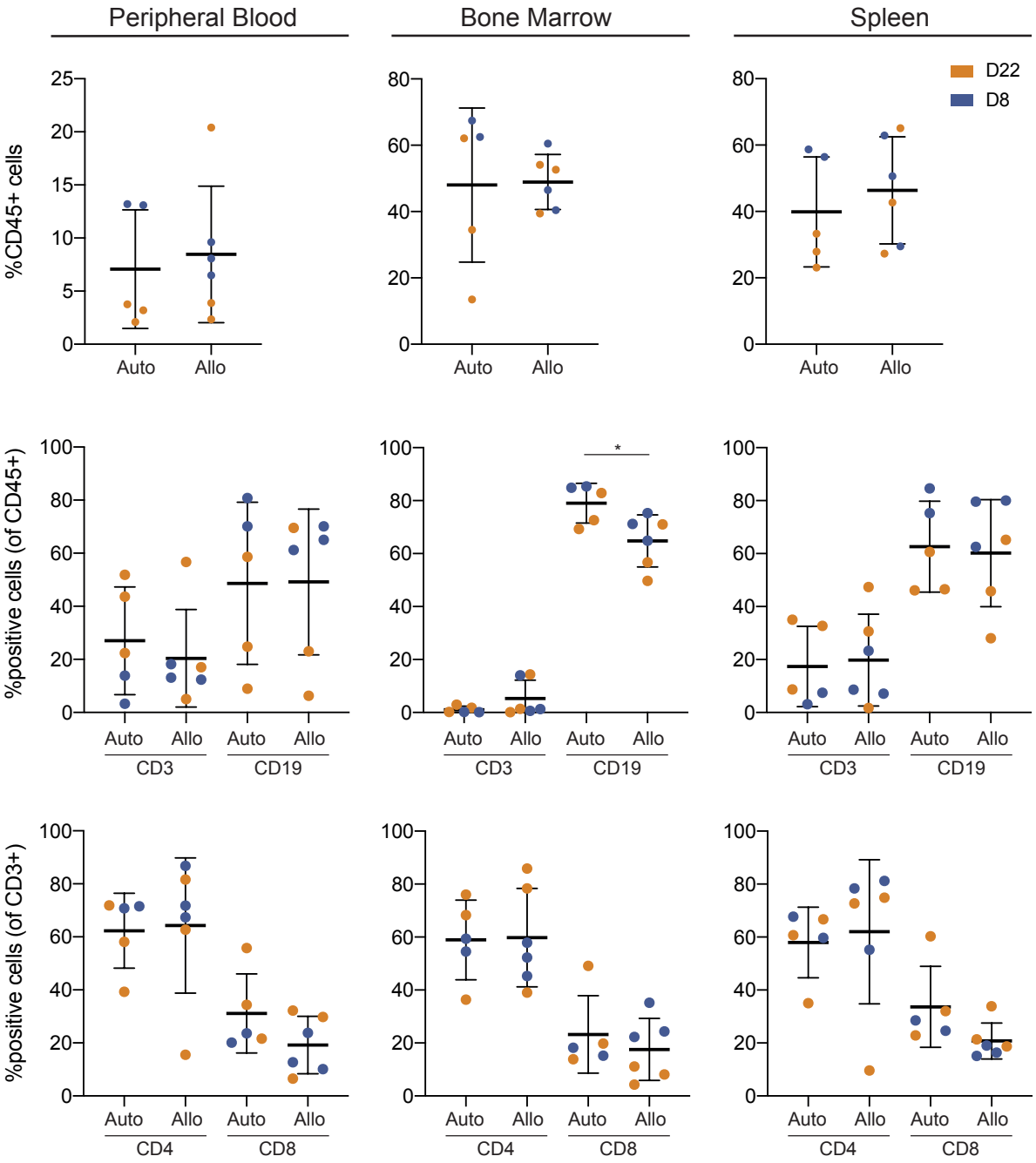

Figure 5.16 Lymphocyte infiltration in peripheral blood, bone marrow and spleen of HSC-HIS mice. Graphs represent levels of human lymphocyte populations in the peripheral blood, bone marrow and spleen of NSG mice 22 weeks post I.V. injections with CD3 depleted HSCs and subsequent transplants with hPOs. Top graphs demonstrate levels of human lymphocytes (CD45+ cells), middle graphs show levels of T cells (CD3+) and B cells (CD19+) as a proportion of CD45+ cells and bottom graphs show levels of T cell subsets CD4+ cells (T-helper cells) and CD8+ cells (Cytotoxic T cells). Experiments were performed on n=3 mice per donor per condition (autologous and allogeneic), with a total of 12 mice. Each dot represents a single mouse. Data is shown as mean± SD. Differences between groups were tested using paired two-tailed t-test. Significant differences are marked by asterisks: * $p \leq 0.05$.

with the exception of CD19+ cells in the bone marrow, with the allogeneic group having less cells (Fig. 16). Furthermore, T cell subsets, CD4+ and CD8+ cells were similar among the three tissue types and the two groups, with CD4+ cells being at higher levels.

In summary, these results show that it is possible to utilise the HSC-HIS mouse model to study rejection of hPOs in an autologous and allogeneic setting. However, it remains unclear whether the graft can have any significant impact on the levels of humanisation in the mice as well as the levels of CD45+ cell subtypes. It is likely that overall levels of humanisation in the mouse are driven by the donor chosen rather than the response against the graft. Moreover, current work is ongoing to section the engrafted pancreases to quantify levels of lymphocyte infiltration and to understand whether autologous cells get rejected and whether allogeneic cells are rejected more than their autologous counterparts. Nevertheless, both SpMC-HIS and HSC-HIS experiments show that in principle, allograft rejection can be assessed using these mouse models while both models are complimentary allowing to use both a T cell driven model and a model that also supports maintenance of B cells.

5.2.4 Generation of a Luciferase+ hPO line for *in vivo* tracking of graft rejection

A significant portion of the work in this project requires transplantation of hPOs *in vivo*, either in the mouse kidney capsule, particularly for the earlier transplants prior to optimisation of the injection protocol, or in the pancreas capsule. Furthermore, identification of the graft and assessment of surviving cells is very time consuming, requiring significant sectioning, at times of the whole organ, and H&E staining in various locations, while quantification is difficult. Importantly, the animal needs to be culled in order to retrieve the organs, therefore more animals are needed in order to have biological replicates at each culling point. Therefore, in order to allow tracking and quantification of graft survival *in vivo* without the need for culling the animal, I chose to generate a luciferase-expressing hPO line which could be imaged *in vivo* using bioluminescence imaging (BLI). Indeed, BLI is commonly used for a variety of *in vivo* research applications such as assessing graft survival or tumour growth[292] and has a major advantage of being able to image animals multiple times while also being relatively easier to perform compared to other imaging applications such as magnetic resonance imaging (MRI) or positron emission tomography (PET)[292]. Therefore, I investigated the ability to generate luciferase-expressing hPOs utilising various constructs, either commercially available or generated in collaboration with other laboratories.

I first utilised constructs which were commercially available in pre-packaged lentiviral particles. The first contained luciferase and green fluorescent protein (GFP), both controlled by the CMV promoter (referred from this point as GFP-virus) while the second contained luciferase controlled by the CAG promoter and linked by an F2A linker to red fluorescent protein (RFP) which was controlled by the RSV promoter (referred to form this point as RFP-virus; Fig.17). hPOs were made into single cells and transduced with the viruses (refer to section 2.6.1) and were subsequently

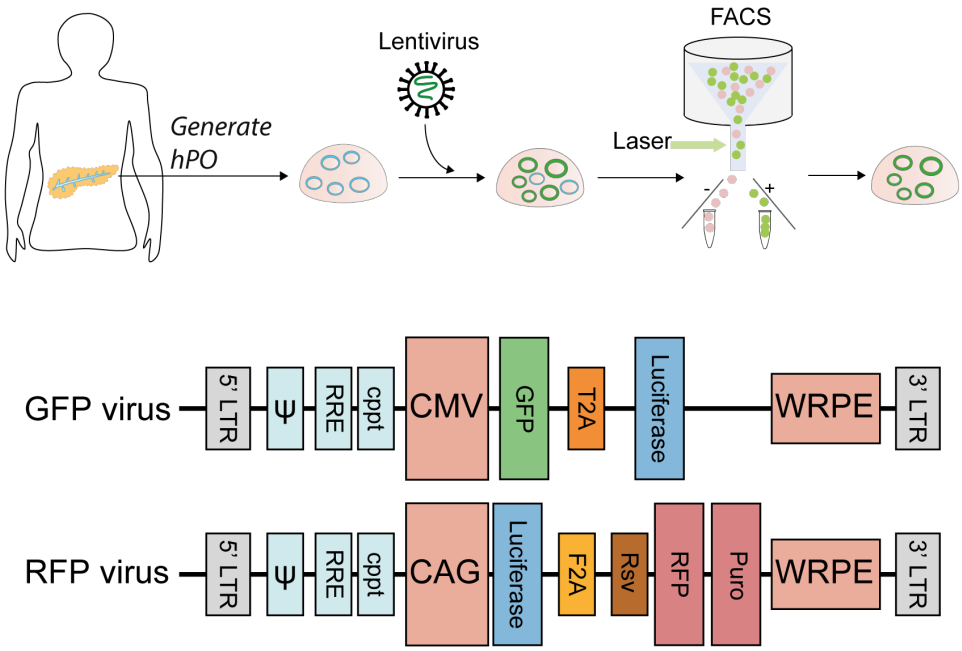

Figure 5.17 Generation of a GFP/RFP-Luciferase+ hPO line using lentiviral vectors. Schematic showing generation of an hPO line which expresses GFP/RFP and Luciferase. hPOs are expanded to passage 3 and are made into single cells followed by transduction using pre-packaged lentiviral preps (see section 2.6.1 for further details). The transduced hPOs are then allowed to expand for a further 2 passages and are imaged for expression of fluorescent GFP or RFP depending on the construct used. hPOs are then subjected to a second single cell step and are FACS sorted to select for GFP- or RFP-positivity and to generate a pure population. The GFP/RFP-negative population is also collected for control experiments.

checked for fluorescence signal and luciferase activity, followed by a second single-cell step and fluorescence activated cell sorting (FACS) to achieve a pure population of luciferase+ cells (Fig 5.17). Fluorescence imaging demonstrated that a large number of hPOs expressed GFP 13 days following transduction while very few organoids expressed RFP at the same timepoint (Fig. 5.18a). Transduced hPOs were allowed to expand for 2 passages after which *in vitro* luciferase activity was assessed. hPOs transduced with GFP-virus had significantly higher luciferase activity than control hPOs, while hPOs transduced with RFP-virus demonstrated some luciferase activity but significantly lower compared to GFP-virus hPOs (Fig. 5.18b). However, RFP-virus transduced hPOs retained *in vitro* luciferase activity at a level significantly higher to control hPOs (Fig. 5.18b). Furthermore, same passage hPOs were also collected for FACS sorting and approximately 20% of GFP-virus transduced cells were GFP+ at the time of sorting (Fig. 5.19a) while for RFP-virus transduced cells, RFP expression was too low to allow collection of any RFP+ cells (data not shown). GFP+ sorted cells could expand and generated a homogenous GFP+ population of cells *in vitro* (Fig. 5.19b). However, after 3 passages post FACS sorting, I could observe loss of GFP+ signal in some hPOs within the culture (Fig. 5.19c). Nonetheless, this data demonstrates that hPOs can be successfully transduced using lentiviral vectors to express both luciferase and a fluorescent protein such as GFP whose expression can be maintained *in vitro*.

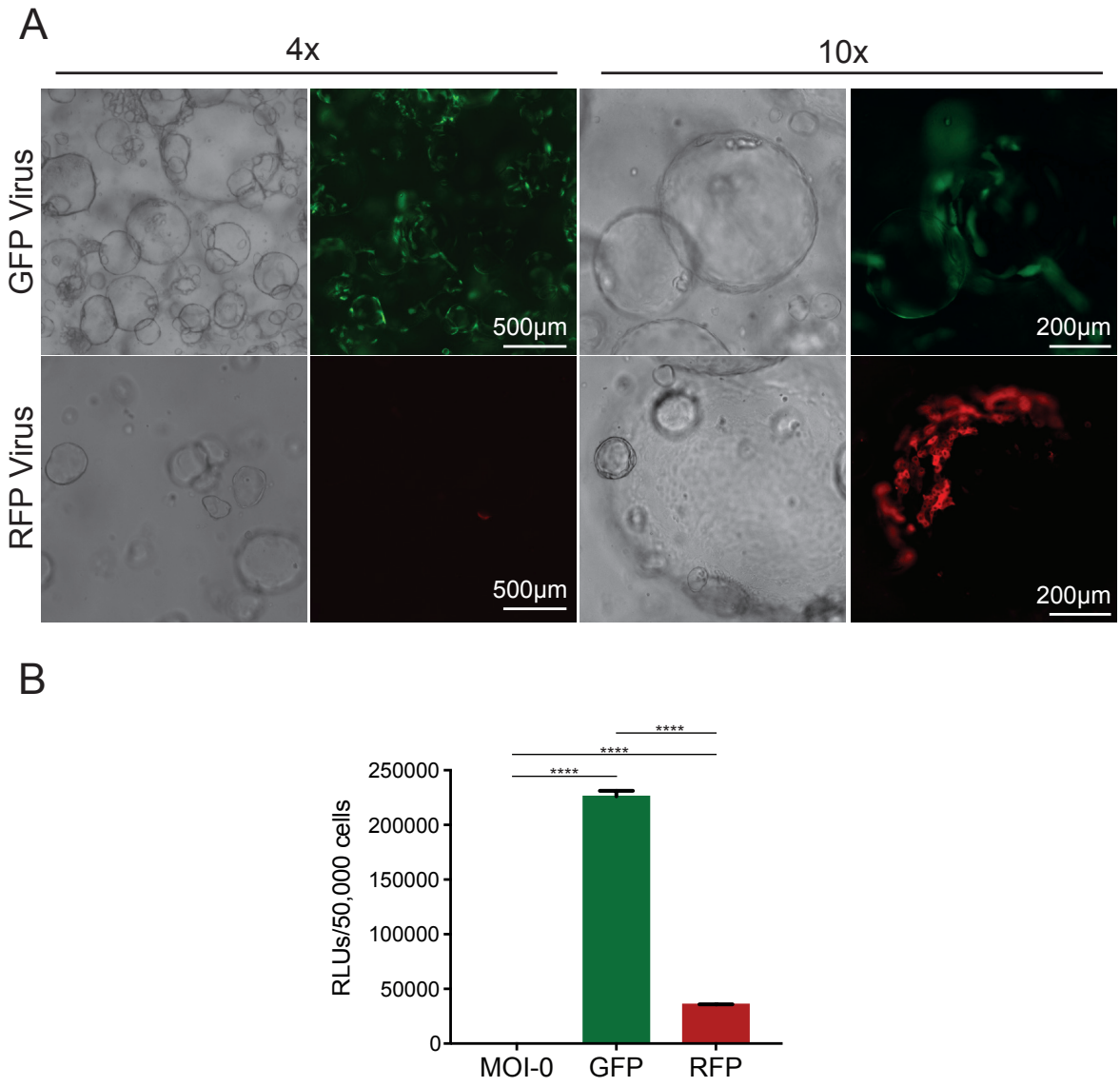

Figure 5.18 hPOs can be transduced with a lentiviral vector carrying GFP/RFP-Luciferase (**A**)Representative images showing hPOs transduced with the CMV-GFP-T2A-Luciferase (GFP-Virus) pre-packaged lentivirus or the CAG-Luciferase-F2A-RFP-RsvPuro (RFP virus) pre-packaged lentivirus at 4x and 10x magnification 13 days post-transduction. Note the low level of RFP signal in the RFP-virus group Experiments were performed for n=2 donors (**B**) Graphs showing luciferase activity as measured by a luminometer and expressed as relative light units (RLUs), for control group (hPOs not having received virus), GFP-virus hPOs and RFP-virus hPOs. Data is shown as mean ± SEM. Differences between groups were tested using one-way repeated measures ANOVA followed by Tukey's honestly significant difference (HSD)test. Significant differences are marked by asterisks: *** $p \leq 0.001$, **** $p \leq 0.0001$.

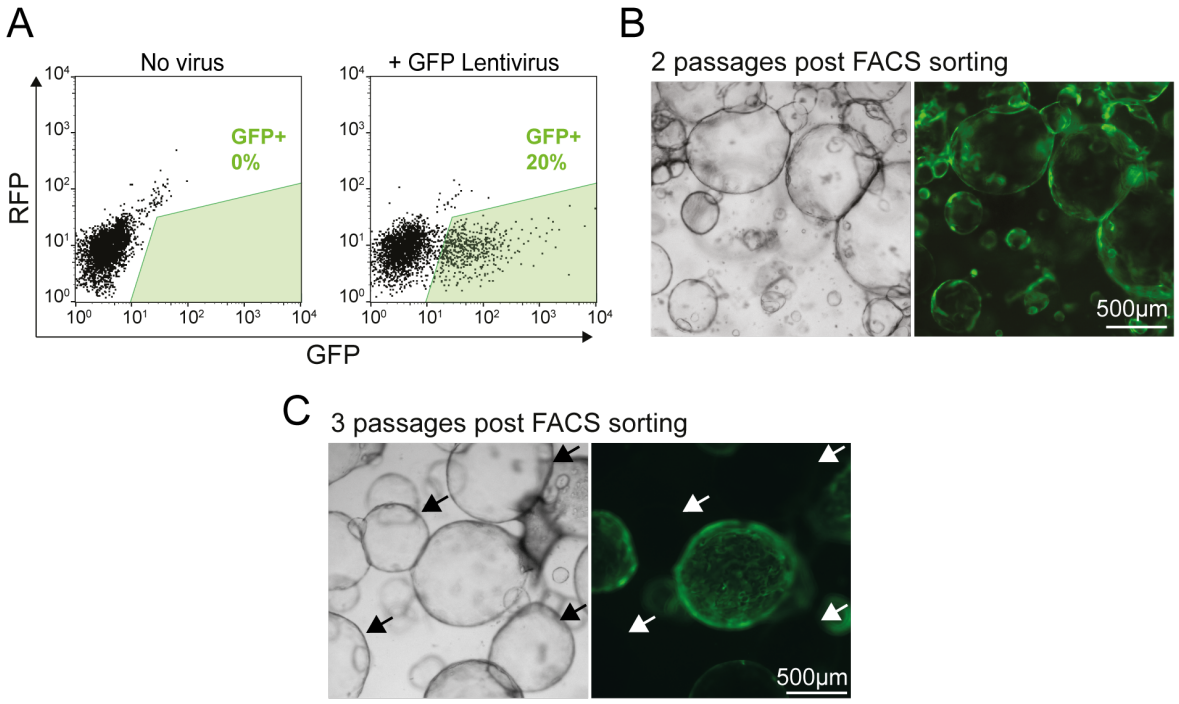

Figure 5.19 A GFP-Luciferase positive pure population of hPOs can be achieved following cell sorting hPOs were dissociated to single cells at passage 3 and transduced with a lentiviral vector carrying a GFP reporter gene. Following viral transduction, the single cells formed hPOs and were expanded for 3 passages. (**A**) hPOs were dispersed into single cells and FACS sorting was used to select for GFP-positivity. The GFP+ cells were isolated and expanded as genetically modified hPOs for a further 3 passages. (**B-C**) Representative images of genetically modified organoids at passage 8 and9 are shown (2 and 3 passages post FACS sorting respectively). Experiments were carried out for n=2 donors.

In order to assess whether luciferase+ hPOs could be used to track graft survival, hPOs which had been FACS-sorted, were expanded and transplanted under the kidney capsule of NSG mice (protocol K-0, please refer to Table 2). As controls, the GFP negative hPO cell population and hPOs from a separate donor were also expanded and transplanted into NSG mice (Fig. 5.20a). BLI was performed 2 days following transplantation and all mice in the GFP-luciferase positive sorted group demonstrated a strong bioluminescence signal. However, a signal was also detected for the GFP-luciferase negative sorted group, although this was significantly lower compared to GFP-Luciferase positive group. This is likely either due to contaminating GFP+ cells in the negative sorted population or due to low-GFP-expressing cells that could not be detected by FACS, but their luciferase activity could (Fig. 5.20b, c). Due to technical issues, hPO control mice were not imaged at this timepoint. However, one mouse from the GFP-luciferase positive group was sacrificed and the kidney and lung were subjected to BLI. Interestingly, the kidney showed a strong signal while the lung did not show any signal apart from the baseline radiance which is automatically detected by the IVIS system (Fig. 5.20b, c). Interestingly however, subsequent imaging at 3 weeks post transplantation demonstrated a complete loss of bioluminescence signal in the GFP-Luciferase positive group and negative group. Imaging of the organs directly following animal sacrifice also failed to detect any signal, confirming the complete

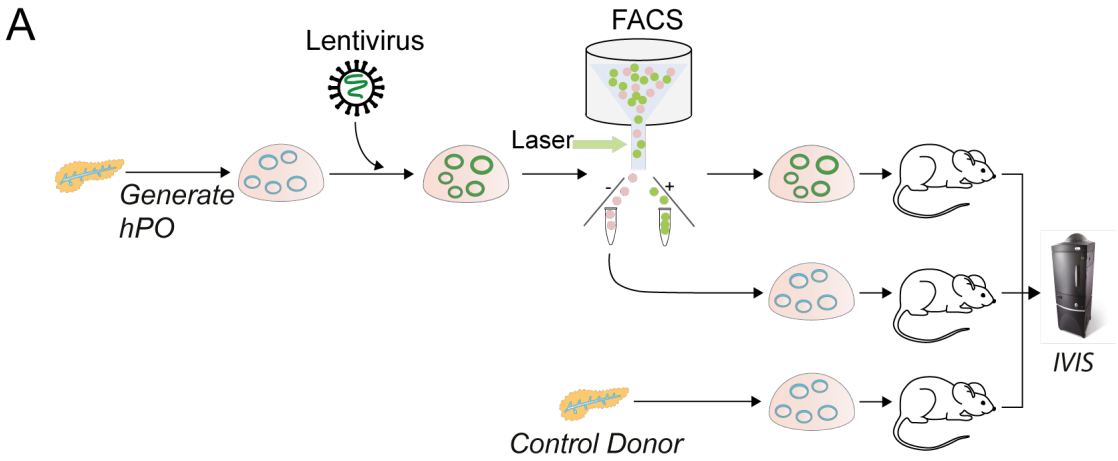
A
Lentivirus
FACS
Laser
Generate
hPO
IVIS
Control Donor

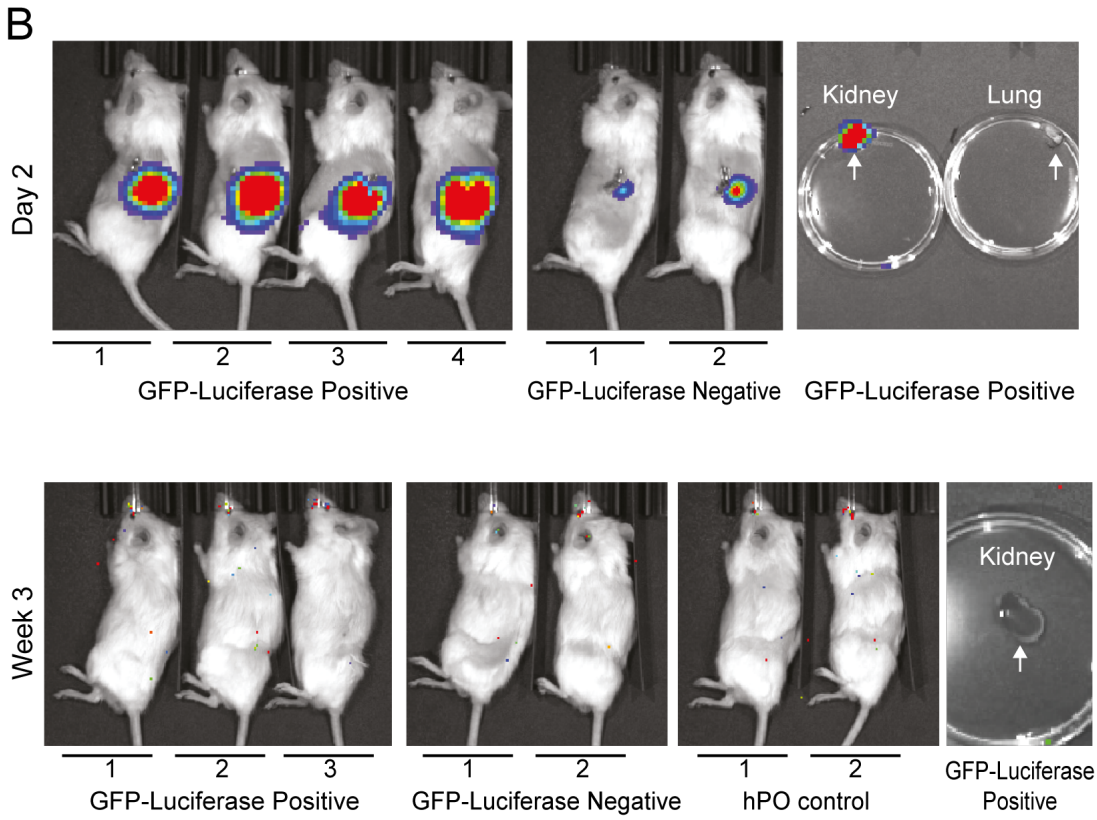
B
Day 2
Kidney
Lung
1
2
3
4
GFP-Luciferase Positive
1
2
GFP-Luciferase Negative
1
2
GFP-Luciferase Positive
Week 3
1
2
3
GFP-Luciferase Positive
1
2
GFP-Luciferase Negative
1
2
hPO control
Kidney
GFP-Luciferase
Positive

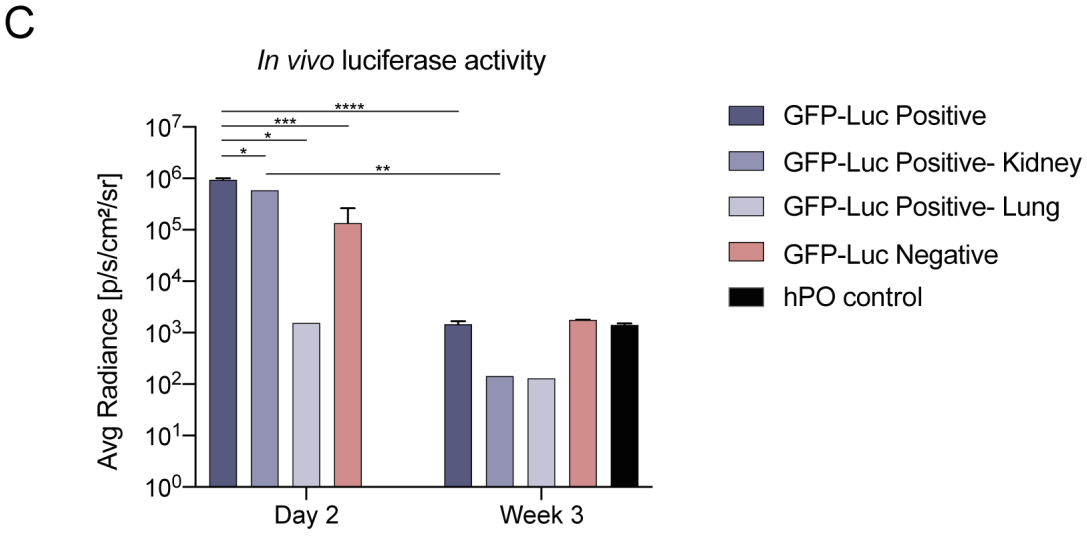
C
In vivo luciferase activity
Avg Radiance [p/s/cm²/sr]
10⁷
10⁶
10⁵
10⁴
10³
10²
10¹
10⁰
****
***
*
*
**
Day 2
Week 3
GFP-Luc Positive
GFP-Luc Positive- Kidney
GFP-Luc Positive- Lung
GFP-Luc Negative
hPO control

Figure 5.20 GFP-Luciferase+ hPOs can be transplanted and tracked *in vivo*. (**A**) Schematic showing experimental design for the transplantation and in vivo tracking of GFP-luciferase expressing hPOs. hPOs were transduced with a GFP-luciferase lentivirus and subjected to FACS sorting to select for GFP positivity. The negative population was also collected. hPOs following FACS sorting were expanded to reach appropriate numbers and were injected into the kidney capsule of NSG mice. hPOs from a separate, non-transduced donors were also injected into NSG mice as control. The mice were then subjected to imaging using a bioluminescent In Vivo Imaging System (IVIS) following I.P. injections with luciferin. (**B**) Representative mages of NSG mice transplanted with hPOs sorted for GFP-luciferase, the negatively sorted GFP-luciferase population or hPO control, imaged using the IVIS system, 2 days and 3 weeks following transplantation. Note that organs from the GFP-luciferase positive group were also removed and imaged directly in the IVIS following injection with luciferin. All images shown are taken with automatic exposure. Experiments were performed for n=2 donors. (**C**) Graphs demonstrating levels of bioluminescence as analysed following IVIS imaging. Analysis was performed on images taken with set exposure of 120 secs. Data is shown as mean± SEM. Differences were assessed between groups in a given time point or matched groups between different time points. Differences were tested using one-way repeated measures ANOVA followed by Tukey's honestly significant difference (HSD)test. Significant differences are marked by asterisks: * $p \leq 0.05$, ** $p \leq 0.01$, *** $p \leq 0.001$, **** $p \leq 0.0001$.

loss of luciferase+ cells in the graft (Fig. 5.20b, c). Furthermore, fluorescent imaging of the organs post removal failed to show a GFP signal in the kidney, lung or liver, suggesting that the GFP-luciferase+ cells had not survived in the transplantation site nor had migrated to other organs (Supp Fig. 12). However, this data demonstrates that while optimisation is required, hPOs can be transduced to express luciferase and can be subjected to BLI following transplantation into mice.

The mechanisms underlying the loss of signal was not clear from these experiments. This could be due to silencing of the promoter and loss of protein expression, or due to GFP-luciferase+ hPOs being outcompeted by non-transduced contaminating hPOs. However, since this loss of expression was observed *in vitro* following FACS sorting, it is likely that the former rather than the latter accounts for this observation. Therefore, I established a collaboration with Dawei Sun, a PhD student in the Rawlins Lab, in order to investigate a different promoter which may result in a more stable expression. Dawei generated a lentiviral vector which contained GFP under the control of the Ef1α promoter which has shown strong expression in difficult-to-transduce cells such as haematopoietic stem cells[293] (HSCs; Fig. 5.21a). Furthermore, this vector has been used in human lung organoids in the Rawlins Lab and resulted in stable expression (personal communication). Utilising this vector packaged into a lentivirus (referred to as Ef1α virus from this point), I transduced an hPO line following the same protocols used for the GFP/RFP viruses. Four days following transduction, many hPOs were GFP+, as assessed by fluorescent microscopy. Contrary to the GFP/RFP viruses, a few hPOs that were transduced with the Ef1α virus grew into larger spherical organoids in a manner reminiscent of healthy non-transduced hPOs. I hand-picked these hPOs in order to purify the GFP+ population resulting in a homogeneously GFP expressing hPO population, reminiscent of the FACS sorted GFP virus hPO population (Fig. 5.21b). Contrastingly, the bulk population demonstrated many multicell GFP+ clusters which were not able to expand larger organoids (Fig. 5.21b). Importantly, the use of this virus allowed a pure GFP+ population to be obtained without the need of FACS sorting. However, due to the shutdown of our laboratory as a result of the

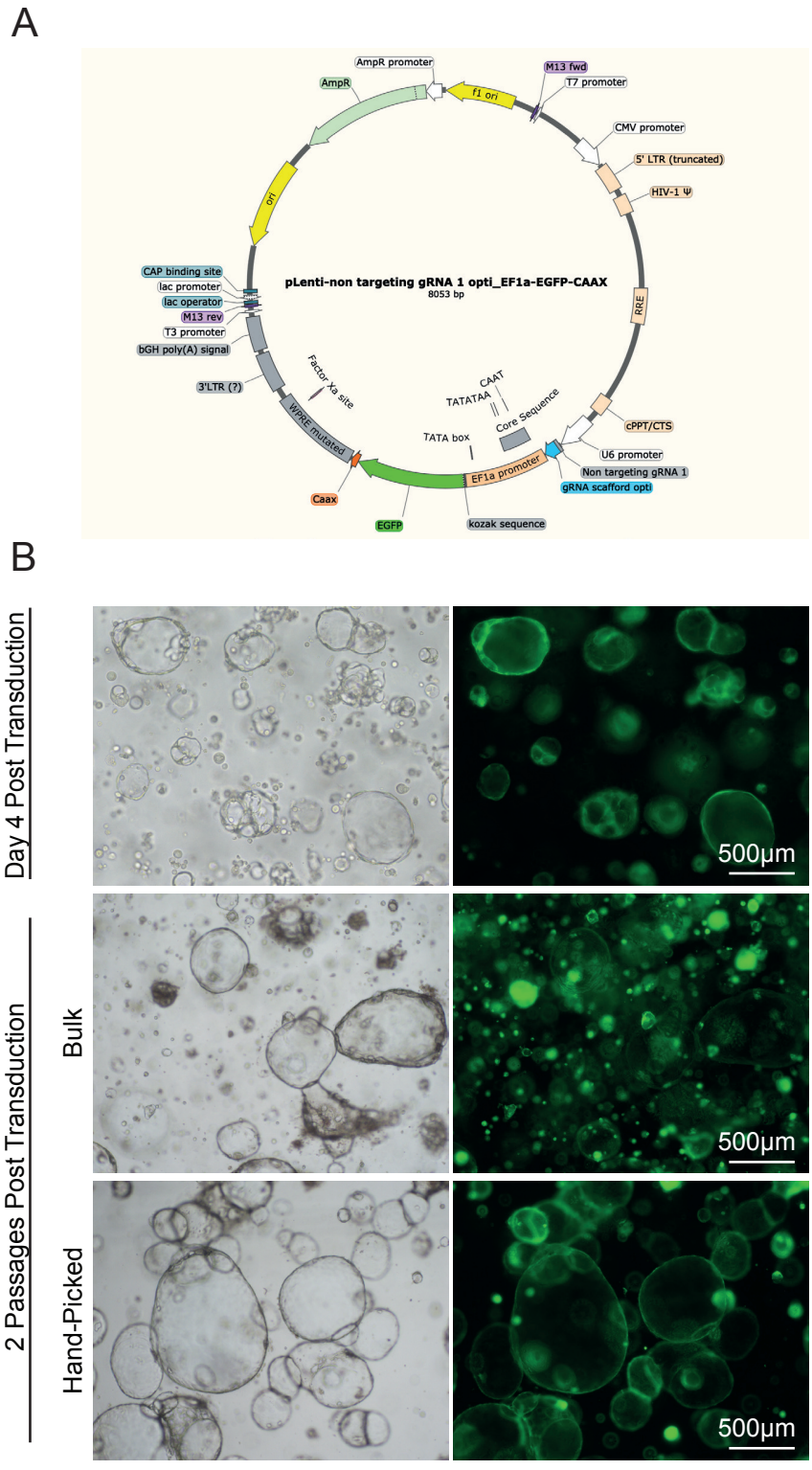

Figure 5.21 Lentiviral induced expression of GFP under the EF1a promoter. (**A**) Plasmid map of the Ef1a-GFP construct obtained from the Rawlins lab (generated by Dawei Sun) which was packaged into lentiviral particles and used to generate GFP+ hPOs. (**B**) Representative brightfield and fluorescence images of hPOs transduced with the Ef1a-GFP virus 4 days post transduction (top images) and 2 passages following transduction (bottom images). Note that in the 'hand-picked' group, hPOs are healthier in morphology, are able to expand and form cysts and are homogeneously expressing GFP whereas in the 'bulk' population they have lost their healthy morphology. (EF1a-GFP viral construct was generated by Dawei Sun in the Rawlins lab.)

restrictions imposed in response to the spread of the SARS-CoV-2 virus, this line was cryopreserved, and I was not able to assess the stability of GFP expression over long-term *in vitro* culture.

5.3 Discussion

5.3.1 Antigenicity assessment of organoids in an inflammatory environment

Cellular therapies offer a promising route to personalised medicine to treat conditions such as macular degeneration, diabetes, cystic fibrosis, cholangiopathies, and cancer, either by being directly transplanted or used as an *in vitro* model for the discovery of novel therapeutics. However, in the case of transplantable cellular therapies, it is important to understand the expression of antigens and the extent of which they risk eliciting an immune response to understand the need for immunomodulatory approaches. In this project I demonstrate that hPOs have low expression of HLA Class I and II under normal culture conditions, similar to pancreatic tissue. However, upon introduction into an inflammatory environment, they upregulate expression of HLA Class II, a phenotype of professional APCs, both at the gene and protein level.

Interestingly, mRNA analysis demonstrated that IFNγ stimulation increases gene expression of the three HLA Class I molecules analysed equally, whereas in the case of HLA Class II molecules, *HLA-DP* and *-DR* demonstrate a higher and significant upregulation while *HLA-DQ* is not significantly upregulated compared to normal hPOs. This is in line with previous literature stating that IFNγ treatment led to increased surface expression of HLA-DP and -DR but had little effect on HLA-DQ expression in melanoma cancer cell lines[294]. IFNγ increases expression of HLA class II molecules through induction of class II trans-activator protein (CIITA) gene, a co-activator of the MHC class II gene promoter[294]. It would therefore be interesting to assess level of CIITA gene expression in response to IFNγ treatment to understand whether upregulation of HLA Class II in hPOs is indeed a direct effect of IFNγ downstream signalling. This might also provide a mechanistic explanation for the observation that IFNγ increases the overall intensity of HLA Class I expression, but not the percentage of cells expressing it, as that is already at a nearly maximal level. Furthermore, it would also be interesting to assess whether this differential HLA Class II molecule upregulation observed at the mRNA level occurs at the protein level. While a pan-class II antibody was used for flow cytometric analysis, future experiments will aim to utilise molecule specific antibodies.

A limitation of this study is the use of primary pancreas tissue rather than ductal cells for the comparison. Therefore, it is unclear whether gene expression of HLA molecules in the pancreas tissue is representative of the ductal compartment or of the acinar/endocrine compartments. This limitation arose due to the fact that hPOs were compared to donor matched tissue and obtaining ductal segments was not always possible from each donor. Future work will focus on obtaining pure ductal populations from primary tissue in order to better understand HLA expression by ductal cells *in vivo*.

Furthermore, although time in culture did not affect marker expression in hPOs, expression of HLA Class I molecules, at the mRNA level, was numerically higher (and significantly higher for *HLA-B*) for late-passage hPOs treated with IFNγ compared to their early counterparts. However, levels of HLA Class II molecules were not significantly different for both early and late passage hPOs. Use of additional donor lines as well as further gene expression analysis such as bulk RNA sequencing and protein-level analysis would be useful to understand whether an increase of culture time correlates with a more inflammatory hPO phenotype. Moreover, while I demonstrated that hPOs do not express two well-known T1D autoantigens, bulk RNA sequencing would allow identification of other antigens. Indeed, it would also be interesting to perform the IFNγ stimulation experiments with lines derived from T1D or T2D patients to understand whether this disease profile leads to higher expression of HLA Class I/II or autoantigens *in vitro*. Interestingly, HLA Class I hyperexpression has been observed in islets of T1D patients[295] while it is unclear whether this is seen in the ductal compartment. Therefore, it would be of interest to understand whether hPOs derived from diseased individuals have increased expression of HLA molecules and would therefore require special considerations for immunosuppressive regimes, particularly in the case of autologous therapies.

The IFNγ stimulation experiment is limited in that it only exposes hPOs to one pro-inflammatory cytokine in a concentration that may not be reflective of physiological conditions. However, while more cytokines need to be tested, the IFNγ stimulation experiments provide an initial starting point for investigation of the alloimmune response to cellular therapies as they provide an indication of how a pro-inflammatory environment can change the cells' phenotype and inform design of more complex *in vitro* or *in vivo* studies.

hPO co-culture with SpMCs

In order to overcome the limitation of the IFNγ stimulation model relating to the supraphysiological concentration of IFNγ used and assessment of a single cytokine, I designed a co-culture model incorporating splenocyte derived mononuclear cells (SpMCs) with hPOs in a medium which contained the full set of growth factors found in hPO-Opt.EM media but contained 50% Basal media and 50% RPMI. This allowed short term culture of the two cell types in order to investigate whether exposure of hPOs to lymphocyte-induced pro-inflammatory environment would result in increased expression of HLA molecules. Interestingly, HLA Class I expression was the same among all conditions in terms of percentage of cells expressing HLA class I while an increase in the intensity of staining was only observed for the IFNγ treated group, similar to previous experiments. Co-culture with SpMCs led to a more modest increase in HLA Class II expression in hPOs. The increase in HLA Class II appeared to be dose-dependent upon the number of activated SpMCs in co-culture. While it was unclear whether activation itself resulted in an increase of HLA Class II expression, increase in the number of SpMCs

led to increased expression of HLA Class II in hPOs which was significantly different between condition 8, i.e. the maximum number of SpMCs used, and condition 1 (hPO control).

Several limitations exist within this model that hinder the understanding of both the interactions between hPOs and lymphocytes and the cause of HLA Class II upregulation. Indeed, this experiment was performed on one donor hPO line with co-culture of allogeneic SpMCs. Therefore, more donors would be required to confirm the findings, including the apparent dose-dependent effect demonstrated in this experiment. Furthermore, as shown in Figure 5.9, activation of SPCMs was below 10% with the lowest activation levels in the co-culture conditions. Moreover, only activated SpMCs were used in increasing numbers while non-activated SpMCs were cultured in low numbers with hPOs (1:2.5- hPOs: SpMCs). Therefore, future experiments will focus on establishing an activation protocol which reaches higher levels of T cell activation and will also include higher numbers of non-activated SpMCs to understand whether the activation or the increase in numbers causes the increase in HLA Class II expression. Moreover, use of conditioned media from cultured T cells or use of trans-wells could also illuminate as to whether the increase in HLA Class II expression occurred as a result of cell-cell contact between lymphocytes and hPOs or as a result of cytokine production from SpMCs. Since an ELISA was not performed in this experiment, the levels of pro-inflammatory cytokines such as IFNγ or TNF α/β, which are typically produced by both T cells and B cells, could not be determined. Furthermore, studies have utilised GFP-labelled lymphocytes with time-lapse imaging to understand the interaction of intraepithelial lymphocytes (IELs) with intestinal organoids[296] and therefore a similar experimental design could be used in future hPO-lymphocyte co-culture experiments.

Furthermore, as this was a preliminary experiment, SpMCs were used in bulk without selection of a specific population of cells. Therefore, although the experiment aimed to activate T cells and an assumption was made that the activated T cells cause the increase in HLA Class II expression, further experiments are needed to verify this. Future experiments which include co-culture of either B cells only, CD4+ T helper cells only, CD8+ cytotoxic T cells only or in various combinations would illuminate the extent of each cell's contribution towards the increased HLA Class II expression of hPOs, as well as whether hPOs have the ability themselves to activate T cells. This would also provide further insight as to whether CD8+ T cells can be activated and provide effector function without help from CD4+ T helper cells, as is the case in classic immune rejection mechanisms[294]. Such experiments would be crucial in order to understand whether hPOs pose a risk for immune rejection upon transplantation and which mechanisms are involved, thereby providing data for amelioration strategies.

Notwithstanding these caveats, my preliminary co-culture experiments provide insight as to the potential implication of a physiologically relevant pro-inflammatory environment on the antigenic expression of hPOs, as well as providing a basis for modelling the interaction of pancreatic ductal cells with lymphocytes or other cell types of interest.

5.3.2 Assessment of the HIS mouse models

In vitro assays such as the co-cultures presented in sections 5.2.1 and 5.2.3 are important in understanding whether hPOs can upregulate immunogenic molecules such as HLA and uncovering specific cell interactions that lead to such events. However, these models offer a simplistic view, while the mechanisms of allograft rejection are incredibly complex and rely on multiple variables. HIS mice are emerging as a valuable *in vivo* model to investigate the human immune response including rejection of a graft (either cells or whole tissue). I have utilised two HIS-mouse models, the HU-PBL and HU-SRC to investigate whether hPOs will result in immune rejection by human immune cells. Furthermore, I have included both autologous and allogeneic arms to understand whether autologous hPOs will still be rejected, much like in the case of iPSCs reported by Zhao *et al.*[208], and whether allogeneic cell rejection is a specific alloimmune response. These experiments are important and difficult to carry out, largely due to the limited access to human tissue, complexity of the experimental design and low animal survival, but can offer insight into the immune rejection mechanisms of allografts *in vivo*. However, several limitations exist both within the models and my experimental design which need to be addressed in future experiments.

The SpMC-HIS mouse model

The SpMC model is one of the easiest methods of humanisation as it requires I.P. injection of splenocytes into immunodeficient mice without delay in engraftment since the lymphocytes are already mature. This model largely introduces T cells with a memory and activated phenotype[297]. However, this can lead to early development of graft *versus* host disease (GvHD) thought to be invoked by the recognition of mouse MHC antigens by the human T cells, causing their subsequent activation and expansion[297]. Moreover, a rapid GvHD event reduces the available window to assess rejection of the engrafted cells while also adding further complication to the interpretation of the results. In order to increase the experimental window and decrease the occurrence of GvHD, I utilised a new strain of NSG mice which lack expression of MHC Class I and II, referred to as NSG-double knockout (NSG-dKO) mice. In my first SpMC-HIS experiment, mice survived up to week 10 at which point the mice were still healthy, while only 1 mouse was lost due to GvHD related illness. In the second SpMC-HIS experiment no mice were lost due to GvHD, although the cull point was relatively early, at 3 weeks. Nevertheless, this supports the idea that severe GvHD was not present when the hPOs were transplanted into the SpMC-HIS mice.

Importantly, I have shown that the NSG-dKO mice successfully engraft with human lymphocytes with the levels of lymphocytes increasing in only the allogeneic groups following transplantation with hPOs. While this perhaps underpins an alloimmune response to the allogeneic cells, it is difficult to make this conclusion with certainty, not least because a similar pattern is not observed in the T cell numbers. This result was indeed surprising, given that Donor 8 and 22 were completely

mismatched for HLA Class I and II and therefore higher levels of T cells would be expected in the allogeneic group following an allograft rejection event. However, it is possible that T cells are already being maximally activated in both autologous and allogeneic groups as a result of a reactions against mouse antigens. This therefore may be the reason why differences of T cells cannot be detected on a global scale such as in the mouse peripheral blood.

Furthermore, an obvious limitation of the data presented in this project is the lack of sectioned grafts and subsequent histological assessment. Once sectioned, it will be essential to understand whether grafts are being infiltrated, by quantifying presence of CD45+ cells and other cell subtypes, and whether the structure of engrafted hPOs has been affected. Furthermore, it is important to understand whether this potential infiltration has caused upregulation of HLA II as observed *in vitro* and hence understand if hPOs truly become immunogenic in an *in vivo* inflammatory scenario. Furthermore, assessment of the pancreas of the non-transplanted SpMC-HIS mice will illuminate whether lymphocytes are infiltrating the pancreas as a result of the engrafted cells or due to general occurrence of GvHD. Furthermore, it would be also possible that lymphocytes are infiltrating the graft due to the damage caused by the surgical procedure to implant hPOs into the pancreas, although this is less likely as the parenchyma is not damaged during this process. Nevertheless, a control of matrix-only injection would answer the question of whether lymphocytes are infiltrating the pancreas as a result of local damage and inflammation. Furthermore, it would be interesting to understand the extent of which hPOs might become more immunogenic than cells derived from the same donor as a result of the culture process. Use of mouse groups that are transplanted with primary ductal cells as well as a positive control cells such as islets, which have previously been used as positive control[291], would help in the understanding whether hPOs are more immunogenic than the starting material and/or positive controls.

The further assessment of grafts with the addition of the controls mentioned above could provide a definitive answer of whether hPOs will result in an alloimmune response and whether autologous hPOs are immunoprotected and do not result in rejection. Further understanding of whether hPOs are expressing HLA Class II as a result of either the transplantation or the interaction with lymphocytes could better inform future strategies on the need to perform HLA matching for recipients receiving hPO-based cellular therapies.

The HSC-HIS mouse model

HU-SRC model can be generated by reconstituting immunodeficient mice with either with umbilical cord blood, bone marrow, or foetal liver[228]. The advantage of this model is that allows engraftment of multiple lineages of human immune cells and the mice can survive with more than 20 weeks without presentation of GvHD. However, the main caveats are the long time it takes for *de novo* generation of lymphocytes and the lack of fully functional cells. T cells do not undergo proper thymic education as they only interact with mouse MHC molecules during haematopoiesis, while there is also a lack of cytokine production to allow maturity of the cells. Furthermore, B cells have impaired antibody

production while there is a lack of splenic germinal centres reported in these mice[227]. Interestingly, it has been reported that cord blood coupled with the use of neonatal mice results in improved engraftment[298]. However, as I aimed to explore rejection of hPOs in an autologous setting and this was only possible with the use of bone marrow, but it is possible that this resulted in reduced levels of engraftment. Furthermore, use of neonates increases the risk of accidental death, therefore I used mice which were 7 weeks of age.

Despite the limitations of the model, I successfully generated HSC-HIS mice with the same two donors that were used for the SpMC-HIS mice. This is a particularly challenging task as it requires samples from bone marrow, spleen and pancreas from the same donor. Furthermore, as there is large donor to donor variability, using the same donors for the two models can help to reduce this variability. Importantly, in both donors used, I demonstrated the production of de novo T cells at week 17 with the maintenance of B cells until the end of the experiment. However, the conclusions from this experiment remain equally ambiguous to the SpMC-HIS model at this point. I was not able to discern any differences in circulating levels of CD45+, CD3+ or CD19+ cells among any of the autologous or allogeneic groups. This indeed may have been a result of existing over-activation of the human lymphocytes as a result of interaction with mouse alloantigens, as described for the SpMC-HIS mice. However, T cells in HSC-HIS mice may be in an anergic state due to the lack of proper thymic education, and therefore may be less likely to mount an adequate allograft response which may also explain the lack of differences detected between allogeneic and autologous groups.

Moreover, due to the limited number of bone marrow cells available, particularly after CD3 depletion, I was not able to include controls of mice that were humanised but not transplanted with cells, as in the case of the SpMC-HIS mouse experiment. Furthermore, ongoing work aims to section the pancreases from these mice to evaluate, on histological level, the amount of infiltration, if any, in the engrafted hPOs. Moreover, the experiment also requires the controls mentioned as lacking in the SpMC-HIS mouse model (i.e., matrix only injections, islet transplants etc.) to understand the immune rejection that may be caused specifically the hPOs grafts.

Despite the limitations of the models and the future work that is needed to derive clearer conclusions, these experiments mark a significant milestone towards understanding the immune rejection kinetics of autologous and allogeneic hPOs. Use of “crossover” experiments utilising both SpMC-HIS mice and HSC-HIS mice with the same donors offers a complimentary platform which allows the reduction of the impact of the limitations from each model and the robust assessment of rejection of hPOs *in vivo*.

5.3.3 Evaluation of the luciferase+ hPO line

To enable improved assessment of graft survival in a more efficient time manner as well as reduce the need for sacrificing animals at the predetermined timepoints, I generated hPOs which express the

enzyme luciferase. This allowed use of bioluminescent imaging to assess survival of hPO grafts following transplantation. However, my initial experiments, although demonstrating some success, were hindered by two main issues: 1) the cells showed a decrease in GFP expression *in vitro* over time and 2) grafts could only be imaged a few days following transplantation and signal was lost very quickly. Interestingly, despite BLI imaging of the organs directly, and clearly showing that no GFP/luciferase+ cells survived at 3 weeks post engraftment, it is unclear whether any non-transduced cells survived. Work is ongoing in order to examine the kidneys from these animals on a histological level to assess whether any cells survived at these timepoints. Notably, in order to facilitate imaging of these cells, luciferase+ hPOs were transplanted into the kidney capsule which I have demonstrated in chapter 4, is a sub-optimal location for the survival of hPOs *in vivo*. Therefore, this early loss of cells could be a result of the niche rather than the hPOs and in future experiments hPOs will be transplanted into the pancreas to ensure that survival of the cells is not affected by the transplant site. However, it is also possible that poor survival of hPOs was a result random integration of the transgene, namely GFP and luciferase. I chose to use a lentiviral transduction system to introduce the GFP/luciferase constructs into the genome of hPOs as this has been previously used in our lab to generate GFP or RFP organoid lines. However, two main limitations can be associated with this system: 1) use of lentivirus which randomly integrates the construct into the genome and 2) use of the CMV or CAG promoters.

With respect to the first problem, use of lentiviral transduction has the limitations of requiring packaging of the transgene plasmid into viral particles and the risk of integration of viral DNA into the genome. Furthermore, as the integration is not targeted, the transgene is integrated randomly into the genome[299]. This can therefore lead to potential integration into an existing gene which can cause an alteration in the cell's function or lead to a malignant transformation by insertional mutagenesis. It is therefore possible that reduced expression of GFP+ *in vitro* and loss of luciferase+ cells *in vivo* was a result of increased cell death due to random integration events following lentiviral transduction[300]. Future work will focus on targeting constructs to integrate luciferase-bearing transgenes in safe genomic regions such the AASV1 locus[301] or under the control of expressed genes through the use of CRISP/Cas9 targeting systems.

With respect to the second limitation of the lentivirus system used in this project, eventual loss of expression of GFP was observed *in vitro* which could be due to the silencing of the CMV promoter. Moreover, the RFP virus, using the CAG promoter, failed to demonstrate any efficiency in transduction of hPOs and the RFP signal was observed in a small fraction of cells. It has been reported that both CMV and CAG promoters can be silenced after certain periods of *in vitro* culture[302,303] while this phenomenon could be more pronounced in a primary cell line such as hPOs. These experiments need to be repeated and samples can be collected upon visualisation of loss of signal. PCR/qPCR analysis with primers for the GFP or luciferase genes from the collected cells could illuminate as to whether the cells in culture retain integration of the transgenes, i.e., silencing of the promoter, or whether the cells collected do not retain the transgene i.e., loss of expression due to being outcompeted by non-transduced

cells. Another problem in the case of the RFP virus is that it relies on the F2A linker for cleaving and appropriate protein folding. However, the F2A linker is known to have low self-cleaving efficiency[304]. Hence, the lack of RFP signal could have resulted from inefficient protein processing rather than silencing of the CAG promoter.

In order to mitigate the risk of losing GFP/luciferase signal over time, particularly due to promoter silencing, I utilised a lentiviral vector with GFP under the control of the Ef1α promoter. Notably, this vector has been reported to have more stable expression in primary cell lines[293]. However, while use of this lentiviral vector allowed me to establish a pure GFP+ population without use of cell sorting, further work is needed in order to assess the stability of expression following long-term culture. Furthermore, as luciferase will need to be cloned into the plasmid, it is uncertain whether this potential stability of GFP expression under the Ef1α promoter will be retained in a GFP-luciferase construct.

Nevertheless, I have demonstrated that hPOs can be genetically modified to express GFP and luciferase using a lentiviral system. These cells can be expanded following two single cell steps and transplanted *in vivo,* allowing bioluminescent imaging of the graft. This demonstrates the robust nature of the hPO culture system and paves the way for generation of optimised protocols aimed at creating improved luciferase+ lines which can be useful for *in vivo* tracking or assessing immune rejection without the need to sacrifice animals.

5.4 Conclusion

In this chapter I have demonstrated the use of *in vitro* co-culture assays of hPOs either with IFNγ or SpMCs to investigate antigenicity of hPOs. I have shown that under *in vitro* inflammatory conditions, hPOs can upregulate HLA Class II but not antigens linked to development of T1D. Furthermore, I demonstrate preliminary experiments that allow investigation of whether hPOs are rejected *in vivo* under autologous or allogeneic conditions. These experiments show that in principle, HIS-mice can be used to assess immunogenicity of cell therapies and inform on future strategies for the clinical implementation of cellular therapies. Furthermore, I demonstrate preliminary experiments for the generation of a GFP-luciferase expressing hPO line. This demonstrates the robust nature of the culture system which allows genetic manipulation of hPOs and subsequent growth following two single-cell steps, while also illustrates a solution to the issue of *in vivo* tracking of human primary cell derived organoids. While further work is required to understand whether hPOs an immunogenic threat in the context of transplantation, these experiments set a foundation for future studies of the immunogenicity of cell therapies.

CHAPTER 6. FUTURE WORK AND CONCLUSIONS

6.1 Introduction

In chapters 3-5, I presented the experimental results of this project and discuss the limitation of the experiments and/or models used, as well as the conclusions of the specific findings while also placing them within the greater scientific context. This chapter aims to provide a high-level summary of the major findings of my dissertation and suggest future work that can stem from the work presented. This is both with the purpose of addressing outstanding questions within this project and to highlight the use of the hPO system in future research and clinical applications.

6.2 Future directions

6.2.1 Modelling healthy and diseased cell types of the human pancreas

In this project I have demonstrated the generation of a 3D-based culture system that can support the expansion of primary tissue derived human pancreatic ductal cells as human pancreas organoids (hPOs). Unlike similar systems that have been previously reported[131,132], the hPO culture system allows expansion of hPOs beyond 180 days in a chemically defined, serum-free medium without need of cell transformation. However, while several limitations exist within the hPO system, including the need to increase the hPO expansion capacity, an important next step would be to uncover the precise cellular identity of hPOs. While many adult epithelial organoid systems have demonstrated that Lgr5 marks the adult stem cell population in the organs from which they are derived[117,118,120,243] this has not been shown for hPOs. First, it would need to be shown that hPOs arise solely from the ductal population, for example, following EpCAM+ cell sorting. Furthermore, generation of an *Lgr5* reporter line could help uncover whether Lgr5 expression is maintained throughout culture and whether it is upregulated under specific conditions such as following passaging as shown by Huch *et al.*[121] for mouse pancreas organoids. Indeed, work to generate an Lgr5 (or other potential gene targets) knockout line could clarify the gene's role and its effect in culture, for example through demonstration of reduced colony formation efficiency (CFE) of hPOs in an *Lgr5*-KO line. Moreover, sorting only LGR5+ hPOs and comparing CFE with the bulk population would help determine whether Lgr5 marks a progenitor pool in hPOs given that a progenitor-rich pool of cells would result in higher numbers of organoids and proliferation.

While the hPO system presented here is novel in that it allows expansion of ductal cells, it is in fact restricted in that it cannot support expansion of acinar or endocrine populations. Indeed, expansion of primary human derived acinar cells has yet to be achieved, while expansion of human islets is equally difficult with the only success reported from the use of iPSC/ESC technology[96,97]. Excitingly, a recent study identified a multipotent progenitor population in mouse islets marked by protein C receptor (Procr+). These cells, when placed in 3D cell culture and co-cultured with endothelial cells, were able to form organoid structures, could be expanded for at least 6 months and maintained expression of

endocrine markers such as insulin, glucagon, and somatostatin[122]. Such a population has not been investigated in the human pancreas. The hPO culture system demonstrated here could be applied and adapted to investigate novel populations of endocrine or acinar cells. Furthermore, co-culture of multiple cell populations of the pancreas, as was reported by Koike and colleagues[111], would help elucidate the interaction between cells *in vivo*, while also allowing the expansion of more complex 3D cell structures.

I have shown that the optimised hPO medium, hPO-Opt.EM, allows expansion of ductal cells from the single-cell level at various stages of *in vitro* expansion. Importantly this allowed generation of clonal populations, which could undergo whole genome sequencing or used to generate GFP-luciferase positive hPOs. The ability to genetically manipulate hPOs offers the potential to develop *in vitro* models for exocrine diseases following step-wise, guided genetic manipulation, as described for colon cancer, where the sequential addition of mutations using CRISPR technology has enabled the identification of the minimal set of mutations that can induce colon cancer in healthy human colon cells[276].

Furthermore, I have shown that the hPO system can support generation of ductal cells from patients with type 2 diabetes. While further work is needed to understand the effects of T2D on the ductal tissue and subsequently derived hPOs, this work also opens up the possibility to study other diseases of the exocrine pancreas. Two such disease candidates are cystic fibrosis, which directly effects the ductal system as well as pancreatitis, which although primarily affects the acinar compartment, causes widespread inflammation that is likely to have an impact on the ductal cells, while issues in the ductal compartment have been linked to an increased risk of acute pancreatitis development[45]. Generating hPOs from patients with pancreatitis can further facilitate the understanding of the potential link between impaired function of the ductal cells and subsequent development of pancreatitis. hPOs therefore present a range of possibilities for further work into understanding the biology of the healthy and diseased state of pancreatic cells.

6.2.2 Differentiation of hPOs into insulin producing cells

The disease which impacts the largest number of people relating to the pancreas is diabetes. The prevalence of diabetes increases every year and while there are a range of medications or treatment strategies to treat diabetes, curative treatments such as solid organ or islet transplantation are restricted by the availability of donors and the need for subsequent immunosuppression of the recipient. Emerging cellular therapies have aimed at providing an alternative source of insulin producing cells which can reduce the dependency on organ donors. Arguably, the generation of clinically applicable insulin producing cells could be a very impactful cell therapy product. While various groups have generated insulin-producing cells *in vitro*, their translation to the clinic is hampered either due to the source being ESC or iPSC cells, or use of integrating vectors, both of which are associated with an increased risk of tumorigenicity.

The body of work presented in this thesis is a continuation of the work published by Huch and colleagues[121] whereby the generation of mouse pancreatic organoids was illustrated, along with their ability to differentiate into insulin producing cells following aggregation with embryonic pancreas cells and transplantation into mice. In our lab, previous work by Daisy Harrison and recent work by Dr. Nicole Prior, involved the investigation of strategies for the differentiation of hPOs into insulin producing cells in a manner that will not prevent their translation to the clinic; the project is still ongoing. These strategies are: use of soluble factors in the culture media that can induce differentiation, mRNA transfection, co-culture with embryonic cells and co-culture with endothelial cells. In the first strategy, promising results have demonstrated that removal of growth factors and inhibition of Notch signalling results in increased expression of PDX1 and NKX6.1 (pancreatic and early endocrine marker) in hPOs. Furthermore, mRNA transfection of the three transcription factors PDX1, Neurogenin-3 and MAFA which are critical for β-cell development and regeneration[305] into hPOs has resulted in increased expression of NKX6.1, Chromogranin A and Insulin at the mRNA level. Further work to elucidate whether this translates to the protein level and if insulin expression can be maintained in culture and following *in vivo* transplantation is currently ongoing. Additionally, while obtaining human embryonic tissue is difficult due to limited availability and ethical restrictions, current work is investigating use of mouse embryonic pancreas explants. This explanted tissue can be maintained for several days in an air-liquid interphase culture while hPOs can be injected directly into the pancreas. While this work is preliminary, the hope is that growth factors from the developing mouse pancreas can push the human ductal cells and/or ductal progenitors towards a more endocrine fate. Lastly, co-culture of mouse or human ESCs with endothelial cells (ECs) has shown to increase differentiation or maturation towards endocrine specification[306,307]. Current work in our lab is aimed at establishing a co-culture system of hPOs with human endothelial cells and investigate whether this can aid in the differentiation of hPOs. Although these strategies are at an early phase, if successful, they would result in the generation of insulin producing cells from a potentially unlimited source of primary adult cells. Importantly, as I have demonstrated in this project, in the undifferentiated or mature ductal state, hPOs do not pose risk of tumorigenicity and while this would also need to be shown for the insulin producing hPOs, my work establishes a pipeline of experiments which can be replicated for a range of cellular therapies.

6.2.3 Development of ECMs for *in vitro* and *in vivo* applications

In this project I have demonstrated that hPOs can be generated and expanded in a chemically defined extracellular matrix in a manner that is comparable to BME 2. This presents the exciting possibility to move away from the commonly used Matrigel or BME 2 both of which are animal derived and therefore result in the difficulty towards clinical translation. However, as I have discussed in chapter 3, the chemically defined hydrogels presented in this project are suboptimal in that they do not allow

expansion of hPOs in a similar manner to BME 2 and also result in loss of the culture and some loss of the expression of markers key for ductal identity. However, while further work is required to generate a hydrogel that is equal to or better than BME 2 in terms of hPO expansion, this work also demonstrates the opportunity for the use of these tuneable hydrogels to study the biology of healthy and diseased states as well as the investigation of the mechano-sensing dynamics which may underlie pancreatic differentiation. It has been shown that in diabetes there is a significant change to the ECM resulting from events such as increased collagen deposition[260]. Furthermore, the ECM is known to be significantly altered in pancreatic cancer with various ECM proteins having pro-tumorigenic effects[308]. The possibility of manipulating the ECM composition might facilitate the *in vitro* modelling of the pathogenic ECM-remodelling often observed in such diseased states.

Furthermore, a link has been reported between mechanosignalling and specification of pancreatic progenitors. Specifically, mechanistic studies from hESCs, differentiated into pancreatic progenitors, showed that interaction with α5 integrin in the ECM acts through the F-actin-YAP1-Notch mechanosignalling axis to control the fate of bipotent progenitors. The signalling resulting from the α5 integrin interaction promotes specification towards the duct lineage while disruption of this signalling cascade results in an endocrine specification[309]. Furthermore, it has been shown that TEAD, an effector of Hippo signalling pathway which is affected by mechanical stimuli, and its co-activator YAP can activate transcription factors leading the expansion of pancreatic progenitors[310]. Therefore, the ability to introduce different components into the hydrogel can shed light into the interactions of pancreatic cells and their surrounding ECM and can also be used in the investigation of the differentiation of mature ductal progenitors towards insulin producing cells.

6.2.4 Continued assessment of the immunogenicity of hPOs

I have assessed the expression of HLA Class I and II in hPOs following two main types of inflammatory environments *in vitro*, either co-culture with IFNγ or with SpMCs. I have demonstrated that hPOs significantly upregulate expression of HLA Class II in both conditions and may pose, at least to a certain extent, a risk for an immune rejection event *in vivo*. However, further experiments are required in order to understand precisely what drives the upregulation of HLA Class II and the mechanisms underlying the interaction with lymphocytes. Future experiments will investigate other pro-inflammatory cytokines such as TNF-α, IL-1 and IL-6 and their effect on the expression of HLA and other immunogenic molecules. Experiments where hPOs are co-cultured with lymphocytes are also needed, including use of more donor lines as well as different types of conditions to include varying numbers of both activated and non-activated SpMCs as well as different lymphocyte sub-populations (CD4+, CD8+ etc.). While my experiments helped to illustrate that SpMCs can lead to HLA Class II upregulation in hPOs, it is essential to understand whether hPOs can in fact drive the activation of lymphocytes. It would also be important to demonstrate if lymphocytes have a direct interaction with hPOs or whether the observed

HLA Class II upregulation on hPOs is a by-product of cytokines produced from the activated lymphocytes. ELISA experiments to assess levels of cytokines in "activated SPMCs only" or "activated SPMCs mixed with hPOs" could answer whether SPMCs are producing cytokines as a result of interacting with hPOs. Furthermore, use of trans-wells to ensure SPMCs are not interacting with hPOs could illuminate whether the hPO-lymphocyte interaction is needed for the subsequent HLA upregulation or whether it is a product of cytokine produced from the SpMCs. Furthermore, use of a GFP-expressing hPO line could allow co-culture with SPMCs followed by cell sorting of hPO cells (or sorting for EpCAM positive cells) in order to perform mRNA analysis to understand the global change in gene expression as a result of the interaction with lymphocytes. These experiments would allow understanding of the specific pathways activated which result in upregulation of immunogenic molecules and could highlight areas for targeted treatments to reduce expression of such molecules.

Furthermore, in this project I present preliminary work on the use of HIS-mice to investigate the immunogenicity of hPOs in an *in vivo* environment under an autologous and allogeneic setting. While the work is ongoing and too preliminary to draw definitive conclusions, it highlights the use of two novel technologies i.e*.,* hPOs and HIS-mice, to uncover the immunogenic risk of hPOs and the ability of an hPO graft to attract and be recognised by human lymphocytes in the peripheral blood. Ongoing work to section the grafts from these animals will allow quantification of graft infiltration as well as understanding of whether allogeneic but not autologous hPOs are rejected. Once this has been established, it will be important to investigate strategies for amelioration of the immune response. One method that is currently used in the clinic to reduce risk of rejection of transplanted organs is HLA matching. The donor lines used in this project to investigate immune rejection in HIS-mice were a complete HLA-mismatch. In the future, I will repeat the HIS-mouse experiments outlined in this project using donor lines that are either HLA-matched or have different degrees of mismatching. Using this approach, I can investigate whether HLA-matching can reduce the alloimmune response. Another method that is currently investigated is the removal or silencing of HLA expression through gene editing. Such lines that can avoid immune rejection would mean that less lines would be required to meet the demands of a particular disease, thus reducing the time and expense to generate the cellular therapy product. A group has recently generated PSC-derived HLA Class I knock-out lines which effectively evade immune recognition. Furthermore, while the lack of HLA Class I expression typically can lead towards cytotoxic killing by Natural Killer (NK) cells, the group also engineered the cells to express HLA-E which presents antigens from other HLA Class I molecules and also inhibits NK cell activity. This way, the cells could avoid recognition from APCs and direct killing by NK cells[311]. Such gene editing strategies can be employed for hPOs and render them less immunogenic. Interestingly, work in our lab is aimed at the generation of HLA Class I KO cholangiocyte organoid lines in collaboration with the Ghevaert group which has generated multiple iPSC HLA Class I KO lines.

6.2.5 Generation of a robust GFP-luciferase expressing hPO line

I have demonstrated in this work the generation of a GFP-luciferase expressing hPO line following a single cell step and transduction with a lentivirus. Importantly this work demonstrated that in principle GFP-luciferase+ hPOs can be tracked *in vivo* following transplantation into the kidney capsule, thereby reducing the need to cull animals to assess survival of the graft. Furthermore, this work can potentially allow the quantification of graft rejection by linking the signal produced following bioluminescent imaging (BLI) to the number of cells engrafted. Indeed, use of BLI imaging to assess hESC allograft rejection in HIS-mice has recently been demonstrated[312]. However, the work presented in this dissertation is currently hampered by the progressive loss of GFP-luciferase expressing cells *in vitro* and the rapid loss of signal following *in vivo* transplants. While I have demonstrated that use of the Ef1α promoter can allow more rapid generation of a homogenously GFP-expressing pool of cells, without the need for a second single-cell step and cell sorting, I have not yet demonstrated use of this promoter in a construct containing luciferase. Future work will aim to utilise the Ef1α-GFP construct, produced by the Rawlins lab, in order to clone in the luciferase gene. Once this construct is generated and packaged into lentivirus particles, the protocol for hPO transduction will be repeated to assess transduction efficacy and longevity of expression *in vitro*. If results are promising, the lines will be transplanted into non-humanised and humanised mice, in parallel with non-transduced hPO controls, to assess the use of the GFP-luciferase hPO line in the quantification of allograft rejection *in vivo*. Furthermore, the line will be further assessed for expression of HLA Class I and II along with other immunogenic antigens to investigate whether the random insertion of the genes causes upregulation of antigens that can induce allograft rejection by lymphocytes. Another option, which may circumvent both the loss of expression and random insertion, is the use of CRISPR/Cas9 technology. In such a case, the GFP-luciferase gene could be targeted in a gene that is strongly expressed in hPOs such as *KRT19, PDX1* or *SOX9* thereby promoting a more stable expression and reducing susceptibility to gene silencing.

6.3 Conclusions

The key outputs of my experimental work are summarised below:

- Generating a culture system that allows efficient and long-term expansion of primary human pancreatic ductal cells as 3D organoids in a chemically defined, serum-free culture medium.
- Successfully cryopreserving primary pancreas tissue that allows subsequent hPO generation.
- Demonstrating that hPOs maintain their ductal architecture and identity over long-term culture.
- Demonstrating that hPOs can be expanded in a chemically defined, biomimetic ECM facilitating the generation of a GMP-compatible protocol.

- Modelling hPOs derived from T2D patients and illustrating the potential for the use of the hPO culture system for disease modelling.
- Generating tumour organoid lines from 3 different pancreatic cancers which can be used as a positive control for tumorigenicity assays.
- Demonstrating that hPOs maintain stable chromosomal numbers and genomic integrity over long-term culture.
- Generating clonally derived hPO lines that can be subjected to whole genome sequencing and uncover the mutational burden of *in vitro* culture.
- Demonstrating that hPOs do not obtain excessive amount of genetic variants during culture nor do they accumulate cancer driver mutations.
- Establishing a tumorigenicity assessment panel and demonstrating that hPOs do not pose a risk for tumour formation even after long-term engraftment in NSG mice.
- Demonstrating that hPOs can upregulate HLA Class II *in vitro* following co-culture with IFNγ and activated lymphocytes.
- Comparing the immune response of autologous and allogeneic hPOs through the use of SpMC-HIS and HSC-HIS mice.
- Generating preliminary results for the creation of a GFP-luciferase expressing hPO line and demonstrating its use for *in vivo* survival and immune rejection tracking.

In conclusion, the work presented in my dissertation demonstrates a novel system that allows expansion of hPOs long-term, form both fresh and cryopreserved human pancreas tissue in a chemically defined serum-free culture system with no detectable tumorigenicity. hPOs represent an abundant source of pancreas ductal cells that retain the characteristics of the tissue-of-origin. Furthermore, they facilitate the investigation of their antigenicity and immunogenicity and can be used in complex *in vivo* immune rejection models. This opens up avenues for modelling diseases of the ductal epithelium, increasing understanding of human pancreas exocrine biology and generation of insulin-secreting cells for the treatment of diabetes with the ability to formulate strategies to remove or reduce allograft rejection.

CHAPTER 7. SUPPLEMENTAL DATA

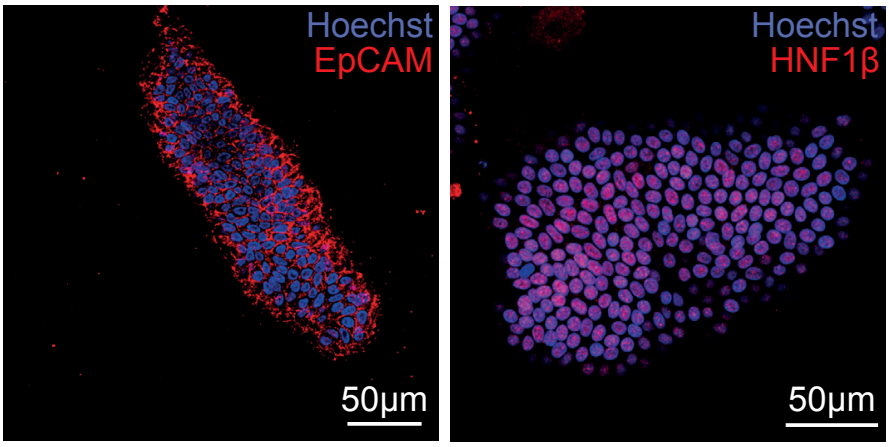

Supplemental Figure 1 hPOs retain protein expression ductal and pancreas specification markers. Immunofluorescence staining of healthy tissue derived hPOs of cytoplasmic EpCAM (red) and nuclear HNF1β (red). Experiments were performed in n=1 donors.

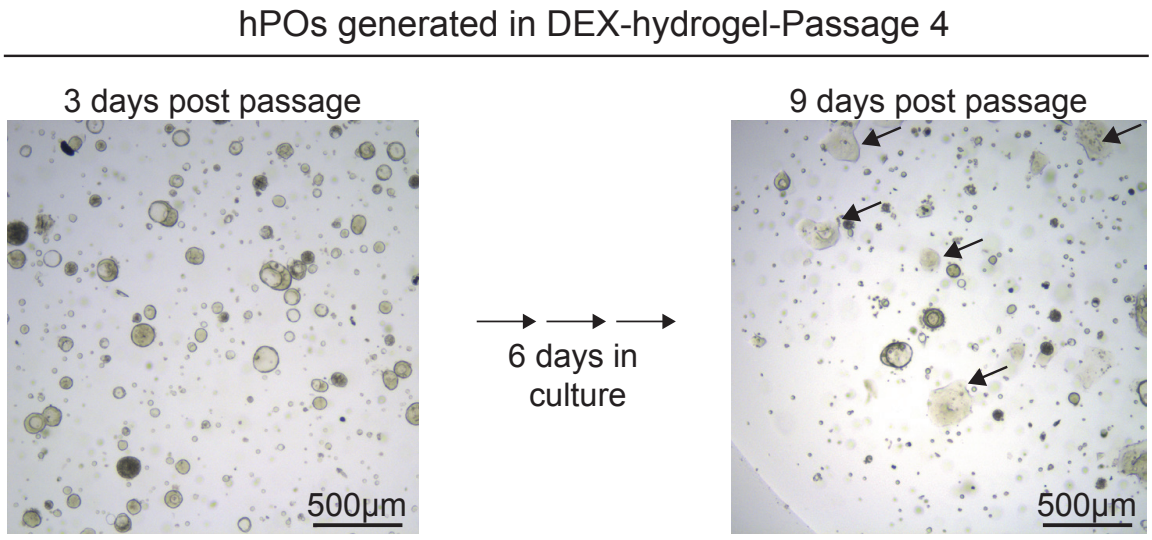

Supplemental Figure 2- Degradation of DEX-hydrogel by residual dextranase.
Representative brightfield images of hPOs generated in DEX-Hydrogel and passaged using dextranase. Note the lack of cyst expansion and increased attachment to the culture plate (indicated by black arrows) after 6 days of culture. Experiments were performed in n=3 donors.

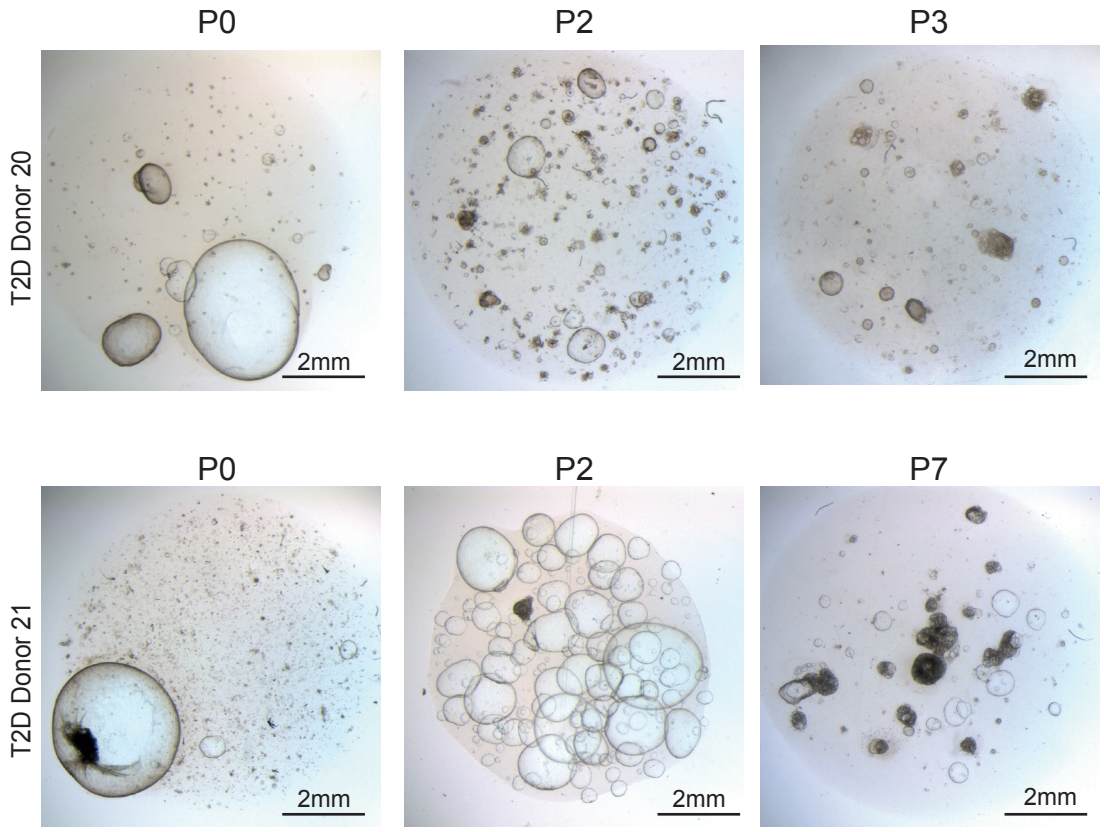

Supplemental Figure 3 Expansion of T2D hPOs demonstrates early deterioration of cultures. Representative brightfield images of hPOs derived from T1D donor 20 (upper panels) and donors 21 (lower panels) show deterioration of organoids following *in vitro* expansion.

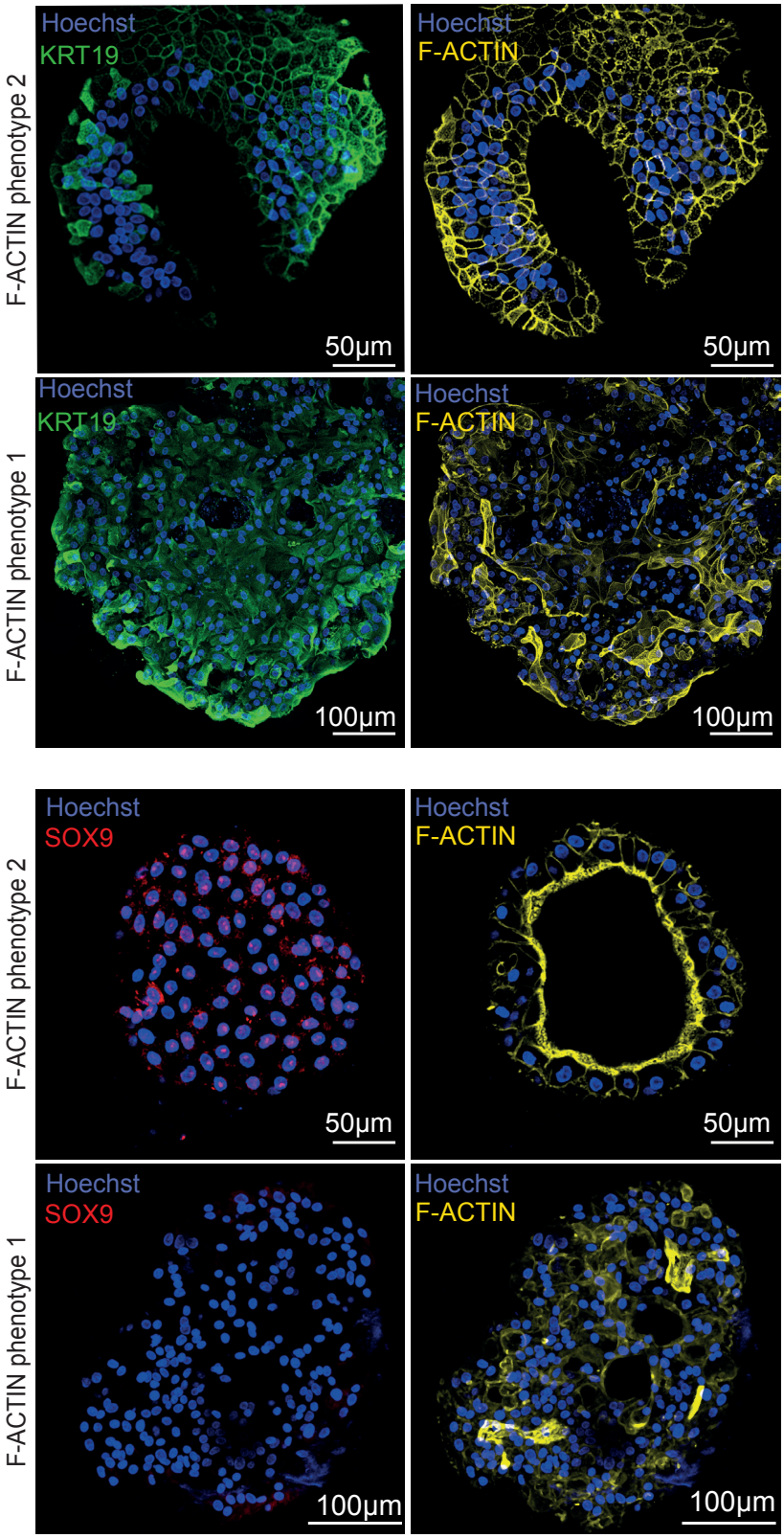

Supplemental Figure 4 T2D Donor 20 hPOs demonstrate contrasting phenotypes of spatial organisation and marker expression.
Immunofluorescence staining of T2D Donor 20 hPOs of cytoplasmic KRT19 (green), nuclear SOX9 (red), nuclear PDX1 (red), and F-ACTIN (yellow). Note that hPOs demonstrate two phenotypes of F-ACTIN staining as well as loss of SOX9 expression in some organoids. (n=1 organoid stained per phenotype).

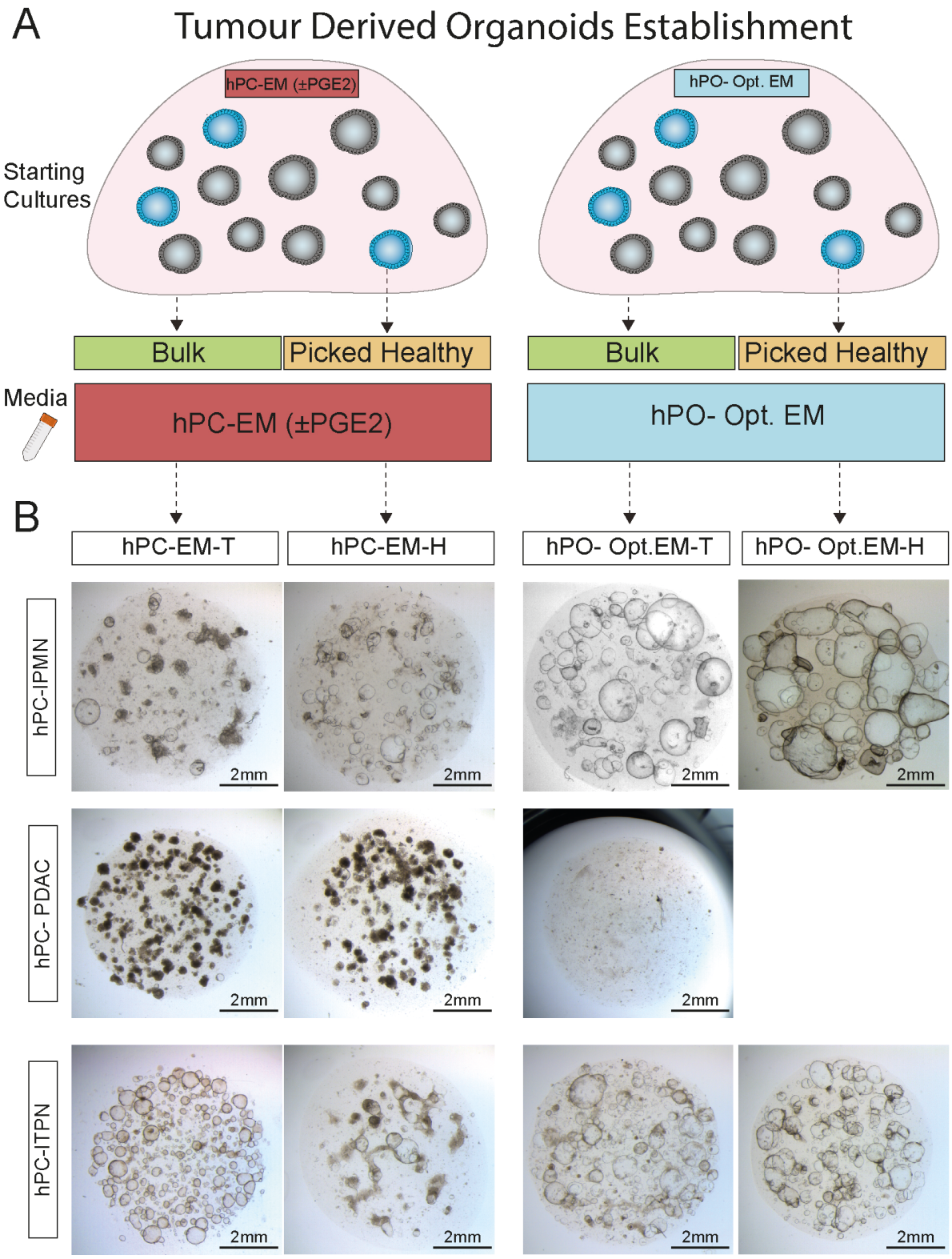

Supplemental Figure 5 Different media compositions trialled to generate organoids from pancreas cancer

(**A**)Schematic depicting experimental design for generation of a tumour organoid line without healthy organoid contamination. (**B**) Representative images showing either bulk cancer organoids or healthy hand-picked organoids expanded in tumour media (hPC-EM) or healthy hPO media (hPO-Opt.EM) among three pancreas cancer lines: hPC-IPMN, hPC-PDAC, hPC-ITPN. Note that hPC-PDAC organoids did not expand in healthy media, hence no 'healthy' organoids could be hand-picked out from that condition.

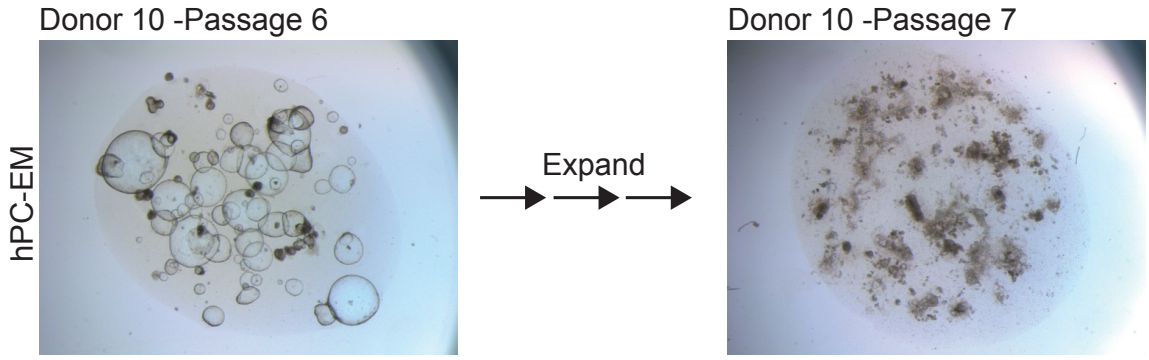

Supplemental Figure 6 Healthy hPOs quickly deteriorate in tumour media
Representative images demonstrate healthy hPOs expanded in hPO-Opt.EM until passage 6 and then placed into tumour media (hPC-EM). hPOs cannot be expanded nor passaged in tumour media and quickly deteriorate.

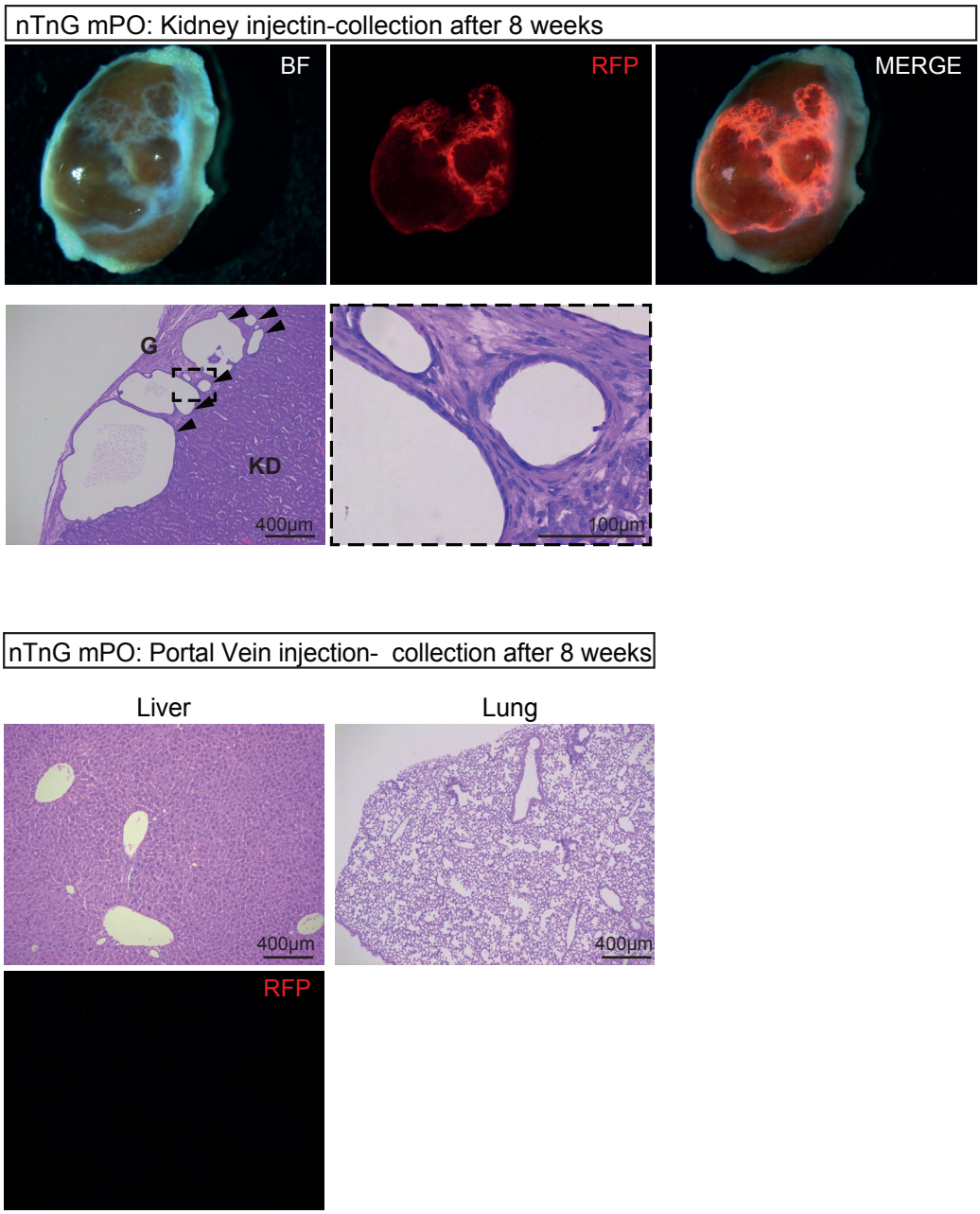

Supplemental Figure 7 nTnG mPOs injected under the kidney capsule or into the portal vein. (Top panel) Representative wholemount fluorescence (Top) and H&E (bottom) images of nTnG mPOs transplanted into the kidney of NSG mice and recovered after 8 weeks. This is confirmed by H&E staining. (Bottom panel) Representative H&E images (top) and wholemount fluorescence images of nTnG mPOs transplanted into the the portal vein of NSG mice and collected after 8 weeks.

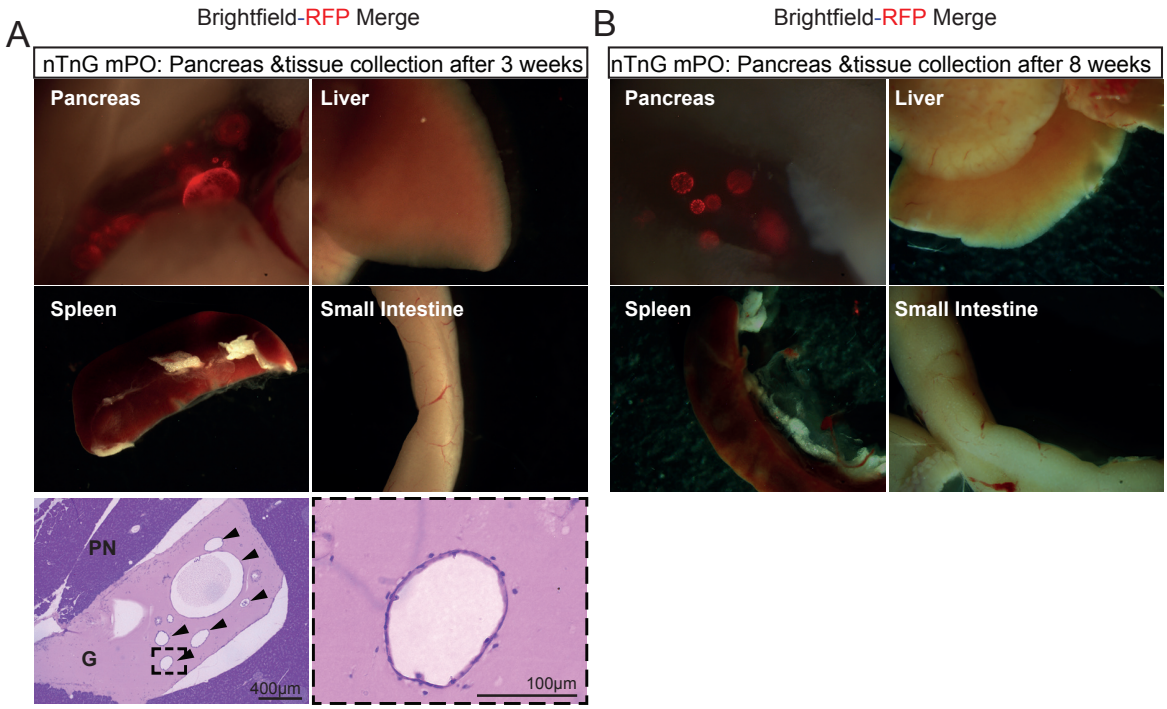

Supplemental Figure 8 nTnG mPOs engrafted in the mouse pancreas are retained in the site of transplantation. Representative wholemount images of nTnG mPOs transplanted into the pancreas of NSG mice and recovered after 3 weeks (**A**) and 8 weeks (**B**). Note that the organoids are in between the pancreas parenchyma and retain their cystic morphology at both 3 and 8 weeks. Organoids were not found in any of the other organs checked, namely liver, spleen and small intestine. H&E staining confirms hPOs at the 3 week time point.

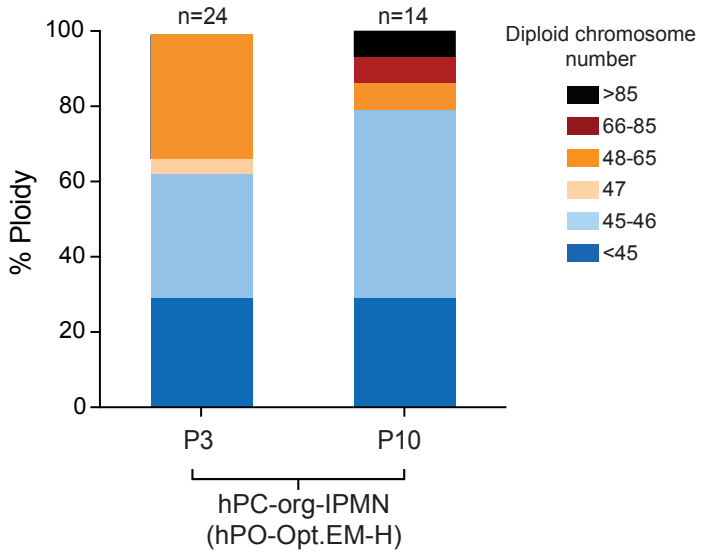

Supplemental Figure 9 Karyotypes of hPC-IPMN organoids expanded in hPO-Opt.EM-H. Graph shows karyotype counts for tumour organoids derived from hPC-IPMN samples and expanded in hPO-Opt.EM media. The organoids expanded had a healthy (**H**) morphology and were handpicked out.

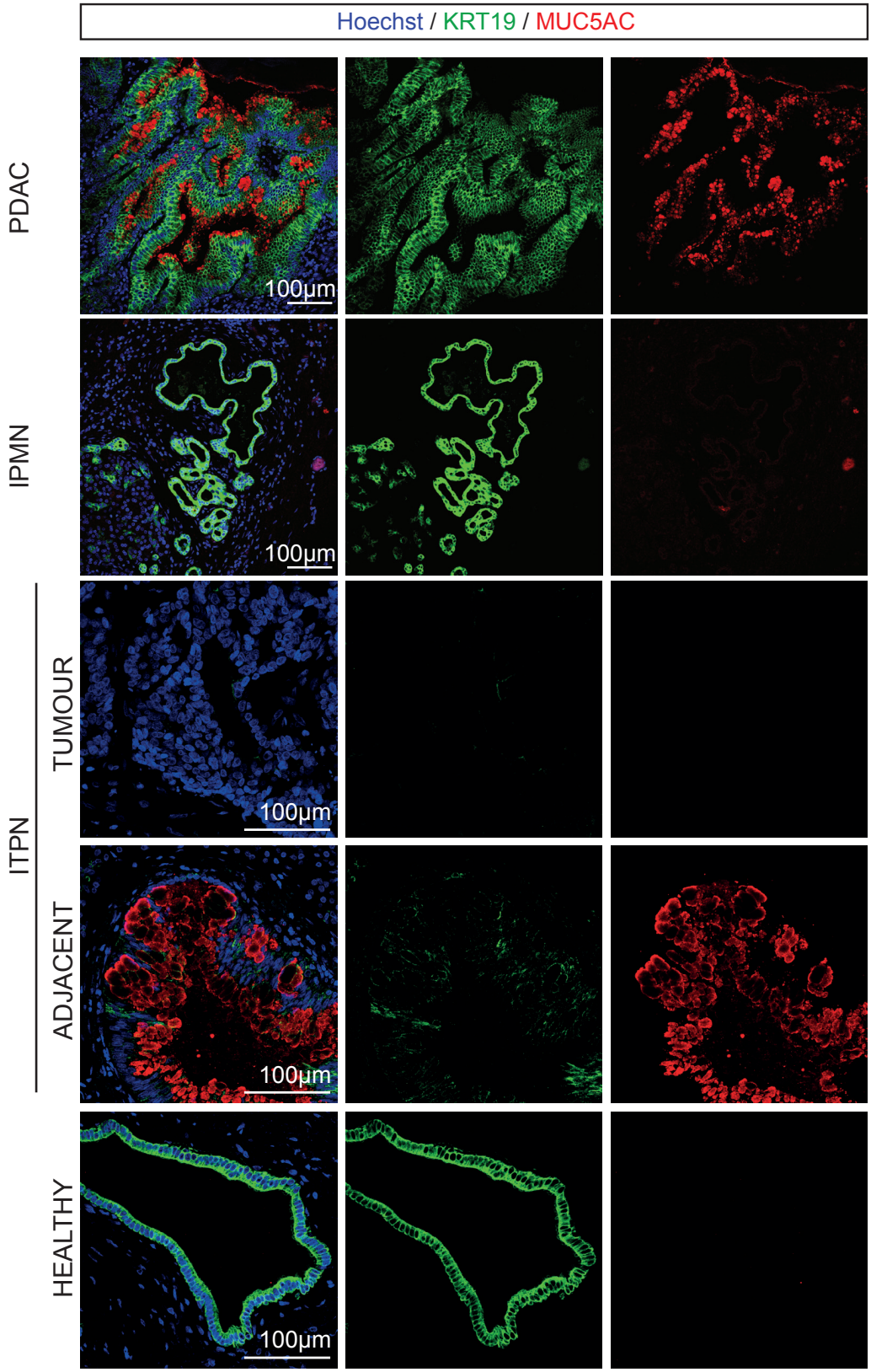

Supplemental Figure 10 Muc5AC antibody validation.
Representative images of immunofluorescence staining for pancreas cancer specific marker MUC5AC(red) and ductal marker KRT19(green) showing MUC5AC positivity for tumour tissue from PDAC(2/3 donors), IPMN (1/2 donors), and ITPN (1/1donors) tumours and lack of expression in healthy pancreas tissue (n=5 independent donors)

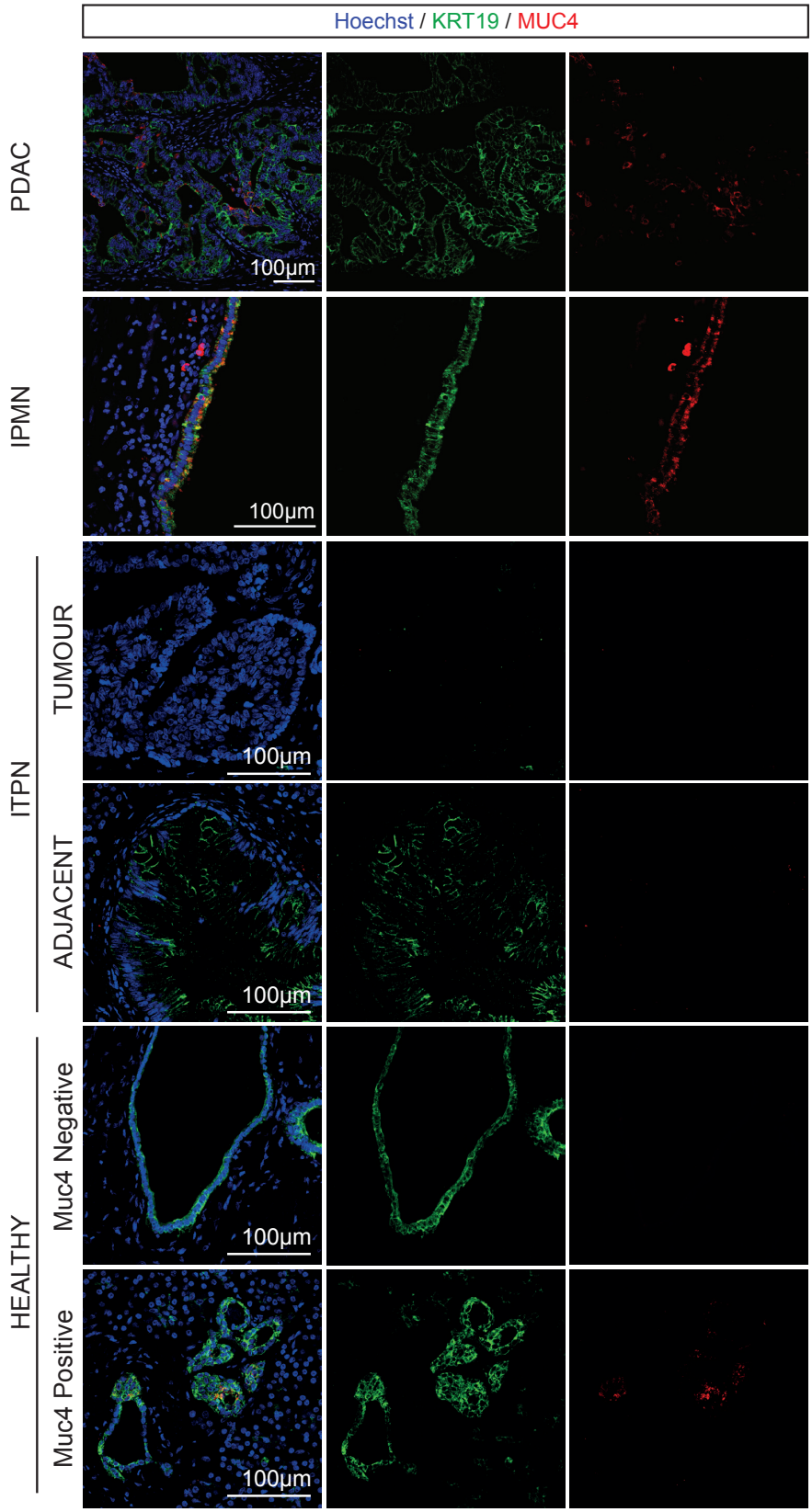

Supplemental Figure 11 MUC4 antibody validation. Representative images of immunofluorescence staining for pancreas cancer specific marker MUC4(red) and ductal marker KRT19(green). Tumour tissue from IPMN and PDAC tumours was positive for MUC4 expression while ITPN tissue showed no detection of MUC4. Healthy primary tissue also showed positivity for MUC4 expression (3/5 donors tested), which brings into question the specificity of this antibody.

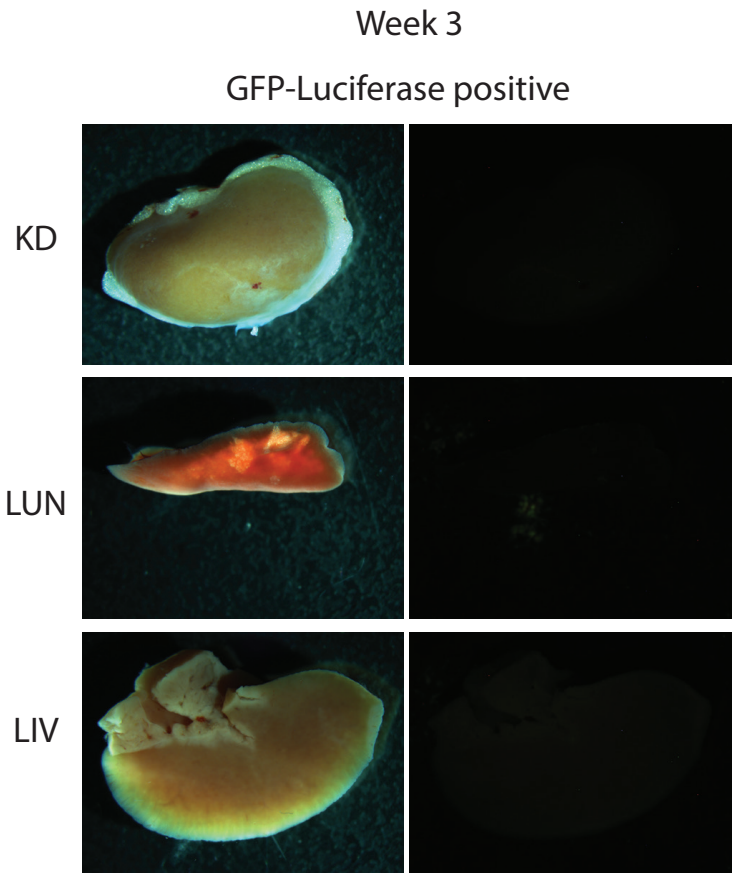

Supplemental Figure 12 GFP-Luciferase engrafted cells do not survive beyond 1-week post-transplantation. Representative wholemount brightfield and fluorescence images of organs collected from NSG mice following 3 weeks engraftment into the kidney capsule with GFP-luciferase positive hPOs.

CHAPTER 8. APPENDIX

8.1.1 Appendix Table 1: Demographics of deceased human organ donors used in experiments

Donor ID	Age of donor (years)	BMI	Tissue ischaemic Time (hrs)	Underlying pathology	Successful organoid isolation	info
1*	58	37.8	24-30	none	Yes	
2	57	33.6	60-72	none	Yes	
3	37	23.1	24-28	none	Yes	
4	53	38.6	40-48	none	Yes	
5	66	25.6	20-24	none	Yes	
6	24	24.3	40-48	none	Yes	
7	46	30.8	7	none	Yes	
8	41	40.65	15-20	none	Yes	
9	43	25.53	48	none	Yes	
10	51	31.1	21	none	Yes	
11	63	28.1	48	none	Yes	
12	58	25.63	19-20	none	Yes	
13	22	23.4	24	none	Yes (contamination) yes from frozen tissue	
14	31	21.37	4-5	none	Yes	
15	63	22	8-10	none	Yes	
16	65	23	30	none	Yes	
17	40	25	29	none	Yes	
18	37	30	24	none	Yes	
19	63	33.36	48	Type 2 diabetes	No	Type 2 diabetes medication: insulin glargine, metformin, glicazide, simvastatin, bisoprolol, nicorandil, venlaflaxine, rivoxaban. Heavy drinker 7-9u/day; smoker;history of pulmonary disease, hypertension, cardiac disease
20	54	35.02	24	Border line diabetic	Yes	No medication. Heavy drinker
21	56	24.69	24	Type 2 diabetes	Yes	Type 2 diabetes, diet controlled.
22	58	22.45	4-5	none	Yes	
23	58	25.8	12	none	Yes	
24	79	23.9	5	none	Yes	
25	50	31.8	18	none	Yes	
26	46	26.71	24	none	Yes	
27	40	32.74	34	none	No (technical issue)	
28*	47	26.4	40	none	Yes	
29	48	28.7	18	none	Yes	
30	53	28.41	80-84	none	Yes	
31	42	34.2	100-103	none	NO (technical issue)	
32	48	28.7	24	none	Yes	
33	51-60	32.4	40-48	none	Yes	
34	41-50	27.7	20	none	Yes	
hPC-IPMN	61-70	(--)	>24	IPMN	Yes	
hPC-PDAC	51-60	33.94	6	PDAC/T1D	Yes	metastasis: Nodal, lymphovascular and perineural
Islets-1	51-60	27.17	(--)	none	N/A	

*Donors used exclusively for media optimisation experiments; Red shading- donors with underlying disease; Yellow shading- islets obtained from the Scottish National Blood Transfusion Service (SNBTS) Islet Isolation Centre

8.1.2 Appendix Table 2: Mouse transplants performed

Type	hPO Donor	lymphocyte donor	Condition as in Table 2	Passage	Condition	Mice Tx	Recipient Mouse	Location	No. engrafted with organoids	Furthest week of organoid engraftment
Healthy-Bulk	11	N/A	K-0	Early	100% BME	4	NSG	KC	2/4	2 weeks
Healthy-Bulk	11	N/A	K-0	Late	100% BME	8	NSG	KC	2/8	4 weeks
Healthy-Bulk	34	N/A	K-0	Early	100% BME	13	NSG	KC	0/9	N/A
Healthy-Clone	7-Clone 1	N/A	K-0	Mid-late	100% BME	6	NSG	KC	0/6	N/A
Healthy-Clone	7-Clone 2	N/A	K-0	Early	100% BME	6	NSG	KC	0/6	N/A
Healthy-Clone	7-Clone 3	N/A	K-0	Mid-late	100% BME	6	NSG	KC	0/6	N/A
Healthy Bulk	7	N/A	K-4	Mid-late	30% Matri, VEGF, Rhoki	3	NSG	KC	3/3	4 weeks
Healthy Bulk	7	N/A	K-2	Mid-late	30% BME, VEGF, Rhoki	3	NSG	KC	3/3	4 weeks
Healthy Bulk	7	N/A	K-5	Mid-late	50% G-HA, VEGF, Rhoki, hPO-EM	3	NSG	KC	3/3	4 weeks
Healthy Bulk	7	N/A	K-3	Mid-late	30% Matri., VEGF, Rhoki, hPO-EM	3	NSG	KC	1/3	4 weeks
Healthy Bulk	7	N/A	P-2	Mid-late	30% Matri., Rhoki	3	NSG	PC	3/3	4 weeks
Healthy Bulk	7	N/A	P-1	Mid-late	100% BME, Rhoki	3	NSG	PC	3/3	4 weeks
Healthy Bulk	7	N/A	K-1	Mid-late	100% BME, Rhoki	3	NSG	KC	2/3	4 weeks
Healthy Bulk	22	N/A	P-4	Early	30% Matri., VEGF, Rhoki, hPO-EM	4	NSG	PC	4/4	12 weeks (n=3)
Healthy Bulk	22	N/A	P-3	Early	50% G-HA, VEGF, Rhoki, hPO-EM	4	NSG	PC	4/4	12 weeks (n=3)
Total Healthy						72				
SPMC-HIS (Control)	N/A	8	N/A	N/A	N/A	3	NSG-dKO	N/A	N/A	N/A
SPMC-HIS (Control)	N/A	22	N/A	N/A	N/A	3	NSG-dKO	N/A	N/A	N/A
SPMC-HIS-1	22	22	P-4	Mid-late	30% Matri., VEGF, Rhoki, hPO-EM	4	NSG-dKO	PC	Ongoing	Ongoing

SPMC-HIS-1	8	22	P-4	Mid-late	30% Matri., VEGF, Rhoki, hPO-EM	3	NSG-dKO	PC	Ongoing	Ongoing
SPMC-HIS-1	8	8	P-4	Mid-late	30% Matri., VEGF, Rhoki, hPO-EM	4	NSG-dKO	PC	Ongoing	Ongoing
SPMC-HIS-1	22	8	P-4	Mid-late	30% Matri., VEGF, Rhoki, hPO-EM	4	NSG-dKO	PC	Ongoing	Ongoing
HSC-HIS-1	22	22	P-4	Mid-late	30% Matri., VEGF, Rhoki, hPO-EM	3	NSG	PC	Ongoing	Ongoing
HSC-HIS-1	8	22	P-4	Mid-late	30% Matri., VEGF, Rhoki, hPO-EM	3	NSG	PC	Ongoing	Ongoing
HSC-HIS-1	8	8	P-4	Mid-late	30% Matri., VEGF, Rhoki, hPO-EM	2	NSG	PC	Ongoing	Ongoing
HSC-HIS-1	22	8	P-4	Mid-late	30% Matri., VEGF, Rhoki, hPO-EM	3	NSG	PC	Ongoing	Ongoing
Cancer	hPC-IPMN	N/A		Mid-late	100% BME	5	NSG	KC	2/5	4 weeks
Cancer	hPC-PDAC	N/A		Mid-late	30% Matri., VEGF, Rhoki, hPO-EM	6	NSG	PC	6/6	8 weeks
mPOs-RFP	nTnG mouse	N/A	P-2	Mid-late	30% Matri., Rhoki	7	NSG	PN	7/7	12 weeks
mPOs-RFP	nTnG mouse	N/A	N/A	Mid-late	30% Matri., Rhoki	2	NSG	KC	2/2	8 weeks
mPOs-RFP	nTnG mouse	N/A	N/A	Mid-late	PBS	4	NSG	PV	0/4	N/A
hPOs-GFP-Luc (negative sort)	8	N/A	K-4	Mid-late	30% Matri, VEGF, Rhoki	4	NSG	KC	N/A	GFP signal at day 2
hPOs-GFP-Luc (sorted)	8	N/A	K-4	Mid-late	30% Matri, VEGF, Rhoki	2	NSG	KC	N/A	GFP signal at day 3
hPO-GFP-Luc (negative control)	23	N/A	K-4	Mid-late	30% Matri, VEGF, Rhoki	2	NSG	KC	N/A	N/A
Total mice						136				

NSG= Nod Scid Gamma; KC- Kidney Capsule; PC-Pancreas Capsule; PV- Portal Vein; G-HA: Glycosil Hyaluronic Acid (ESI Bio); VEGF- Animal Free; Recombinant Human Vascular Endothelial Growth Factor (Peprotech) - used at conc. 50ng/ml; Rhoki-Rho kinase inhibitor used at 1:1000; HIS-human immune system; SpMC- splenocyte mononuclear cells; HSC- haematopoietic stem cells; Early

passage 1-6, Mid-Late 7-10, Late passage 11-15; Blue shading- hPO survival experiments; Yellow shading- HIS mice experiments; Red shading- nTnG mPO experiments; Green shading- GFP-luciferase hPO experiments

8.1.3 Appendix Table 3: Single nucleotide variant (SNV) counts in clone and subclone samples

Donor	Clone	Sub-clone	Coverage (X)	SNV Counts	Contamination
14	1	N.A.	20.71	763	No
14	4	N.A.	44.53	824	No
14	4	3	25.94	34329	Yes
14	4	1	22.12	3624	Yes
14	4	5	26.86	42932	Yes
14	5	N.A.	80.99	874	No
14	5	5	22.37	49169	Yes
14	5	4	30.11	1144	No
14	5.5	N.A.	41.8	823	No
14	5.5	3	21.37	941	No
10	1	N.A.	14.99	1075	No
10	2	N.A.	17.59	1272	No
10	3	N.A.	12.52	1075	No
10	4	N.A.	23.38	1315	No

Table shows raw variants calculated after basic set of bioinformatic filters. Note that Clones 5 and 5.5 have been expanded from the same clonal organoid.

8.1.4 Appendix Table 4: HLA typing of donors used in HIS-mouse experiments

Donor	HLA A	HLA B	HLA C	HLA DR	HLA DQ
Donor 8	A*30:01 A*31:01	B*27:02 B*52:01	C*01:02 C*12:02	DRB1*01:01 DRB1*15:01	DQB1*05:01 DQB1*06:01
Donor 22	A*03:01 A*24:02	B*07:02 B*39:06	C*07:01 C*07:01	DRB1*04:01 DRB1*15:01	DQB1*03:01 DQB1*06:02

Table shows 4-digit resolution of HLA typing. The letter (A,B, DRB1 etc.) denotes the HLA gene locus. The number following the asterisk denotes the allele group. The number following the semicolon denotes the specific allele found.

8.1.5 Appendix Table 5: List of antibodies related to experimental procedures

Antigen	Supplier	Cat. number	Clonality	Origin	dilution IF	Application
Human KRT19	ATLAS	HPA002465	Poly.	Rabbit	1:300	IF/IHC-P-IF
SOX9	EMD Millipore	AB5535	Poly.	Rabbit	1:200	IF
PDX1	R&D Systems	AF2419	Poly.	Goat	1:20	IF

Phalloidin-FITC	Thermofisher	F432	N/A	N/A	1:300	IF
Phalloidin-647	Thermofisher	A22287	N/A	N/A	1:300	IF
Muc5AC(AB)	Abcam	AB212636	Mono.	Mouse	1:500	IHC-IP-IF
Muc5AC	Thermofisher	MS-145-P0	Mono.	Mouse	1:300	IHC-IP-IF
Muc4 (8G7)	Santa-Cruz	SC-53945	Mono.	Mouse	1:100	IHC-IP-IF
Muc1	SigmaAldrich	HPA004179	Poly.	Rabbit	1:100	IHC-IP-IF
Muc2	Santa-Cruz	SC-7314	Mono.	Mouse	1:100	IHC-IP-IF
Muc4(1G8)	Thermofisher	35-4900	Mono.	Mouse	1:100	IHC-IP-IF
Hnf1b	Santa-Cruz	SC-7411	Poly.	Goat	1:100	IF
hEpCAM-AF647	eBiosciences	51-9326-73	Poly.	Mouse	1:300	IF
Ki67	Thermofisher	RM 9106 S1	Mono.	Rabbit	1:200	IF/IHC-P-IF
Anti-RFP	Rockland	600-401-379	Poly.	Rabbit	1:300	IHC-IP-IF
Anti-Rabbit Alexa 488	Thermofisher	A21206	Poly.	Donkey	1:250	IF
Anti-Rabbit Alexa 647	Thermofisher	A31573	Poly.	Donkey	1:250	IF
Anti-Goat Alexa 568	Thermofisher	A11057	Poly.	Donkey	1:250	IF
Anti-Mouse Alexa 555	Thermofisher	A31570	Poly.	Donkey	1:250	IF
hCD45-FITC	eBiosciences	11-0459-42	Mono.	Mouse	1:50	Flow-Cyt
hCD4-PE	Thermofisher	25-0049-42	Mono.	Mouse	1:50	Flow-Cyt
7AAD-PerCP-Cy5.5	Biolegend	420404	N/A	N/A	1:20	Flow-Cyt
mCD45.1-PE-Cy7	eBiosciences	25-0049-42	Mono.	Mouse	1:125	Flow-Cyt
hCD3-APC	Biolegend	300439	Mono.	Mouse	1:50	Flow-Cyt
hCD8-APC-Cy7	Invitrogen	A15448	Mono.	Mouse	1:50	Flow-Cyt
hCD8-PE-Cy7	Biolegend	344712	Mono.	Mouse	1:51	Flow-Cyt
hCD19-PE	Biolegend	363004	Mono.	Mouse	1:50	Flow-Cyt

hCD14-APC-Cy7	Thermofisher	A15453	Mono.	Mouse	1:50	Flow-Cyt
CD25- APC-Cy7	BD Biosciences	561782	Mono.	Mouse	1:50	Flow-Cyt
EpCAM-PE	Biolegend	324206	Mono.	Mouse	1:40	Flow-Cyt
EpCAM-FITC	Biolegend	324204	Mono.	Mouse	1:40	Flow-Cyt
HLA-ABC-PE-cy7	Biolegend	311430	Mono.	Mouse	1:100	Flow-Cyt
HLA-DP/DQ/DR-APC	MACS Miltenyi	130-104-824	Mono.	Mouse	1:100	Flow-Cyt

N/A- not applicable; Poly. - polyclonal; Mono.- Monoclonal IHC-P- Immunohistochemistry-Paraffin; IF- immunofluorescence

8.1.6 Appendix Table 6: List of primers used

PRIMERS	Sequence (5'--------3')
Hprt	AAGAGCTATTGTAATGACCAGT CAAAGTCTGCATTGTTTTGC
Krt19	CGCGGCGTATCCGTGTCCTC AGCCTGTTCCGTCTCAAACTTGGT
Sox9	GGAAGTCGGTGAAGAACGGG TGTTGGAGATGACGTCGCTG
Pdx1	CAGCTGCCTTTCCCATGGAT TCCGCTTGTTCTCCTCCG
Insulin	AAGAGGCCATCAAGCAGATCA CAGGAGGCGCATCCACA
Lgr5	GACTTTAACTGGAGCACAGA AGCTTTATTAGGGATGGCAA
CFTR	AGTTGCAGATGAGGTTGGGC AAAGAGCTTCACCCTGTCGG
HLA-A	TCACAGACTGACCGAGTGGA ATGGTGTGAGAACCGGCCT
HLA-B	AGCAGTTGTGGTCATCGGAG TCCCTCCTTTTCCACCTGAAC
HLA-C	GGTTGTCCTAGCTGTCCTTGG AGGCAGCTGTCTCAGGCTTT
HLA-DQ	GCTACAACTCTACCGCTGCT CCCATTGCTCAGCCATGTG
HLA-DR	GGTGGACAACTACTGCAGACA CACCTTAGGATGGACTCGCC
HLA-DP	CGTTCCAACCACACTCAGG TGTCAATGTGGCAGATGAGG
Gad65	CTTTTGGTCTTTCGGGTCGG GCACAGTTTGTTTCCGATGC
IA-2	TCTCCGGCTGCTCCTCTG GCACACCTTGTAAGCGTTGG
Cd44	AGCACAATCCAGGCAACTCC CTGGTATGAGCTGAGGCTGC

8.1.7 Appendix Table 7: List of kits used related to experimental procedures

KIT/Reagent	Supplier	Cat. number
RNeasy Micro Kit	QIAGEN	74004
RNeasy Mini Kit	QIAGEN	74104
Paraffin	Thermofisher	6774006
Eosin	Merck	HT110316
Haematoxylin	Merck	MHS16
VEGF	Peprotech	AF-100-20A
Glycosil Hyaluronic Acid	ESI Bio	GS222
CMV-GFP-T2A-Luciferase pre-packaged virus	Systems Bioscience	BLIV101VA-1
CAG-Luciferase-F2A-RFP-RsvPuro pre-packaged virus	GenTarget Inc.	LVP572
TransDux™	Systems Bioscience	LV850A
MAX Enhancer	Systems Bioscience	LV860A
Reporter Lysis 5X Buffer	Promega	E3971
Luciferase Assay Buffer	Promega	E152A
Luciferase Assay Substrate	Promega	E151A

CHAPTER 9. REFERENCES

1. Jennings, R. E., Berry, A. A., Strutt, J. P., Gerrard, D. T. & Hanley, N. A. Human pancreas development. *Development* **142**, 3126–3137 (2015).
2. Grapin-Botton, A. Ductal cells of the pancreas. *International Journal of Biochemistry and Cell Biology* **37**, 504–510 (2005).
3. Leung, P. S. & Ip, S. P. Pancreatic acinar cell: Its role in acute pancreatitis. *International Journal of Biochemistry and Cell Biology* **38**, 1024–1030 (2006).
4. Bouwens, L. & Pipeleers, D. G. Extra-insular beta cells associated with ductules are frequent in adult human pancreas. *Diabetologia* **41**, 629–633 (1998).
5. Ionescu-Tirgoviste, C. *et al.* A 3D map of the islet routes throughout the healthy human pancreas. *Sci. Rep.* **5**, 1–14 (2015).
6. Jørgensen, M. C. *et al.* An illustrated review of early pancreas development in the mouse. *Endocr. Rev.* **28**, 685–705 (2007).
7. Pan, F. C. & Wright, C. Pancreas organogenesis: From bud to plexus to gland. *Developmental Dynamics* **240**, 530–565 (2011).
8. Jennings, R. E. *et al.* Development of the human pancreas from foregut to endocrine commitment. *Diabetes* **62**, 3514–3522 (2013).
9. Bhushnan, A. *et al.* Fgf10 is essential for maintaining the proliferative capacity of epithelial progenitor cells during early pancreatic organogenesis. *Development* **128**, 5109–5117 (2001).
10. Bonfanti, P. *et al.* Ex Vivo Expansion and Differentiation of Human and Mouse Fetal Pancreatic Progenitors Are Modulated by Epidermal Growth Factor. *Stem Cells Dev.* **24**, 1766–1778 (2015).
11. Lemaire, L. A. *et al.* Bicaudal C1 promotes pancreatic NEUROG3+ endocrine progenitor differentiation and ductal morphogenesis. *Development* **142**, 858–70 (2015).
12. staff, B. co. & staff, B. co. Medical gallery of Blausen Medical 2014. *WikiJournal Med.* **1**, 10 (2014).
13. Gu, G., Dubauskaite, J. & Melton, D. A. Direct evidence for the pancreatic lineage: NGN3+ cells are islet progenitors and are distinct from duct progenitors. *Development* **129**, 2447 LP – 2457 (2002).
14. Kim, S. K. & MacDonald, R. J. Signaling and transcriptional control of pancreatic organogenesis. *Current Opinion in Genetics and Development* **12**, 540–547 (2002).
15. Pulkkinen, M. A., Spencer-Dene, B., Dickson, C. & Otonkoski, T. The IIIb isoform of fibroblast growth factor receptor 2 is required for proper growth and branching of pancreatic ductal epithelium but not for differentiation of exocrine or endocrine cells. *Mech. Dev.* **120**, 167–175 (2003).
16. Saint-Criq, V. & Gray, M. A. Role of CFTR in epithelial physiology. *Cellular and Molecular*

Life Sciences **74**, 93–115 (2017).

17. Ishiguro, H. *et al.* CFTR Functions as a bicarbonate channel in pancreatic duct cells. *J. Gen. Physiol.* **133**, 315–326 (2009).
18. Christodoulopoulos, J. B., Jacobs, W. H. & Klotz, A. P. Action of secretin on pancreatic secretion. *Am. J. Physiol.* **201**, 1020–1024 (1961).
19. Rutter, G. A., Pullen, T. J., Hodson, D. J. & Martinez-Sanchez, A. Pancreatic β-cell identity, glucose sensing and the control of insulin secretion. *Biochemical Journal* **466**, 203–218 (2015).
20. Da Silva Xavier, G. The Cells of the Islets of Langerhans. *J. Clin. Med.* **7**, 54 (2018).
21. Briant, L., Salehi, A., Vergari, E., Zhang, Q. & Rorsman, P. Glucagon secretion from pancreatic α-cells. *Upsala Journal of Medical Sciences* **121**, 113–119 (2016).
22. Rorsman, P. *et al.* Glucose-inhibition of glucagon secretion involves activation of GABAA-receptor chloride channels. *Nature* **341**, 233–236 (1989).
23. Kropp, P. A., Zhu, X. & Gannon, M. Regulation of the Pancreatic Exocrine Differentiation Program and Morphogenesis by Onecut 1/Hnf6. *CMGH* **7**, 841–856 (2019).
24. Hoang, C. Q. *et al.* Transcriptional Maintenance of Pancreatic Acinar Identity, Differentiation, and Homeostasis by PTF1A. *Mol. Cell. Biol.* **36**, 3033–3047 (2016).
25. Hale, M. A. *et al.* The nuclear hormone receptor family member NR5A2 controls aspects of multipotent progenitor cell formation and acinar differentiation during pancreatic organogenesis. *Dev.* **141**, 3123–3133 (2014).
26. Pin, C. L., Michael Rukstalis, J., Johnson, C. & Konieczny, S. F. The bHLH transcription factor Mist1 is required to maintain exocrine pancreas cell organization and acinar cell identity. *J. Cell Biol.* **155**, 519–530 (2001).
27. Siddiqui, A. A. *et al.* Diabetes: Mechanism, Pathophysiology and Management-A Review SGC college of Pharmacy, Baghpat(UP). *Drug Dev. Res* **5**, 1–23
28. Diabetes UK. *Diabetes Facts and Stats: 2015*. (2015).
29. *Quality and Outcomes Framework (2014/15), Diabetes Prevalence Model 2016 (Public Health England) and 2012 APHO Diabetes Prevalence Model.*
30. Saeedi, P. *et al.* Global and regional diabetes prevalence estimates for 2019 and projections for 2030 and 2045: Results from the International Diabetes Federation Diabetes Atlas, 9th edition. *Diabetes Res. Clin. Pract.* **157**, (2019).
31. Pirot, P., Cardozo, A. K. & Eizirik, D. L. Mediators and Mechanisms of Pancreatic Beta-cell Death in Type 1 Diabetes. *Arq Bras Endrocrinol Metab* **52**, 156–165 (2008).
32. Atkinson, M. A., Eisenbarth, G. S. & Michels, A. W. Type 1 diabetes. *Lancet* **383**, 69–82 (2014).
33. Hartman, I. Insulin analogs: impact on treatment success, satisfaction, quality of life, and adherence. *Clin. Med. Res.* **6**, 54–67 (2008).

34. Mathieu, C., Gillard, P., Benhalima, K. & Chantal Mathieu, P. G. and K. B. Insulin analogues in type 1 diabetes mellitus: getting better all the time. *Nat. Rev. Endocrinol.* **13**, 385–399 (2017).
35. Gingras, V. *et al.* Efficacy of dual-hormone artificial pancreas to alleviate the carbohydrate-counting burden of type 1 diabetes: A randomized crossover trial. *Diabetes Metab.* **42**, 47–54 (2016).
36. El-Khatib, F. H. *et al.* Home use of a bihormonal bionic pancreas versus insulin pump therapy in adults with type 1 diabetes: a multicentre randomised crossover trial. *Lancet* **389**, 369–380 (2017).
37. NHS Blood and Transplant. Annual report on pancreas and islet transplantation. Available at: https://nhsbtdbe.blob.core.windows.net/umbraco-assets-corp/16776/nhsbt-pancreas-and-islet-transplantation-annual-report-2018-2019.pdf. (Accessed: 12th May 2020)
38. Burke, G. W., Ciancio, G. & Sollinger, H. W. Advances in pancreas transplantation. *Transplantation* **77**, 62–67 (2004).
39. Shapiro, A. M. J. *et al.* Islet transplantation in seven patients with type 1 diabetes mellitus using a glucocorticoid-free immunosuppressive regimen. *N. Engl. J. Med.* **343**, 230–238 (2000).
40. Nathan, D. M. Diabetes Advances in Diagnosis and Treatment. *JAMA* **314**, 1052 (2015).
41. Ratjen, F. *et al.* Cystic fibrosis. *Nature reviews. Disease primers* **1**, 15010 (2015).
42. Wilschanski, M. & Novak, I. The cystic fibrosis of exocrine pancreas. *Cold Spring Harb. Perspect. Med.* **3**, (2013).
43. Mitchell, R. M. S., Byrne, M. F. & Baillie, J. Pancreatitis. in *Lancet* **361**, 1447–1455 (Elsevier Limited, 2003).
44. Brock, C., Nielsen, L. M., Lelic, D. & Drewes, A. M. Pathophysiology of chronic pancreatitis. *World Journal of Gastroenterology* **19**, 7231–7240 (2013).
45. Hegyi, P. & Rakonczay, Z. The role of pancreatic ducts in the pathogenesis of acute pancreatitis. *Pancreatology* **15**, S13–S17 (2015).
46. Office for National Statistics. *Cancer Survival in England-adults diagnosed*. (2019).
47. De Angelis, R. *et al.* Cancer survival in Europe 1999-2007 by country and age: Results of EUROCARE-5 - A population-based study. *Lancet Oncol.* **15**, 23–34 (2014).
48. McGuigan, A. *et al.* Pancreatic cancer: A review of clinical diagnosis, epidemiology, treatment and outcomes. *World Journal of Gastroenterology* **24**, 4846–4861 (2018).
49. Hruban, R. H., Maitra, A. & Goggins, M. Update on Pancreatic Intraepithelial Neoplasia. *Int. J. Clin. Exp. Pathol.* **1**, 306–316 (2008).
50. Grützmann, R., Post, S., Saeger, H. D. & Niedergethmann, M. Intraductal papillary mucinous neoplasia (IPMN) of the pancreas: its diagnosis, treatment, and prognosis. *Dtsch. Arztebl. Int.* **108**, 788–94 (2011).

51. Chen, J., Beal, E. W., Pawlik, T. M., Cloyd, J. & Dillhoff, M. E. Molecular Diagnosis of Cystic Neoplasms of the Pancreas: a Review. *Journal of Gastrointestinal Surgery* **24**, 1201–1214 (2020).
52. Maitra, A. & Hruban, R. H. Pancreatic Cancer. *Annu. Rev. Pathol. Mech. Dis.* **3**, 157–188 (2008).
53. Hruban, R. H. & Fukushima, N. Pancreatic adenocarcinoma: Update on the surgical pathology of carcinomas of ductal origin and panins. *Mod. Pathol.* **20**, 61–70 (2007).
54. Nagasue, N., Yukaya, H., Ogawa, Y., Kohno, H. & Nakamura, T. Human liver regeneration after major hepatic resection. A study of normal liver and livers with chronic hepatitis and cirrhosis. *Ann. Surg.* **206**, 30–39 (1987).
55. Lin, T. Y., Lee, C. S., Chen, C. C., Liau, K. Y. & Lin, W. S. Regeneration of human liver after hepatic lobectomy studied by repeated liver scanning and repeated needle biopsy. *Ann. Surg.* **190**, 48–53 (1979).
56. Menge, B. A. *et al.* Partial pancreatectomy in adult humans does not provoke β-cell regeneration. *Diabetes* **57**, 142–149 (2008).
57. Zhou, Q. & Melton, D. A. *Pancreas regeneration*. *Nature* **557**, 351–358 (Nature Publishing Group, 2018).
58. Zhong, F. & Jiang, Y. Endogenous pancreatic β cell regeneration: A potential strategy for the recovery of β cell deficiency in diabetes. *Front. Endocrinol. (Lausanne).* **10**, 101 (2019).
59. Hull, R. L. *et al.* Dietary-fat-induced obesity in mice results in beta cell hyperplasia but not increased insulin release: Evidence for specificity of impaired beta cell adaptation. *Diabetologia* **48**, 1350–1358 (2005).
60. Sorenson, R. L. & Brelje, T. C. Adaptation of islets of Langerhans to pregnancy: β-cell growth, enhanced insulin secretion and the role of lactogenic hormones. in *Hormone and Metabolic Research* **29**, 301–307 (Georg Thieme Verlag, 1997).
61. Saisho, Y. *et al.* β-Cell mass and turnover in humans: Effects of obesity and aging. *Diabetes Care* **36**, 111–117 (2013).
62. Butler, A. E. *et al.* Adaptive changes in pancreatic beta cell fractional area and beta cell turnover in human pregnancy. *Diabetologia* **53**, 2167–2176 (2010).
63. Dor, Y., Brown, J., Martinez, O. I. & Melton, D. A. Adult pancreatic β-cells are formed by self-duplication rather than stem-cell differentiation. *Nature* **429**, 41–46 (2004).
64. Meier, J. J. *et al.* β-cell replication is the primary mechanism subserving the postnatal expansion of β-cell mass in humans. *Diabetes* **57**, 1584–1594 (2008).
65. Wang, Y. J. *et al.* Single-Cell Mass Cytometry Analysis of the Human Endocrine Pancreas. *Cell Metab.* **24**, 616–626 (2016).
66. Avrahami, D., Klochendler, A., Dor, Y. & Glaser, B. Beta cell heterogeneity: an evolving concept. *Diabetologia* **60**, 1363–1369 (2017).

67. Johnston, N. R. *et al.* Beta Cell Hubs Dictate Pancreatic Islet Responses to Glucose. *Cell Metab.* **24**, 389–401 (2016).
68. Dorrell, C. *et al.* Human islets contain four distinct subtypes of β cells. *Nat. Commun.* **7**, 1–9 (2016).
69. Bader, E. *et al.* Identification of proliferative and mature β-cells in the islets of langerhans. *Nature* **535**, 430–434 (2016).
70. Puri, S. *et al.* Replication confers β cell immaturity. *Nat. Commun.* **9**, 1–12 (2018).
71. Talchai, C., Xuan, S., Lin, H. V., Sussel, L. & Accili, D. Pancreatic β cell dedifferentiation as a mechanism of diabetic β cell failure. *Cell* **150**, 1223–1234 (2012).
72. Smukler, S. R. *et al.* The adult mouse and human pancreas contain rare multipotent stem cells that express insulin. *Cell Stem Cell* **8**, 281–293 (2011).
73. Thorel, F. *et al.* Conversion of adult pancreatic α-cells to β-cells after extreme β-cell loss. *Nature* **464**, 1149–1154 (2010).
74. Chera, S. *et al.* Diabetes recovery by age-dependent conversion of pancreatic δ-cells into insulin producers. *Nature* **514**, 503–507 (2014).
75. Bonner-Weir, S., Baxter, L. A., Schuppin, G. T. & Smith, F. E. *A Second Pathway for Regeneration of Adult Exocrine and Endocrine Pancreas A Possible Recapitulation of Embryonic Development*. *Diabetes* **42**, (1993).
76. Domínguez-Bendala, J., Qadir, M. M. F. & Pastori, R. L. Pancreatic Progenitors: There and Back Again. *Trends in Endocrinology and Metabolism* **30**, 4–11 (2019).
77. Bonner-Weir, S. *et al.* Transdifferentiation of pancreatic ductal cells to endocrine β-cells. in *Biochemical Society Transactions* **36**, 353–356 (Portland Press, 2008).
78. Solar, M. *et al.* Pancreatic Exocrine Duct Cells Give Rise to Insulin-Producing β Cells during Embryogenesis but Not after Birth. *Dev. Cell* **17**, 849–860 (2009).
79. Criscimanna, A. *et al.* Duct cells contribute to regeneration of endocrine and acinar cells following pancreatic damage in adult mice. *Gastroenterology* **141**, 1451 (2011).
80. Huch, M. *et al.* IN vitro expansion of single Lgr5+ liver stem cells induced by Wnt-driven regeneration. *Nature* **494**, 247–250 (2013).
81. Pan, F. C. *et al.* Spatiotemporal patterns of multipotentiality in Ptf1aexpressing cells during pancreas organogenesis and injuryinduced facultative restoration. *Dev.* **140**, 751–764 (2013).
82. Xu, X. *et al.* β Cells Can Be Generated from Endogenous Progenitors in Injured Adult Mouse Pancreas. *Cell* **132**, 197–207 (2008).
83. El-Gohary, Y. *et al.* Intraislet pancreatic ducts can give rise to insulin-positive cells. *Endocrinology* **157**, 166–175 (2016).
84. Qadir, M. M. F. *et al.* Single-cell resolution analysis of the human pancreatic ductal progenitor cell niche. *Proc. Natl. Acad. Sci.* 201918314 (2020). doi:10.1073/pnas.1918314117
85. Russ, H. A., Ravassard, P., Kerr-Conte, J., Pattou, F. & Efrat, S. Epithelial-Mesenchymal

Transition in Cells Expanded In Vitro from Lineage-Traced Adult Human Pancreatic Beta Cells. *PLoS One* **4**, e6417 (2009).

86. Evans, M. Discovering pluripotency: 30 years of mouse embryonic stem cells. *Nat. Rev. Mol. Cell Biol.* **12**, 680–686 (2011).
87. Takahashi, K. *et al.* Induction of Pluripotent Stem Cells from Adult Human Fibroblasts by Defined Factors. *Cell* **131**, 861–872 (2007).
88. Bilic, J. & Belmonte, J. C. I. Concise Review: Induced Pluripotent Stem Cells Versus Embryonic Stem Cells: Close Enough or Yet Too Far Apart? *Stem Cells* **30**, 33–41 (2012).
89. Shih, C.-C., Forman, S. J., Chu, P. & Slovak, M. Human Embryonic Stem Cells Are Prone to Generate Primitive, Undifferentiated Tumors in Engrafted Human Fetal Tissues in Severe Combined Immunodeficient Mice. *Stem Cells Dev.* **16**, 893–902 (2007).
90. Bjorklund, L. M. *et al.* Embryonic stem cells develop into functional dopaminergic neurons after transplantation in a Parkinson rat model. *Proc. Natl. Acad. Sci. U. S. A.* **99**, 2344–9 (2002).
91. Ben-David, U. & Benvenisty, N. The tumorigenicity of human embryonic and induced pluripotent stem cells. *Nat. Rev. Cancer* **11**, 268–277 (2011).
92. Na, J., Baker, D., Zhang, J., Andrews, P. W. & Barbaric, I. Aneuploidy in pluripotent stem cells and implications for cancerous transformation. *Protein Cell* **5**, 569–79 (2014).
93. Zhao, T., Zhang, Z.-N., Rong, Z. & Xu, Y. Immunogenicity of induced pluripotent stem cells. *Nature* **474**, 212–215 (2011).
94. Johannesson, B., Sui, L., Freytes, D. O., Creusot, R. J. & Egli, D. Toward beta cell replacement for diabetes. *EMBO J.* **34**, 841–55 (2015).
95. Thakur, G., Lee, H. J., Jeon, R. H., Lee, S. L. & Rho, G. J. Small molecule-induced pancreatic β-like cell development: Mechanistic approaches and available strategies. *International Journal of Molecular Sciences* **21**, 2388 (2020).
96. Pagliuca, F. W. *et al.* Generation of Functional Human Pancreatic β Cells In Vitro. *Cell* **159**, 428–439 (2014).
97. Rezania, A. *et al.* Reversal of diabetes with insulin-producing cells derived in vitro from human pluripotent stem cells. *Nat. Biotechnol.* **32**, 1121–1133 (2014).
98. Millman, J. R. *et al.* Generation of stem cell-derived β-cells from patients with type 1 diabetes. *Nat. Commun.* **7**, 11463 (2016).
99. Pellegrini, S., Piemonti, L. & Sordi, V. Pluripotent stem cell replacement approaches to treat type 1 diabetes. *Current Opinion in Pharmacology* **43**, 20–26 (2018).
100. Heremans, Y. *et al.* Recapitulation of embryonic neuroendocrine differentiation in adult human pancreatic duct cells expressing neurogenin 3. *J. Cell Biol.* **159**, 303–311 (2002).
101. Swales, N. *et al.* Plasticity of Adult Human Pancreatic Duct Cells by Neurogenin3-Mediated Reprogramming. *PLoS One* **7**, e37055 (2012).

102. Collombat, P. *et al.* The Ectopic Expression of Pax4 in the Mouse Pancreas Converts Progenitor Cells into α and Subsequently β Cells. *Cell* **138**, 449–462 (2009).
103. Zhou, Q., Brown, J., Kanarek, A., Rajagopal, J. & Melton, D. A. In vivo reprogramming of adult pancreatic exocrine cells to β-cells. *Nature* **455**, 627–632 (2008).
104. Lima, M. J. *et al.* Generation of functional beta-like cells from human exocrine pancreas. *PLoS One* **11**, e0156204 (2016).
105. Clayton, H. W. *et al.* Pancreatic Inflammation Redirects Acinar to β Cell Reprogramming. *Cell Rep.* **17**, 2028–2041 (2016).
106. Huch, M. & Koo, B.-K. Modeling mouse and human development using organoid cultures. *Development* **142**, (2015).
107. Lancaster, M. A. & Huch, M. Disease modelling in human organoids. *DMM Dis. Model. Mech.* **12**, (2019).
108. Lancaster, M. A. & Knoblich, J. A. Organogenesis in a dish: Modeling development and disease using organoid technologies. *Science (80-.).* **345**, 1247125 (2014).
109. Greggio, C. *et al.* Artificial three-dimensional niches deconstruct pancreas development in vitro. *Development* **140**, 4452–4462 (2013).
110. Kim, Y. *et al.* Islet-like organoids derived from human pluripotent stem cells efficiently function in the glucose responsiveness in vitro and in vivo. *Sci. Rep.* **6**, 35145 (2016).
111. Koike, H. *et al.* Modelling human hepato-biliary-pancreatic organogenesis from the foregut–midgut boundary. *Nature* **574**, 112–116 (2019).
112. Barrandon, Y. & Green, H. Three clonal types of keratinocyte with different capacities for multiplication. *Proc. Natl. Acad. Sci. U. S. A.* **84**, 2302–6 (1987).
113. Hao, H. X., Jiang, X. & Cong, F. Control of Wnt receptor turnover by R-spondin-ZNRF3/RNF43 signaling module and its dysregulation in cancer. *Cancers* **8**, (2016).
114. Feng, Q. & Gao, N. Keeping Wnt Signalosome in Check by Vesicular Traffic. *J. Cell. Physiol.* **230**, 1170–1180 (2015).
115. Clevers, H. & Nusse, R. Wnt/β-Catenin Signaling and Disease. *Cell* **149**, 1192–1205 (2012).
116. Barker, N. *et al.* Identification of stem cells in small intestine and colon by marker gene Lgr5. *Nature* **449**, 1003–1007 (2007).
117. Barker, N. *et al.* Lgr5(+ve) stem cells drive self-renewal in the stomach and build long-lived gastric units in vitro. *Cell Stem Cell* **6**, 25–36 (2010).
118. Sato, T. *et al.* Single Lgr5 stem cells build crypt–villus structures in vitro without a mesenchymal niche. *Nature* **459**, 262–265 (2009).
119. Zhan, T., Rindtorff, N. & Boutros, M. Wnt signaling in cancer. *Oncogene* **36**, 1461–1473 (2017).
120. Huch, M. *et al.* Long-term culture of genome-stable bipotent stem cells from adult human liver. *Cell* **160**, 299–312 (2015).

121. Huch, M. *et al.* Unlimited in vitro expansion of adult bi-potent pancreas progenitors through the Lgr5/R-spondin axis. *EMBO J.* **32**, 2708–21 (2013).
122. Wang, D. *et al.* Long-Term Expansion of Pancreatic Islet Organoids from Resident Procr+ Progenitors. *Cell* **180**, 1198-1211.e19 (2020).
123. Broutier, L. *et al.* Culture and establishment of self-renewing human and mouse adult liver and pancreas 3D organoids and their genetic manipulation. *Nat. Protoc.* **11**, 1724–43 (2016).
124. Lin, J.-Y. *et al.* In vitro expansion of pancreatic islet clusters facilitated by hormones and chemicals. *Cell Discov.* **6**, 20 (2020).
125. Bonner-Weir, S. *et al.* In vitro cultivation of human islets from expanded ductal tissue. *Proc. Natl. Acad. Sci. U. S. A.* **97**, 7999–8004 (2000).
126. Rescan, C. *et al.* EGF-induced proliferation of adult human pancreatic duct cells is mediated by the MEK/ERK cascade. *Lab. Investig.* **85**, 65–74 (2005).
127. Yatoh, S. *et al.* Differentiation of affinity-purified human pancreatic duct cells to β-cells. *Diabetes* **56**, 1802–1809 (2007).
128. Klein, D. *et al.* BMP-7 Induces Adult Human Pancreatic Exocrine-to-Endocrine Conversion. *Diabetes* **64**, 4123–34 (2015).
129. Qadir, M. M. F. *et al.* P2RY1/ALK3-Expressing Cells within the Adult Human Exocrine Pancreas Are BMP-7 Expandable and Exhibit Progenitor-like Characteristics. *Cell Rep.* **22**, 2408–2420 (2018).
130. Lee, J. *et al.* Expansion and conversion of human pancreatic ductal cells into insulin-secreting endocrine cells. *Elife* **2**, e00940 (2013).
131. Boj, S. F. S. F. *et al.* Organoid models of human and mouse ductal pancreatic cancer. *Cell* **160**, 324–38 (2015).
132. Loomans, C. J. M. *et al.* Expansion of Adult Human Pancreatic Tissue Yields Organoids Harboring Progenitor Cells with Endocrine Differentiation Potential. *Stem Cell Reports* **10**, 712–724 (2018).
133. Chen, Y.-J. *et al.* De Novo Formation of Insulin-Producing "Neo-β Cell Islets" from Intestinal Crypts. *Cell Rep.* **6**, 1046–1058 (2014).
134. Ariyachet, C. *et al.* Reprogrammed Stomach Tissue as a Renewable Source of Functional β Cells for Blood Glucose Regulation. *Cell Stem Cell* **18**, 410–421 (2016).
135. Ben-David, U. *et al.* Genetic and transcriptional evolution alters cancer cell line drug response. *Nature* **560**, 325–330 (2018).
136. Hidalgo, M. *et al.* Patient-derived Xenograft models: An emerging platform for translational cancer research. *Cancer Discov.* **4**, 998–1013 (2014).
137. Tiriac, H. *et al.* Organoid Profiling Identifies Common Responders to Chemotherapy in Pancreatic Cancer. *Cancer Discov.* **8**, 1112–1129 (2018).
138. Driehuis, E. *et al.* Pancreatic cancer organoids recapitulate disease and allow personalized

drug screening. *Proc. Natl. Acad. Sci. U. S. A.* **116**, 26580–26590 (2019).

139. Sachs, N. *et al.* A Living Biobank of Breast Cancer Organoids Captures Disease Heterogeneity. *Cell* **172**, 373-386.e10 (2018).
140. Vlachogiannis, G. *et al.* Patient-derived organoids model treatment response of metastatic gastrointestinal cancers. *Science (80-.).* **359**, 920–926 (2018).
141. Ooft, S. N. *et al.* Patient-derived organoids can predict response to chemotherapy in metastatic colorectal cancer patients. *Sci. Transl. Med.* **11**, (2019).
142. Tsai, S. *et al.* Development of primary human pancreatic cancer organoids, matched stromal and immune cells and 3D tumor microenvironment models. *BMC Cancer* **18**, 335 (2018).
143. EudraLex - Volume 4 - Good Manufacturing Practice (GMP) guidelines | Public Health. Available at: https://ec.europa.eu/health/documents/eudralex/vol-4_en. (Accessed: 17th August 2020)
144. Giancola, R., Bonfini, T. & Iacone, A. Cell therapy: cGMP facilities and manufacturing. *Muscles, Ligaments and Tendons Journal* **2**, 243–247 (2012).
145. Fink, D. W. FDA regulation of stem cell-based products. *Science* **324**, 1662–1663 (2009).
146. Andrews, P. W. *et al.* Assessing the Safety of Human Pluripotent Stem Cells and Their Derivatives for Clinical Applications. in *Stem Cell Reports* **9**, 1–4 (Cell Press, 2017).
147. Sato, Y. *et al.* Tumorigenicity assessment of cell therapy products: The need for global consensus and points to consider. *Cytotherapy* **21**, 1095–1111 (2019).
148. Thomson, J. A. *et al.* Embryonic Stem Cell Lines Derived from Human Blastocysts. *Science (80-.).* **282**, (1998).
149. Hentze, H., Graichen, R. & Colman, A. Cell therapy and the safety of embryonic stem cell-derived grafts. *Trends Biotechnol.* **25**, 24–32 (2007).
150. Werbowetski-Ogilvie, T. E. *et al.* Characterization of human embryonic stem cells with features of neoplastic progression. *Nat. Biotechnol.* **27**, 91–97 (2009).
151. Roy, N. S. *et al.* Functional engraftment of human ES cell-derived dopaminergic neurons enriched by coculture with telomerase-immortalized midbrain astrocytes. *Nat. Med.* **12**, 1259–1268 (2006).
152. Song, W. K. *et al.* Treatment of macular degeneration using embryonic stem cell-derived retinal pigment epithelium: Preliminary results in Asian patients. *Stem Cell Reports* **4**, 860–872 (2015).
153. Schwartz, S. D. *et al.* Human embryonic stem cell-derived retinal pigment epithelium in patients with age-related macular degeneration and Stargardt's macular dystrophy: Follow-up of two open-label phase 1/2 studies. *Lancet* **385**, 509–516 (2015).
154. Takahashi, K. & Yamanaka, S. Induction of pluripotent stem cells from mouse embryonic and adult fibroblast cultures by defined factors. *Cell* **126**, 663–76 (2006).
155. Yu, J. *et al.* Induced Pluripotent Stem Cell Lines Derived from Human Somatic Cells. *Science*

(80-.). **318**, 1917–1920 (2007).

156. Stadtfeld, M., Nagaya, M., Utikal, J., Weir, G. & Hochedlinger, K. Induced pluripotent stem cells generated without viral integration. *Science (80-.).* **322**, 945–949 (2008).
157. Hussein, S. M. *et al.* Copy number variation and selection during reprogramming to pluripotency. *Nature* **471**, 58–62 (2011).
158. Gore, A. *et al.* Somatic coding mutations in human induced pluripotent stem cells. *Nature* **471**, 63–67 (2011).
159. Mayshar, Y. *et al.* Identification and classification of chromosomal aberrations in human induced pluripotent stem cells. *Cell Stem Cell* **7**, 521–531 (2010).
160. Kwon, E. M. *et al.* iPSCs and fibroblast subclones from the same fibroblast population contain comparable levels of sequence variations. *Proc. Natl. Acad. Sci. U. S. A.* **114**, 1964–1969 (2017).
161. Martincorena, I. *et al.* Universal Patterns of Selection in Cancer and Somatic Tissues. *Cell* **171**, 1029-1041.e21 (2017).
162. Martincorena, I. & Campbell, P. J. Somatic mutation in cancer and normal cells. *Science* **349**, 1483–9 (2015).
163. Martincorena, I. *et al.* High burden and pervasive positive selection of somatic mutations in normal human skin. *Science (80-.).* **348**, 880–886 (2015).
164. Weaver, J. M. J. *et al.* Ordering of mutations in preinvasive disease stages of esophageal carcinogenesis. *Nat. Genet.* **46**, 837–843 (2014).
165. Alexandrov, L. B. *et al.* Signatures of mutational processes in human cancer. *Nature* **500**, 415–421 (2013).
166. Alexandrov, L. B. *et al.* Mutational signatures associated with tobacco smoking in human cancer. *Science (80-.).* **354**, 618–622 (2016).
167. Zhang, Y., Chen, W., Feng, B. & Cao, H. The clinical efficacy and safety of stem cell therapy for diabetes mellitus: A systematic review and meta-analysis. *Aging and Disease* **11**, 141–153 (2020).
168. *European Medicines Agency. EMA/CAT/571134/2009: Reflection paper on stem cell-based medicinal products*. (2011).
169. *US Food and Drug Administration: Guidance for Industry Preclinical Assessment of Investigational Cellular and Gene Therapy Products*. (2013).
170. Blokzijl, F. *et al.* Tissue-specific mutation accumulation in human adult stem cells during life. *Nature* **538**, 260–264 (2016).
171. Kuijk, E. *et al.* The mutational impact of culturing human pluripotent and adult stem cells. *Nat. Commun.* **11**, 2493 (2020).
172. Hughes, C. S., Postovit, L. M. & Lajoie, G. A. Matrigel: a complex protein mixture required for optimal growth of cell culture. *Proteomics* **10**, 1886–1890 (2010).

173. Gjorevski, N. *et al.* Designer matrices for intestinal stem cell and organoid culture. *Nature* **539**, 560–564 (2016).
174. Broguiere, N. *et al.* Growth of Epithelial Organoids in a Defined Hydrogel. *Adv. Mater.* **30**, 1801621 (2018).
175. Hernandez-Gordillo, V. *et al.* Fully synthetic matrices for in vitro culture of primary human intestinal enteroids and endometrial organoids. *Biomaterials* **254**, 120125 (2020).
176. Gotham, D., Barber, M. J. & Hill, A. Production costs and potential prices for biosimilars of human insulin and insulin analogues. *BMJ Glob Heal.* **3**, 850 (2018).
177. ten Ham, R. M. T. *et al.* What does cell therapy manufacturing cost? A framework and methodology to facilitate academic and other small-scale cell therapy manufacturing costings. *Cytotherapy* **22**, 388–397 (2020).
178. Kanavos, P., Van Den Aardweg, S. & Schurer, W. *Diabetes expenditure, burden of disease and management in 5 EU countries*. (2012).
179. Lipsitz, Y. Y. *et al.* A roadmap for cost-of-goods planning to guide economic production of cell therapy products. *Cytotherapy* **19**, 1383–1391 (2017).
180. Moreau, A., Varey, E., Anegon, I. & Cuturi, M. C. Effector mechanisms of rejection. *Cold Spring Harbor Perspectives in Medicine* **3**, (2013).
181. Michaels, P. J. *et al.* Humoral rejection in cardiac transplantation: Risk factors, hemodynamic consequences and relationship to transplant coronary artery disease. *J. Hear. Lung Transplant.* **22**, 58–69 (2003).
182. Ingulli, E. Mechanism of cellular rejection in transplantation. *Pediatr. Nephrol.* **25**, 61–74 (2010).
183. LaRosa, D. F., Rahman, A. H. & Turka, L. A. The Innate Immune System in Allograft Rejection and Tolerance. *J. Immunol.* **178**, 7503–7509 (2007).
184. Sacks, S. H. & Zhou, W. Allograft rejection: Effect of local synthesis of complement. *Springer Seminars in Immunopathology* **27**, 332–344 (2005).
185. Ali, J. M., Bolton, E. M., Bradley, J. A. & Pettigrew, G. J. Allorecognition Pathways in Transplant Rejection and Tolerance. *Transplant. J.* **96**, 681–688 (2013).
186. Ali, J. M. *et al.* Diversity of the CD4 T Cell Alloresponse: The Short and the Long of It. *Cell Rep.* **14**, 1232–1245 (2016).
187. Lee, R. S., Grusby, M. J., Glimcher, L. H., Winn, H. J. & Auchincloss, H. Indirect recognition by helper cells can induce donor-specific cytotoxic T lymphocytes in vivo. *J. Exp. Med.* **179**, 865–872 (1994).
188. Kurosaki, T., Kometani, K. & Ise, W. Memory B cells. *Nat. Rev. Immunol.* **15**, 149–159 (2015).
189. Sanchez-Fueyo, A. & Strom, T. B. Immunologic basis of graft rejection and tolerance following transplantation of liver or other solid organs. *Gastroenterology* **140**, 51-64.e2

(2011).

190. Afzali, B., Lombardi, G. & Lechler, R. I. Pathways of major histocompatibility complex allorecognition. *Curr. Opin. Organ Transplant.* **13**, 438–44 (2008).
191. Pelletier, R. P. *et al.* Clinical Significance of MHC-Reactive Alloantibodies that Develop after Kidney or Kidney-pancreas Transplantation. *Am. J. Transplant.* **2**, 134–141 (2002).
192. Herrera, O. B. *et al.* A Novel Pathway of Alloantigen Presentation by Dendritic Cells. *J. Immunol.* **173**, 4828–4837 (2004).
193. Xing, Y. & Hogquist, K. A. T-Cell tolerance: Central and peripheral. *Cold Spring Harb. Perspect. Biol.* **4**, 1–15 (2012).
194. Wood, K. J. & Sakaguchi, S. Regulatory T cells in transplantation tolerance. *Nature Reviews Immunology* **3**, 199–210 (2003).
195. Salisbury, E. M., Game, D. S. & Lechler, R. I. Transplantation tolerance. *Pediatric Nephrology* **29**, 2263–2272 (2014).
196. Page, E. K., Dar, W. A. & Knechtle, S. J. Tolerogenic therapies in transplantation. *Front. Immunol.* **3**, 198 (2012).
197. Sheldon, S. & Poulton, K. HLA typing and its influence on organ transplantation. *Methods in molecular biology (Clifton, N.J.)* **333**, 157–174 (2006).
198. Robinson, J. *et al.* The IPD and IMGT/HLA database: allele variant databases. *Nucleic Acids Res.* **43**, D423–D431 (2015).
199. Rudolph, E. N. *et al.* HLA-A, -B, -C, -DR, and -DQ Matching in Pancreas Transplantation: Effect on Graft Rejection and Survival. *Am. J. Transplant.* **16**, 2401–2412 (2016).
200. Moini, M., Schilsky, M. L. & Tichy, E. M. Review on immunosuppression in liver transplantation. *World Journal of Hepatology* **7**, 1355–1368 (2015).
201. Enderby, C. & Keller, C. A. An Overview of Immunosuppression in Solid Organ Transplantation. *Am J Manag Care* **21**, 12–23 (2015).
202. Iwatsuki, S. *et al.* Experience in 1,000 liver transplants under cyclosporine-steroid therapy: A survival report. *Transplant. Proc.* **20**, 498–504 (1988).
203. Bamoulid, J. *et al.* The need for minimization strategies: Current problems of immunosuppression. *Transplant International* **28**, 891–900 (2015).
204. Wood, K. J., Issa, F. & Hester, J. Understanding Stem Cell Immunogenicity in Therapeutic Applications. *Trends Immunol.* **37**, 5–16 (2016).
205. Drukker, M. *et al.* Characterization of the expression of MHC proteins in human embryonic stem cells. *Proc. Natl. Acad. Sci. U. S. A.* **99**, 9864–9869 (2002).
206. Robertson, N. J. *et al.* Embryonic stem cell-derived tissues are immunogenic but their inherent immune privilege promotes the induction of tolerance. *Proc. Natl. Acad. Sci.* **104**, 20920 LP – 20925 (2007).
207. Thanasegaran, S., Cheng, Z., Ito, S., Nishio, N. & Isobe, K. No Immunogenicity of IPS Cells

in Syngeneic Host Studied by *In Vivo* Injection and 3D Scaffold Experiments. *Biomed Res. Int.* **2013**, 378207 (2013).

208. Zhao, T. *et al.* Humanized Mice Reveal Differential Immunogenicity of Cells Derived from Autologous Induced Pluripotent Stem Cells. *Cell Stem Cell* **17**, 353–359 (2015).
209. Pujol-Borrell, R., Todd, I., Doshi, M., Gray, D. & Feldmannt, M. Differential expression and regulation of MHC products in the endocrine and exocrine cells of the human pancreas. *Clin. exp. Immunol* **65**, 128–139 (1986).
210. Lu, W.-G., Pipeleers, D. G., Kl6ppel, G. & Bouwens, L. Comparative immunocytochemical study of MHC class II expression in human donor pancreas and isolated islets. *Virchows Arch* **429**, 205–211 (1996).
211. Vosters, O. *et al.* CD40 expression on human pancreatic duct cells: Role in nuclear factor-kappa B activation and production of pro-inflammatory cytokines. *Diabetologia* **47**, 660–668 (2004).
212. Klein, D. *et al.* A functional CD40 receptor is expressed in pancreatic beta cells. *Diabetologia* **48**, 268–276 (2005).
213. Klein, D., Timoneri, F., Ichii, H., Ricordi, C. & Pastori, R. L. CD40 activation in human pancreatic islets and ductal cells. *Diabetologia* **51**, 1853–1861 (2008).
214. Zhao, Y. *et al.* Mouse pancreatic beta cells express MHC class II and stimulate $CD4^+$ T cells to proliferate. *Eur. J. Immunol.* **45**, 2494–2503 (2015).
215. Kawasaki, E. Type 1 diabetes and autoimmunity. *Clin. Pediatr. Endocrinol. case reports Clin. Investig. Off. J. Japanese Soc. Pediatr. Endocrinol.* **23**, 99–105 (2014).
216. Wachlin, G. *et al.* IL-1β, IFN-γ and TNF-α increase vulnerability of pancreatic beta cells to autoimmune destruction. *J. Autoimmun.* **20**, 303–312 (2003).
217. Barrett, J. C. *et al.* Genome-wide association study and meta-analysis find that over 40 loci affect risk of type 1 diabetes. *Nat. Genet.* **41**, 703–707 (2009).
218. Nakayama, M., Simmons, K. M. & Michels, A. W. Molecular Interactions Governing Autoantigen Presentation in Type 1 Diabetes. *Curr. Diab. Rep.* **15**, 113 (2015).
219. Devendra, D., Liu, E. & Eisenbarth, G. S. Type 1 diabetes: recent developments. *BMJ* **328**, 750–4 (2004).
220. Mandrup-Poulsen, T. β-cell apoptosis: Stimuli and signaling. in *Diabetes* **50**, (Diabetes, 2001).
221. Hughes, K. J., Chambers, K. T., Meares, G. P. & Corbett, J. A. Nitric oxides mediates a shift from early necrosis to late apoptosis in cytokine-treated β-cells that is associated with irreversible DNA damage. *Am. J. Physiol. - Endocrinol. Metab.* **297**, (2009).
222. Campbell, I. L., Kay, T. W., Oxbrow, L. & Harrison, L. C. Essential role for interferon-gamma and interleukin-6 in autoimmune insulin-dependent diabetes in NOD/Wehi mice. *J. Clin. Invest.* **87**, 739–42 (1991).
223. Bosma, G. C., Custer, R. P. & Bosma, M. J. A severe combined immunodeficiency mutation

in the mouse. *Nature* **301**, 527–530 (1983).

224. Shultz, L. D., Ishikawa, F. & Greiner, D. L. Humanized mice in translational biomedical research. *Nat. Rev. Immunol.* **7**, 118–130 (2007).
225. Shultz, L. D. *et al.* Multiple defects in innate and adaptive immunologic function in NOD/LtSz-scid mice. *J. Immunol.* **154**, 180–91 (1995).
226. Ishikawa, F. *et al.* Development of functional human blood and immune systems in NOD/SCID/IL2 receptor {gamma} chain(null) mice. *Blood* **106**, 1565–73 (2005).
227. Shultz, L. D., Brehm, M. A., Garcia-Martinez, J. V. & Greiner, D. L. Humanized mice for immune system investigation: progress, promise and challenges. *Nat. Rev. Immunol.* **12**, 786–798 (2012).
228. Curran, M. *et al.* Recent Advancements and Applications of Human Immune System Mice in Preclinical Immuno-Oncology. *Toxicol. Pathol.* **48**, 302–316 (2019).
229. Brehm, M. A., Shultz, L. D. & Greiner, D. L. Humanized mouse models to study human diseases. *Curr. Opin. Endocrinol. Diabetes. Obes.* **17**, 120–5 (2010).
230. Pearson, T., Greiner, D. L. & Shultz, L. D. Creation of 'humanized' mice to study human immunity. *Curr. Protoc. Immunol.* **Chapter 15**, Unit 15.21 (2008).
231. King, M. *et al.* A new Hu-PBL model for the study of human islet alloreactivity based on NOD-scid mice bearing a targeted mutation in the IL-2 receptor gamma chain gene. *Clin. Immunol.* **126**, 303–314 (2008).
232. Brehm, M. A. *et al.* Lack of acute xenogeneic graft-versus-host disease, but retention of T-cell function following engraftment of human peripheral blood mononuclear cells in NSG mice deficient in MHC class I and II expression. *FASEB J.* **33**, 3137–3151 (2019).
233. Georgakopoulos, N. *et al.* Long-term expansion, genomic stability and in vivo safety of adult human pancreas organoids. *BMC Dev. Biol.* **20**, 4 (2020).
234. Santhanam, S., Liang, J., Baid, R. & Ravi, N. Investigating thiol-modification on hyaluronan via carbodiimide chemistry using response surface methodology. *J. Biomed. Mater. Res. Part A* **103**, 2300–2308 (2015).
235. D'Este, M., Eglin, D. & Alini, M. A systematic analysis of DMTMM vs EDC/NHS for ligation of amines to Hyaluronan in water. *Carbohydr. Polym.* **108**, 239–246 (2014).
236. Ellman, G. L. A colorimetric method for determining low concentrations of mercaptans. *Arch. Biochem. Biophys.* **74**, 443–450 (1958).
237. Li, H. Aligning sequence reads, clone sequences and assembly contigs with BWA-MEM. (2013).
238. Jones, D. *et al.* cgpCaVEManWrapper: Simple execution of caveman in order to detect somatic single nucleotide variants in NGS data. *Curr. Protoc. Bioinforma.* **2016**, 15.10.1-15.10.18 (2016).
239. Van Loo, P. *et al.* Allele-specific copy number analysis of tumors. *Proc. Natl. Acad. Sci. U. S.*

A. **107**, 16910–5 (2010).

240. Jun, G. *et al.* Detecting and estimating contamination of human DNA samples in sequencing and array-based genotype data. *Am. J. Hum. Genet.* **91**, 839–848 (2012).
241. Sampaziotis, F. *et al.* Reconstruction of the mouse extrahepatic biliary tree using primary human extrahepatic cholangiocyte organoids. *Nat. Med.* **23**, 954–963 (2017).
242. Bartfeld, S. *et al.* In Vitro Expansion of Human Gastric Epithelial Stem Cells and Their Responses to Bacterial Infection. *Gastroenterology* **148**, 126-136.e6 (2015).
243. Sato, T. *et al.* Long-term Expansion of Epithelial Organoids From Human Colon, Adenoma, Adenocarcinoma, and Barrett's Epithelium. *Gastroenterology* **141**, 1762–1772 (2011).
244. Suzuki, A. *et al.* PTH/cAMP/PKA signaling facilitates canonical Wnt signaling via inactivation of glycogen synthase kinase-3β in osteoblastic Saos-2 cells. *J. Cell. Biochem.* **104**, 304–317 (2008).
245. Coradini, D., Casarsa, C. & Oriana, S. Epithelial cell polarity and tumorigenesis: New perspectives for cancer detection and treatment. *Acta Pharmacologica Sinica* **32**, 552–564 (2011).
246. Koo, B. K. & Clevers, H. Stem cells marked by the r-spondin receptor LGR5. *Gastroenterology* **147**, 289–302 (2014).
247. Gerecht, S. *et al.* Hyaluronic acid hydrogel for controlled self-renewal and differentiation of human embryonic stem cells. *Proc. Natl. Acad. Sci. U. S. A.* **104**, 11298–11303 (2007).
248. Baker, L. A. & Tuveson, D. A. Generation and Culture of Tumor and Metastatic Organoids from Murine Models of Pancreatic Ductal Adenocarcinoma. in 117–133 (Humana Press, New York, NY, 2019). doi:10.1007/978-1-4939-8879-2_10
249. Baker, M. 1,500 Scientists Lift the Lid on Reproducibility. *Nature* **533**, 452–454 (2016).
250. Dossena, M. *et al.* Standardized GMP-compliant scalable production of human pancreas organoids. *Stem Cell Res. Ther.* **11**, 94 (2020).
251. Johnson, J. D. *et al.* Insulin protects islets from apoptosis via Pdx1 and specific changes in the human islet proteome. *Proc. Natl. Acad. Sci. U. S. A.* **103**, 19575–80 (2006).
252. Rimland, C. A. *et al.* Regional differences in human biliary tissues and corresponding *in vitro* derived organoids. *Hepatology* (2020). doi:10.1002/hep.31252
253. Dekkers, J. F. *et al.* A functional CFTR assay using primary cystic fibrosis intestinal organoids. *Nat. Med.* **19**, 939–945 (2013).
254. Lu, P., Takai, K., Weaver, V. M. & Werb, Z. Extracellular Matrix degradation and remodeling in development and disease. *Cold Spring Harb. Perspect. Biol.* **3**, (2011).
255. Cruz-Acuña, R. *et al.* Synthetic hydrogels for human intestinal organoid generation and colonic wound repair. *Nat. Cell Biol.* **19**, 1326–1335 (2017).
256. Barczyk, M., Carracedo, S. & Gullberg, D. Integrins. *Cell and Tissue Research* **339**, 269–280 (2010).

257. Bordeleau, F., Myrand Lapierre, M.-E., Sheng, Y. & Marceau, N. Keratin 8/18 Regulation of Cell Stiffness-Extracellular Matrix Interplay through Modulation of Rho-Mediated Actin Cytoskeleton Dynamics. *PLoS One* **7**, e38780 (2012).
258. Ravassard, P. *et al.* A genetically engineered human pancreatic β cell line exhibiting glucose-inducible insulin secretion. *J. Clin. Invest.* **121**, 3589–3597 (2011).
259. John, W. G. Use of HbA 1c in the diagnosis of diabetes mellitus in the UK. The implementation of World Health Organization guidance 2011. *Diabetic Medicine* **29**, 1350–1357 (2012).
260. Hayden, M. R. *et al.* Attenuation of endocrine-exocrine pancreatic communication in type 2 diabetes: pancreatic extracellular matrix ultrastructural abnormalities. *Journal of the cardiometabolic syndrome* **3**, 234–243 (2008).
261. Park, H. W. *et al.* Alternative Wnt Signaling Activates YAP/TAZ. *Cell* **162**, 780–794 (2015).
262. Kumar, D. & Lassar, A. B. The Transcriptional Activity of Sox9 in Chondrocytes Is Regulated by RhoA Signaling and Actin Polymerization. *Mol. Cell. Biol.* **29**, 4262–4273 (2009).
263. Pera, M. F. Stem cells: The dark side of induced pluripotency. *Nature* **471**, 46–47 (2011).
264. Schwartz, S. D., Tan, G., Hosseini, H. & Nagiel, A. Subretinal transplantation of embryonic stem cell–derived retinal pigment epithelium for the treatment of macular degeneration: An assessment at 4 years. *Investig. Ophthalmol. Vis. Sci.* **57**, ORSFc1–ORSFc9 (2016).
265. Da Cruz, L. *et al.* Phase 1 clinical study of an embryonic stem cell-derived retinal pigment epithelium patch in age-related macular degeneration. *Nat. Biotechnol.* **36**, 1–10 (2018).
266. Sharma, R. *et al.* Clinical-grade stem cell-derived retinal pigment epithelium patch rescues retinal degeneration in rodents and pigs. *Sci. Transl. Med.* **11**, 5580 (2019).
267. Petrus-Reurer, S. *et al.* Preclinical safety studies of human embryonic stem cell-derived retinal pigment epithelial cells for the treatment of age-related macular degeneration. *Stem Cells Transl. Med.* **9**, 936–953 (2020).
268. Fritz, S. *et al.* Intraductal tubular papillary neoplasm (ITPN), a novel entity of pancreatic epithelial neoplasms and precursor of cancer: A case report and review of the literature. *Int. J. Surg. Case Rep.* **55**, 187–191 (2019).
269. Broutier, L. *et al.* Human primary liver cancer-derived organoid cultures for disease modeling and drug screening. *Nat. Med.* **23**, 1424–1435 (2017).
270. Nicholson, J. M. & Cimini, D. Cancer karyotypes: Survival of the fittest. *Frontiers in Oncology* **3 JUN**, 148 (2013).
271. Zmuda, E. J., Powell, C. A. & Hai, T. A method for murine islet isolation and subcapsular kidney transplantation. *J. Vis. Exp.* e2096–e2096 (2011). doi:10.3791/2096
272. Prigge, J. R. *et al.* Nuclear double-fluorescent reporter for in vivo and ex vivo analyses of biological transitions in mouse nuclei. *Mamm. Genome* **24**, 389–399 (2013).
273. Hohwieler, M. *et al.* Human pluripotent stem cell-derived acinar/ductal organoids generate

human pancreas upon orthotopic transplantation and allow disease modelling. *Gut* **66**, 473–486 (2017).

274. Kaur, S., Kumar, S., Momi, N., Sasson, A. R. & Batra, S. K. Mucins in pancreatic cancer and its microenvironment. *Nat. Rev. Gastroenterol. &Amp; Hepatol.* **10**, 607 (2013).
275. Horinouchi, M. *et al.* Expression of Different Glycoforms of Membrane Mucin(MUC1) and Secretory Mucin (MUC2, MUC5AC and MUC6) in Pancreatic Neoplasms. *ACTA Histochem. Cytochem.* **36**, 443–453 (2003).
276. Drost, J. & Clevers, H. Translational applications of adult stem cell-derived organoids. *Development* (2017). doi:10.1242/dev.140566
277. Huang, L. *et al.* Ductal pancreatic cancer modeling and drug screening using human pluripotent stem cell- and patient-derived tumor organoids. *Nat. Med.* **21**, 1364–1371 (2015).
278. Seino, T. *et al.* Human Pancreatic Tumor Organoids Reveal Loss of Stem Cell Niche Factor Dependence during Disease Progression. *Cell Stem Cell* **22**, 454-467.e6 (2018).
279. Barkholt, L. *et al.* Risk of tumorigenicity in mesenchymal stromal cell-based therapies - Bridging scientific observations and regulatory viewpoints. *Cytotherapy* **15**, 753–759 (2013).
280. Goonetilleke, K. S. & Siriwardena, A. K. Systematic review of carbohydrate antigen (CA 19-9) as a biochemical marker in the diagnosis of pancreatic cancer. *European Journal of Surgical Oncology* **33**, 266–270 (2007).
281. Cheng, L. *et al.* Low incidence of DNA sequence variation in human induced pluripotent stem cells generated by nonintegrating plasmid expression. *Cell Stem Cell* **10**, 337–344 (2012).
282. Schneider, G., Schmidt-Supprian, M., Rad, R. & Saur, D. Tissue-specific tumorigenesis: Context matters. *Nature Reviews Cancer* **17**, 239–253 (2017).
283. Yamaguchi, J. *et al.* Pancreatic duct glands (PDGs) are a progenitor compartment responsible for pancreatic ductal epithelial repair. *Stem Cell Res.* **15**, 190–202 (2015).
284. Chang, C. Y. *et al.* Hyaluronic acid-human blood hydrogels for stem cell transplantation. *Biomaterials* **33**, 8026–8033 (2012).
285. (CITR) Collaborative Islet Transplant Registry. *CITR Tenth Annual Report*. (2017).
286. Pisania, A. *et al.* Quantitative analysis of cell composition and purity of human pancreatic islet preparations. *Lab. Investig.* **90**, 1661–1675 (2010).
287. Darnell, J. E., Kerr, I. M. & Stark, G. R. Jak-STAT pathways and transcriptional activation in response to IFNs and other extracellular signaling proteins. *Science (80-.).* **264**, 1415–1421 (1994).
288. de Vasconcellos Machado, C., da Silva Telles, P. D. & Nascimento, I. L. O. Immunological characteristics of mesenchymal stem cells. *Revista Brasileira de Hematologia e Hemoterapia* **35**, 62–67 (2013).
289. Johnson, P. & Ruffell, B. CD44 and its role in inflammation and inflammatory diseases. *Inflamm. Allergy Drug Targets* **8**, 208–20 (2009).

290. Pouliquen, E. *et al.* Anti-Donor HLA Antibody Response After Pancreatic Islet Grafting: Characteristics, Risk Factors, and Impact on Graft Function. *Am. J. Transplant.* **17**, 462–473 (2017).
291. Kenney, L. L., Shultz, L. D., Greiner, D. L. & Brehm, M. A. Humanized Mouse Models for Transplant Immunology. *Am. J. Transplant.* **16**, 389–397 (2016).
292. De Jong, M., Essers, J. & Van Weerden, W. M. Imaging preclinical tumour models: Improving translational power. *Nature Reviews Cancer* **14**, 481–493 (2014).
293. Woods, N.-B., Ooka, A. & Karlsson, S. Development of gene therapy for hematopoietic stem cells using lentiviral vectors. *Leukemia* **16**, 563–569 (2002).
294. Rodríguez, T. *et al.* Patterns of constitutive and IFN-γ inducible expression of HLA class II molecules in human melanoma cell lines. *Immunogenetics* **59**, 123–133 (2007).
295. Richardson, S. J. *et al.* Islet cell hyperexpression of HLA class I antigens: a defining feature in type 1 diabetes. *Diabetologia* **59**, 2448–2458 (2016).
296. Nozaki, K. *et al.* Co-culture with intestinal epithelial organoids allows efficient expansion and motility analysis of intraepithelial lymphocytes. *J. Gastroenterol.* **51**, 206–213 (2016).
297. King, M. A. *et al.* Human peripheral blood leucocyte non-obese diabetic-severe combined immunodeficiency interleukin-2 receptor gamma chain gene mouse model of xenogeneic graft-versus-host-like disease and the role of host major histocompatibility complex. *Clin. Exp. Immunol.* **157**, 104–118 (2009).
298. Lepus, C. M. *et al.* Comparison of human fetal liver, umbilical cord blood, and adult blood hematopoietic stem cell engraftment in NOD-scid/γc-/-, Balb/c-Rag1-/-γc-/-, and C.B-17-scid/bg immunodeficient mice. *Hum. Immunol.* **70**, 790–802 (2009).
299. Pauwels, K. *et al.* State-of-the-Art Lentiviral Vectors for Research Use: Risk Assessment and Biosafety Recommendations. *Curr. Gene Ther.* **9**, 459–474 (2009).
300. Hacein-Bey-Abina, S. *et al.* Insertional oncogenesis in 4 patients after retrovirus-mediated gene therapy of SCID-X1. *J. Clin. Invest.* **118**, 3132–3142 (2008).
301. Oceguera-Yanez, F. *et al.* Engineering the AAVS1 locus for consistent and scalable transgene expression in human iPSCs and their differentiated derivatives. *Methods* **101**, 43–55 (2016).
302. Jones, S. *et al.* Lentiviral vector design for optimal T cell receptor gene expression in the transduction of peripheral blood lymphocytes and tumor-infiltrating lymphocytes. *Hum. Gene Ther.* **20**, 630–640 (2009).
303. Wang, X. *et al.* The EF-1α promoter maintains high-level transgene expression from episomal vectors in transfected CHO-K1 cells. *J. Cell. Mol. Med.* **21**, 3044–3054 (2017).
304. Velychko, S. *et al.* Fusion of Reprogramming Factors Alters the Trajectory of Somatic Lineage Conversion. *Cell Rep.* **27**, 30-39.e4 (2019).
305. Zhu, Y., Liu, Q., Zhou, Z. & Ikeda, Y. PDX1, Neurogenin-3, and MAFA: Critical transcription regulators for beta cell development and regeneration. *Stem Cell Research and*

Therapy **8**, (2017).

306. Talavera-Adame, D. *et al.* Endothelial Cells in Co-culture Enhance Embryonic Stem Cell Differentiation to Pancreatic Progenitors and Insulin-Producing Cells through BMP Signaling. *Stem Cell Rev. Reports* **7**, 532–543 (2011).
307. Jaramillo, M. & Banerjee, I. Endothelial cell co-culture mediates maturation of human embryonic stem cell to pancreatic insulin producing cells in a directed differentiation approach. *J. Vis. Exp.* (2012). doi:10.3791/3759
308. Weniger, M., Honselmann, K. C. & Liss, A. S. The extracellular matrix and pancreatic cancer: A complex relationship. *Cancers* **10**, (2018).
309. Mamidi, A. *et al.* Mechanosignalling via integrins directs fate decisions of pancreatic progenitors. *Nature* **564**, 114–118 (2018).
310. Cebola, I. *et al.* TEAD and YAP regulate the enhancer network of human embryonic pancreatic progenitors. *Nat. Cell Biol.* **17**, 615–626 (2015).
311. Gornalusse, G. G. *et al.* HLA-E-expressing pluripotent stem cells escape allogeneic responses and lysis by NK cells. *Nat. Biotechnol.* **35**, 765–772 (2017).
312. Kooreman, N. G. *et al.* Alloimmune Responses of Humanized Mice to Human Pluripotent Stem Cell Therapeutics. *Cell Rep.* **20**, 1978–1990 (2017).